THÈSE / UNIVERSITÉ DE BRETAGNE OCCIDENTALE

sous le sceau de l'Université européenne de Bretagne

pour obtenir le titre de

DOCTEUR DE L'UNIVERSITÉ DE BRETAGNE OCCIDENTALE

Mention : (Électronique)

École DoctoraleSICMA (Santé, Information-Communication, Mathématiques, Matière) [ED 373]

présentée par

Naheed SAJJAD

Préparée à l'Ecole Nationale Supérieure de Techniques Avancées Bretagne (ENSTA-Bretagne)

au sein du laboratoires E3I2- Extraction et Exploitation de l'Information en Environnements Incertaines (EA 3876)

Electromagnetic wave scattering by using an improved two-scale model: Application to sea and bare soil surface

Thèse soutenue le 7 juillet 2011

devant le jury composé de :

Christian BROUSSEAU, président du jury
Professeur à l'UBO

Jihad ZALLAT, rapporteur
Professeur à l'Université de Strasbourg

Ala SHARAIHA, rapporteur
Professeur à Rennes 1

Abdelaziz BENSRHAIR, examinateur
Professeur à l'INSA Caen

Gabriel SORIANO, examinateur
Maitre de Conférences à l'Université Aix-Marseille

Ali KHENCHAF, directeur de thèse
Professeur à l'ENSTA-Bretagne

Arnaud COATANHAY, co-encadrant
Enseignant-Chercheur à à l'ENSTA-Bretagne

Contents

List of Figures

List of Tables

Notations

E : Electric field vector

H : Magnetic field vector

D : electric induction

B : magnetic induction

ρ : charge density

J : current density vector

ε_r : relative permittivity

μ_r : relative permeability

$\mathbf{K_i}$: incident wave vector

K : wave number of incident wave

k_i : transverse incident wave vector

θ_i : incident angle

θ_s: observation angle angle

ϕ_i: incident azimuth angle

ϕ_s : observed azimuth angle

σ_{pq}: scattering coefficient with transmitter polarization p and receiver polarization q

h : rms height of rough surface

l : correlation length of rough surface

W(K) : power spectrum of rough surface

Abstract

We use the contribution of second order scattering effects from a rough surface to obtain the enhanced backscattering cross section at grazing angles and the accurate predictions of depolarization in a radar return. We begin by reviewing the classically used scattering models like the Krichhoff Approximation (KA), first order Small Perturbation Method (SPM1) and the classical Two Scale Method (TSM1). Then by using the extended boundary condition method we study the SPM up to second order (SPM2). Comparisons between the numerical results obtained by using SPM1 and SPM2 reveal a greater accuracy and backscattering enhancement at grazing angles by SPM2 (for relatively rougher surfaces and/or for certain configurations). Moreover, SPM2 predicts non-zero backscattering results for cross polarization as opposed to SPM1. Motivated by these observations we develop an improved TSM (TSM2) by including the second order scattering effects into first order at small scale.

In the second part of the thesis, firstly we consider the applications of the newly developed model at grazing angles for sea and bare soil surface by using Elfouhaily and exponential spectrum respectivly. Secondly, we study the depolarization of electromagnetic waves from sea and bare soil surface by using TSM2. For both cases the results computed by TSM2 are compared with the available experimental data and the other approximate analytical methods like small slope approximation and weighted curvature approximation, in order to validate the model and demonstrate the obtained improvement in accuracy.

Acknowledgements

All praises to Almighty Allah, the most benevolent and merciful, who enabled me to complete this research work successfully.

First and foremost, I acknowledge the valuable role played by my respectable Supervisor Professor Ali KHENCHAF, whose continued encouragement, confidence and willing support kept me going to the end. I appreciate his vast knowledge and skill in many areas, his assistance in writing reports, his patience, invaluable guidance and excellent advice throughout this study.

My deep gratitude also goes to my co-supervisor Dr. Arnaud COATANHAY forhis guidance, assistance and valuable discussions during my work.

I also appreciate the help and technical support from my lab fellow Slah-Eddine BEN KHADRA. Sincere thanks to my friends Ania and Ayda for their caring behavior and moral support.

I am forever indebted to my parents and parents in law for their enormous love, support and prayers. I would like to give special thanks to my brothers and sisters for encouraging me with their best wishes, supporting me and being there whenever help was needed.

Words fail me to express my appreciation to my husband Sajjad whose encouragement, love and constant support enabled me to finish this journey. I also would like to thank to my kids Ayesha Ali, Muhammad Umar and Fatimah Zahra, who are powerful source of inspiration and energy and for giving me unlimited happiness and pleasure. I dedicate this dissertation to the four of you.

Chapter 1

Introduction

Predicting scattering cross sections of randomly rough surfaces is critical for designing terrain and sea surface remote sensing systems. The particular problem of wave scattering at low grazing angles is of great interest because of its importance for the low-altitude/long-range radar surveillance, target tracking, communication and navigation systems operating at low grazing conditions above the rough surface. The radar cross section from a rough surface becomes very small at grazing incidence, since most part of the incident power is scattered around the specular direction. Moreover, the dominant scattering mechanisms at low and high grazing angles are different e.g., the effects of multiple scattering (or higher order scattering) [1, 2, 3, 4], shadowing [5, 6, 7, 8], fading [9] and mechanisms attributable to wave breaking [10, 11, 12, 13, 14] are particularly marked in the low grazing angle regime. Therefore, the inclusion of these effects while developing a rigorous model can help to estimate accurately the radar bistatic scattering at grazing angles.

The mechanism of multiple scattering due to target surface roughness also causes depolarization (change in polarization state or cross polarization) [15]. Depolarization in a radar return results in corruption of the received signal. It is an undesired effect for a given transmitter, limiting the useful radar coverage distance. However, the cross-polarization in conjunction with co-polarization information can be used to retrieve the surface roughness parameters [16, 17], the geometrical configuration of scatterers while giving important clues to the electrical properties of surfaces etc [18]. Hence the study of depolarization cannot be used only to discriminate the unwanted reflections but it is also used for the identification and optimization purposes since it permits a deeper insight into physical phenomena.

In this context, the objective of this thesis is to study the bistatic scattering enhancement at grazing angles and the accurate depolarization estimation in a radar return by developing an analytical approximate scattering model which takes into ac-

count the contribution of higher-order scattering (multiple scattering). To this end we begin by reviewing the classically used scattering models like the Kirchhoff Approximation (KA)[19, 20, 21, 22], first order Small Perturbation Method (SPM1) [23, 24, 25, 26] and the classical Two Scale Method (TSM1) [1, 27, 28, 29, 30]. TSM1 combines KA and SPM1 and has larger domain of validity wrt. these models but it is inaccurate for grazing angles and there is a gap in the regions of validity of SPM1 and KA. Moreover, the predictions for cross polarization in backscattering case are not exact. We study the SPM up to second order and the comparisons between the simulated results obtained by SPM1 and SPM2 based on Gaussian spectrum reveal a greater accuracy and backscattering enhancement at grazing angles by SPM2 for certain configurations. Moreover the depolarization predictions by SPM2 are non-zero as opposed to SPM1. Motivated by these observations we develop an improved TSM (TSM2) by including the second order scattering effect by SPM [31]. The applications of TSM2 are presented for sea and bare soil surfaces by using Elfouhaily and exponential spectrum respectively [32]. Comparisons of the numerical results obtained from TSM2 with experimental data [9, 33, 34, 35, 36] and other analytical approximate techniques like Small Slope Approximation (SSA) [37] and Weighted Curvature Approximation (WCA) [38] demonstrate the validity and efficiency of TSM2 at grazing angles and accurate depolarization estimation [39, 40, 41, 42].

This dissertation consists of five chapters.

The second chapter is devoted to the review of some fundamental concepts related to electromagnetic wave theory, definitions and notations used subsequently and the principle tools concerning the propagation of electromagnetic waves. Then we study the different statistical techniques to characterize the random rough surface.

In the third chapter, at first we study the classically used scattering models (KA and SPM) which are characterized by a restricted angular domain of validity. Then, by using the extended boundary condition method we study the SPM up to second order. Some comparisons between the numerical results obtained by SPM1 and SPM2 based on Gaussian spectrum are also presented. Next, we start by reviewing the TSM1 and then by replacing the SPM1 with SPM1+SPM2 in TSM1, the development of TSM2 is given.

The objective of the fourth chapter is to provide a statistical description of the sea and soil surface to estimate the electromagnetic field scattered by these surfaces. Thus, we characterize the marine surface using some geometrical models like Gaussian and Elfouhaily for the spectral representation and Gauss and Cox & Munk for the representation of slopes. For bare soil surface the exponential spectrum and Gaussian slope distribution is used. Similarly, we propose in this chapter the analytical expressions of Debys's model and Peplinski model for the electric permittivity of sea water and soil

surface respectively.

The fifth and final chapter shows the numerical results obtained by TSM2. In the first part applications of TSM2 are considered for sea and bare soil surfaces at grazing angles. The results obtained are compared with available experimental data, TSM1, SSA and WCA in backscattering case. Then the simulation results are given for bistatic case and compared with TSM1. The prediction of depolarization (or cross-polarization) by TSM2 are evaluated in the second part of this chapter. The validity limit in each case is also given.

Finally, the dissertation is concludes by a summary of our main contributions and a list of suggestions for future research.

Chapter 2

Fundamentals of Electromagnetic Wave Scattering

This chapter presents the principles of propagation of EM wave along with the notations and definitions used subsequently. Then we introduce the polarimetric behavior of a target which permits us to determine the characteristics of a reflected wave from a target as a function of incident angle. Different statistical techniques to characterize the random rough surface are also studied.

2.1 Electromagnetic Waves

Electromagnetic wave theory is well-established scientific discipline, whose applications include, but are not limited to, remote sensing, digital and analog electronics, power systems, wireless and wired communications, radar systems, optics, and astronomy. Each application involves the creation, manipulation, and/or reception of electric and magnetic fields. The behavior of electromagnetic fields is completely described by Maxwell's Equations [43, 44] that relate electric and magnetic fields in time and space, given by

$$\nabla.\mathbf{D} = \rho \qquad \text{Gauss'law-electrostatics} \qquad (2.1)$$

$$\nabla.\mathbf{B} = \mathbf{0} \qquad \text{Gauss' law-magnetostatics} \qquad (2.2)$$

$$\nabla \times \mathbf{E} = -\frac{\partial \mathbf{B}}{\partial t} \qquad \text{Faraday's law} \qquad (2.3)$$

$$\nabla \times \mathbf{H} = \mathbf{J} + \frac{\partial \mathbf{D}}{\partial t} \qquad \text{Ampère-Maxwell law} \qquad (2.4)$$

where $\mathbf{E}$ is the electric field and $\mathbf{H}$ is the magnetic field: the two fields constitutes the electromagnetic field. *Subsequently, the vectors will be designated by boldface characters and the unit vectors with a hat on a boldface character.* The quantities $\mathbf{D}$ and $\mathbf{B}$

Symbol	Name	Numerical Value	SI Unit of Measure
ε_0	vacuum permittivity	8.854×10^{-12}	farads per meter
μ_0	vacuum permeability	1.256×10^{-6}	henries per meter
c	Speed of light in vacuum	2.998×10^{8}	meters per second

Table 2.1: Numerical values of permittivity, permeability and speed of light in vacuum

designate respectively the electric and magnetic induction (magnetic flux density), ρ is the charge density and $\mathbf{J}$ is the current density vector. The curl and divergence operator are denoted by $\nabla\times$ and $\nabla.$ respectively. The units used above are the standard SI units.

The electric displacement field $\mathbf{D}$, the magnetic flux density $\mathbf{B}$ and the current density $\mathbf{J}$ are related to the electric and magnetic fields by the following relations

$$\mathbf{D} = \varepsilon\mathbf{E} \tag{2.5}$$

$$\mathbf{B} = \mu\mathbf{H} \tag{2.6}$$

$$\mathbf{J} = \sigma\mathbf{E} \tag{2.7}$$

where ε, μ and σ are the permittivity, permeability and conductivity of the material respectively. In vacuum these quantities are denoted by ε_0 and μ_0; satisfies the relationship $c = 1/\sqrt{\varepsilon_0\mu_0}$, and summarized in the table 2.1.

In general, in the absence of charge and current, we commonly uses the relative permittivity $\varepsilon_r = \frac{\varepsilon}{\varepsilon_0}$ and relative permeability $\mu_r = \frac{\mu}{\mu_0}$ in the propagation, which allows to express the speed of wave propagation as a function of the speed of light:

$$v = \frac{c}{\sqrt{\varepsilon_r\mu_r}} \tag{2.8}$$

The Maxwell equations are applicable for an infinite medium, which does not reflect reality as every medium possess boundaries. Therefore, for practical applications of the electromagnetism theory it is important to treat the boundary value problem between two mediums with different electromagnetic properties. Suppose an arbitrary interface S_{01} separating two semi-infinite mediums denoted by Σ_0 for the upper half medium and Σ_1 for the lower medium respectively, and $\widehat{\mathbf{n}}$ is the the unit normal vector to the interface conventionally oriented to the upper half medium Σ_0 (see Fig. 2.1).

The boundary conditions [26, 45] can be written under the local form as follows:

$$\widehat{\mathbf{n}}.\,(\mathbf{B}_1 - \mathbf{B}) = \mathbf{0} \tag{2.9}$$

$$\widehat{\mathbf{n}}.\,(\mathbf{D}_1 - \mathbf{D}) = \rho_s \tag{2.10}$$

$$\widehat{\mathbf{n}}\times(\mathbf{E}_1 - \mathbf{E}) = \mathbf{0} \tag{2.11}$$

$$\widehat{\mathbf{n}}\times(\mathbf{H}_1 - \mathbf{H}) = \mathbf{J_s}\times\widehat{\mathbf{n}} \tag{2.12}$$

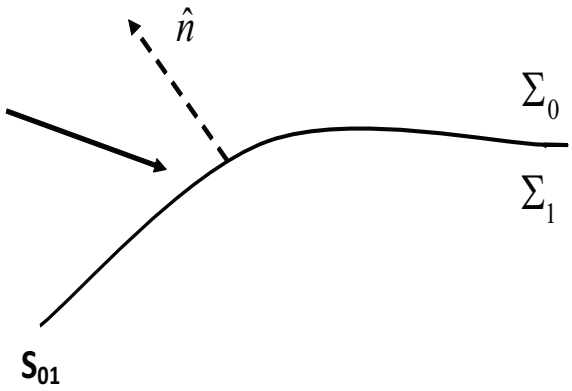

Figure 2.1: Interface between two semi infinite mediums Σ_0 and Σ_1.

where $\rho_{\mathbf{s}}$ and $\mathbf{J_s}$ represents the surface charge density and surface current density respectively, which can exist on the interface separating the two mediums ($\rho_{\mathbf{s}} = 0$ for dielectric medium, $\rho_{\mathbf{s}} = 0$ and $\mathbf{J_s} = 0$ for perfectly dielectric medium). The equations (2.9) and (2.11) are called the continuity relations at interface describing the continuity of the normal component of $\mathbf{B}$ and the tangential component of $\mathbf{E}$ respectively.

2.1.1 Propagation of a plane wave

Furthermore, from Maxwell's equations, one can deduce the wavy behavior of electromagnetic field. For a linear, homogeneous and isotropic medium with permittivity ε and permeability μ, in the absence of charge and current ($\rho = 0$ and $\mathbf{J} = \mathbf{0}$) it can be shown easily that any electric field $\mathbf{E}$ satisfies the homogeneous wave equation [46]

$$\nabla^2\mathbf{E} - \varepsilon\mu\frac{\partial^2\mathbf{E}}{\partial t^2} = \mathbf{0} \tag{2.13}$$

Similarly, the magnetic field $\mathbf{H}$ verify:

$$\nabla^2\mathbf{H} - \varepsilon\mu\frac{\partial^2\mathbf{H}}{\partial t^2} = \mathbf{0} \tag{2.14}$$

Equations (2.13) and (2.14) are the electric and magnetic *wave equations*.

In the particular case of a monochromatic wave of pulsation ω, The second derivative with respect to time is equivalent to multiplication by the factor $-\omega^2$

$\Big($ i. e., $\frac{\partial^2\mathbf{E}}{\partial t^2} = -i\omega.-i\omega.\mathbf{E} = -\boldsymbol{\omega}^2\mathbf{E}\Big)$. Under these conditions, the wave equation takes the form:

$$\nabla^2\mathbf{E} - \varepsilon\mu\frac{\partial^2\mathbf{E}}{\partial t^2} = \nabla^2\mathbf{E} - \left(-\omega^2\right)\varepsilon\mu\mathbf{E} = \nabla^2\mathbf{E} + K^2\mathbf{E} \tag{2.15}$$

where $\mathbf{K}$ is the wave vector such that $K = |\mathbf{K}| = \omega\sqrt{\mu\varepsilon} = \frac{2\pi}{\lambda}$, with ω is the angular frequency and λ is the wave length. Finally, $\mathbf{E}$ verify the Helmholtze equation [46]:

$$\left(\nabla^2 + K^2\right)\mathbf{E} = \mathbf{0} \tag{2.16}$$

Similarly the magnetic field $\mathbf{H}$ verify the Helmholtz equation.

For electric field the planar traveling wave solution of the wave equations is

$$\mathbf{E} = \widehat{\mathbf{e}} E e^{i(\mathbf{K}.\mathbf{R} - \omega t)} \tag{2.17}$$

where $\mathbf{R} = x\widehat{\mathbf{x}} + y\widehat{\mathbf{y}} + z\widehat{\mathbf{z}}$ is the position vector. In (2.17) E is the amplitude of the electric field and $\widehat{\mathbf{e}}$ is the direction of electric field. Figure 2.2 shows an illustration of the propagation of a plane electromagnetic wave towards z axis. The associated

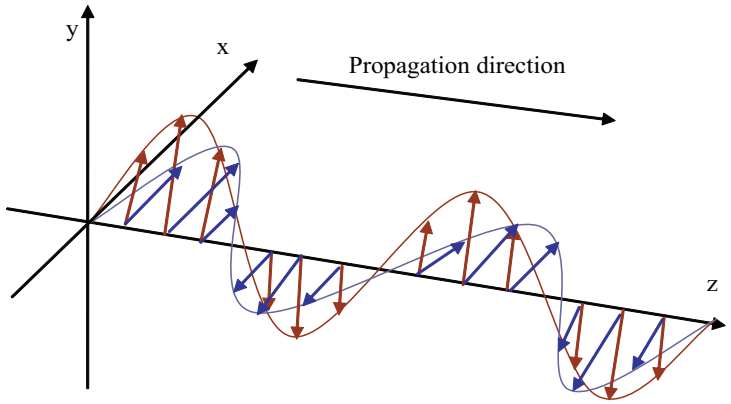

Figure 2.2: Polarized plane wave

magnetic field is given by

$$\mathbf{H} = \frac{1}{\eta}\widehat{\mathbf{K}} \times \mathbf{E} \tag{2.18}$$

where $\eta = \sqrt{\mu/\varepsilon}$ is the wave impedance.

2.2 Diffraction and diffusion of electromagnetic waves by a rough interface

2.2.1 Presentation of Problem

Figure 2.3 shows a geometric illustration of the phenomenon of scattering with the notation used for this manuscript. We have chosen the cartesian coordinate system ($\widehat{\mathbf{x}}$, $\widehat{\mathbf{y}}$, $\widehat{\mathbf{z}}$) whose origin is at the center of the illuminated surface.

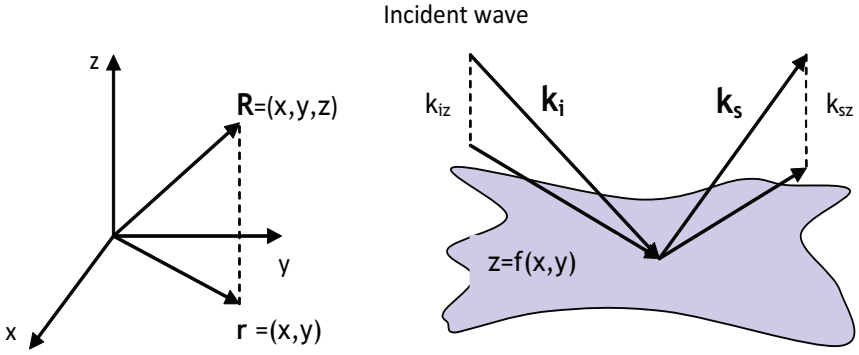

Figure 2.3: Graphical illustration of the vectorial parameters

Let $\mathbf{E}^i(\mathbf{R})$ be an electromagnetic plane wave propagating in the upper half medium Σ_0, towards a rough interface S_{01} separating the lower half medium medium Σ_1. The vector $\mathbf{R}$ is the position vector of the considered point expressed by $\mathbf{R} = x\widehat{\mathbf{x}} + y\widehat{\mathbf{y}} + z\widehat{\mathbf{z}}$. The incident wave propagates along the direction $\mathbf{K}_i = K\widehat{\mathbf{K}}_\mathbf{i} = k_{ix}\widehat{\mathbf{x}} + k_{iy}\widehat{\mathbf{y}} + k_{iz}\widehat{\mathbf{z}}$, which makes an angle θ_i with the vertical axis and φ_i with the x axis in the $x-y$ plane s.t.,

$$\begin{cases} k_{ix} = K\sin\theta_i\cos\varphi_i \\ k_{iy} = K\sin\theta_i\sin\varphi_i \\ k_{iz} = K\cos\theta_i \end{cases} \tag{2.19}$$

Suppose $\mathbf{r}$ and $\mathbf{k}$ denote the "transverse" wave vectors (i.e., vectors in $x-y$ plane) s.t., $\mathbf{r} = x\widehat{\mathbf{x}} + y\widehat{\mathbf{y}}$ and $\mathbf{k_i} = k_{ix}\widehat{\mathbf{x}} + k_{iy}\widehat{\mathbf{y}}$, then the incident wave (2.17) in the direction $\widehat{\mathbf{K}}_\mathbf{i}$ with unit amplitude can be written as

$$\mathbf{E}^i(\mathbf{R},t) = \widehat{\mathbf{e}}_i \exp\left(-i\left[\omega t - (\mathbf{k_i}.\mathbf{r} - k_{iz}z)\right]\right) \tag{2.20}$$

If we suppress the time harmonic dependence $\exp(-i\omega t)$ the expression of incident wave becomes:

– For the waves propagating in negative z direction:

$$\mathbf{E}^i(\mathbf{R}) = \widehat{\mathbf{e}}_i \exp\left[i\left(\mathbf{k_i}.\mathbf{r} - k_{iz}z\right)\right] \tag{2.21}$$

– For the waves propagating in positive z direction:

$$\mathbf{E}^i(\mathbf{R}) = \widehat{\mathbf{e}}_i \exp\left[i\left(\mathbf{k_i}.\mathbf{r} + k_{iz}z\right)\right] \tag{2.22}$$

The incident wave generates a reflected wave in the direction $\widehat{\mathbf{K}}_\mathbf{r}$ and a transmitted wave in direction $\widehat{\mathbf{K}}_\mathbf{t}$. The total field on the dielectric surface Σ_0 in the upper half

medium is the sum of the incident field and the reflected field i.e.,

$$\mathbf{E}(\mathbf{R}) = \mathbf{E}^i(\mathbf{R}) + \mathbf{E}^r(\mathbf{R}) \tag{2.23}$$

where $\mathbf{E}^r(\mathbf{R})$ is the reflected field in the direction $\widehat{\mathbf{K}}_\mathbf{r}$ and (θ_r, φ_r) are the associated angles in spherical domain. The total field on the dielectric surface S_{01} as regard to the transmission medium is equal to the transmitted field $\mathbf{E^t}(\mathbf{R})$ in the direction $\widehat{\mathbf{K}}_\mathbf{t}$ with (θ_t, φ_t) are the associated angles in spherical coordinate system.The unknowns of the problem are therefore the diffracted fields in reflection $\mathbf{E}^r(\mathbf{R})$ and transmission $\mathbf{E^t}(\mathbf{R})$ by the rough surface, at any point $\mathbf{R}$ of the space.

The incident and diffracted waves in reflection verifies the Helmholtz equation in the upper half medium Σ_0 and diffracted wave in transmission verify the Helmholtz equation in the lower half medium Σ_1

$$\nabla^2 + K_\alpha^2 \mathbf{E} = \mathbf{0} \tag{2.24}$$

where $\alpha = 0$ in the upper half medium and $\alpha = 1$ in the lower half medium. The diffracted waves in refection and transmission are related to the incident wave on the rough interface by the boundary conditions (2.9) to (2.12). Finally, to formulate the problem completely there must a be a radiation condition at infinity, $R \to +\infty$, verified by a functions called Green functions, that we will use in the sequel [47].

2.2.2 Dyadic Green's Function

The integral formulation of the field permits us to solve a three dimensional diffraction problem by resolving a system of integral equations defined on a bidimensional surface, provided that the medium is homogeneous. These integrals equations can be expressed with the help of Green's function, which gives the elementary solution of Helmholtz equation and satisfying the radiation conditions at infinity.

The Green's function is the solution of the field equation for a point source. Using the principle of linear superposition, the solution of the field due to a general source is just the convolution of the Green's function with the source. The equation for the Green's function for the scalar wave equation is

$$\left(\nabla^2 + K_0^2\right) g\left(\mathbf{R}, \mathbf{R}_d\right) = -\delta\left(\mathbf{R} - \mathbf{R}_d\right) \tag{2.25}$$

where $\delta\left(\mathbf{R} - \mathbf{R}_d\right)$ is the three-dimensional Dirac delta function with the source located at $\mathbf{R}_d$. The solution of (2.25) is [26, 48]

$$g\left(\mathbf{R}, \mathbf{R}_d\right) = g\left(\mathbf{R} - \mathbf{R}_d\right) = \frac{e^{iK_0|\mathbf{R}-\mathbf{R}_d|}}{4\pi\left|\mathbf{R} - \mathbf{R}_d\right|} \tag{2.26}$$

The dyadic Green's function relates the vector electromagnetic fields to vector current sources.

From the Maxwell equations in frequency domain with $exp(i\omega t)$ time convention

$$\nabla \times \mathbf{E} = i\omega\mu\mathbf{H} \tag{2.27}$$

$$\nabla \times \mathbf{H} = -i\omega\mu\mathbf{E} + \mathbf{J} \tag{2.28}$$

$$\nabla.\mu\mathbf{H} = 0 \tag{2.29}$$

$$\nabla.\varepsilon\mathbf{E} = \rho \tag{2.30}$$

it follows that the electric field obeys the vector wave equation

$$\nabla \times \nabla \times \mathbf{E} - K_0^2\mathbf{E} = i\omega\mu\mathbf{J} \tag{2.31}$$

where $K_0^2 = \omega^2\mu\varepsilon$.

In source-free region, $\mathbf{J} = \mathbf{0}$, and we have

$$\nabla \times \nabla \times \mathbf{E} - K_0^2\mathbf{E} = \mathbf{0} \tag{2.32}$$

The free space dyadic Green's function satisfies the equation

$$\nabla \times \nabla \times \mathbf{G}(\mathbf{R}, \mathbf{R}_d) - K_0^2\mathbf{G}(\mathbf{R}, \mathbf{R}_d) = \mathbf{I}\delta(\mathbf{R} - \mathbf{R}_d) \tag{2.33}$$

where $\mathbf{I}$ is the unit dyad.

Using the dyadic Green's function [49, 50] the electric field is equal to the convolution of the dyadic Green's function with the current source

$$\mathbf{E}(\mathbf{R}) = i\omega\mu \int \mathbf{G}(\mathbf{R}, \mathbf{R}_d) .\mathbf{J}(\mathbf{R}_d)\, d\mathbf{R}_d \tag{2.34}$$

The solution to (2.33) is

$$\mathbf{G}(\mathbf{R}, \mathbf{R}_d) = \left(\mathbf{I} + \frac{1}{K_0^2}\nabla\nabla\right) g(\mathbf{R}, \mathbf{R}_d) \tag{2.35}$$

2.2.3 Huygens' Principle and Extinction Theorem

Huygens'- Fresnel Principle

The Huygens'- Fresnel principle [44, 51, 52] is a method of analysis applied to problems of wave propagation (both in the far field limit and in near field diffraction). According to Huygens' construction, *every point of a wave front may be considered as a center of a secondary disturbance which gives rise to spherical wavelets, and the wave-front at any later instant may be regarded as the envelope of these wavelets.* Fresnel was able to account for diffraction by supplementing Huygens' construction with the postulate that

the secondary wavelets mutually interfere. This combination of Huygens' construction with the principle of interference is called the Huygens-Fresnel principle.

For **example**, if two rooms are connected by an open doorway and a sound is produced in a remote corner of one of them, a person in the other room will hear the sound as if it originated at the doorway. As far as the second room is concerned, the vibrating air in the doorway is the source of the sound.

In electromagnetic wave theory Huygens' principle formulation gives an exact relation that expresses the field in a region of space to the fields on a surface that encloses the region. Thus if the surface fields are determined, then the fields at any point in space can be calculated readily.

Extinction Theorem

Extinction theorem demonstrates that when an electromagnetic wave, propagating with the vacuum velocity of light c, is incident on a homogeneous medium with a sharp boundary, it is extinguished inside the medium in the process of interaction and is replaced by a wave propagated in the medium with a velocity c/n, where n is the refractive index of the medium. A classical theorem by P. P. Ewald [53] and C. W. Oseen [54] expresses the extinction of the incident wave in terms of an integral relation, that involves the induced field on the boundary of the medium.We know that under the influence of the incident electromagnetic field another field will be generated inside the dielectric, which will have a different wave number and hence a different phase velocity.

This theorem gives a non-local boundary conditions subject to which the field equations provide *unique* solution for the fields $\mathbf{E}$ and $\mathbf{H}$ inside the scattering medium (i.e., inside the volume V), when an electromagnetic field $\mathbf{E}^i$, $\mathbf{H}^i$ is incident on the medium. Once the solution inside the scattering medium has been obtained the solution outside it may be determined by substituting the boundary values into the surface integrals [51].

Mathematical representation of Huygens' principle and Extinction theorem

Both Huygens' principle and extinction theorem can be derived using the wave equation and the vector Green's theorem [26]. Vector Green's theorem states that for any two vectors $\mathbf{P}$ and $\mathbf{Q}$ in a region of space V,

$$\int_V \{\mathbf{P}.\nabla\times\nabla\times\mathbf{Q} - \mathbf{Q}.\nabla\times\nabla\times\mathbf{P}\}\,dV = \int \hat{\mathbf{n}}.\{\mathbf{Q}\times\nabla\times\mathbf{P} - \mathbf{P}\times\nabla\times\mathbf{Q}\}\,dS \quad (2.36)$$

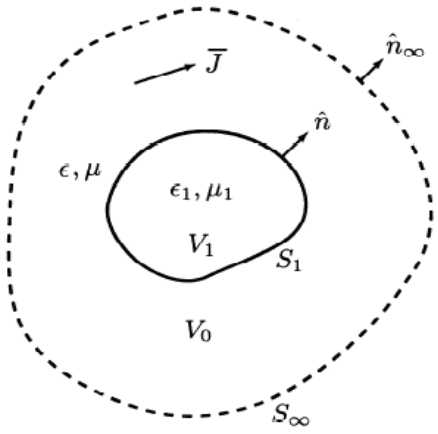

Figure 2.4: Electromagnetic scattering with source $\mathbf{J}$ in volume V_0.

where S is a surface that encloses volume V and $\widehat{\mathbf{n}}$ is the outward normal of S that points away from volume V.

Consider electromagnetic wave scattering with source $\mathbf{J}$ in region 0 that has permittivity ε and permeability μ while region 1 has permittivity ε_1 and permeability μ_1 (Fig. 2.4). Let S_1 denote the surface that encloses V_1 with outward normal $\widehat{\mathbf{n}}$, and let S_∞ be the surface at infinity with outward normal $\widehat{\mathbf{n}}_\infty$ that encloses the all of space. From the Maxwell equations, we have

$$\nabla \times \nabla \times \mathbf{E} - K^2 \mathbf{E} = i\omega\mu \mathbf{J} \tag{2.37}$$

$$\nabla \times \nabla \times \mathbf{E}_1 - K_1^2 \mathbf{E}_1 = 0 \tag{2.38}$$

with the boundary conditions $\widehat{\mathbf{n}} \times \mathbf{E} = \widehat{\mathbf{n}} \times \mathbf{E}_1$ and $\widehat{\mathbf{n}} \times \mathbf{H} = \widehat{\mathbf{n}} \times \mathbf{H}_1$ on S_1.

The free space Green's function $\mathbf{G}_o$ obeys the equation

$$\nabla \times \nabla \times \mathbf{G}_o(\mathbf{R}, \mathbf{R}_d) - K^2 \mathbf{G}_o(\mathbf{R}, \mathbf{R}_d) = \mathbf{I}\delta(\mathbf{R} - \mathbf{R}_d) \tag{2.39}$$

$$\mathbf{G}_o(\mathbf{R}, \mathbf{R}_d) = \left(\mathbf{I} + \frac{1}{K^2}\nabla\nabla\right) \frac{e^{iK|\mathbf{R}-\mathbf{R}_d|}}{4\pi|\mathbf{R} - \mathbf{R}_d|} \tag{2.40}$$

However, $\mathbf{R}_d$ as given in $\mathbf{G}_o(\mathbf{R}, \mathbf{R}_d)$ can be in either region 0 or region 1. Let $\mathbf{P} = \mathbf{E}$ in (2.36) and $\mathbf{Q} = \mathbf{G}_o(\mathbf{R}, \mathbf{R}_d).\mathbf{a}$ and $V = V_o$ in the vector Green's theorem of (2.36), with $\mathbf{a}$ being an arbitrary constant vector. We have

$$\begin{aligned} & \int_{V_o} \{\mathbf{E}(\mathbf{R}).\nabla \times \nabla \times \mathbf{G}_o(\mathbf{R}, \mathbf{R}_d).\mathbf{a} - \mathbf{G}_o(\mathbf{R}, \mathbf{R}_d).\mathbf{a}.\nabla \times \nabla \times \mathbf{E}(\mathbf{R})\}\, dV \\ = & -\int_{S_1} \widehat{\mathbf{n}}.\{\mathbf{G}_o(\mathbf{R}, \mathbf{R}_d).\mathbf{a} \times \nabla \times \mathbf{E} - \mathbf{E} \times \nabla \times \mathbf{G}_o(\mathbf{R}, \mathbf{R}_d).\mathbf{a}\}\, dS \\ & + \int_{S_\infty} \widehat{\mathbf{n}}_\infty.\{\mathbf{G}_o(\mathbf{R}, \mathbf{R}_d).\mathbf{a} \times \nabla \times \mathbf{E} - \mathbf{E} \times \nabla \times \mathbf{G}_o(\mathbf{R}, \mathbf{R}_d).\mathbf{a}\}\, dS \end{aligned} \tag{2.41}$$

The surface integral over S_∞ vanishes because of the radiation condition. Using (2.39) and (2.37) in (2.41), we have

$$\begin{aligned} & \int_{V_o} \left\{ \mathbf{E}\left(\mathbf{R}\right).\mathbf{a}\delta\left(\mathbf{R}-\mathbf{R}_d\right) - \left(\mathbf{G}_o\left(\mathbf{R},\mathbf{R}_d\right).\mathbf{a}\right).i\omega\mu\mathbf{J}\left(\mathbf{R}\right)\right\} dV \\ = & -\int_{S_1} \widehat{\mathbf{n}}.\left\{ \mathbf{G}_o\left(\mathbf{R},\mathbf{R}_d\right).\mathbf{a}\times\nabla\times\mathbf{E} - \mathbf{E}\times\nabla\times\mathbf{G}_o\left(\mathbf{R},\mathbf{R}_d\right).\mathbf{a}\right\} dS \end{aligned} \tag{2.42}$$

The Dirac delta function in (2.42) only contributes if $\mathbf{R}_d$ is in region 0. The other terms can be simplified by using the symmetry relation of Green's 'function,

$$\mathbf{G}_o^t\left(\mathbf{R},\mathbf{R}_d\right) = \mathbf{G}_o\left(\mathbf{R}_d,\mathbf{R}\right) \tag{2.43}$$

$$\left(\nabla\times\mathbf{G}_o\left(\mathbf{R},\mathbf{R}_d\right)\right)^t = \nabla'\times\mathbf{G}_o\left(\mathbf{R}_d,\mathbf{R}\right) \tag{2.44}$$

where superscript t denotes the transpose of the dyad and the properties of triple scalar product of vectors. Thus

$$\begin{aligned} & \begin{cases} \mathbf{E}\left(\mathbf{R}_d\right).\mathbf{a} & \text{if } \mathbf{R}_d\in V_o \\ 0 & \text{if } \mathbf{R}_d\in V_1 \end{cases} = \int_{V_o} \mathbf{a}.\mathbf{G}_o\left(\mathbf{R}_d,\mathbf{R}\right).i\omega\mu\mathbf{J}\left(\mathbf{R}\right)dV \\ & + \int_{S_1} \left[\mathbf{a}.G_o\left(\mathbf{R}_d,\mathbf{R}\right).\widehat{\mathbf{n}}\times i\omega\mu\mathbf{H}\left(\mathbf{R}\right) + \mathbf{a}.\nabla'\times G_o\left(\mathbf{R}_d,\mathbf{R}\right).\widehat{\mathbf{n}}\times\mathbf{E}\left(\mathbf{R}\right)\right] dS \end{aligned} \tag{2.45}$$

The constant vector $\mathbf{a}$ can be canceled from both sides of the equation. The first term on the right-hand side is the field generated by current source in an unbounded medium with permittivity ε and permeability μ and corresponds to the incident field $\mathbf{E}^i$. Thus

$$\begin{aligned} & \begin{cases} \mathbf{E}\left(\mathbf{R}_d\right) & \text{if } \mathbf{R}_d\in V_o \\ 0 & \text{if } \mathbf{R}_d\in V_1 \end{cases} \\ = & \mathbf{E}^i\left(\mathbf{R}_d\right) + \int_{S_1} \left[G_o\left(\mathbf{R}_d,\mathbf{R}\right).\widehat{\mathbf{n}}\times i\omega\mu\mathbf{H}\left(\mathbf{R}\right) + \nabla_p\times G_o\left(\mathbf{R}_d,\mathbf{R}\right).\widehat{\mathbf{n}}\times\mathbf{E}\left(\mathbf{R}\right)\right] dS \end{aligned} \tag{2.46}$$

In (2.46), the relation for $\mathbf{R}_d\in V_o$ is known as Huygens' principle and expresses the scattered electric field in terms of tangential electric and magnetic fields on the surface of the scatterer. The relation in (2.46) for $\mathbf{R}_d\in V_1$ is known as the extinction theorem and shows that the radiation of the surface field using $\mathbf{G}_o$, as the propagator into V_1 extinguishes the incident wave.

2.3 Polarization of a Plane Wave

Polarization, or direction of polarization, refers to the orientation of the field vectors of an electromagnetic wave at a given point during one period of oscillation. In radio physics, polarization refers to the direction of the electric field strength vector $\mathbf{E}$.

Polarization is the property of electromagnetic waves that describes the direction of the transverse electric field. More generally, the polarization of a transverse wave describes the direction of oscillation in the plane perpendicular to the direction of travel.

For the electric field the plane sinusoidal solution for an electromagnetic wave traveling in the z direction is

$$\mathbf{E}(z,t) = \begin{bmatrix} E_x(z,t) \\ E_y(z,t) \\ E_z(z,t) \end{bmatrix} = \begin{bmatrix} |E_x|\cos(\omega t - kz + \delta_x) \\ |E_y|\cos(\omega t - kz + \delta_y) \\ 0 \end{bmatrix} \tag{2.47}$$

where $|E_x|$ and $|E_y|$ are the amplitudes of the components of electric field E_x and E_y, $\lambda = c/f$ is the wave length and f is the frequency. δ_x and δ_y are the absolute phases of the field components at the origin $(t = 0, z = 0)$.

We can show that independent of time, the components E_x and E_y verify the quadratic equation equation of the form

$$\left(\frac{E_x}{|E_x|}\right)^2 - 2\frac{E_x E_y}{|E_x|\,|E_y|}\cos\delta + \left(\frac{E_y}{|E_y|}\right)^2 = \sin^2\delta \tag{2.48}$$

where $\delta = \delta_x - \delta_y$ shows the phase difference. This relation corresponds to an equation of ellipse (see figure 2.5). The state of polarization of a wave will be completely specified

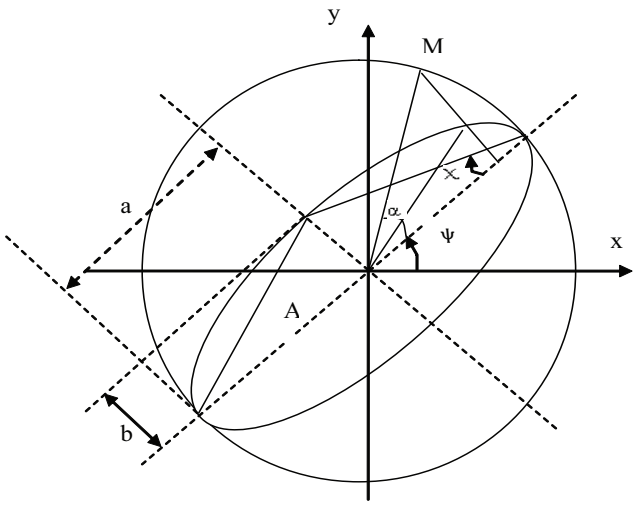

Figure 2.5: Ellipse of polarization with orientation angle ψ and ellipticity angle χ which are functions of major axis a and minor axis b.

by the parameters characterizing this ellipse, known as ellipse of polarization [55]. The

angle of orientation ψ is defined as the angle between the major semi-axis of the ellipse and the x-axis. The domain of this angle is $\left[-\frac{\pi}{2}, \frac{\pi}{2}\right]$.

The ellipticity is characterized by the angle χ which represents the opening of the ellipse, defined as the arctangent of the ratio of the minor and major axes. The domain of this angle is $\left[-\frac{\pi}{4}, \frac{\pi}{4}\right]$ and its sign, by convention, gives the direction of polarization

- right polarization when $-\frac{\pi}{4} < \chi < 0$,
- left polarization $0 < \chi < \frac{\pi}{4}$.

Moreover if the ellipticity is zero, the wave is linearly polarized and if the ellipticity is $\pm\frac{\pi}{4}$ degrees, the wave is circularly polarized.

The amplitude A is defined as a function of the length of minor axis and major axis by

$$A = \sqrt{a^2 + b^2} \tag{2.49}$$

A^2 characterizes the density of energy of the wave collected at the point of observation. The absolute phase is represented by the angle α between the major axis of the ellipse to M point This point M is defined as the intersection of the circle circumscribed to the ellipse and the orthogonal projection from the major axis of the ellipse, of the electric field at $t = 0$. The domain of this angle α is the interval $[-\pi, \pi]$.

Finally, the polarization of a wave is characterized by the couple (ψ, χ), which infer the variations of the components E_x and E_y of the electric field $\mathbf{E}(t)$ w.r.t., the axis x and y defined in the plane orthogonal to z-axis.

$$\tan(2\psi) = \tan(2\chi)\cos(\delta) \tag{2.50}$$

$$\sin(2\psi) = \sin(2\chi)\sin(\delta) \tag{2.51}$$

where

$$\tan(\chi) = \frac{|E_y|}{|E_x|} \tag{2.52}$$

Two particular cases can be noted

- $\chi = 0$ correspond to linear polarization

$$\begin{cases} \psi = 0\text{: horizontal polarization} \\ \psi = \frac{\pi}{2}\text{: vertical polarization} \end{cases} \tag{2.53}$$

- $\chi = \pm\frac{\pi}{4}$ correspond to vertical polarization

$$\begin{cases} \psi = \frac{\pi}{4}\text{: right polarization} \\ \psi = -\frac{\pi}{4}\text{: left polarization} \end{cases} \tag{2.54}$$

We will now write the electromagnetic wave in analytical form and introduce the representation of the polarization through Jones vector.

2.3.1 Jones vector

In the preceding paragraph, the electric field of a plane monochromatic wave of arbitrary polarization is given by (2.47) in real form. This electric field can also be written in complex form as follows

$$\mathbf{E}(z,t) = \begin{bmatrix} |E_x|\, e^{j(\omega t - kz + \delta_x)} \\ |E_y|\, e^{j(\omega t - kz + \delta_y)} \\ 0 \end{bmatrix} \tag{2.55}$$

For a monochromatic wave, the electric field components oscillate at the same frequency in a sinusoidal manner and therefore temporal term can be removed. Hence equation (2.55) can be written as

$$\mathbf{E}(z,t) = e^{-jkz} \begin{bmatrix} |E_x|\, e^{j\delta_x} \\ |E_y|\, e^{j\delta_y} \\ 0 \end{bmatrix} \tag{2.56}$$

In addition, the electric field $\mathbf{E}(z)$ has an identical phase at every point in the plane of a wave (z constant). Thus, while considering the case $z = 0$, the information on the amplitudes and the phases of the components of electric field is preserved. So in original form the electric field can be written as

$$\mathbf{E}(0) = \begin{bmatrix} |E_x|\, e^{j\delta_x} \\ |E_y|\, e^{j\delta_y} \\ 0 \end{bmatrix} \tag{2.57}$$

This vector is called the Jones vector, linked to the basis $(\widehat{x}, \widehat{y})$, the projection of the electric field components. The spatio-temporal vector electric field can be perfectly rebuilt from the Jones vector, according to following relation

$$\mathbf{E}(z,t) = \mathrm{Re}\left(\mathbf{E}(0)\, e^{j(\omega t - Kz)}\right) \tag{2.58}$$

Since the Jones vector characterizes completely the state of polarization of the wave, the parameters of the ellipse of polarization can be rediscovered.

Any state of polarization, represented by its Jones vector Jones $\mathbf{E}$, may be expressed in an orthonormal basis $(\widehat{x}, \widehat{y})$ called core polarization as

$$\mathbf{E} = E_x \widehat{x} + E_y \widehat{y} \tag{2.59}$$

The Jones vector is usually expressed in linear basis or circular basis. The most commonly used basis are the linear basis $(\widehat{\mathbf{h}}, \widehat{\mathbf{v}})$ where h is the state of horizontal polarization and v represents the state of vertical polarization. These basis will be used afterward.

2.3.2 Diffusion Matrix of a Target

The polarization of the electromagnetic plane wave scattered by a target is generally different from that of the incident wave. Let E^i and E^r represent the Jones vector of the transmitting and receiving electromagnetic waves, respectively. This polarization change represents the properties of the target expressed by the coherent scattering matrix S also known as the Sinclair (1950) matrix [56]. This matrix is a 2×2 complex matrix relating the Jones vectors of the transmitting wave and the receiving wave [55]. It depends on the polarization basis as presented by Mott (1986, 1992) [57]. Using an orthogonal linear (HV) polarization basis, the components of the received E^r and transmitted E^i electric field expressed in the polarization bases $(\mathbf{v}_r, \mathbf{h}_r)$, and $(\mathbf{v}, \mathbf{h})$ respectively, are related by

$$E^r = \begin{bmatrix} E^r_{v_r} \\ E^r_{h_r} \end{bmatrix} = \begin{bmatrix} S_{v_r v} & S_{v_r h} \\ S_{h_r v} & S_{h_r h} \end{bmatrix} \begin{bmatrix} E^i_v \\ E^i_h \end{bmatrix} = S^{BSA} E^i \tag{2.60a}$$

The scattering matrix is expressed in (1) using the backscattering alignment (BSA) convention.

In the forward scattering alignment (FSA) convention the scattered field is expressed in the $(\mathbf{v}_s, \mathbf{h}_s)$ basis such as [57]

$$E^s = \begin{bmatrix} E^s_{v_s} \\ E^s_{h_s} \end{bmatrix} = \begin{bmatrix} S_{v_s v} & S_{v_s h} \\ S_{h_s v} & S_{h_s h} \end{bmatrix} \begin{bmatrix} E^i_v \\ E^i_h \end{bmatrix} = S^{FSA} E^i \tag{2.61}$$

The scattering matrices expressed in both conventions are related by [57]

$$S^{FSA} = \begin{bmatrix} 1 & 0 \\ 0 & -1 \end{bmatrix} S^{BSA} \tag{2.62}$$

The coefficients of the scattering matrix depend on the geometrical and physical (permittivity and conductivity) features of the target. They are also functions of the target observation angles (locations of the transmitter and the receiver compared with the target) and of the frequency of the transmitted wave.

Considering the chosen convention (Fig. 2.6) for the angles characterizing the incident and diffused directions, the unit vectors defining the bases of polarisation in convention FSA and BSA can be expressed in local coordinate plane $(\widehat{x}, \widehat{y}, \widehat{z})$ as

$$\begin{cases} \widehat{\mathbf{K}} = \sin\theta\cos\varphi.\widehat{x} + \sin\theta\sin\varphi.\widehat{y} - \cos\theta.\widehat{z} \\ \widehat{\mathbf{v}} = -\cos\theta\cos\varphi.\widehat{x} - \cos\theta\sin\varphi.\widehat{y} - \sin\theta.\widehat{z} \\ \widehat{\mathbf{h}} = -\sin\varphi.\widehat{x} + \cos\varphi.\widehat{y} \end{cases} \tag{2.63}$$

$$\begin{cases} \widehat{\mathbf{K}}_s = \sin\theta_s\cos\varphi_s.\widehat{x} + \sin\theta_s\sin\varphi.\widehat{y} + \cos\theta_s.\widehat{z} \\ \widehat{\mathbf{v}}_s = \cos\theta_s\cos\varphi_s.\widehat{x} + \cos\theta_s\sin\varphi_s.\widehat{y} - \sin\theta_s.\widehat{z} \\ \widehat{\mathbf{h}}_s = -\sin\varphi_s.\widehat{x} + \cos\varphi_s.\widehat{y} \end{cases} \tag{2.64}$$

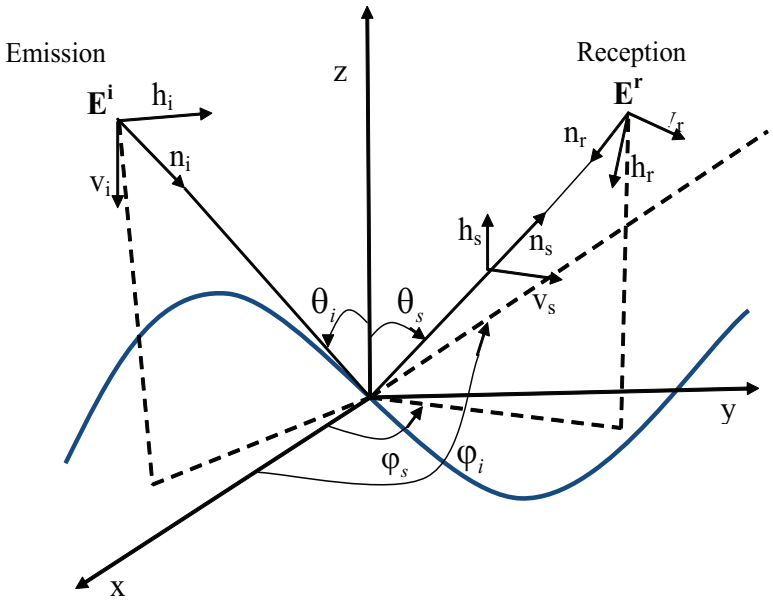

Figure 2.6: Geometrical configuration of bistatic scattering.

and

$$\begin{cases} \widehat{\mathbf{K}}_r = -\widehat{\mathbf{K}}_s \\ \widehat{\mathbf{v}}_r = \widehat{\mathbf{v}}_s \\ \widehat{\mathbf{h}}_r = -\widehat{\mathbf{h}}_s \end{cases} \tag{2.65}$$

These equations are related to a bistatic configuration whatsoever. On the other hand geometry of forward propagation is defined by $\theta_s = \theta$ and $\varphi_s = \varphi$. The backscattering is obtained by taking $\theta_s = \theta$ and $\varphi_s = \varphi + \pi$.

2.4 Characteristics of Random Rough Surfaces

No two surfaces are identical and even those formed by a well controlled process, such as turning, will each possess a unique surface form. Statistical techniques are required for describing such a surfaces.

A rough surface is usually described in terms of its deviation from a smooth 'reference surface'. There are two aspects to the nature of a random rough surface: the spread of heights about the reference surface and variation of height along surface. A variety of statistical distributions and parameters may be used to describe these surface properties. We here concentrate on surface height distribution functions and surface correlation functions.

2.4.1 Height Probability Distribution

The deviation of a surface from the smooth reference surface is represented by the function $z(\mathbf{m})$, where z is the height of the surface from the reference surface and $\mathbf{m}$ is the position vector of points on the reference surface (Fig. 2.7). The surface is thus assumed to be part of a continuous random process, z. The distribution of surface heights is described by the statistical height distribution, $p(z)$, where $p(z)dz$ is the probability of any surface point being at a height between z and $z + dz$ away from the mean surface.

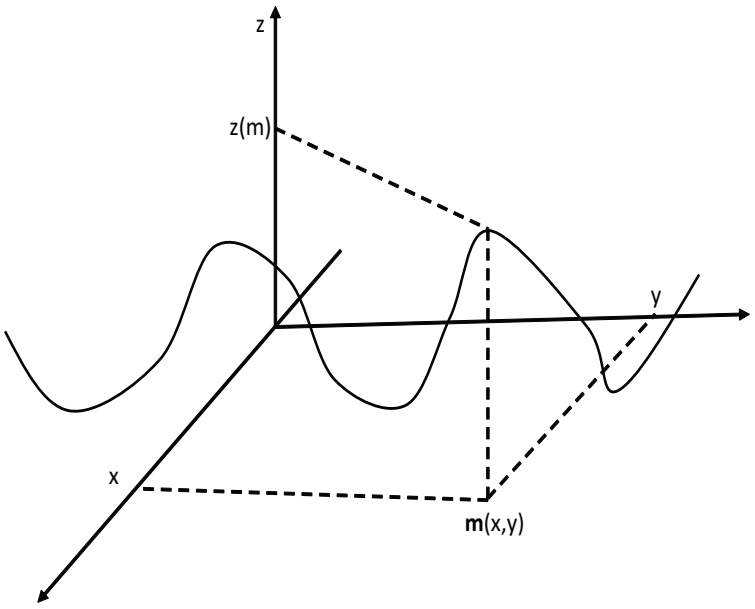

Figure 2.7: Illustration of hight distribution of a random rough surface.

It is usual to ensure that z satisfies

$$\langle z \rangle_s = \int_{-\infty}^{\infty} z p(z) dz = 0 \tag{2.66}$$

where $\langle ... \rangle_s$ denotes the process of spatial averaging, that is, averaging across the surface. The root mean square (rms) height of the surface is then equal to the standard deviation and is given by

$$h = \sqrt{\langle z^2 \rangle_s} = \sqrt{\int_{-\infty}^{\infty} z^2 p(z) dz} \tag{2.67}$$

In case of a random surface, the variance h^2 characterize the degree of vertical roughness of the surface, this degree is often expressed w.r.t. the emitted wave length.

One of the process mostly used in literature to define a random process is a Gaussian process and is characterized by the density function given by [22]

$$p(z) = \frac{1}{h\sqrt{2\pi}} \exp\left(-\frac{z^2}{2h^2}\right) \tag{2.68}$$

It has 96% of its distribution within two standard deviations of the mean. This distribution is symmetrical about zero so that Gaussian surfaces have an equal number of surface points above and below the reference surface and all odd order moments of z vanish.

In first approximation the profile of natural surface is supposed Gaussian. In fact the natural surfaces which are the result of a large number of local events, obey a statistical distribution which approaches to a Gaussian distribution. This result approaches to central limit theorem. If a random variable z is the sum of random variables z_i, where z_i are independent, then under fairly general conditions the distribution of z is Gaussian. Here the random variable z_i correspond to surface heights from the i^{th} independent process, each process contributing cumulatively to the final surface height.

2.4.2 Surface Correlations

The distribution of surface height does not characterize a surface completely. For example, the three surfaces shown in Fig. 2.8 have a Gaussian height distribution and same rms (root mean square) height

However the surface profiles are different because of the 'different length scales' over which length changes occur along the surface.

Such surfaces may be distinguished by their correlation functions (or autocorrelation functions), defined as

$$\rho(M) = \frac{\langle z(m)\, z(m+M)\rangle}{h^2} \tag{2.69}$$

The correlation function has the property that $\rho(0) = 1$. As M increases $\rho(M)$ will decay to zero, with the shape of the decay depends on surface profile.

The theory of wave scattering from rough surfaces often assumes that surface correlation functions are Gaussian and may be given by

$$\rho(M) = \exp\left(\frac{M^2}{l^2}\right) \tag{2.70}$$

where l is the correlation length.

Another type of correlation functions the exponential, and has the form

$$\rho(M) = \exp\left(\frac{|M|}{l}\right) \tag{2.71}$$

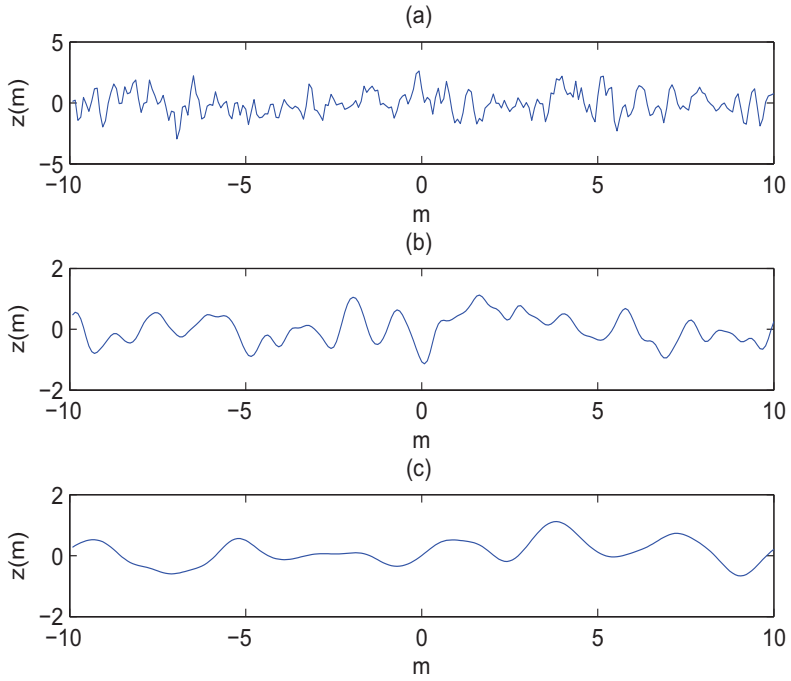

Figure 2.8: Profile of a Gaussian distribution with unit variance and different correlation lengths: (a)$l = 0.1$; (b)$l = 0.4$; (c)$l = 1$.

2.4.3 Other Descriptions

Characteristic function

The one-dimensional characteristic function of a rough surface is the Fourier transform of the probability density function:

$$\chi(s) = \int_{-\infty}^{\infty} p(h) e^{jsh} dh \tag{2.72}$$

This function provides a measure of the phase modulation of a wave at a rough surface. The two-dimensional characteristic function is given by

$$\chi(s_1, s_2) = \int_{-\infty}^{\infty} p(h_1, h_2) e^{j(s_1 h_1 + s_2 h_2)} dh_1 dh_2 \tag{2.73}$$

where h_1 and h_2 are surface heights measured at different surface points.

Power spectrum

An alternative description of a randomly rough surface is obtained through the power spectrum. This is defined as the Fourier transform of the correlation function:

$$W(K) = \frac{1}{2\pi} \int_{-\infty}^{\infty} \rho(M)\, e^{jKM} dM \tag{2.74}$$

where K is the wave number. The total area under the power spectrum gives the variance of the surface:

$$\int_{-\infty}^{\infty} p(K) dK = h^2 \tag{2.75}$$

For the case of stationary Gaussian height distribution with zero mean and rms height h the spectral density is equal to

$$W(K) = \frac{1}{2\sqrt{\pi}} \exp\left(-\frac{K^2 l^2}{4}\right) \tag{2.76}$$

and for anisotropic surface with Gaussian correlation function it takes the form

$$W(k_1, k_2) = \frac{h^2 l_x l_y}{4\pi} \exp\left(-\frac{k_x^2 l_x^2}{4} - \frac{k_y^2 l_y^2}{4}\right) \tag{2.77}$$

when k_x and k_y are components of wave vector in x and y direction. For exponential correlation function the power spectrum is given by

$$W(k_1, k_2) = \frac{h^2}{l_x l_y \pi^2} \frac{1}{(1/l_x^2 + k_x^2)} \frac{1}{(1/l_y^2 + k_y^2)} \tag{2.78}$$

Isotropy, stationarity and ergodicity

Several assumptions are often implicit in the statistical theory of random rough surface. These assumptions are described as follows.

A rough surface is isotropic if the statistics of that surface are independent of direction along the surface. If the statistics of one section of the surface is same as the statistics determined from a different section of the same surface then it is said to be a stationary surface and it is ergodic if the spatial average (average taken over many different parts of one surface realization) is equal to the ensemble average (average over many realizations).

2.5 Statistical description of the diffused field

Natural surfaces (e.g., sea surface, snowy covered surface and vegetation canopies etc.) can be considered as rough, and the roughness is the dominant factor for the scattering

behavior of an EM wave. The roughness of any scattering surfaces is not an intrinsic property of that surface but depends on the properties of a wave being transmitted. Both, the frequency and the local angle of incidence of the transmitted wave, determine how rough and smooth any surface appears to be. The relation of the EM wave in terms of its wave length λ to the statistical roughness parameter h is given by kh. Thus with increasing wavelength, the roughness term is decreasing, consequently, the indication of relative roughness for any surface is depending on the wavelength as $K = 2\pi/\lambda$. Also the local incidence angle plays an important role for defining the roughness condition of a surface. In the near field of the propagating EM wave, the surface appears rougher than in the far field, which can be compared with the reflection of the sunset over the sea [19, 22].

2.5.1 The Rayleigh criterion

Wave scattering from rough surface was first studied by Rayleigh in 1877, who considered the problem of a plane monochromatic wave incident normally onto a sinusoidal surface. Consider a plane monochromatic wave incident at some angle θ onto a rough surface (Fig. 2.9), it is a simple matter to to calculate the phase difference between two rays scattered from separate points on the surface:

$$\Delta\varphi = 2h\frac{2\pi}{\lambda}\cos\theta \tag{2.79}$$

where h is the standard deviation of the roughness height regarding to a reference height and θ is the local incident angle. The Rayleigh criterion states that if the phase

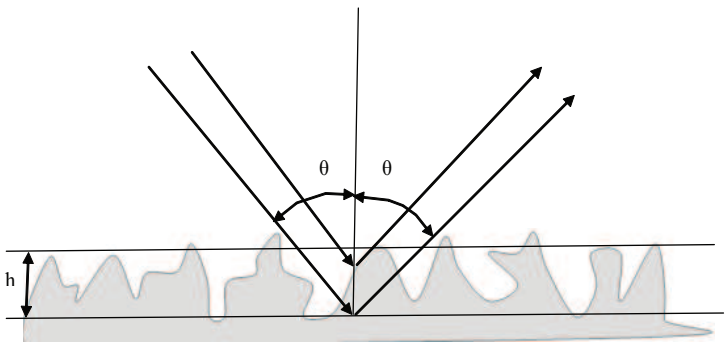

Figure 2.9: Diagram for determining the phase difference between two parallel waves scattered from different points on a rough surface

difference $\Delta\varphi$ between two reflected waves is less than $\pi/2$ radians, then the surface

is 'smooth', otherwise it is 'rough' or in terms of wave length and surface standard deviation this criterion can be stated as

$$\sigma < \frac{\lambda}{8\cos\theta} \tag{2.80}$$

Another more stringent criterion was proposed by Fraunhofer as [21]

$$\sigma < \frac{\lambda}{32\cos\theta} \tag{2.81}$$

Experimental measurements have confirmed that the Fraunhofer criteria is better suited to determining if a surface may be considered smooth enough to model with a simple decrease in the coherent reflection coefficient [21].

2.5.2 Phase Considerations

In the natural environment the surface condition varies from medium to rough. The backscattered EM wave on a surface consists of two components, a reflected or coherent (i.e., $h1 = h2$) and a scattered and incoherent one (i.e.,$h1 \neq h2$ and $\Delta\varphi$ varies) as shown in Fig. 2.10. The coherent component reacts as a specular reflection on a smooth surface. The incoherent component is a diffuse scatterer and distributes the scattering power in all directions. As the surface become rougher, the coherent

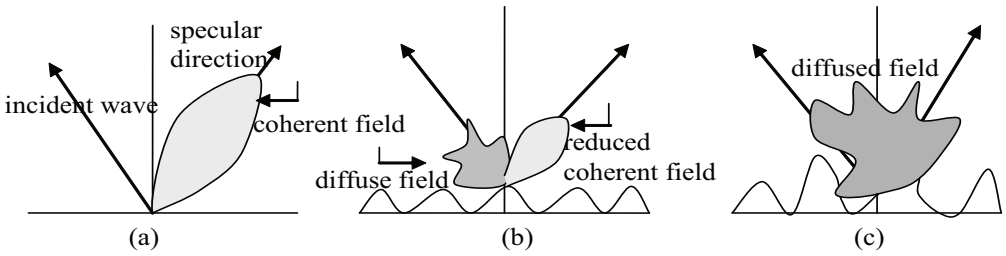

Figure 2.10: Rates of roughness components on a (a) smooth, (b) rough and (c) very rough surface

component becomes negligible and the incoherent component consists of only diffuse scattering.

Chapter 3

Models of diffusion

Many natural surfaces are rough in varying degrees, and this roughness affects the propagation and scattering characteristics of a wave. For example, the propagation characteristics of a wave over such a surface are different from the characteristics over a smooth surface. The aim of our work is the thorough understanding of this phenomenon and develop a reliable electromagnetic diffusion model which can predicts accurately the bistatic scattering from moderate to low grazing angles and can be used for better depolarization estimation. This problem is of interest in many practical radar applications, for examples radar systems operating on naval ships which are designed to provide protection against low cross section sea-skimming anti-ship missiles.

The radar equation is introduced in the first part of this chapter. It permits us to express the received power as function of emitted power, the system characteristics and the properties of the illuminated target. In the second part we start by presenting some classically used scattering models in the context of bistatic configuration (Kirchhoff Approximation: KA [19]–[22], and first order Small Perturbation Method: SPM1 [23]–[26]). Then by using the extended boundary condition method we study the SPM upto second order. Some comparisons between the numerical results obtained by SPM1 and SPM2 based on Gaussian spectrum are also presented. We observe that SPM2 has greater accuracy and enhanced results at grazing angles for certain roughness conditions and it also produce non-zero results for cross polarization in backscattering direction. Next, we take a review of classical Two Scale Model (TSM1) [27]–[30] which combines KA and SPM1. TSM1 has broader range of validity as compared to KA and SPM1 but it is inaccurate at grazing angles. Moreover in backscattering case the cross polarization estimation by TSM1 are not exact. The observation during the comparisons between SPM1 and SPM12 led us to develop and improved TSM (TSM2) by including the effects of second order scattering estimated by SPM2. Hence the development is presented in the third part of this chapter. Our objective is to implement this model in marine

and bare soil surface applications for the study of bistatic scattering enhancement from moderate to small grazing angles and cross polarization estimations.

3.1 Polarimetry of a Radar target

An object illuminated by an electromagnetic wave re-emit a diffused field in space which is mainly a function of, among others, frequency, initial polarization of incident wave and the geometric position of target with respect to the emitting and receiving antennas. However, in general the polarimetric properties of diffused wave are different from the incident wave.

Generally speaking, radar reflectivity of a contributor can be characterized by a magnitude called Surface Equivalent Radar σ (SER) of the target, homogenous to a surface. It is customary to quantify the electromagnetic response of a rough surface by scattering coefficient $\sigma^0 = \frac{\sigma}{A}$, which is the ratio of the surface equivalent radar to the illuminated surface. It is expressed in units of reciprocal distance [21].

3.1.1 Problem statement

The measurements in active remote sensing are done generally in monostatic (transmitter and receiver is placed on the same place) or quasi-monostatic configuration. In this case we take a measure of backscattering. The measurements can also be taken everywhere in space (bistatic configuration). In this case the transmission and reception antennas are situated in different locations (see Fig. 3.1).

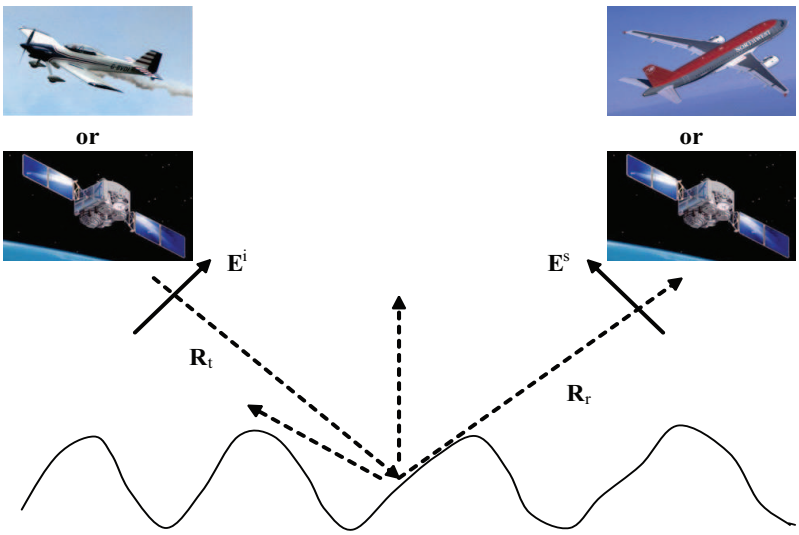

Figure 3.1: Bistatic scattering of an electromagnetic wave by a rough surface

3.1.2 Radar Equation

The fundamental relation between the characteristics of the radar, the target, and the received signal is called the radar equation. While considering a bistatic system with transmitting antenna gain G_t and receiving antenna gain G_r, located respectively at distances R_t and R_r on the surface, the power received by a receptor is given by [21]

$$P_r = \frac{\lambda^2}{(4\pi)^3} \int_{A_0} \frac{P_t G_t G_r}{R_r^2 R_t^2} \sigma^0_{\alpha\alpha_0} dA \tag{3.1}$$

where P_t represents the emitted power, λ is the wave length of the emitted wave, A_0 designates the illuminated surface and $\sigma^0_{\alpha\alpha_0}$ is the coefficient of diffusion of a illuminated surface by a wave with polarisation α (v or h) and observed with polarization α_0 (v or h).

The coefficient of bistatic scattering $\sigma_{\alpha\alpha_0}$ is a function that depends on many parameters such as the physical and geometric characteristics of the enlightened surface, the wave length as well as the emitter and receiver polarization. Its calculation requires the choice of frame and appropriate modeling.

3.1.3 Scattering coefficient

The incident and scattered fields $\mathbf{E}^i$ and $\mathbf{E}^s$ can be decomposed in their basis of polarization respectively

$$\begin{aligned} \mathbf{E}^i &= \mathbf{E}_{ih_i}\widehat{h}_i + \mathbf{E}_{iv_i}\widehat{v}_i \\ \mathbf{E}^s &= \mathbf{E}_{sh_s}\widehat{h}_s + \mathbf{E}_{sv_s}\widehat{v}_s \end{aligned}$$

The complete description of scattering from a target is obtained by its diffusion matrix $[S]_{HV}$ which relates the incident field with its scattered field [56]

$$\begin{bmatrix} \mathbf{E}_{sh_s} \\ \mathbf{E}_{sv_s} \end{bmatrix} = \frac{e^{-ikr}}{r} \begin{bmatrix} S_{h_s h_i} & S_{h_s v_i} \\ S_{s_s h_i} & S_{v_s v_i} \end{bmatrix} \begin{bmatrix} \mathbf{E}_{ih_i} \\ \mathbf{E}_{iv_i} \end{bmatrix} = [S]_{HV}\, \mathbf{E}^i \tag{3.2}$$

where $S_{h_s v_i}$ is a complex number proportional to the component $\widehat{\mathbf{h}}_s$ of scattered field in the direction $\widehat{K}_s$ such that a surface is illuminated by vertically polarized wave i.e.,

$$\mathbf{E}_{sh_s} = S_{h_s v_i} \mathbf{E}_{iv_i} \quad \text{with } \mathbf{E}_{ih_i} = 0.$$

The relation 3.2 makes sense for a given polarization. In this thesis we have chosen linear polarization. $\left(\widehat{\mathbf{v}}_i, \widehat{\mathbf{h}}_i\right)$ are the polarization basis for emitter and $\left(\widehat{\mathbf{v}}_s, \widehat{\mathbf{h}}_s\right)$ are the polarisation basis for receptor.

The bistatic scattering coefficient σ_{pq} can be expressed as a function of incident electric field $\mathbf{E}^i$ and scattered field $\mathbf{E}^s$, given by

$$\sigma_{pq} = \frac{4\pi r^2}{A} \frac{\left\langle E^s_{pq} E^{s*}_{pq} \right\rangle}{E^i_q E^{i*}_q} \tag{3.3}$$

where $\langle . \rangle$ denotes mathematical expectation and A is the illuminated area.

3.2 Models of diffusion scattered by a rough surface

Even though the scattering of electromagnetic waves from a randomly rough surface has been studied for many decades, no exact closed-form solutions have been obtained [58] because of the complexity of the problem. Instead, approximate models are available for a limited range of random surface parameters. We will briefly describe such approximate analytic models.

Two commonly used classical models are the KA [19]–[22] and SPM (or SPM1) [23]–[26]. The KA is applicable to the random surface of which the correlation length is larger than the incident wavelength and the rms height is small enough so that the average radius of curvature is larger than the incident wavelength [21]. The KA method employs the so called tangent plane approximation to apply the boundary conditions on the surface. Under the tangent plane approximation, the surface fields at any point of the surface are approximated by the fields that would be present on the tangent plane at that point. However, even with the tangent plane approximation, the scattered field in the Kirchhoff-approximated diffraction integral is still difficult to solve analytically. Therefore, additional assumptions are required to obtain an analytical solution. A commonly used approximation is to expand the integrand of the diffraction integral in terms of the surface slope, keeping only the lower order terms. This additional approximation provides the physical optics (PO) model, which is valid when the surface rms slope is small relative to the wavelength. In the high frequency, the geometrical optics (GO) model can be obtained using the methods of stationary-phase. The GO model is independent of the frequency, and is valid when the rms height is large relative to the wavelength [21, 59, 60]. On the other hand SPM can be used for random surface of which the surface rms height is much smaller than the wavelength and the surface rms slope is relatively small. In SPM, the surface field is expanded in a perturbation series to solve for the scattered field from a random surface [21, 61].

In the following we will first review the KA and then study the SPM.

3.2.1 Kirchhoff Approximation

The Kirchhoff approximation approximates the surface fields using the tangent plane approximation. Using the tangent plan approximation, the fields at any point on the surface are approximated by the fields that would be present on the tangent plane at that point. For that to be valid, it is required that every point on the surface has a large radius of curvature relative to the wavelength of the incident field. In our case the approach will be effective for areas dominated by the gravity waves.

We will start by taking a review of the general principle of this method, then we will establish an expression of the scattering matrix for different configurations (backscattering, forward scattering and bistatic scattering).

Basic scattering formulation

The vector formulation of the Kirchhoff method [22] is based upon the vector second Green's theorem, which states that the scattered field at any point within a source free region bounded by a closed surface can be expressed in terms of the tangential fields on the surface. A mathematical statement of this fact formulated by Stratton and Chu [46] and modified for the far zone by Silver is as follows [62]

$$\mathbf{E}^s = -jk\frac{e^{-jkR_r}}{4\pi R_r}\widehat{\mathbf{n}}_s \wedge \int \left[\widehat{\mathbf{n}} \wedge \mathbf{E} - \eta \widehat{\mathbf{n}}_s \wedge (\widehat{\mathbf{n}} \wedge \mathbf{H})\right] e^{jk\mathbf{R}.\widehat{\mathbf{n}}_s} ds \tag{3.4}$$

where

$\widehat{\mathbf{n}}_s$	:	unit vector in the scattered direction,
$\widehat{\mathbf{n}}$	:	unit vector normal to the surface,
η_s	=	$\sqrt{\mu/\varepsilon}$: intrinsic impedance of the medium,
R_r	:	distance from the center of the illuminated area to the point of observation,
$\mathbf{E}$	:	total electric field,
$\mathbf{H}$	:	total magnetic field.

To calculate the scattered field we have to evaluate the quantities $\widehat{\mathbf{n}} \wedge \mathbf{E}$ and $\widehat{\mathbf{n}} \wedge \mathbf{H}$ But generally, these quantities are difficult to evaluate, therefore it is necessary to make simplifying assumptions. By adopting a surface whose radius of curvature is greater than the incident electrogenic wavelength, we can assimilate the profile of the surface to an infinite plane tangent to the surface. Under these conditions, the laws of Snell-Descartes can be applied. Then, the tangential field components can be written as a function of Fresnel coefficients [63].

In the following, we will specify the local geometry adopted for this method, then we will give the details of mathematical calculations, which comes back to to find the analytical expression of the diffusion matrix.

Local Geometry

The incident field $\mathbf{E}^i$ is taken parallel to the polarization vector $\mathbf{a}$ (either equal to $\mathbf{h}$, vector in the plane perpendicular to the incident plane or $\mathbf{v}$,vector contains the incident plane) be the incident field defined by the expression, it can be written in the form

$$\mathbf{E}^i = \mathbf{a}e^{-jK(\widehat{\mathbf{n}}_i.\mathbf{R})} \tag{3.5}$$

where $\widehat{\mathbf{n}}_i$ is the unit vector in the direction of incident field and K is the wave number.

Figure 3.2 illustrate the local reference plane at a point of the scattered surface.

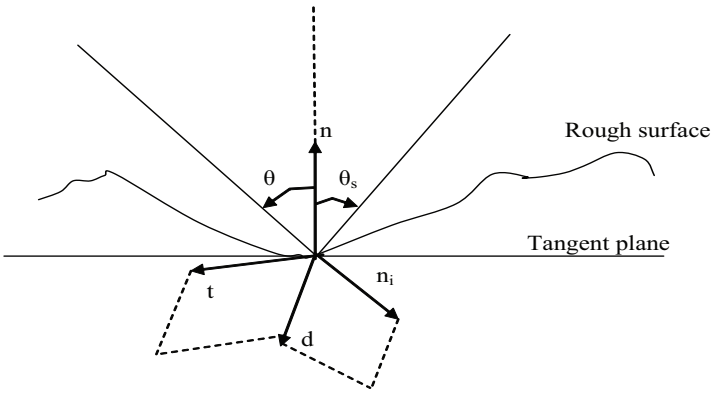

Figure 3.2: Local geometry of the scattering problem

The local reference expresses itself according to the orientation of the incident ray $\widehat{\mathbf{n}}_i$ and of local normal $\widehat{\mathbf{n}}$ to the surface

$$\begin{cases} \mathbf{t} = \frac{\widehat{\mathbf{n}}_i \wedge \widehat{\mathbf{n}}}{\|\widehat{\mathbf{n}}_i \wedge \widehat{\mathbf{n}}\|} \\ \mathbf{d} = \widehat{\mathbf{n}}_i \wedge \mathbf{t} \end{cases} \tag{3.6}$$

Under the approximation of tangent plane, the scattered field by the surface is the sum of incident field and the reflected field by the infinite tangent plane, at the surface of considered point. with these conditions the tangential components of electric and magnetic fields are given by

$$\begin{cases} \widehat{\mathbf{n}} \wedge \mathbf{E} = E_0 \left[(1 + R_h) (\mathbf{a}.\mathbf{t}) (\widehat{\mathbf{n}} \wedge \mathbf{t}) - (1 - R_v) (\widehat{\mathbf{n}}.\widehat{\mathbf{n}}_i) (\mathbf{a}.\mathbf{d}) \mathbf{t} \right] e^{-jk(\widehat{\mathbf{n}}_i.\mathbf{R})} \\ \eta (\widehat{\mathbf{n}} \wedge \mathbf{H}) = -E_0 \left[(1 - R_h) (\mathbf{a}.\mathbf{t}) (\widehat{\mathbf{n}}.\widehat{\mathbf{n}}_i) \mathbf{t} + (1 + R_v) (\widehat{\mathbf{n}} \wedge \mathbf{t}) (\mathbf{a}.\mathbf{d}) \mathbf{t} \right] e^{-jk(\widehat{\mathbf{n}}_i.\mathbf{R})} \end{cases} \tag{3.7}$$

where R_h and R_v represent the Fresnel coefficients of reflection in horizontal and vertical polarization.They are expressed as a function of local incident angle

$$\begin{cases} R_h = \frac{\cos\theta_l - \sqrt{\varepsilon_r - \sin^2\theta_l}}{\cos\theta_l + \sqrt{\varepsilon_r - \sin^2\theta_l}} \\ R_v = \frac{\varepsilon_r\cos\theta_l - \sqrt{\varepsilon_r - \sin^2\theta_l}}{\varepsilon_r\cos\theta_l + \sqrt{\varepsilon_r - \sin^2\theta_l}} \end{cases} \tag{3.8}$$

Analytical Expression

By using the relation (3.4) and (3.7) the scattered field by the surface enlightened by an incident wave is written as

$$\mathbf{E}^s = -jk\frac{e^{-jkR_r}}{4\pi R_r}\widehat{\mathbf{n}}_s \wedge \int \left[\widehat{\mathbf{n}} \wedge \mathbf{E} - \eta\widehat{\mathbf{n}}_s \wedge (\widehat{\mathbf{n}} \wedge \mathbf{H})\right] e^{jk\overline{r}(\widehat{\mathbf{n}}_s - \widehat{\mathbf{n}}_i)} ds \tag{3.9}$$

Even with the approximation of tangent plane, equation (3.9) contains a complex vectorial integral which necessitates the other approximations to manage this problem. The mostly used approximation is called the stationary phase or the geometric optics approximation. According to this approximation the points which contribute in the scattering are are the specular points, i,e,. the points where the specular reflection is produced between the direction of incident wave and the direction of scattered wave. These are the points where the vector is normal to the surface. Mathematically if we take Q having the phase

$$Q = k\left(\mathbf{R}.\left(\widehat{\mathbf{n}}_s - \widehat{\mathbf{n}}_i\right)\right) = q_x x' + q_y y' + q_z z' \tag{3.10}$$

$\mathbf{R} = [x',\ y',\ z']$ is the coordinates of the point of scattered surface, and

$$\begin{cases} q_x = K\left(\sin\theta_s\cos\varphi_s - \sin\theta\cos\varphi\right) \\ q_y = K\left(\sin\theta_s\sin\varphi_s - \sin\theta\sin\varphi\right) \\ q_z = K\left(\cos\theta_s + \cos\theta\right) \end{cases} \tag{3.11}$$

The stationary condition is verified if we have

$$\begin{cases} \frac{\partial Q}{\partial x'} = 0 = q_x + q_z\frac{\partial z'}{\partial x'} = q_x + q_z Z_x \\ \frac{\partial Q}{\partial y'} = 0 = q_y + q_z\frac{\partial z'}{\partial y'} = q_y + q_z Z_y \end{cases} \tag{3.12}$$

where Z_x and Z_y designates the slopes of the surface following the directions x and y.

This hypothesis of stationarity simplify the evaluation of $\widehat{\mathbf{n}} \wedge \mathbf{E}$ and $\widehat{\mathbf{n}} \wedge \mathbf{H}$ given in equation (3.9). In fact by considering the points uniquely for which the phase is stationary, the unitary vectors $\widehat{\mathbf{n}}$, $\mathbf{t}$, and $\mathbf{d}$ become independent of $\mathbf{R}$ and can be expressed in the form

$$\begin{cases} \widehat{\mathbf{n}} = \frac{k|q_z|}{q^2 q_z D}\left(\widehat{\mathbf{n}}_i - \widehat{\mathbf{n}}_s\right) \\ \mathbf{t} = \frac{|q_z|}{q_z D}\left(\widehat{\mathbf{n}}_i \wedge \widehat{\mathbf{n}}_s\right) \\ \mathbf{d} = \frac{|q_z|}{q_z D}\left(\left(\widehat{\mathbf{n}}_i.\widehat{\mathbf{n}}_s\right)\widehat{\mathbf{n}}_i - \widehat{\mathbf{n}}_s\right) \end{cases} \tag{3.13}$$

with $q^2 = q_x^2 + q_y^2 + q_z^2 = 2k^2\left(1 - \widehat{\mathbf{n}}_i.\widehat{\mathbf{n}}_s\right)$, and $D = \sqrt{\left(\widehat{\mathbf{n}}_i.\mathbf{v}_s\right)^2 + \left(\widehat{\mathbf{n}}_i.\mathbf{h}_s\right)^2}$. This permits to write

$$\mathbf{E}^s = -jk\frac{e^{-jkR_r}}{4\pi R_r}\widehat{\mathbf{n}}_s \wedge \left\{\widehat{\mathbf{n}} \wedge \mathbf{E} - \eta\widehat{\mathbf{n}}_s \wedge \left(\widehat{\mathbf{n}} \wedge \mathbf{H}\right)\right\} \int e^{jQ} ds \tag{3.14}$$

by using the equations (3.7), (3.13) and (3.14) the scattered field written in simplified form as

$$E_{pq}^s = kIE_0U_{pq} \tag{3.15}$$

with $I = \iint \exp\left(jq_x x' + jq_y y' + jq_z z' z\left(x',\ y'\right)\right) dx'dy'$, and U_{pq} are the polarization terms.

The field E_{pq}^s correspond to scattered field by the surface for the state of polarization q ($\mathbf{h}_i$ or $\mathbf{v}_i$) at the emission and p ($\mathbf{h}_s$ or $\mathbf{v}_s$) at reception. After (3.12), it is possible to calculate the scattering coefficients σ_{pq}^s. We have

$$\sigma_{pq}^s = \frac{4\pi R_r^2}{A_0}\frac{\left\langle E_{pq}^s E_{pq}^{s*}\right\rangle}{E_{pq}^i E_{pq}^{i*}} \tag{3.16}$$

Also the calculation of mathematical expectation $\left\langle E_{pq}^s E_{pq}^{s*}\right\rangle$ permit us to determine the coefficients of diffusion in bistatic case. These coefficients are given in the form

$$\sigma_{pq}^s = \frac{\pi k^2 q^2}{q_z^4}\left|U_{pq}\right|^2 \Pr\left(Z_x, Z_y\right) \tag{3.17}$$

where Pr is the probability density of slopes for which the phase is stationary.

Backscattering

The backscattering or monostatic case corresponds to an incident angle equal to observation angle ($\theta_i = \theta_s$) and the azimuth difference between incident and observed is π ($\varphi_s = \varphi_i + \pi$). The coefficients of polarizations then become

$$\begin{cases} U_{hh} = 2R_h \\ U_{hv} = 0 \\ U_{vh} = 0 \\ U_{vv} = 2R_v \end{cases} \tag{3.18}$$

The equations (3.17) and (3.18) permits us to deduce the scattering monostatic coefficients as

$$\begin{cases} \sigma_{hh} = \frac{\pi}{\cos^4\theta}\left|R_v\right|^2 \Pr\left(\tan\theta, 0\right) = \sigma_{vv} \\ \sigma_{vh} = \sigma_{hv} = 0 \end{cases} \tag{3.19}$$

In Fig. 3.3 we have traced the backscattering coefficients in vertical σ_{vv} (a) and horizontal σ_{hh} (b) polarization as a function of observation angle for three different roughness levels of gaussian surfaces.

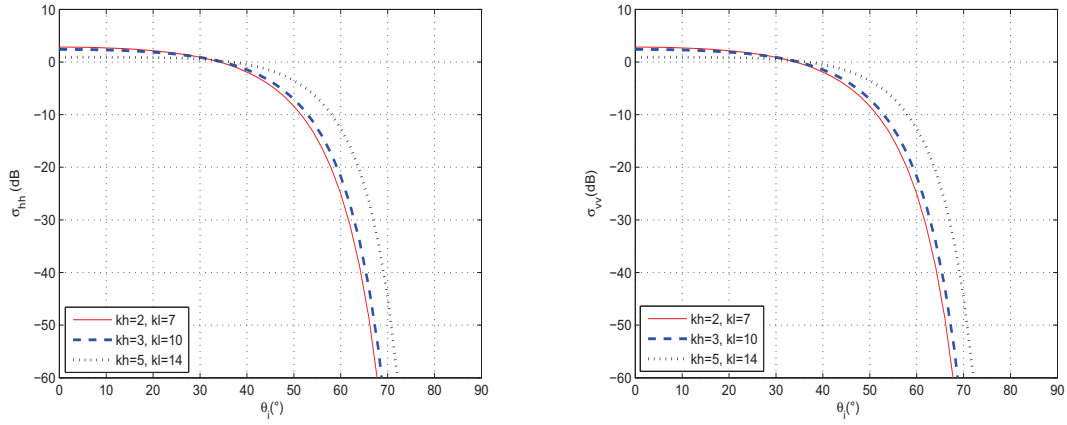

(a)horizontal polarization (b)vertical polarization

Figure 3.3: Coefficients of backscattering using KA-GO for three types of gaussian surfaces with different roughness levels

Forward scattering

The forward scattering differs from monostatic scattering in azimuth angle, in fact we have $(\varphi_s = \varphi_i)$ and $(\theta_s = \theta_i)$ which gives

$$\begin{cases} U_{hh} = -2R_h \cos\theta \\ U_{hv} = 0 \\ U_{vh} = 0 \\ U_{vv} = 2R_v \cos\theta \end{cases} \tag{3.20}$$

and deduce the coefficients of diffusion as

$$\begin{cases} \sigma_{hh} = \pi \left|R_h\right|^2 \Pr\left(0,0\right) \\ \sigma_{vv} = \pi \left|R_v\right|^2 \Pr\left(0,0\right) \\ \sigma_{vh} = \sigma_{hv} = 0 \end{cases} \tag{3.21}$$

3.2.2 Small Perturbation Method

The scattering of electromagnetic waves from a slightly rough surface can be studied using SPM. It is assume that the surface variations are much smaller than the incident wavelength and the slopes of the rough surface are relatively small. This method has been studied and applied extensively to problems in optics, remote sensing, and propagation and yields the Bragg scatter phenomenon of rough-surface scattering when only first-order terms are considered.

Two approaches are generally used to derive the expression for scattered field. The classical approach is named as the Rayleigh-Rice method [24]. In this method, the scattered field is represented as a superposition of outgoing waves and assumed that this representation is valid arbitrarily close to the rough surface (Rayleigh hypothesis). The field amplitudes are then determined from the boundary conditions and the divergence relations. The second method is Extended Boundary Condition (EBC) method, [64, 65]which uses the the Extinction Theorem [25, 44, 66] to solve the surface currents on the rough surface.The scattered fields can then be calculated from the diffraction integral by making use of the calculated surface fields.

The relationship between the Rayleigh method and extinction theorem (EBC method) for the solution of the problem of scattering from a rough surface are investigated in detailby Toigo [67]. Both of the forms of perturbation theory lead to identical results [68] for the scattered field because the expansions of amplitudes of the scattered fields are unique within their circle of convergence. We have used the second method to study the scattering effects by SPM and derive the results up to second order.

This formulation also permits us the evaluation of depolarization, which is a second order effect in the plane of incidence. The depolarization of electromagnetic waves by slightly rough surface using Rice's theory is investigated by Valenzuela [15], where he inferred that depolarization from slightly rough surface is due to multiple scattering because the expression for the depolarized scattered power he obtained is of the form obtained in multiple scattering investigations.

Electromagnetic Wave Scattering by a Dielectric Rough Surface

Consider a plane electromagnetic wave $\mathbf{E^i}$

$$\mathbf{E}^i = \widehat{\mathbf{e}}_\mathbf{i} \exp\left(i\mathbf{k_i}.\mathbf{r} - ik_{iz}z\right) \tag{3.22}$$

incident upon a dielectric rough surface S. Let ε and ε_1 denote the permittivity of the upper and lower half space respectively. In (3.22), $k_{ix} = k\sin\theta_i\cos\varphi_i$, $k_{iy} = k\sin\theta_i\sin\varphi_i$, and $k_{iz} = k\cos\theta_i$. We also have $k_{i\rho} = k\sin\theta_i$. The rough surface is characterized by a random height function $z = f(x,y)$, where $f(x,y)$ is a random function with zero mean $\langle f(x,y)\rangle = 0$ (Fig.3.4). From Huygens' principle and the extinction theorem (2.46) for the field $\mathbf{E}(\mathbf{R})$ in region 0 and the transmitted field

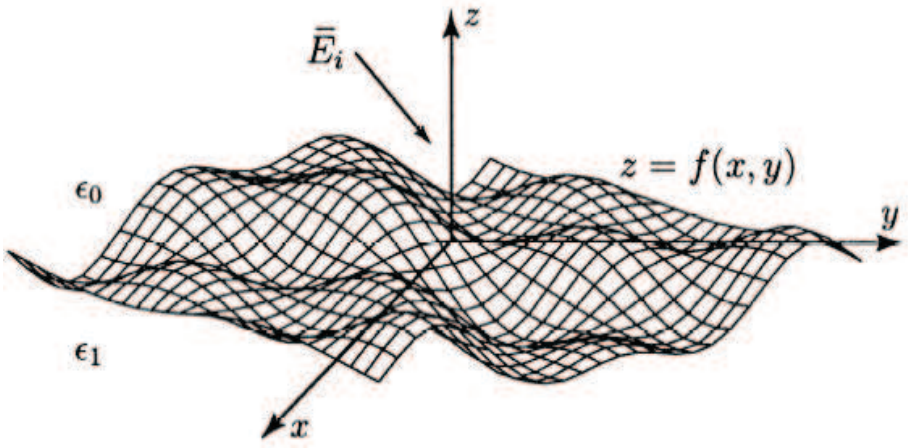

Figure 3.4: Electromagnetic scattering by a 2-D dielectric surface.

$\mathbf{E}_1(\mathbf{R})$ in the dielectric medium, we obtain [69]

$$\begin{aligned} & \mathbf{E}^i(\mathbf{R}) + \int_{S_d} \{i\omega\mu_0 G(\mathbf{R}, \mathbf{R}_d) \cdot [\hat{\mathbf{n}} \times \mathbf{H}(\mathbf{R}_d)] + \nabla \times G(\mathbf{R}, \mathbf{R}_d) \cdot [\hat{\mathbf{n}} \times \mathbf{E}(\mathbf{R}_d)]\} \, dS_d \\ = & \begin{cases} \mathbf{E}(\mathbf{R}) & z > f(\mathbf{r}) \\ 0, & z < f(\mathbf{r}) \end{cases} \end{aligned} \tag{3.23}$$

$$\begin{aligned} & \int_{S_d} \{i\omega\mu_1 G_1(\mathbf{R}, \mathbf{R}_d) \cdot [\hat{\mathbf{n}}_d \times \mathbf{H}_1(\mathbf{R}_d)] + \nabla \times G_1(\mathbf{R}, \mathbf{R}_d) \cdot [\hat{\mathbf{n}}_d \times \mathbf{E}_1(\mathbf{R}_d)]\} \, dS_d \\ = & \begin{cases} 0 & z > f(\mathbf{r}) \\ \mathbf{E}(\mathbf{R}), & z < f(\mathbf{r}) \end{cases} \end{aligned} \tag{3.24}$$

where S_d denotes the rough surface in which the surface integration is to be carried out, $\hat{\mathbf{n}}$ and $\hat{\mathbf{n}}_d$ are the unit vectors normal to the rough surface and pointing into the free space and the dielectric medium, respectively, and G and G_1 are the respective dyadic Green's functions for free space and the homogeneous dielectric of region 1.

Since tangential electric and magnetic fields are continuous, for $z_d = f(x_d, y_d)$ we can define surface field unknowns as follows

$$dS_d \eta \hat{\mathbf{n}} \times \mathbf{H}(\mathbf{R}_d) = d\mathbf{R}_d \mathbf{a}(\mathbf{r}_d) = dS_d \eta \hat{\mathbf{n}} \times \mathbf{H}_1(\mathbf{R}_d) \tag{3.25}$$

$$dS_d \hat{\mathbf{n}} \times \mathbf{E}(\mathbf{R}_d) = d\mathbf{r}_d \mathbf{b}(\mathbf{r}_d) = dS_d \hat{\mathbf{n}} \times \mathbf{E}_1(\mathbf{R}_d) \tag{3.26}$$

Next we make use of the integral representation of dyadic Green's function. For $z <$

$f(\mathbf{r}_d)$ we have [69, 70]

$$\begin{aligned} G(\mathbf{R},\mathbf{R}_d) &= \frac{i}{8\pi^2}\int d\mathbf{k} e^{i\mathbf{k}.\mathbf{r}-ik_z z}e^{-i\mathbf{k}.\mathbf{r}_d+ik_z f(\mathbf{r}_d)} \\ &\quad .\frac{1}{k_z}\left[\widehat{e}(-k_z)\widehat{e}(-k_z)+\widehat{h}(-k_z)\widehat{h}(-k_z)\right] \end{aligned} \tag{3.27}$$

$$\begin{aligned} \nabla\times G(\mathbf{R},\mathbf{R}_d) &= \frac{-1}{8\pi^2}\int d\mathbf{k} e^{i\mathbf{k}.\mathbf{r}-ik_z z}e^{-i\mathbf{k}.\mathbf{r}_d+ik_z f(\mathbf{r}_d)} \\ &\quad .\frac{K}{k_z}\left[-\widehat{h}(-k_z)\widehat{e}(-k_z)+\widehat{e}(-k_z)\widehat{h}(-k_z)\right] \end{aligned} \tag{3.28}$$

on the other hand, for $z > f(\mathbf{r}_d)$ we obtain

$$\begin{aligned} G_1(\mathbf{R},\mathbf{R}_d) &= \frac{i}{8\pi^2}\int d\mathbf{k} e^{i\mathbf{k}.\mathbf{r}+ik_{1z}z}e^{-i\mathbf{k}.\mathbf{r}_d-ik_{1z}f(\mathbf{r}_d)} \\ &\quad .\frac{1}{k_{1z}}\left[\widehat{e}_1(k_{1z})\widehat{e}_1(k_{1z})+\widehat{h}_1(k_{1z})\widehat{h}_1(k_{1z})\right] \end{aligned} \tag{3.29}$$

where

$$\begin{cases} K_1 = K\sqrt{\varepsilon_r\mu_r} \\ k_{1z} = K\sqrt{\varepsilon_r-(\sin\theta_s)^2} \end{cases} \tag{3.30}$$

(since $\mu_r = 1$ for sea surface so $K_1 = K\sqrt{\varepsilon_r}$) . Now

$$\begin{aligned} \nabla\times G_1(\mathbf{R},\mathbf{R}_d) &= \frac{-1}{8\pi^2}\int d\mathbf{k} e^{i\mathbf{k}.\mathbf{r}+ik_{1z}z}e^{-i\mathbf{k}.\mathbf{r}_d-ik_{1z}f(\mathbf{r}_d)} \\ &\quad .\frac{K_1}{k_{1z}}\left[-\widehat{h}(k_{1z})\widehat{e}_1(k_{1z})+\widehat{e}_1(k_{1z})\widehat{h}_1(k_{1z})\right] \end{aligned} \tag{3.31}$$

Substitute these into (3.23) and (3.24). Let $f_{\min}$ and $f_{\max}$ be, respectively, the minimum and maximum values of the surface profile $f(\mathbf{r}_d)$. Evaluating (3.23) for $x < f_{\min}$ and (3.24) for $x > f_{\max}$, we obtain the equations of the two extinction theorems [69, 71]

$$\begin{aligned} \mathbf{E}^i(\mathbf{R}) &= \frac{1}{8\pi^2}\int d\mathbf{k} e^{i\mathbf{k}.\mathbf{r}-ik_z z}\frac{K}{k_z}\int d\mathbf{r}_d e^{-i\mathbf{k}.\mathbf{r}_d+ik_z f(\mathbf{r}_d)} \\ &\quad .\Big(\left[\widehat{e}(-k_z)\widehat{e}(-k_z)+\widehat{h}(-k_z)\widehat{h}(-k_z)\right].\mathbf{a}(\mathbf{r}_d) \\ &\quad \left[-\widehat{h}(-k_z)\widehat{e}(-k_z)+\widehat{e}(-k_z)\widehat{h}(-k_z)\right].\mathbf{b}(\mathbf{r}_d)\Big) \end{aligned} \tag{3.32}$$

$$\begin{aligned} 0 &= \frac{1}{8\pi^2}\int d\mathbf{k} e^{i\mathbf{k}.\mathbf{r}+ik_{1z}z}\frac{K_1}{k_{1z}}\int d\mathbf{r}_d e^{-i\mathbf{k}.\mathbf{r}_d-ik_{1z}f(\mathbf{r}_d)} \\ &\quad .\Big(\frac{K}{K_1}\left[\widehat{e}_1(k_{1z})\widehat{e}_1(k_{1z})+\widehat{h}_1(k_{1z})\widehat{h}_1(k_{1z})\right].\mathbf{a}(\mathbf{r}_d) \\ &\quad \left[-\widehat{h}(k_{1z})\widehat{e}_1(k_{1z})+\widehat{e}_1(k_{1z})\widehat{h}_1(k_{1z})\right].\mathbf{b}(\mathbf{r}_d)\Big) \end{aligned} \tag{3.33}$$

The above equations are the extended boundary conditions and can be used to solve for the surface fields along with the following equations, which are results of (3.25) and

(3.26),

$$\widehat{\mathbf{n}}\left(\mathbf{r}_d\right).\mathbf{a}\left(\mathbf{r}_d\right) = 0 \tag{3.34}$$

$$\widehat{\mathbf{n}}\left(\mathbf{r}_d\right).\mathbf{b}\left(\mathbf{r}_d\right) = 0 \tag{3.35}$$

Since

$$\widehat{\mathbf{n}} = \frac{\left(-\frac{\partial f}{\partial x}\widehat{x} - \frac{\partial f}{\partial y}\widehat{y} + \frac{\partial f}{\partial z}\widehat{z}\right)}{\sqrt{1+\left(\frac{\partial f}{\partial x}\right)^2 + \left(\frac{\partial f}{\partial y}\right)^2}} \tag{3.36}$$

from (3.34) and (3.35) we have

$$a_z\left(\mathbf{r}_d\right) = \left(\widehat{x}\frac{\partial f\left(\mathbf{r}_d\right)}{\partial x_d} + \widehat{y}\frac{\partial f\left(\mathbf{r}_d\right)}{\partial y_d}\right).\mathbf{a}\left(\mathbf{r}_d\right) \tag{3.37}$$

$$b_z\left(\mathbf{r}_d\right) = \left(\widehat{x}\frac{\partial f\left(\mathbf{r}_d\right)}{\partial x_d} + \widehat{y}\frac{\partial f\left(\mathbf{r}_d\right)}{\partial y_d}\right).\mathbf{b}\left(\mathbf{r}_d\right) \tag{3.38}$$

with a_z, and b_z, as the z-components of $\mathbf{a}$ and $\mathbf{b}$, respectively.

Once the surface fields are obtained, the scattered field in region 0 and the transmitted field in medium 1 can be derived by using (3.23) and (3.24). The scattered fields and transmitted fields are calculated by evaluating (3.23) and (3.24) for $z > f_{\max}$ and $z < f_{\min}$, respectively. For $z > f\left(\mathbf{r}_d\right)$ [69, 71]

$$\begin{aligned} G\left(\mathbf{R},\mathbf{R}_d\right) &= \frac{i}{8\pi^2}\int d\mathbf{k} e^{i\mathbf{k}.\mathbf{r}+ik_z z}e^{-i\mathbf{k}.\mathbf{r}_d - ik_{1z}f(\mathbf{r}_d)} \\ &\quad .\frac{1}{k_z}\left[\widehat{e}\left(k_z\right)\widehat{e}\left(k_z\right)+\widehat{h}\left(k_z\right)\widehat{h}\left(k_z\right)\right] \end{aligned} \tag{3.39}$$

$$\begin{aligned} \nabla\times G\left(\mathbf{R},\mathbf{R}_d\right) &= \frac{-1}{8\pi^2}\int d\mathbf{k} e^{i\mathbf{k}.\mathbf{r}+ik_z z}e^{-i\mathbf{k}.\mathbf{r}_d - ik_{z}f(\mathbf{r}_d)} \\ &\quad .\frac{K}{k_z}\left[-\widehat{h}\left(k_z\right)\widehat{e}\left(k_z\right)+\widehat{e}\left(k_z\right)\widehat{h}\left(k_z\right)\right] \end{aligned} \tag{3.40}$$

$$\begin{aligned} \mathbf{E}^s\left(\mathbf{R}\right) &= \frac{-1}{8\pi^2}\int d\mathbf{k} e^{i\mathbf{k}.\mathbf{r}+ik_z z}\frac{K}{k_z}\int d\mathbf{r}_d e^{-i\mathbf{k}.\mathbf{r}_d - ik_z f(\mathbf{r}_d)} \\ &\quad .\left(\left[\widehat{e}\left(k_z\right)\widehat{e}\left(k_z\right)+\widehat{h}\left(k_z\right)\widehat{h}\left(k_z\right)\right].\mathbf{a}\left(\mathbf{r}_d\right).\right. \\ &\quad \left.+\left[-\widehat{h}\left(k_z\right)\widehat{e}\left(k_z\right)+\widehat{e}\left(k_z\right)\widehat{h}\left(k_z\right)\right].\mathbf{b}\left(\mathbf{r}_d\right)\right) \end{aligned} \tag{3.41}$$

We note that the expression for the scattered field is similar to that of the extinction theorem. The property can be exploited later on in simplifying the analysis. Similarly for transmitted fields, we have [71]

$$\begin{aligned} \mathbf{E}^t\left(\mathbf{R}\right) &= \frac{1}{8\pi^2}\int d\mathbf{k} e^{i\mathbf{k}.\mathbf{r}-ik_{1z}z}\frac{K_1}{k_{1z}}\int d\mathbf{r}_d e^{-i\mathbf{k}.\mathbf{r}_d + ik_{1z}f(\mathbf{r}_d)} \\ &\quad .\left(\frac{K}{K_1}\left[\widehat{e}_1\left(-k_{1z}\right)\widehat{e}_1\left(-k_{1z}\right)+\widehat{h}_1\left(-k_{1z}\right)\widehat{h}_1\left(-k_{1z}\right)\right].\mathbf{a}\left(\mathbf{r}_d\right)\right. \\ &\quad \left.+\left[-\widehat{h}\left(-k_{1z}\right)\widehat{e}_1\left(-k_{1z}\right)+\widehat{e}_1\left(-k_{1z}\right)\widehat{h}_1\left(-k_{1z}\right)\right]\mathbf{b}\left(\mathbf{r}_d\right)\right) \end{aligned} \tag{3.42}$$

The objective is to solve for the surface fields using (3.32), (3.33), (3.34) and (3.35) and then to solve for the scattered and transmitted fields using (3.41) and (3.42).

Equations (3.32) and (3.33) through (3.42) are exact. To solve for the surface fields, the perturbation method makes use of series expansions.Let

$$\mathbf{a}(\mathbf{r}_d) = \sum_{m=0}^{\infty} \mathbf{a}^{(m)}(\mathbf{r}_d) \tag{3.43}$$

$$\mathbf{b}(\mathbf{r}_d) = \sum_{m=0}^{\infty} \mathbf{b}^{(m)}(\mathbf{r}_d) \tag{3.44}$$

where superscript (m) denotes mth order solution. We also have

$$e^{\pm ik_z f(\mathbf{r}_d)} = \sum_{m=0}^{\infty} \frac{[\pm ik_z f(\mathbf{r}_d)]^m}{m\,!} \tag{3.45}$$

$$e^{\pm ik_{1z} f(\mathbf{r}_d)} = \sum_{m=0}^{\infty} \frac{[\pm ik_{1z} f(\mathbf{r}_d)]^m}{m\,!} \tag{3.46}$$

In SPM, $f(\mathbf{r}_d)$ and its derivatives are regarded as small parameters. Thus not only the rms heights are small but also the slopes have to be small. The expansions of (3.43), (3.44), (3.45) and (3.46) are substituted into (3.32) and (3.33) to obtain the set of equations for the different-order solutions. From (3.37), (3.38), (3.43) and (3.44) we obtain

$$a_z^{(0)}(\mathbf{r}_d) = b_z^{(0)}(\mathbf{r}_d) = 0 \tag{3.47}$$

$$a_z^{(m)}(\mathbf{r}_d) = \left(\widehat{x}\frac{\partial f(\mathbf{r}_d)}{\partial x_d} + \widehat{y}\frac{\partial f(\mathbf{r}_d)}{\partial y_d}\right).\mathbf{a}^{(m-1)}(\mathbf{r}_d) \tag{3.48}$$

$$b_z^{(m)}(\mathbf{r}_d) = \left(\widehat{x}\frac{\partial f(\mathbf{r}_d)}{\partial x_d} + \widehat{y}\frac{\partial f(\mathbf{r}_d)}{\partial y_d}\right).\mathbf{b}^{(m-1)}(\mathbf{r}_d) \tag{3.49}$$

The assumptions are

$$k_z f(\mathbf{r}_d),\ k_{1z} f(\mathbf{r}_d),\ \frac{\partial f}{\partial x_d},\ \frac{\partial f}{\partial y_d} \ll 1 \tag{3.50}$$

Note that the $\widehat{z}$ components of the surface fields are of a lower order than the horizontal components because of the small slope approximation. Substituting (3.43), (3.44), (3.45) and (3.46) into (3.32), (3.33) and (3.37) through (3.38) and equating the same-order terms, we can calculate the surface fields to the zeroth-order, the first-order, and so on. Then, from (3.41) and (3.42) the scattered fields can be obtained to different orders. In the following, we solve for the surface fields and scattered fields up to the second order. The zeroth-order solutions are just the reflected and transmitted fields of a flat surface. The first-order solution gives the lowest-order incoherent scattered intensities. However, the first-order solution does not give the depolarization effect in

the backscattering direction. The second-order solution gives the lowest-order correction to the coherent reflection and transmission coefficients. Also, the depolarization of the backscattered power is manifested.

We define Fourier transforms of surface fields, or surface fields in the spectral domain:

$$\mathbf{A}(\mathbf{k}) = \frac{1}{(2\pi)^2}\int d\mathbf{r}_d \mathbf{a}(\mathbf{r}_d)\, e^{-i\mathbf{k}.\mathbf{r}_d} \tag{3.51}$$

$$\mathbf{B}(\mathbf{k}) = \frac{1}{(2\pi)^2}\int d\mathbf{r}_d \mathbf{b}(\mathbf{r}_d)\, e^{-i\mathbf{k}.\mathbf{r}_d} \tag{3.52}$$

In spectral domain, (3.48) and (3.49) gives

$$\mathbf{a}_z(\mathbf{k}) = i\int_{-\infty}^{\infty} d\mathbf{k}_d (\mathbf{k}-\mathbf{k}_d).\mathbf{a}(\mathbf{k}) F(\mathbf{k}-\mathbf{k}_d) \tag{3.53}$$

$$\mathbf{b}_z(\mathbf{k}) = i\int_{-\infty}^{\infty} d\mathbf{k}_d (\mathbf{k}-\mathbf{k}_d).\mathbf{b}(\mathbf{k}) F(\mathbf{k}-\mathbf{k}_d) \tag{3.54}$$

Using the Fourier transform of the surface fields and expanding

$$e^{\pm ik_z f(\mathbf{r}_d)} = 1 \pm ik_z f(\mathbf{r}_d) - \frac{k_z^2}{2} f^2(\mathbf{r}_d)$$

in (3.32) and (3.33), we have, up to the second order [71],

$$\begin{aligned}\mathbf{E}^i(\mathbf{R}) = \frac{1}{2}\int d\mathbf{k} e^{i\mathbf{k}.\mathbf{r}+ik_z z}\frac{K}{k_z}.\Big(&\left[\widehat{e}(-k_z)\widehat{e}(-k_z)+\widehat{h}(-k_z)\widehat{h}(-k_z)\right]\\ &\left[\mathbf{A}(\mathbf{k})+ik_z\int d\mathbf{k}_d\mathbf{A}(\mathbf{k})F(\mathbf{k}-\mathbf{k}_d)-\frac{k_z^2}{2}\int d\mathbf{k}\mathbf{A}(\mathbf{k})F^{(2)}(\mathbf{k}-\mathbf{k}_d)\right]\\ &+\left[-\widehat{h}(-k_z)\widehat{e}(-k_z)+\widehat{e}(-k_z)\widehat{h}(-k_z)\right]\left[\mathbf{B}(\mathbf{k})+ik_z\int d\mathbf{k}_d\mathbf{B}(\mathbf{k})F(\mathbf{k}-\mathbf{k}_d)\right.\\ &\left.-\frac{k_z^2}{2}\int d\mathbf{k}\mathbf{B}(\mathbf{k})F^{(2)}(\mathbf{k}-\mathbf{k}_d)\right]\Big)\end{aligned} \tag{3.55}$$

The extinction theorem of (3.33) is [69, 71]

$$\begin{aligned}0 = \frac{1}{2}\int d\mathbf{k} e^{i\mathbf{k}.\mathbf{r}+ik_{1z}z}\frac{K_1}{k_{1z}}.\Big(&\frac{K}{K_1}\left[\widehat{e}_1(k_{1z})\widehat{e}_1(k_{1z})+\widehat{h}_1(k_{1z})\widehat{h}_1(k_{1z})\right]\\ &\left[\mathbf{A}(\mathbf{k})-ik_{1z}\int d\mathbf{k}_d\mathbf{A}(\mathbf{k}_d)F(\mathbf{k}-\mathbf{k}_d)-\frac{k_{1z}^2}{2}\int d\mathbf{k}_d\mathbf{A}(\mathbf{k}_d)F^{(2)}(\mathbf{k}-\mathbf{k}_d)\right]\\ &+\left[-\widehat{h}_1(k_{1z})\widehat{e}_1(k_{1z})+\widehat{e}_1(k_{1z})\widehat{h}_1(k_{1z})\right]\left[\mathbf{B}(\mathbf{k})-ik_{1z}\int d\mathbf{k}_d\mathbf{B}(\mathbf{k})F(\mathbf{k}-\mathbf{k}_d)\right.\\ &\left.-\frac{k_{1z}^2}{2}\int d\mathbf{k}_d\mathbf{B}(\mathbf{k})F^{(2)}(\mathbf{k}-\mathbf{k}_d)\right]\Big)\end{aligned} \tag{3.56}$$

Similarly, for the scattered field we have

$$\begin{aligned}\mathbf{E}^s(\mathbf{R}) &= \frac{-1}{2}\int d\mathbf{k}e^{i\mathbf{k}.\mathbf{r}+ik_z z}\frac{K}{k_z}\Big(\Big[\widehat{e}(k_z)\,\widehat{e}(k_z)+\widehat{h}(k_z)\,\widehat{h}(k_z)\Big] \\ &\Big[\mathbf{A}(\mathbf{k})-ik_z\int d\mathbf{k}_d\mathbf{A}(\mathbf{k}_d)F(\mathbf{k}-\mathbf{k}_d)-\frac{k_z^2}{2}\int d\mathbf{k}_d\mathbf{A}(\mathbf{k})F^{(2)}(\mathbf{k}-\mathbf{k}_d)\Big] \\ &+\Big[-\widehat{h}(k_z)\,\widehat{e}(k_z)+\widehat{e}(k_z)\,\widehat{h}(k_z)\Big]\Big[\mathbf{B}(\mathbf{k})-ik_z\int d\mathbf{k}_d\mathbf{B}(\mathbf{k}_d)F(\mathbf{k}-\mathbf{k}_d) \\ &-\frac{k_z^2}{2}\int d\mathbf{k}_d\mathbf{B}(\mathbf{k})F^{(2)}(\mathbf{k}-\mathbf{k}_d)\Big]\Big) \qquad (3.57)\end{aligned}$$

To solve the surface fields, it is convenient to define $\widehat{q}$ and $\widehat{p}$, which are the unit vectors that are parallel to the projections of $\widehat{e}$ and $\widehat{h}$ on the horizontal plane,

$$\widehat{q}(\mathbf{k})=\widehat{e}(-k_z)=\frac{\widehat{x}k_y-\widehat{y}k_x}{k_\rho} \qquad (3.58)$$

is the same as $\widehat{e}$, and

$$\widehat{p}(\mathbf{k})=\widehat{z}\times\widehat{q}(\mathbf{k})=\frac{\widehat{x}k_x+\widehat{y}k_y}{k_\rho}=\widehat{\mathbf{k}} \qquad (3.59)$$

is the projection of $\widehat{h}(-k_z)$ on the $x-y$ plane and is also the unit vector in the projection of $\mathbf{K}$ onto $x-y$ plane. We use two orthonormal systems ($\widehat{\mathbf{h}}$, $\widehat{\mathbf{e}}$, $\widehat{\mathbf{K}}$) and ($\widehat{\mathbf{z}}$, $\widehat{\mathbf{q}}$, $\widehat{\mathbf{p}}$), Let $\mathbf{k}=k_\rho\cos\varphi_k\widehat{x}+k_\rho\sin\varphi_k\widehat{y}$ and $\mathbf{k}_d=k_{d\rho}\cos\varphi_k\widehat{x}+k_{d\rho}\sin\varphi_k\widehat{y}$. Then

$$\widehat{h}(\pm k_z) = \mp\frac{k_z}{K}\widehat{p}(\mathbf{k})+\frac{k_\rho}{K}\widehat{z} \qquad (3.60)$$

$$\widehat{h}_1(\pm k_{1z}) = \mp\frac{k_{1z}}{K_1}\widehat{p}(\mathbf{k})+\frac{k_\rho}{K_1}\widehat{z} \qquad (3.61)$$

We decompose surface fields in the spectral domains into $\widehat{\mathbf{q}}$, $\widehat{\mathbf{p}}$ and $\widehat{\mathbf{z}}$ components

$$\mathbf{A}(\mathbf{k}) = A_q(\mathbf{k})\,\widehat{q}(\mathbf{k})+A_p(\mathbf{k})\,\widehat{p}(\mathbf{k})+A_z(\mathbf{k})\,\widehat{z} \qquad (3.62)$$

$$\mathbf{B}(\mathbf{k}) = B_q(\mathbf{k})\,\widehat{q}(\mathbf{k})+B_p(\mathbf{k})\,\widehat{p}(\mathbf{k})+B_z(\mathbf{k})\,\widehat{z} \qquad (3.63)$$

The $\widehat{z}$ components of surface fields, in terms of the horizontal components, using (3.51), are

$$A_z^{(m)}(\mathbf{k}) = i\int d\mathbf{k}_d F(\mathbf{k}-\mathbf{k}_d)(\mathbf{k}-\mathbf{k}_d).A^{(m-1)}(\mathbf{k}_d) \qquad (3.64)$$

$$B_z^{(m)}(\mathbf{k}) = i\int d\mathbf{k}_d F(\mathbf{k}-\mathbf{k}_d)(\mathbf{k}-\mathbf{k}_d).B^{(m-1)}(\mathbf{k}_d) \qquad (3.65)$$

After expanding $exp(ik_zf)$ and the $exp(-ik_zf)$ to the second order in f respectively, in (3.32) and (3.33) and doing some calculations we get [69, 71]

$$\begin{aligned}\widehat{e}_i\delta\left(\mathbf{k}-\mathbf{k_i}\right) &= \frac{1}{2}\frac{K}{k_z}.\Big(\Big[\widehat{e}\left(-k_z\right)\widehat{e}\left(-k_z\right)+\widehat{h}\left(-k_z\right)\widehat{h}\left(-k_z\right)\Big]\\ &\quad\Big[\mathbf{A}\left(\mathbf{k}\right)+ik_z\int d\mathbf{k}_d\mathbf{A}\left(\mathbf{k}\right)F\left(\mathbf{k}-\mathbf{k}_d\right)\\ &\quad-\frac{k_z^2}{2}\int d\mathbf{k}_d\mathbf{A}\left(\mathbf{k}\right)F^{(2)}\left(\mathbf{k}-\mathbf{k}_d\right)\Big]\\ &\quad+\frac{1}{2}\frac{K}{k_z}\Big[-\widehat{h}\left(-k_z\right)\widehat{e}\left(-k_z\right)+\widehat{e}\left(-k_z\right)\widehat{h}\left(-k_z\right)\Big].\\ &\quad\Big[\mathbf{B}\left(\mathbf{k}\right)+ik_z\int d\mathbf{k}_d\mathbf{B}\left(\mathbf{k}\right)F\left(\mathbf{k}-\mathbf{k}_d\right)\\ &\quad-\frac{k_z^2}{2}\int d\mathbf{k}_d\mathbf{B}\left(\mathbf{k}\right)F^{(2)}\left(\mathbf{k}-\mathbf{k}_d\right)\Big]\Big)\end{aligned} \tag{3.66}$$

$$\begin{aligned}0 &= \frac{1}{2}\frac{K}{k_{1z}}.\Big(\Big[\widehat{e}_1\left(k_{1z}\right)\widehat{e}_1\left(k_{1z}\right)+\widehat{h}_1\left(k_{1z}\right)\widehat{h}_1\left(k_{1z}\right)\Big]\\ &\quad\Big[\mathbf{A}\left(\mathbf{k}\right)-ik_{1z}\int d\mathbf{k}_d\mathbf{A}\left(\mathbf{k}_d\right)F\left(\mathbf{k}-\mathbf{k}_d\right)\\ &\quad-\frac{k_{1z}^2}{2}\int d\mathbf{k}_d\mathbf{A}\left(\mathbf{k}_d\right)F^{(2)}\left(\mathbf{k}-\mathbf{k}_d\right)\Big]\\ &\quad+\frac{1}{2}\frac{K_1}{k_{1z}}\Big[-\widehat{h}_1\left(k_{1z}\right)\widehat{e}_1\left(k_{1z}\right)+\widehat{e}_1\left(k_{1z}\right)\widehat{h}_1\left(k_{1z}\right)\Big]\\ &\quad.\Big[\mathbf{B}\left(\mathbf{k}\right)-ik_{1z}\int d\mathbf{k}_d\mathbf{B}\left(\mathbf{k}_d\right)F\left(\mathbf{k}-\mathbf{k}_d\right)\\ &\quad-\frac{k_{1z}^2}{2}\int d\mathbf{k}_d\mathbf{B}\left(\mathbf{k}\right)F^{(2)}\left(\mathbf{k}-\mathbf{k}_d\right)\Big]\Big)\end{aligned} \tag{3.67}$$

where the Fourier transforms of the height function and the products of height functions are defined as

$$\frac{1}{\left(2\pi\right)^2}\int d\mathbf{r}e^{-i\mathbf{k}.\mathbf{r}}f\left(\mathbf{r}\right) = F\left(\mathbf{k}\right) \tag{3.68}$$

$$\frac{1}{\left(2\pi\right)^2}\int d\mathbf{r}e^{-i\mathbf{k}.\mathbf{r}}f^{(2)}\left(\mathbf{r}\right) = F^{(2)}\left(\mathbf{k}\right) \tag{3.69}$$

$$\int_{-\infty}^{\infty} d\mathbf{k}_d F\left(\mathbf{k}_d\right)F\left(\mathbf{k}-\mathbf{k}_d\right) = F^{(2)}\left(\mathbf{k}\right) \tag{3.70}$$

Equations (3.66) and (3.67) can be solved up to second order. Again note that here we only summarize the first- and second-order results and refer readers to [71] for the detailed derivation.

First-Order Solutions

The first-order bistatic scattering coefficients are given by eq. (1.2.56) from [71]. These expressions are given in Appendix A. By using the transformations (2.19) & (3.30) we simplify these coefficient and polarization dependent terms and write them in more

comprehensible form. In simplified form the bistatic scattering coefficient and polarization dependent terms are given by

$$\sigma_{pq} = 16\pi \left| k^2 \cos\theta_i \cos\theta_s \alpha_{pq}^{(1)} \right|^2 W\left(k_{sx} - k_{ix}, k_{sy} - k_{ix}\right)$$

where $\alpha_{pq}^{(1)}$ are polarization dependent terms defined as

$$\begin{aligned}
\alpha_{hh}^{(1)} &= \frac{(\varepsilon_r - 1)\cos(\varphi_s - \varphi_i)}{\left(\cos\theta_s + \sqrt{\varepsilon_r - \sin^2\theta_s}\right)\left(\cos\theta_i + \sqrt{\varepsilon_r - \sin^2\theta_i}\right)} \\
\alpha_{hv}^{(1)} &= \frac{(\varepsilon_r - 1)\sqrt{\varepsilon_r - \sin^2\theta_i}\sin(\varphi_s - \varphi_i)}{\left(\cos\theta_s + \sqrt{\varepsilon_r - \sin^2\theta_s}\right)\left(\varepsilon_r\cos\theta_i + \sqrt{\varepsilon_r - \sin^2\theta_i}\right)} \\
\alpha_{vh}^{(1)} &= \frac{(\varepsilon_r - 1)\sqrt{\varepsilon_r - \sin^2\theta_s}\sin(\varphi_s - \varphi_i)}{\left(\varepsilon_r\cos\theta_s + \sqrt{\varepsilon_r - \sin^2\theta_s}\right)\left(\cos\theta_i + \sqrt{\varepsilon_r - \sin^2\theta_i}\right)} \\
\alpha_{vv}^{(1)} &= \frac{(\varepsilon_r - 1)\left\{\sqrt{\varepsilon_r - \sin^2\theta_s}\sqrt{\varepsilon_r - \sin^2\theta_i}\cos(\varphi_s - \varphi_i) - \varepsilon_r \sin\theta_i \sin\theta_s\right\}}{\left(\varepsilon_r\cos\theta_s + \sqrt{\varepsilon_r - \sin^2\theta_s}\right).\left(\varepsilon_r\cos\theta_i + \sqrt{\varepsilon_r - \sin^2\theta_i}\right)}
\end{aligned}$$

Backscattering Backscattering is a particular case for which:

$$\theta_s = \theta_i,\ \varphi_s = \pi + \varphi_i \text{ and } \mathbf{k}_s = -\mathbf{k}_i$$

For $\theta_s = \theta_i$, $\varphi_s = \pi$ so $\varphi_i = 0$, the backscattering coefficients are given by the expression

$$\sigma_{pq} = 16\pi k^4 \cos^4\theta_i \left|\alpha_{pq}^{(1)}\right|^2 W(-2\mathbf{k}_i) \tag{3.71}$$

where

$$\begin{aligned}
\alpha_{hh}^{(1)} &= -(\varepsilon_r - 1)\left(\cos\theta_i + \sqrt{\varepsilon_r - \sin^2\theta_i}\right)^{-2} && (3.72)\\
\alpha_{hv}^{(1)} &= 0 && (3.73)\\
\alpha_{vh}^{(1)} &= 0 && (3.74)\\
\alpha_{vv}^{(1)} &= (\varepsilon_r - 1)\left\{\sin^2\theta_i - \varepsilon_r\left(1 + \sin^2\theta_i\right)\right\}\left(\varepsilon_r\cos\theta_i + \sqrt{\varepsilon_r - \sin^2\theta_i}\right)^{-2} && (3.75)
\end{aligned}$$

Second-Order Solutions

The second-order bistatic scattering coefficients are obtained from (1.3.64) [71]and written in the Appendix A. Again by using the transformations (2.19),(3.30) & (A.12) and with a small change of notation we simplify them and write them in more comprehensible form. The second order bistatic scattering coefficients are given by

$$\sigma_{pq}^{(2)} = 4\pi K^4 \cos^2\theta_s \int_0^{2\pi}\int_0^{\pi/2} \sin\theta_d \cos\theta_d d\theta_d d\varphi_d W(\mathbf{k}_s - \mathbf{k}_d) W(\mathbf{k}_d - \mathbf{k}_i) .\alpha_{pq}^{(2)} \left[\alpha_{pq}^{(2)*} + \beta_{pq}^{(2)*}\right] \quad (3.76)$$

where the simplified polarization dependent terms $\alpha_{pq}^{(2)}$ and $\beta_{pq}^{(2)}$ are obtained form (A.29)-(A.36).

Backscattering In backscattering configuration these results become

$$\sigma_{pq}^{(2)} = 4\pi K^4 \cos^2\theta_s \int_0^{2\pi}\int_0^{\pi/2} \sin\theta_d \cos\theta_d d\theta_d d\varphi_d W(\mathbf{k}_i - \mathbf{k}_d) W(\mathbf{k}_d - \mathbf{k}_i) .\alpha_{pq}^{(2)} \left[\alpha_{pq}^{(2)*} + \beta_{pq}^{(2)*}\right] \quad (3.77)$$

where the polarization dependent terms become

Backscattering : Again in case of back scattering they become

$$\alpha_{hh}^{(2)} = \frac{\varepsilon_r - 1}{\left(\cos\theta_i + \sqrt{\varepsilon_r - \sin^2\theta_i}\right)^2} \left[-2\sqrt{\varepsilon_r - \sin^2\theta_i} + 2(\varepsilon_r - 1) \left\{\frac{\sin^2\phi \cos\theta \sqrt{\varepsilon_r - \sin^2\theta}}{\varepsilon_r \cos\theta + \sqrt{\varepsilon_r - \sin^2\theta}} + \frac{\cos^2\phi}{\cos\theta + \sqrt{\varepsilon_r - \sin^2\theta}}\right\}\right] \quad (3.78)$$

$$\beta_{hh}^{(2)} = \frac{\varepsilon_r - 1}{\left(\cos\theta_i + \sqrt{\varepsilon_r - \sin^2\theta_i}\right)^2} \left[-2\sqrt{\varepsilon_r - \sin^2\theta_i} + 2(\varepsilon_r - 1) \left\{\sin^2\phi_1 \frac{(2\cos\theta_i - \cos\theta)\sqrt{\varepsilon_r - \sin^2\theta}}{\varepsilon_r (2\cos\theta_i - \cos\theta) + \sqrt{\varepsilon_r - \sin^2\theta}} + \frac{\cos^2\phi_1}{(2\cos\theta_i - \cos\theta) + \sqrt{\varepsilon_r - \sin^2\theta}}\right\}\right] \quad (3.79)$$

$$\alpha_{hv}^{(2)} = \frac{-(2\varepsilon_r - 1)}{\left(\cos\theta_i + \sqrt{\varepsilon_r - \sin^2\theta_i}\right)\left(\varepsilon_r \cos\theta_i + \sqrt{\varepsilon_r - \sin^2\theta_i}\right)} \left[\frac{\varepsilon_r \sin\theta \sin\theta_i \sin\phi}{\sin^2\theta + \cos\theta\sqrt{\varepsilon_r - \sin^2\theta}} + \frac{(\varepsilon_r - 1)\sqrt{\varepsilon_r - \sin^2\theta_i}}{\varepsilon_r \cos\theta - \sqrt{\varepsilon_r - \sin^2\theta}} \left\{\sin\phi\cos\phi\cos\theta\sqrt{\varepsilon_r - \sin^2\theta} - \cos\phi\sin\phi\left(\sin^2\theta + \cos\theta\sqrt{\varepsilon_r - \sin^2\theta}\right)\right\}\right] \quad (3.80)$$

$$\beta_{hv}^{(2)} = \frac{-(2\varepsilon_r - 1)}{\left(\cos\theta_i + \sqrt{\varepsilon_r - \sin^2\theta_i}\right)\left(\varepsilon_r \cos\theta_i + \sqrt{\varepsilon_r - \sin^2\theta_i}\right)} \left[\frac{\varepsilon_r \sin\theta \sin\theta_i \sin\phi_1}{\sin^2\theta + (2\cos\theta_i - \cos\theta)\sqrt{\varepsilon_r - \sin^2\theta}} + \frac{(\varepsilon_r - 1)\sqrt{\varepsilon_r - \sin^2\theta_i}}{\varepsilon_r(2\cos\theta_i - \cos\theta) + \sqrt{\varepsilon_r - \sin^2\theta}} \left\{\sin\phi_1\cos\phi(2\cos\theta_i - \cos\theta)\sqrt{\varepsilon_r - \sin^2\theta} - \cos\phi_1\sin\phi_1\left(\sin^2\theta + (2\cos\theta_i - \cos\theta)\sqrt{\varepsilon_r - \sin^2\theta}\right)\right\}\right] \quad (3.81)$$

$$\alpha_{vh}^{(2)} = \frac{-2(\varepsilon_r - 1)}{\left(\cos\theta_i + \sqrt{\varepsilon_r - \sin^2\theta_i}\right)\left(\varepsilon_r \cos\theta_i + \sqrt{\varepsilon_r - \sin^2\theta_i}\right)} \left[\frac{\varepsilon_r \sin\theta \sin\theta_i \sin\phi}{\sin^2\theta + \cos\theta\sqrt{\varepsilon_r - \sin^2\theta}} + \frac{(\varepsilon_r - 1)\sqrt{\varepsilon_r - \sin^2\theta_i}}{\left(\varepsilon_r \cos\theta + \sqrt{\varepsilon_r - \sin^2\theta}\right)} \left\{-\sin\phi\cos\phi\cos\theta\sqrt{\varepsilon_r - \sin^2\theta} + \left(\sin^2\theta + \cos\theta\sqrt{\varepsilon_r - \sin^2\theta}\right)\sin\phi\cos\phi\right\}\right] \quad (3.82)$$

$$\beta_{vh}^{(2)} = \frac{-2(\varepsilon_r - 1)}{\left(\varepsilon_r \cos\theta_i + \sqrt{\varepsilon_r - \sin^2\theta_i}\right)\left(\cos\theta_i + \sqrt{\varepsilon_r - \sin^2\theta_i}\right)} \left[\frac{\varepsilon_r \sin\phi_1 \sin\theta_i \sin\theta}{\sin^2\theta + (2\cos\theta_i - \cos\theta)\sqrt{\varepsilon_r - \sin^2\theta}} + \frac{\sqrt{\varepsilon_r - \sin^2\theta_i}(\varepsilon_r - 1)}{\left(\varepsilon_r(2\cos\theta_i - \cos\theta) + \sqrt{\varepsilon_r - \sin^2\theta}\right)} \left\{-(2\cos\theta_i - \cos\theta)\sqrt{\varepsilon_r - \sin^2\theta} . \cos\phi_1\sin\phi_1 + \left(\sin^2\theta + (2\cos\theta_i - \cos\theta)\sqrt{\varepsilon_r - \sin^2\theta}\right)\sin\phi_1\cos\phi_1\right\}\right] \quad (3.83)$$

$$\alpha_{vv}^{(2)} = \frac{\varepsilon_r - 1}{\left(\varepsilon_r \cos\theta_i + \sqrt{\varepsilon_r - \sin^2\theta_i}\right)^2} \Big[2\varepsilon_r \sqrt{\varepsilon_r - \sin^2\theta_i} - 2\left\{\left(\varepsilon_r - \sin^2\theta_i\right)\sin^2\phi \right.$$
$$\frac{(\varepsilon_r - 1)}{\left(\cos\theta + \sqrt{\varepsilon_r - \sin^2\theta}\right)} + \frac{1}{\left(\varepsilon_r \cos\theta + \sqrt{\varepsilon_r - \sin^2\theta}\right)}$$
$$\left.\left(\varepsilon_r\left(\varepsilon_r - 1\right)\sin^2\theta_i \sin^2\theta + \cos\theta\left(\varepsilon_r - 1\right)\sqrt{\varepsilon_r - \sin^2\theta}\left(\varepsilon_r - \sin^2\theta_i\right)\cos\phi\cos\pi\right)\right\}\Big] \tag{3.84}$$

$$\beta_{vv}^{(2)} = \frac{(\varepsilon_r - 1)}{\left(\varepsilon_r \cos\theta_i + \sqrt{\varepsilon_r - \sin^2\theta_i}\right)^2} \Big[2\varepsilon_r \sqrt{\varepsilon_r - \sin^2\theta_i} - 2\left\{\left(\varepsilon_r - \sin^2\theta_i\right)\right.$$
$$\frac{(\varepsilon_r - 1)\sin^2\phi_1 \sin^2\phi_1}{\left((2\cos\theta_i - \cos\theta) + \sqrt{\varepsilon_r - \sin^2\theta}\right)} + \frac{1}{\left(\varepsilon_r\left(2\cos\theta_i - \cos\theta\right) + \sqrt{\varepsilon_r - \sin^2\theta}\right)}$$
$$. \left(\varepsilon_r\left(\varepsilon_r - 1\right)\sin^2\theta_i \sin^2\theta + (2\cos\theta_i - \cos\theta)\right.$$
$$\left.\left.\sqrt{\varepsilon_r - \sin^2\theta}\left(\varepsilon_r - 1\right)\left(\varepsilon_r - \sin^2\theta_i\right)\cos^2\phi_1\right)\right\}\Big] \tag{3.85}$$

Numerical simulations

Backscattering In this paragraph we present the comparisons between the numerical results obtained by SPM1 and SPM2 based on Gaussian spectrum. We perform the calculations for kh values of 0.1, 0.2,..., 0.6 and kl values of 1, 2,...,6. The relative permittivity of rough surface is taken as $4+i$ for all configurations. Some representative results are shown here.

Figures 3.5, 3.6 and 3.7 present the comparisons between SPM1 and SPM2 for surfaces with a constant value of $kl = 1$ and three different values of kh i.e., 0.1, 0.3 and 0.5.

For all three cases the simulated results obtained from SPM2 are weaker than those of SPM1 for HH and VV polarization, but they are becoming stronger as the value of kh increases. The depolarization (or cross polarization i. e., HV and VH) results are absent as SPM1 does not produce depolarized results in backscattering direction. However, the predictions by SPM2 for cross polarization are non-zero and can be seen in these figures.

Next, in figures 3.8, 3.9 and 3.10 we have traced the backscattering coefficients σ_{hh}, σ_{hh}, σ_{hh} and σ_{vv} by SPM1 and SPM2 as a function of incident angle by using the same parameters as used previously except the vale of kl which is increased to 3. Again we observe that the second order scattering intensity increases as the roughness level of the surface increase (or when kh become large). Moreover, the increased value of kl also contribute to enhance the predictions by SPM2. Another important feature, which is also very interesting is that the second order scattering effects are more dominant on

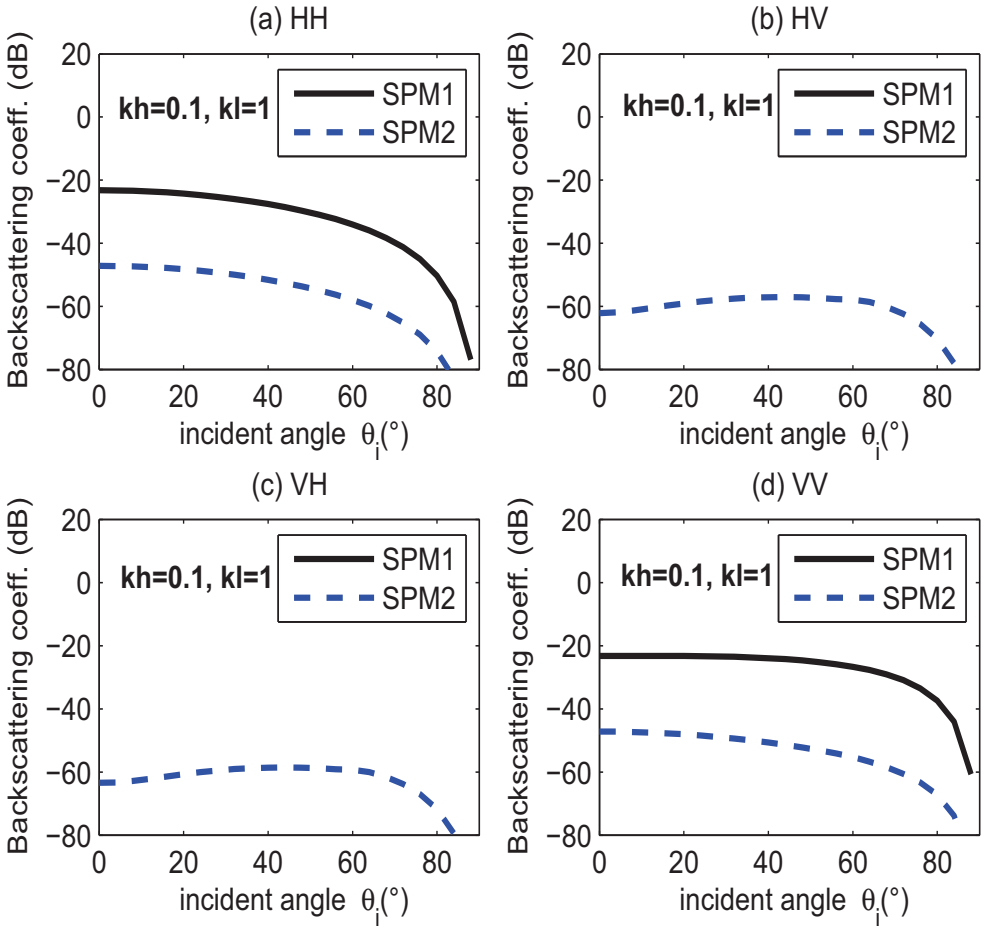

Figure 3.5: Backscattering coeff. : Comparisons between SPM1 and SPM2, Gaussian spectrum, $kh = 0.1$, $kl = 1$, (a)HH-pol; (b)HV-pol; (c)VH-pol and (d) VV-pol.

the grazing angles than the specular domain. Hence for the configurations $kh = 0.3$, $kl = 3$(ref Fig. 3.9) and $kh = 0.5$, $kl = 3$ (ref Fig. 3.10), SPM2 predicts enhanced results than those of SPM1, from moderate to small grazing angles, for HH and VV polarization. The estimated results by SPM2 for cross polarizations HV and VH are also shown in these figures.

The same type of observations can be done for three other rough surfaces with parameters $kh = 0.1$, $kl = 4$; $kh = 0.3$, $kl = 4$ and $kh = 0.5$, $kl = 4$ from the Figs. 3.11, 3.12 and 3.13 respectively.

These results motivated us to develop a model by including the second order scattering effects with larger domain of validity, as compared to KA and SPM, and which can give improved results on grazing angles and better depolarization predictions in

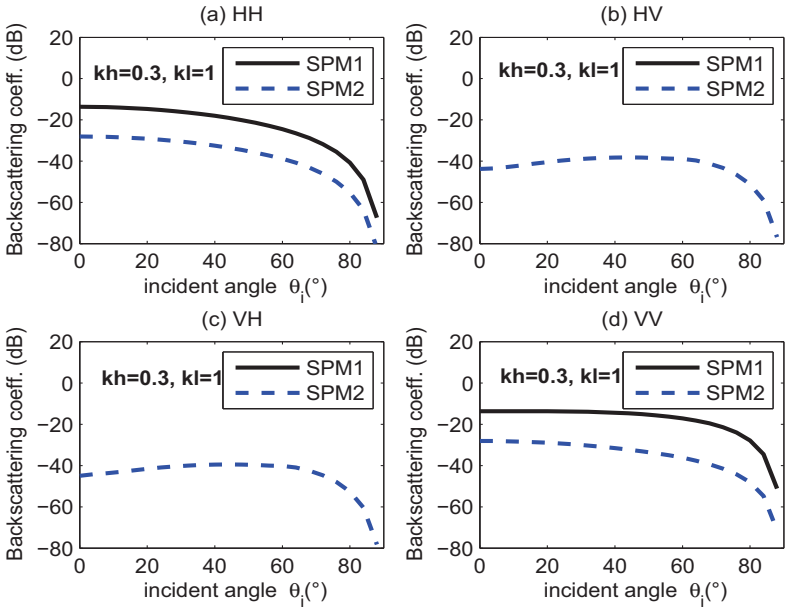

Figure 3.6: Backscattering coeff. : Comparisons between SPM1 and SPM2, Gaussian spectrum, $kh = 0.3$, $kl = 1$, (a)HH-pol; (b)HV-pol; (c)VH-pol and (d) VV-pol.

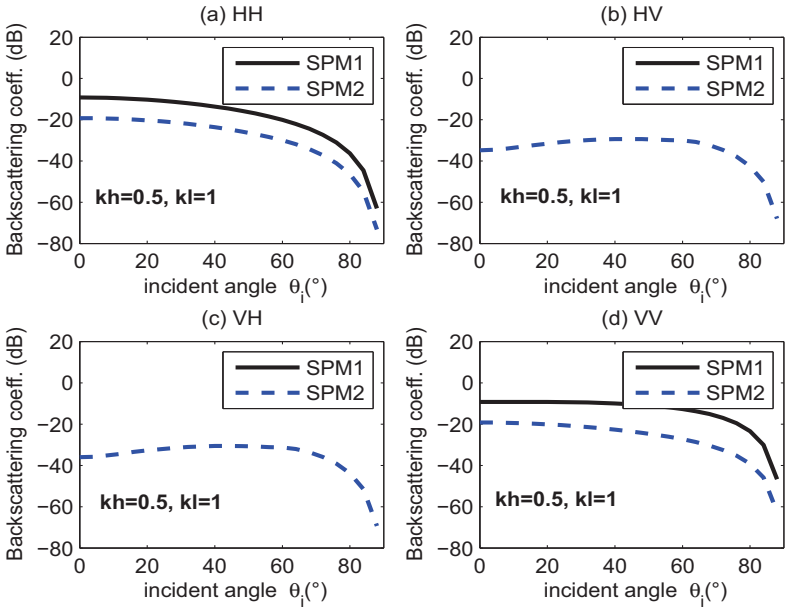

Figure 3.7: Backscattering coeff. : Comparisons between SPM1 and SPM2, Gaussian spectrum, $kh = 0.5$, $kl = 1$, (a)HH-pol; (b)HV-pol; (c)VH-pol and (d) VV-pol.

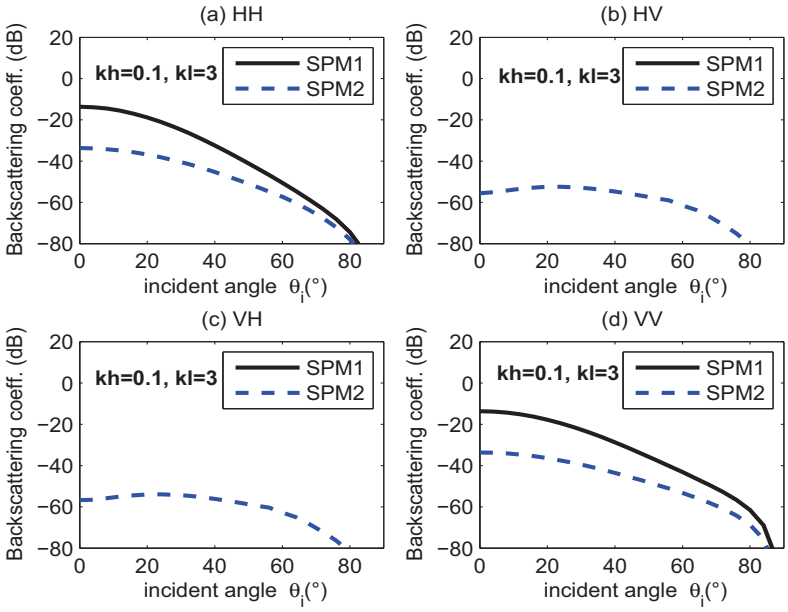

Figure 3.8: Backscattering coeff. : Comparisons between SPM1 and SPM2, Gaussian spectrum, $kh = 0.1$, $kl = 3$, (a)HH-pol; (b)HV-pol; (c)VH-pol and (d) VV-pol.

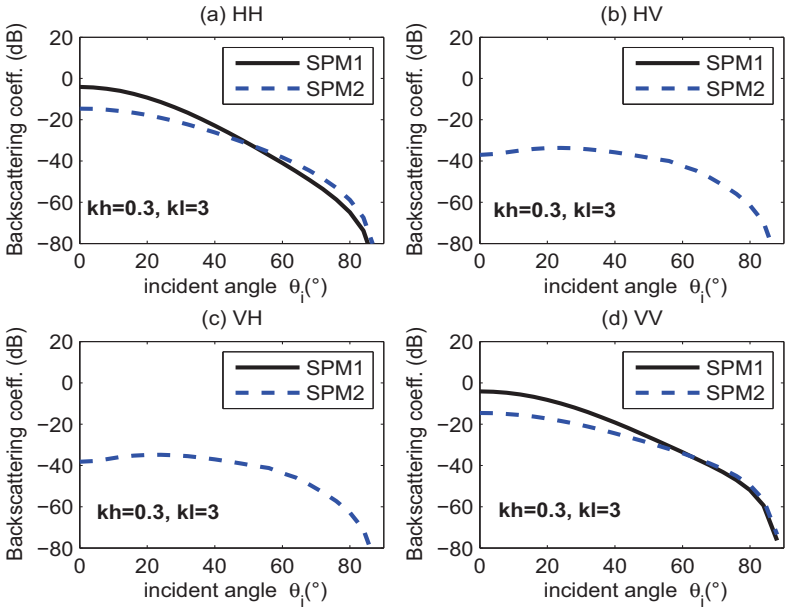

Figure 3.9: Backscattering coeff. : Comparisons between SPM1 and SPM2, Gaussian spectrum, $kh = 0.3$, $kl = 3$, (a)HH-pol; (b)HV-pol; (c)VH-pol and (d) VV-pol.

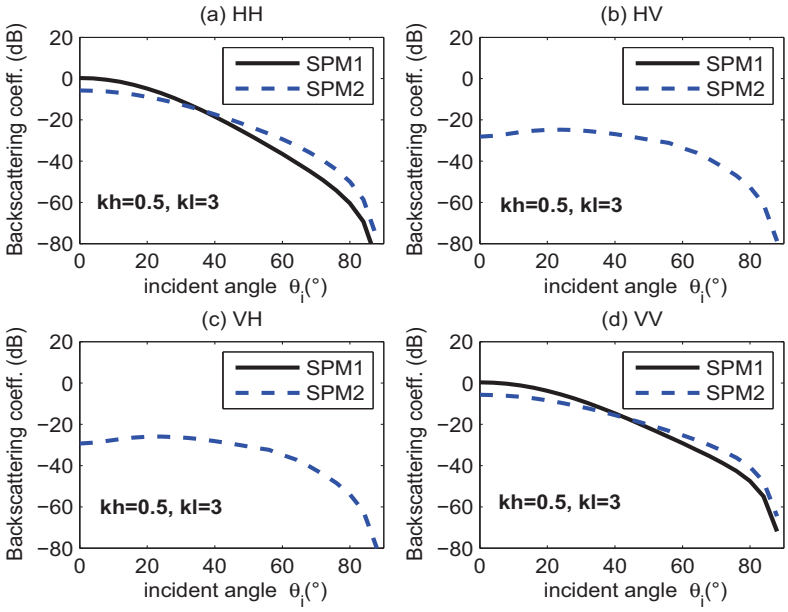

Figure 3.10: Backscattering coeff. : Comparisons between SPM1 and SPM2, Gaussian spectrum, $kh = 0.5$, $kl = 3$, (a)HH-pol; (b)HV-pol; (c)VH-pol and (d) VV-pol.

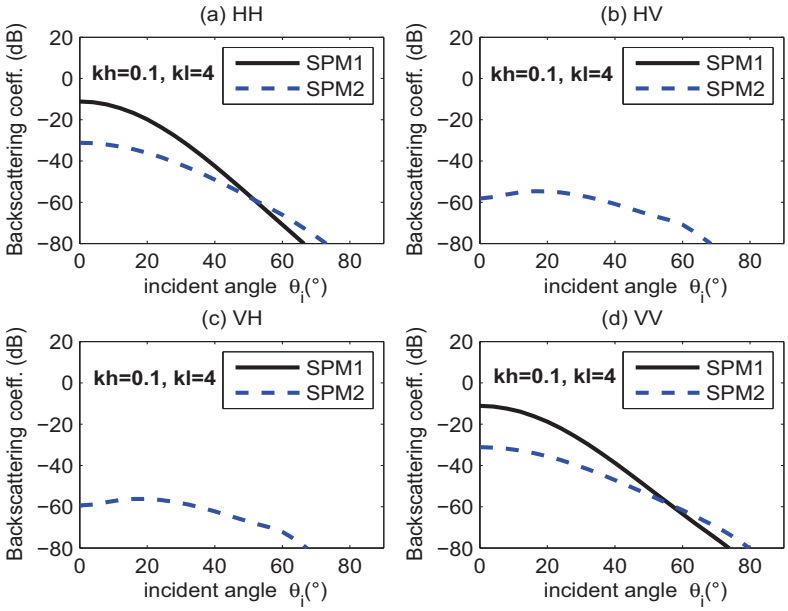

Figure 3.11: Backscattering coeff. : Comparisons between SPM1 and SPM2, Gaussian spectrum, $kh = 0.1$, $kl = 4$, (a)HH-pol; (b)HV-pol; (c)VH-pol and (d) VV-pol.

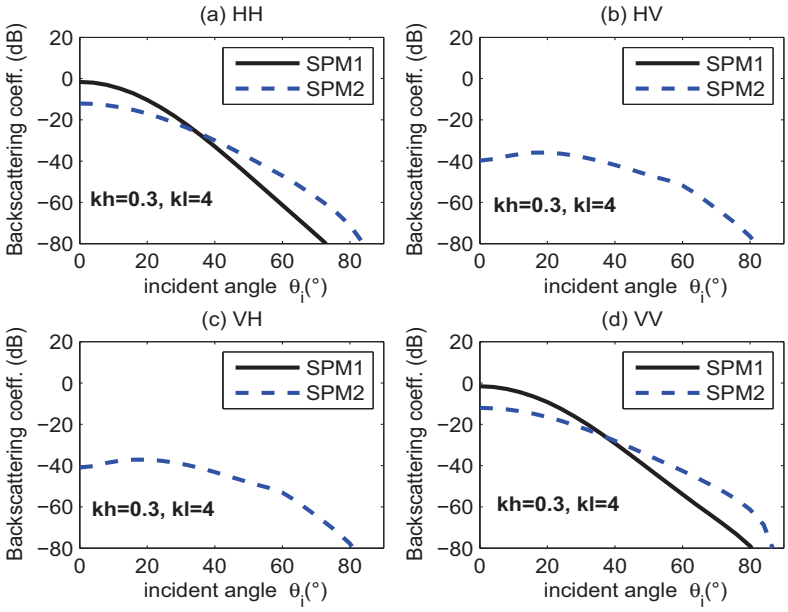

Figure 3.12: Backscattering coeff. : Comparisons between SPM1 and SPM2, Gaussian spectrum, $kh = 0.3$, $kl = 4$, (a)HH-pol; (b)HV-pol; (c)VH-pol and (d) VV-pol.

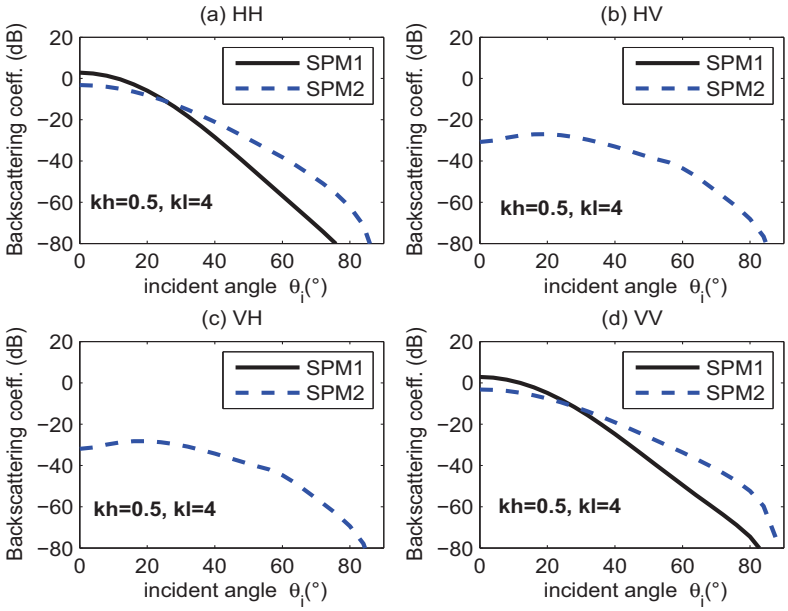

Figure 3.13: Backscattering coeff. : Comparisons between SPM1 and SPM2, Gaussian spectrum, $kh = 0.5$, $kl = 4$, (a)HH-pol; (b)HV-pol; (c)VH-pol and (d) VV-pol.

backscattering direction. The development of such model is given in the next section.

Bistatic scattering To study the second order scattering effects on grazing angles by SPM2 in bistatic direction we choose a sample surface with roughness parameters $kh = 0.5$, $kl = 3$ and plotted the bistatic scattering coefficient as a function of observed angle θ_s in Figs 3.14 and 3.15. The incident angle θ_i is taken as 80°. The transmitter azimuth angle is set ti 0° and the receptor azimuth angle is fixed to 45° and then to 135°. In the first case SPM2 does not give some important results. However, for large value of φ_s SPM2 predictions are stronger than SPM1 from moderate to small grazing angles.

Figure 3.14: Bistatic scattering coeff. : Comparisons between SPM1 and SPM2, Gaussian spectrum, $kh = 0.5$, $kl = 3$, $\theta_i = 80°$, $\varphi_i = 0°$, $\varphi_s = 45°$, (a)HH-pol; (b)HV-pol; (c)VH-pol and (d) VV-pol.

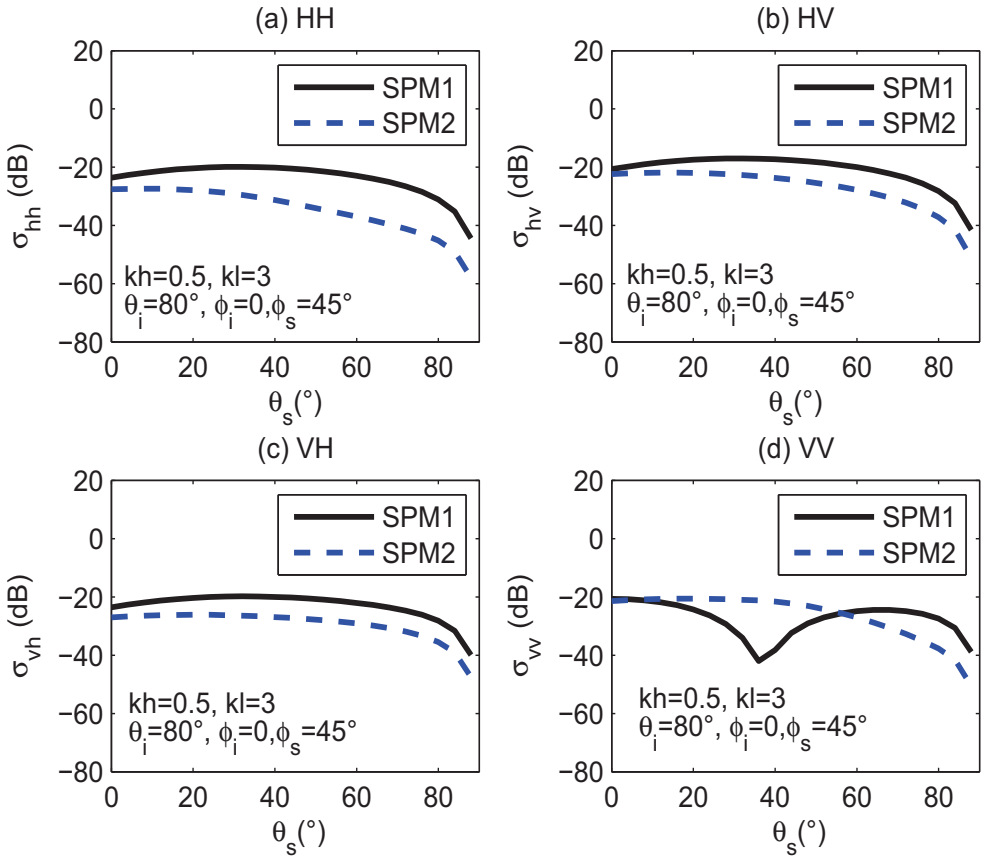

Figure 3.16 shows the variation of bistatic scattering coefficient as a function of

Figure 3.15: Bistatic scattering coeff. : Comparisons between SPM1 and SPM2, Gaussian spectrum, $kh = 0.5$, $kl = 3$, $\theta_i = 80°$, $\varphi_i = 0°$, $\varphi_s = 135°$, (a)HH-pol; (b)HV-pol; (c)VH-pol and (d) VV-pol.

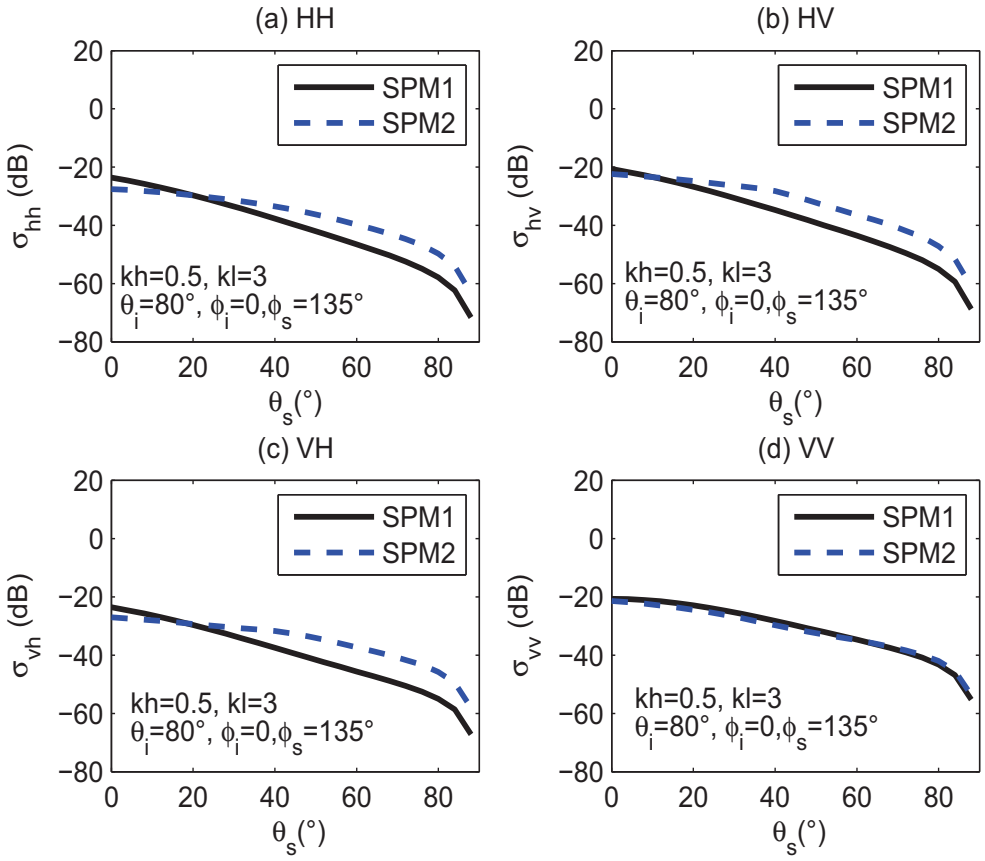

receptor azimuth for the same surface ($kh = 0.5$, $kl = 3$). The incident and scattered angles are equal to 80° and the transmitter azimuth is set to 0°. It can be seen that for the considered example the maximum enhancement by SPM2 is found when φ_s is equal ti 180° i.e., in backscattering direction.

3.2.3 Regions of Validity

It is interesting to have an idea of the domains of validity of the simple asymptotic methods in order to use them properly. However its rather delicate to determine the precise domain of validity of each method, firstly because it depends on the desired accuracy of the method (and it is good to study the qualitative domains of validity),

Figure 3.16: Bistatic scattering coeff. : Comparisons between SPM1 and SPM2, Gaussian spectrum, $kh = 0.5$, $kl = 3$, $\theta_i = \theta_s = 80°$, $\varphi_i = 0°$, (a)HH-pol; (b)HV-pol; (c)VH-pol and (d) VV-pol.

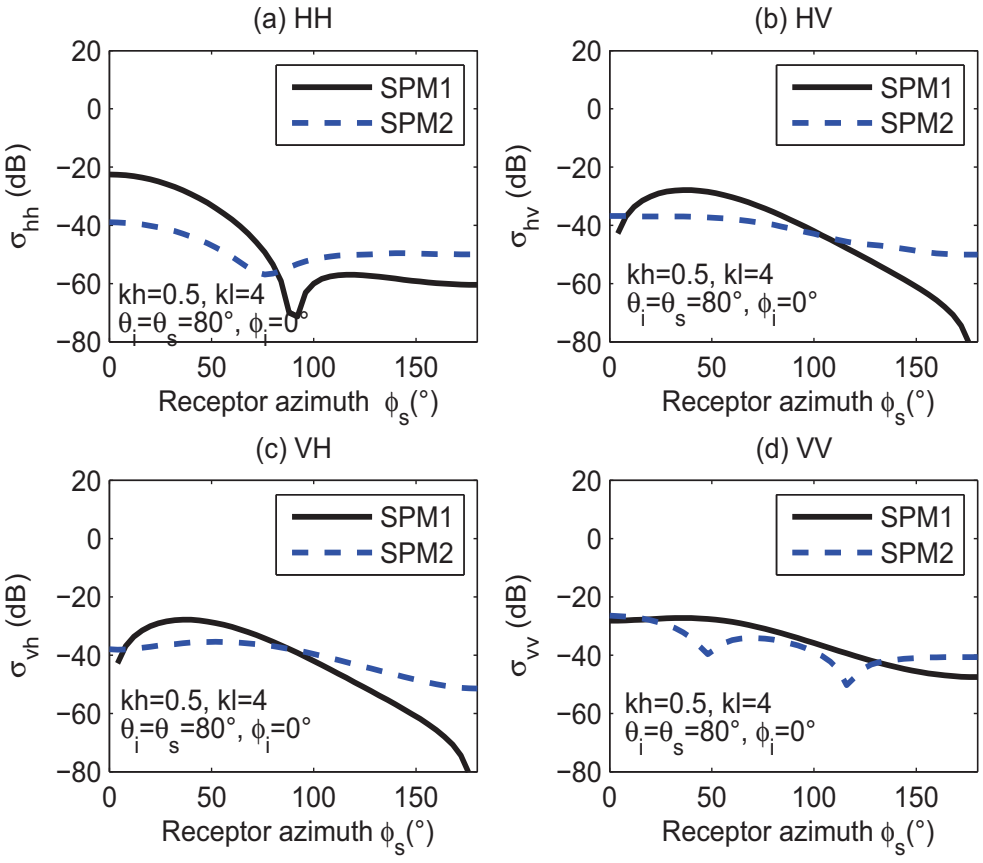

and secondly and more importantly because many parameters are involved. These include the height distribution and autocorrelation function of the surface (Gaussian, Lorentzian, exponential, of sea ..), the values of incidence and /or scattered angles (mono-or bi-static configuration) and the permittivity of the lower medium etc.

To give a qualitative domain of validity of asymptotic methods we consider the surfaces with gaussian statistics and take the moderate incident and scattered angles. It is represented as a function of the product of wave number by correlation length, kl, and the wave number by standard deviation of height kh. As stated earlier the first order SPM (SPM1) is valid if $kh < 0.3$ and $h < 0.3$; conditions to which one must add the condition on correlation length $kl < 1.3$ [21, 61]. To summarize, the SPM1 is valid

if

$$kh < 0.3 \text{ and } h < 0.3 \text{ and } kl < 1.3 \tag{3.86}$$

If θ_i increases the accuracy of SPM1 improves [72] e.g., it is valid for $kh < 0.502$ for horizontal polarization and $kh < 0.4398$ for vertical polarization [73, 74]. For vertical polarization the first order SPM seems to apply at small incident angles up to a point where it appears to fail when the angle of incidence is in the vicinity of the Brewster angle θ_B [74]. This discrepancy has been overcome by modifying the perturbation approach by including the effect of impedance/admittance boundary condition [75, 76].

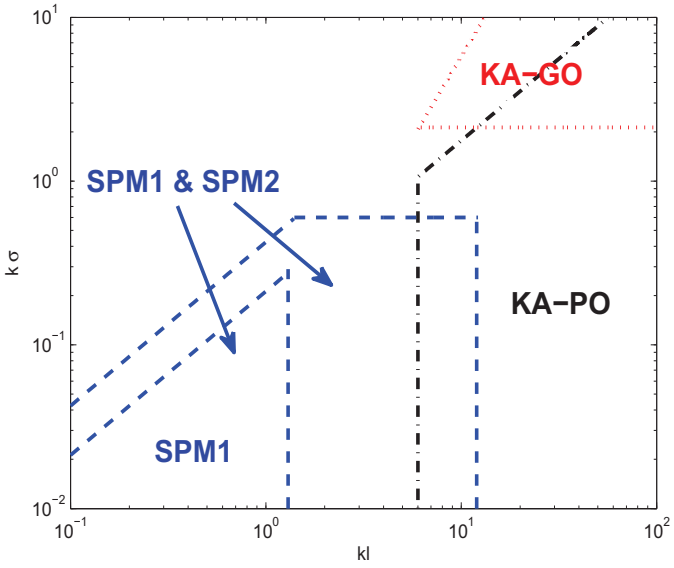

Figure 3.17: Qualitative regions of validity of some asymptotic methods (gaussian statistics, moderate angles...

Taking into account the second order (SPM2), it extends the range of validity of SPM (SPM2 & SPM1) for heights and slopes (and therefore the correlation lengths) somewhat higher as shown in Fig. 3.17. Moreover when kl becomes large compared to 1, the second-order terms give larger contribution to the scattering cross section than does the first order term [72].

The validity conditions, based on analytic considerations, for the Kirchhoff Approximation have been quoted in the literature $kl > 6$ and $R_c > \lambda$ [21, 61, 77], where R_c is the average radius of curvature for the rough surface. For process with Gaussian correlation coefficient the average radius of curvature $R_c = \frac{l^2}{2h}\sqrt{\frac{\pi}{6}}$.

Then the validity conditions becomes [63]:

$$kl > 6 \text{ and } kl > 2\sqrt{kh\sqrt{6\pi}} \approx 4.17\sqrt{kh} \tag{3.87}$$

To evaluate the scattered field analytically, two additional simplifying approximations have appeared in the literature: the stationary phase approximation and the scalar approximation. The validity conditions for the stationary phase are $kh > \frac{\sqrt{10}}{|\cos\theta_s+\cos\theta_i|}$, $kl > 6$ and $R_c > \lambda$. When the surface height is Gaussian distributed the conditions become

$$k\sigma > \frac{\sqrt{10}}{|\cos\theta_s + \cos\theta_i|},\ kl > 6 \text{ and } kl > 2\sqrt{kh\sqrt{6\pi}} \tag{3.88}$$

and the validity conditions for the scalar approximation (physical optics) are $kl > 6$, $R_c > \lambda$ and $m < 0.25$ with $m = \sqrt{2}h/l$. When the surface height is Gaussian distribution, the conditions become [63]

$$kl > 6 \text{ and } kl > \frac{\sqrt{2}}{0.25}kh \tag{3.89}$$

These different criteria are summarized in Fig. 3.17

3.3 Mathematical development of improved Two Scale Model (TSM2)

In previous two sections two special types of rough surfaces were considered. Loosely speaking the surface roughnesses had to be either large or small compared with the incident wave length.

Naturally occurring surfaces, however, may include both types of roughness in various proportions. Some surfaces may have one continuous distribution of roughness instead of two significantly different average sizes. Analytically, there is no simple method to treat surfaces with a continuous distribution of roughness. However for, "two-scale" surfaces which can be modeled as having only two average sizes of roughness with one large and the other small compared with the incident wavelength, a simple approximate treatment of this two scale surface problem is possible.

The classical TSM (TSM1) [1, 5], [27]–[30], [59, 60], [78]–[82] approximate the rough surface as a two-scale surface with small-scale waves riding on the top of large-scale waves. Then scattering coefficients are estimated in two steps. Firstly, the classical TSM uses SPM1 on small scale waves and then determine the diffuse component in the global reference by a tilting process. It has larger validity domain as compared to KA and SPM1 but gives inaccurate results at grazing angles. Moreover in backscattering

direction the depolarization estimation by TSM1 is basically due to the tilt of reflecting plane as both method (i.e., KA, SPM) do not predict cross polarization when studied upto first order. To overcome these problems we develop an improved TSM by replacing the SPM1 by SPM1+SPM2 at small scale. The details of development are given in this section.

We start by reviewing the TSM1 firstly and then derive the analytic expressions for bistatic scattering coefficients by TSM2.

3.3.1 Classical TSM (TSM1)

Principle of the model

Comparing the classical models studied previously this model is characterized by its large domain of application. At near-vertical incidence (hence the incidence angle θ is small), the Kirchhoff model may be used. For large incidence angles we consider two types of coordinate systems, one local to represent the slightly-rough-surface scattering problem and another coordinate system for the two scale problem. It then follows that these two problems are related simply by a coordinate transformation.

In the global frame the transmitter and the receiver are located in a reference (x, y, z) by the angles θ_i, φ_i, θ_s and φ_s. Let (x', y', z') represent the local reference frame of which the origin can be taken as the point of incidence of the electromagnetic wave and z' is the local normal to the surface as shown in the following figure (Fig. 3.18). In the global frame we can define the basis at emission and reception as follows

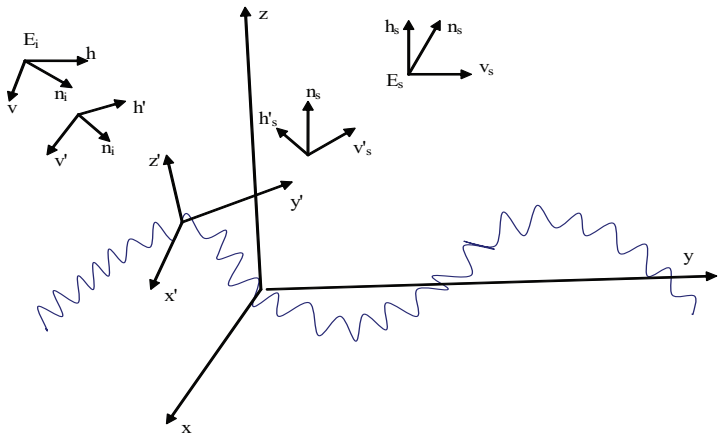

Figure 3.18: Geometry of surface bistatic scattering of a two-scale model

$$\begin{cases} \widehat{\mathbf{n}}_i = \sin\theta_i\cos\varphi_i\mathbf{x} + \sin\theta_i\sin\varphi_i\mathbf{y} - \cos\theta_i\mathbf{z} \\ \widehat{\mathbf{v}}_i = -\cos\theta_i\cos\varphi_i\mathbf{x} - \cos\theta_i\sin\varphi_i\mathbf{y} - \sin\theta_i\mathbf{z} \\ \widehat{\mathbf{h}}_i = -\sin\varphi_i\mathbf{x} + \cos\varphi_i\mathbf{y} \end{cases} \tag{3.90}$$

$$\begin{cases} \widehat{\mathbf{n}}_s = \sin\theta_s\cos\varphi_s\mathbf{x} + \sin\theta_s\sin\varphi_s\mathbf{y} + \cos\theta_s\mathbf{z} \\ \widehat{\mathbf{v}}_s = \cos\theta_s\cos\varphi_s\mathbf{x} + \cos\theta_s\sin\varphi_s\mathbf{y} - \sin\theta_s\mathbf{z} \\ \widehat{\mathbf{h}}_s = -\sin\varphi_s\mathbf{x} + \cos\varphi_s\mathbf{y} \end{cases} \tag{3.91}$$

As for the local reference frame it is defined by x', y' and z' and we write [59]

$$\mathbf{z}' = \widehat{\mathbf{n}} = D_0\left[-Z_x\mathbf{x} - Z_y\mathbf{y} + \mathbf{z}\right] \tag{3.92}$$

$$\begin{aligned} \mathbf{y}' &= \frac{\widehat{\mathbf{n}}\wedge\widehat{\mathbf{n}}_i}{\|\widehat{\mathbf{n}}\wedge\widehat{\mathbf{n}}_i\|} = D_1[(Z_y\cos\theta_i - \sin\theta_i\sin\varphi_i)\,\mathbf{x} + (\sin\theta_i\cos\varphi_i - Z_x\cos\theta_i)\,\mathbf{y} \\ &\quad + (-Z_x\sin\theta_i\sin\varphi_i + Z_y\sin\theta_i\cos\varphi_i)\,.\mathbf{z}] \end{aligned} \tag{3.93}$$

$$\begin{aligned} \mathbf{x}' &= \mathbf{y}'\wedge\mathbf{z}' = D_0D_1[\{(\sin\theta_i\cos\varphi_i - Z_x\cos\theta_i) + Z_y\sin\theta_i\,(-Z_x\sin\varphi_i + Z_y\cos\varphi_i)\}\,\mathbf{x} \\ &\quad + \{-Z_x\sin\theta_i\,(-Z_x\sin\varphi_i + Z_y\cos\varphi_i) - (Z_y\cos\theta_i - \sin\theta_i\sin\varphi_i)\}\,\mathbf{y} \\ &\quad + \{-Z_y\,(Z_y\cos\theta_i - \sin\theta_i\sin\varphi_i)\}\,\mathbf{z}] \end{aligned} \tag{3.94}$$

with

$$D_0 = \left[Z_x^2 + Z_y^2 + 1\right]^{-\frac{1}{2}} \tag{3.95}$$

$$\begin{aligned} D_1 = \Big((Z_y\cos\theta_i - \sin\theta_i\sin\varphi_i)^2 + (\sin\theta_i\cos\varphi_i - Z_x\cos\theta_i)^2 \\ + (-Z_x\sin\theta_i\sin\varphi_i + Z_y\sin\theta_i\cos\varphi_i)^2\Big)^{-\frac{1}{2}} \end{aligned} \tag{3.96}$$

with respect to this local frame, we define th polarization bases at emission ($\widehat{\mathbf{v}}'_i$, $\widehat{\mathbf{h}}'_i$) and at reception ($\mathbf{v}'_s$, $\mathbf{h}'_s$)

$$\begin{cases} \widehat{\mathbf{v}}'_i = -\cos\theta'_i\cos\varphi'_i\mathbf{x}' - \cos\theta'_i\sin\varphi'_i\mathbf{y} - \sin\theta'_i\mathbf{z} \\ \widehat{\mathbf{h}}'_i = -\sin\varphi'_i\mathbf{x}' + \cos\varphi'_i\mathbf{y}' \end{cases} \tag{3.97}$$

$$\begin{cases} \mathbf{v}'_s = \cos\theta'_s\cos\varphi'_s\mathbf{x}' - \cos\theta'_s\sin\varphi'_s\mathbf{y} - \sin\theta'_s\mathbf{z} \\ \mathbf{h}'_s = -\sin\varphi'_s\mathbf{x}' - \cos\varphi'_s\mathbf{y}' \end{cases} \tag{3.98}$$

The local incident angles can be written as

$$\begin{cases} \cos\theta'_i = -\widehat{\mathbf{n}}.\widehat{\mathbf{n}}_i = D_0\left\{Z_x\sin\theta_i\cos\varphi + Z_y\sin\theta_i\sin\varphi + \cos\theta_i\right\} \\ \sin\theta'_i = \frac{D1}{D_0} \end{cases} \tag{3.99}$$

and

$$\begin{cases} \cos\varphi'_i = \frac{D1}{D_0}\widehat{\mathbf{n}}_i.\mathbf{x}' \\ \sin\varphi'_i = \frac{D1}{D_0}\widehat{\mathbf{n}}_i.\mathbf{y}' \end{cases} \tag{3.100}$$

$$\begin{cases} \cos\theta'_s = \widehat{\mathbf{n}}.\widehat{\mathbf{n}}_s \\ \sin\theta'_s = \sqrt{1-(\widehat{\mathbf{n}}.\widehat{\mathbf{n}}_s)^2} \end{cases} \tag{3.101}$$

$$\begin{cases} \cos\varphi'_s = \frac{\widehat{\mathbf{n}}_s.\mathbf{x}'}{\sin\theta'_s} \\ \sin\varphi'_s = \frac{\widehat{\mathbf{n}}_s.\mathbf{y}'}{\sin\theta'_s} \end{cases} \tag{3.102}$$

The 2×1 complex element vectors $\mathbf{E}^i$ and $\mathbf{E}^s$ describe the polarizations of the incident and scattered electric fields, respectively. The incident wave E^i can be written as [59]

$$\mathbf{E}^i = \mathbf{a}E_0 \quad \text{with} \quad E_0 = |E_0| \exp\{-jK(\widehat{\mathbf{n}}_i.\mathbf{r})\} \tag{3.103}$$

where $\mathbf{a}$ is the unit polarization vector (vertical polarization $\mathbf{v}$ or horizontal polarization $\mathbf{h}$), K is the wave number of transmitted wave, and $\widehat{\mathbf{n}}_i$ is the unit vector in the incident direction. In the local reference the incident field can be rewritten as

$$\mathbf{E}^i = E^i_{v'}\widehat{\mathbf{v}}'_i + E^i_{h'}\widehat{\mathbf{h}}'_i = \left[\left(\mathbf{a}.\widehat{\mathbf{v}}'_i\right)\widehat{\mathbf{v}}'_i + \left(\mathbf{a}.\widehat{\mathbf{h}}'_i\right)\widehat{\mathbf{h}}'_i\right] E_0 \tag{3.104}$$

and the scattering field expressed in the $(\mathbf{h}'_s, \mathbf{v}'_s)$ basis by [59]

$$\begin{bmatrix} E^s_{v'} \\ E^s_{h'} \end{bmatrix} = \begin{bmatrix} S_{v'_s v'_i} & S_{v'_s h'_i} \\ S_{h'_s v'_i} & S_{h'_s h'_i} \end{bmatrix} \begin{bmatrix} E^i_{v'} \\ E^i_{h'} \end{bmatrix} \tag{3.105}$$

where $S_{p'q'}$ is the scattered field for unit incident fields.

Diffusion coefficients

The scattered field can be rewritten in the $(\mathbf{h}_s, \mathbf{v}_s)$ basis as

$$\mathbf{E}^s = \begin{bmatrix} E^s_{vs} \\ E^s_{hs} \end{bmatrix} = S\mathbf{E}^i \tag{3.106}$$

where S denotes the scattering matrix.In the global frame of reference it is expressed by [59]

$$S = \begin{bmatrix} \widehat{\mathbf{v}}'_s.\widehat{\mathbf{v}}_s & \widehat{\mathbf{h}}'_s.\widehat{\mathbf{v}}_s \\ \widehat{\mathbf{v}}'_s.\widehat{\mathbf{h}}_s & .\widehat{\mathbf{h}}'_s.\widehat{\mathbf{h}}_s \end{bmatrix} \begin{bmatrix} S_{v'_s v'_i} & S_{v'_s h'_i} \\ S_{h'_s v'_i} & S_{h'_s h'_i} \end{bmatrix} \begin{bmatrix} \widehat{\mathbf{v}}'_i.\widehat{\mathbf{v}}_i & \widehat{\mathbf{v}}'_i.\widehat{\mathbf{h}}_i \\ \widehat{\mathbf{h}}'_i.\widehat{\mathbf{v}}_i & .\widehat{\mathbf{h}}'_i.\widehat{\mathbf{h}}_i \end{bmatrix} \tag{3.107}$$

Generally, for a polarization q ($\widehat{\mathbf{v}}_i$ or $\widehat{\mathbf{h}}_i$) at emission and p ($\widehat{\mathbf{v}}_s$or $\widehat{\mathbf{h}}_s$) at reception the components of the scattered field is given by the expression

$$E^s_{pq} = \left(\widehat{\mathbf{v}}'_s.p\right)\left\{\left(q.\widehat{\mathbf{v}}'_i\right)S_{v'_s v'_i} + \left(q.\widehat{\mathbf{h}}'_i\right)S_{v'_s h'_i}\right\}E_0 + \left(\widehat{\mathbf{h}}'_s.p\right)\left\{\left(q.\widehat{\mathbf{v}}'\right)S_{h'_s v'_i} + \left(q.\widehat{\mathbf{h}}'_i\right)S_{h'_s h'_i}\right\}E_0 \tag{3.108}$$

The scattering coefficients σ^s_{pq} as a function of p and q are given by the following relation [59]

$$\begin{aligned}
\sigma^{1s}_{pq} &= \frac{4\pi R^2}{A}\frac{\left\langle \left|E^s_{pq}\right|^2\right\rangle}{\left|E^i_q\right|^2} \\
&= \Big\langle \left(p.\widehat{\mathbf{h}}'_s\right)^2 \left(\widehat{\mathbf{h}}'_i.q\right)^2 \sigma^s_{h'h'} + \left(p.\widehat{\mathbf{h}}'_s\right)^2 \left(\widehat{\mathbf{v}}'_i.q\right)^2 \sigma^s_{h'v'} \\
&\quad + \left(p.\widehat{\mathbf{v}}'_s\right)^2 \left(\widehat{\mathbf{h}}'_i.q\right)^2 \sigma^s_{v'h'} + \left(p.\widehat{\mathbf{v}}'_s\right)^2 \left(\widehat{\mathbf{v}}'_i.q\right)^2 \sigma^s_{v'v'} \\
&\quad + \left(p.\widehat{\mathbf{h}}'_s\right)^2 \left(\widehat{\mathbf{v}}'_i.q\right)\left(\widehat{\mathbf{h}}'_i.q\right) \sigma^s_{h'h'h'v'} + \left(p.\widehat{\mathbf{v}}'_s\right)\left(\widehat{\mathbf{h}}'_i.q\right)^2 \left(\widehat{\mathbf{h}}'_s.p\right) \sigma^s_{h'h'v'h'} \\
&\quad + \left(p.\widehat{\mathbf{v}}'_s\right)\left(\widehat{\mathbf{v}}'_i.q\right)\left(\mathbf{h}'_s.p\right)\left(\widehat{\mathbf{h}}'_i.q\right)\left(\sigma^s_{v'v'h'h'}\right) + \left(p.\widehat{\mathbf{v}}'_s\right)\left(\widehat{\mathbf{v}}'_i.q\right)\left(\widehat{\mathbf{h}}'_s.p\right)\left(\widehat{\mathbf{h}}'_i.q\right)\sigma^s_{h'v'v'h'} \\
&\quad + \left(p.\widehat{\mathbf{v}}'_s\right)\left(\widehat{\mathbf{v}}'_i.q\right)^2\left(\widehat{\mathbf{h}}'_s.p\right)\sigma^s_{h'v'v'v'} + \left(p.\widehat{\mathbf{v}}'_s\right)^2\left(\widehat{\mathbf{v}}'_i.q\right)\left(\widehat{\mathbf{h}}'_i.q\right)\sigma^s_{v'v'v'h'}\Big\rangle
\end{aligned} \tag{3.109}$$

where $\sigma_{p'q'}$ and $\sigma_{p'q'm'n'}$ are obtained from SPM1 and and calculated at local angles as

$$\begin{cases}
\sigma_{pq} = 16\pi k^4 \cos^2\theta'_i \cos^2\theta'_s \left|\alpha^{(1)}_{p'q'}\right|^2 W\left(k_{sx}-k_{ix}, k_{sy}-k_{ix}\right) \\
\sigma_{pqmn} = 16\pi k^4 \cos^2\theta'_i \cos^2\theta'_s \alpha^{(1)}_{p'q'}\alpha^{(1)*}_{m'n'} W\left(k_{sx}-k_{ix}, k_{sy}-k_{ix}\right)
\end{cases} \tag{3.110}$$

$\alpha^{(1)}_{p'q'}$ can be obtained from (A.13)-(A.16) at local angles θ'_i, ϕ'_i, θ'_s and ϕ'_s.

The average $\langle . \rangle$ in the scattering coefficients may then be calculated by using any model of the surface slopes distribution as

$$\langle G \rangle = \int\int G\left(Z_x, Z_y\right) \Pr\left(Z_x, Z_y\right) I dZ_x dZ_y \tag{3.111}$$

where Pr is the probability density function of the surface slopes, Z_x and Z_y are slopes of the surface in x and y directions respectively., of the large scale roughness function $z = z(x, y)$. The term I is defined as

$$I = \begin{cases}
 & \text{if } n_i.n < 0 \text{ (the surface element is seen} \\
1 & \text{by transmitter) and } n_s.n > 0 \text{ (the surface} \\
 & \text{element is seen by receiver)} \\
0 & \text{elsewhere}
\end{cases} \tag{3.112}$$

Backscattering

Let us consider the backscattering case by taking $\theta_s = \theta_i$, $\phi_s = \pi$ and $\phi_i = 0$. Since SPM1 does not produce results for cross polarized fields so most of the cross correlation terms will become zero in (3.109) and the expression reduces to

$$\begin{aligned}
\sigma^{1s}_{pq} &= \Big\langle \left(\mathbf{p}.\widehat{\mathbf{h}}'_s\right)^2 \left(\widehat{\mathbf{h}}'.\mathbf{q}\right)^2 \sigma^s_{h'_s h'} + \left(\mathbf{p}.\widehat{\mathbf{v}}'_s\right)^2 \left(\widehat{\mathbf{v}}'.\mathbf{q}\right)^2 \sigma^s_{v'_s v'} \\
&\quad + \left(\mathbf{p}.\widehat{\mathbf{v}}'_s\right)\left(\widehat{\mathbf{v}}'.\mathbf{q}\right)\left(\widehat{\mathbf{h}}'_s.\mathbf{p}\right)\left(\widehat{\mathbf{h}}'.\mathbf{q}\right)\left(\sigma^s_{v'_s v' h'_s h'}\right)\Big\rangle
\end{aligned} \tag{3.113}$$

where the reduced first order polarization dependent factors are given by (3.72)-(3.75) and calculated at local angles.

3.3.2 Improved TSM (TSM2)

To include the contribution of second order scattering effects we add the second order scattered field $S_{pq}^{(2)}$ in to $S_{pq}^{(1)}$, for unit incident field, in a local domain. Hence the local scattering matrix will become

$$S' = \begin{bmatrix} S^{(1)}_{h'_s h'_i} + S^{(2)}_{h'_s h'_i} & S^{(1)}_{h'_s v'_i} + S^{(2)}_{h'_s v'_i} \\ S^{(1)}_{v'_s h'_i} + S^{(2)}_{v'_s h'_i} & S^{(1)}_{v'_s v'_i} + S^{(2)}_{v'_s v'_i} \end{bmatrix} \tag{3.114}$$

and in global frame of reference the scattering matrix S is given by

$$S = \begin{bmatrix} \widehat{\mathbf{v}}'_s.\widehat{\mathbf{v}}_s & \widehat{\mathbf{h}}'_s.\widehat{\mathbf{v}}_s \\ \widehat{\mathbf{v}}'_s.\widehat{\mathbf{h}}_s & .\widehat{\mathbf{h}}'_s.\widehat{\mathbf{h}}_s \end{bmatrix} \begin{bmatrix} S^{(1)}_{h'_s h'_i} + S^{(2)}_{h'_s h'_i} & S^{(1)}_{h'_s v'_i} + S^{(2)}_{h'_s v'_i} \\ S^{(1)}_{v'_s h'_i} + S^{(2)}_{v'_s h'_i} & S^{(1)}_{v'_s v'_i} + S^{(2)}_{v'_s v'_i} \end{bmatrix} \begin{bmatrix} \widehat{\mathbf{v}}'_i.\widehat{\mathbf{v}}_i & \widehat{\mathbf{v}}'_i.\widehat{\mathbf{h}}_i \\ \widehat{\mathbf{h}}'_i.\widehat{\mathbf{v}}_i & .\widehat{\mathbf{h}}'_i.\widehat{\mathbf{h}}_i \end{bmatrix} \tag{3.115}$$

Now the components of scattered field, in global frame of reference, are given as

$$\begin{aligned} E^s_{pq} &= \left[\left(\mathbf{p}.\widehat{\mathbf{h}}'_s\right) \left\{ \left(\widehat{\mathbf{h}}'_i.\mathbf{q}\right) \left(S^{(1)}_{h'_s h'} + S^{(2)}_{h'_s h'}\right) + \left(\widehat{\mathbf{v}}'_i.\mathbf{q}\right) \left(S^{(1)}_{h'_s v'} + S^{(2)}_{h'_s v'}\right) \right\} \right. \\ &\quad \left. + \left(\mathbf{p}.\widehat{\mathbf{v}}'_s\right) \left\{ \left(\widehat{\mathbf{h}}'_i.\mathbf{q}\right) \left(S^{(1)}_{v'_s h'} + S^{(2)}_{v'_s h'}\right) + \left(\widehat{\mathbf{v}}'_i.\mathbf{q}\right) \left(S^{(1)}_{v'_s v'} + S^{(2)}_{v'_s v'}\right) \right\} \right] E_0 \end{aligned} \tag{3.116}$$

The improved scattering coefficient σ^s_{pq} as a function of the transmitter polarization q and the receiver polarization p is given by (3.117)

$$
\begin{aligned}
\sigma_{pq}^{2s} &= \Big\langle \left(\mathbf{p}.\widehat{\mathbf{h}}_s'\right)^2 \left(\widehat{\mathbf{h}}_i'.\mathbf{q}\right)^2 \left(\sigma_{h_s'h'}^{(1)} + \sigma_{h_s'h'}^{(12)} + \sigma_{h_s'h'}^{(21)} + \sigma_{h_s'h'}^{(2)}\right) \\
&+ \left(\mathbf{p}.\widehat{\mathbf{h}}_s'\right)^2 \left(\widehat{\mathbf{v}}_i'.\mathbf{q}\right)^2 \left(\sigma_{h_s'v'}^{(1)} + \sigma_{h_s'v'}^{(12)} + \sigma_{h_s'v'}^{(21)} + \sigma_{h_s'v'}^{(2)}\right) \\
&+ \left(\mathbf{p}.\widehat{\mathbf{v}}_s'\right)^2 \left(\widehat{\mathbf{h}}_i'.\mathbf{q}\right)^2 \left(\sigma_{v_s'h'}^{(1)} + \sigma_{v_s'h'}^{(12)} + \sigma_{v_s'h'}^{(21)} + \sigma_{v_s'h'}^{(2)}\right) \\
&+ \left(\mathbf{p}.\widehat{\mathbf{v}}_s'\right)^2 \left(\widehat{\mathbf{v}}_i'.\mathbf{q}\right)^2 \left(\sigma_{v_s'v'}^{(1)} + \sigma_{v_s'v'}^{(12)} + \sigma_{v_s'v'}^{(21)} + \sigma_{v_s'v'}^{(2)}\right) \\
&+ \left(\mathbf{p}.\widehat{\mathbf{v}}_s'\right)^2 \left(\widehat{\mathbf{h}}_i'.\mathbf{q}\right) \left(\widehat{\mathbf{v}}_i'.\mathbf{q}\right) \left(\sigma_{v_s'h'v_s'v'}^{(1)} + \sigma_{v_s'h'v_s'v'}^{(12)} + \sigma_{v_s'h'v_s'v'}^{(21)} + \sigma_{v_s'h'v_s'v'}^{(2)}\right) \\
&+ \left(\mathbf{p}.\widehat{\mathbf{v}}_s'\right)^2 \left(\widehat{\mathbf{h}}_i'.\mathbf{q}\right) \left(\widehat{\mathbf{v}}_i'.\mathbf{q}\right) \left(\sigma_{v_s'v'v_s'h'}^{(1)} + \sigma_{v_s'v'v_s'h'}^{(12)} + \sigma_{v_s'v'v_s'h'}^{(21)} + \sigma_{v_s'v'v_s'h'}^{(2)}\right) \\
&+ \left(\mathbf{p}.\widehat{\mathbf{h}}_s'\right) \left(\mathbf{p}.\widehat{\mathbf{v}}_s'\right) \left(\widehat{\mathbf{v}}_i'.\mathbf{q}\right)^2 \left(\sigma_{h_s'v'v_s'v'}^{(1)} + \sigma_{h_s'v'v_s'v'}^{(12)} + \sigma_{h_s'v'v_s'v'}^{(21)} + \sigma_{h_s'v'v_s'v'}^{(2)}\right) \\
&+ \left(\mathbf{p}.\widehat{\mathbf{h}}_s'\right) \left(\mathbf{p}.\widehat{\mathbf{v}}_s'\right) \left(\widehat{\mathbf{v}}_i'.\mathbf{q}\right)^2 \left(\sigma_{v_s'v'h_s'v'}^{(1)} + \sigma_{v_s'v'h_s'v'}^{(12)} + \sigma_{v_s'v'h_s'v'}^{(21)} + \sigma_{v_s'v'h_s'v'}^{(2)}\right) \\
&+ \left(\mathbf{p}.\widehat{\mathbf{h}}_s'\right)^2 \left(\widehat{\mathbf{h}}_i'.\mathbf{q}\right) \left(\widehat{\mathbf{v}}_i'.\mathbf{q}\right) \left(\sigma_{h_s'h'h_s'v'}^{(1)} + \sigma_{h_s'h'h_s'v'}^{(12)} + \sigma_{h_s'h'h_s'v'}^{(21)} + \sigma_{h_s'h'h_s'v'}^{(2)}\right) \\
&+ \left(\mathbf{p}.\widehat{\mathbf{h}}_s'\right)^2 \left(\widehat{\mathbf{h}}_i'.\mathbf{q}\right) \left(\widehat{\mathbf{v}}_i'.\mathbf{q}\right) \left(\sigma_{h_s'v'h_s'h''}^{(1)} + \sigma_{h_s'v'h_s'h'}^{(12)} + \sigma_{h_s'v'h_s'h'}^{(21)} + \sigma_{h_s'v'h_s'h'}^{(2)}\right) \\
&+ \left(\mathbf{p}.\widehat{\mathbf{h}}_s'\right) \left(\mathbf{p}.\widehat{\mathbf{v}}_s'\right) \left(\widehat{\mathbf{h}}_i'.\mathbf{q}\right)^2 \left(\sigma_{h_s'h'v_s'h'}^{(1)} + \sigma_{h_s'h'v_s'h'}^{(12)} + \sigma_{h_s'h'v_s'h'}^{(21)} + \sigma_{h_s'h'v_s'h'}^{(2)}\right) \\
&+ \left(\mathbf{p}.\widehat{\mathbf{h}}_s'\right) \left(\mathbf{p}.\widehat{\mathbf{v}}_s'\right) \left(\widehat{\mathbf{v}}_i'.\mathbf{q}\right) \left(\widehat{\mathbf{h}}_i'.\mathbf{q}\right) \left(\sigma_{h_s'v'v_s'h'}^{(1)} + \sigma_{h_s'v'v_s'h'}^{(12)} + \sigma_{h_s'v'v_s'h'}^{(21)} + \sigma_{h_s'v'v_s'h'}^{(2)}\right) \\
&+ \left(\mathbf{p}.\widehat{\mathbf{h}}_s'\right) \left(\mathbf{p}.\widehat{\mathbf{v}}_s'\right) \left(\widehat{\mathbf{v}}_i'.\mathbf{q}\right) \left(\widehat{\mathbf{h}}_i'.\mathbf{q}\right) \left(\sigma_{v_s'h'h_s'v'}^{(1)} + \sigma_{v_s'h'h_s'v'}^{(12)} + \sigma_{v_s'h'h_s'v'}^{(21)} + \sigma_{v_s'h'h_s'v'}^{(2)}\right) \\
&+ \left(\mathbf{p}.\widehat{\mathbf{h}}_s'\right) \left(\mathbf{p}.\widehat{\mathbf{v}}_s'\right) \left(\widehat{\mathbf{h}}_i'.\mathbf{q}\right) \left(\widehat{\mathbf{v}}_i'.\mathbf{q}\right) \left(\sigma_{h_s'h'v_s'v'}^{(1)} + \sigma_{h_s'h'v_s'v'}^{(12)} + \sigma_{h_s'h'v_s'v'}^{(21)} + \sigma_{h_s'h'v_s'v'}^{(2)}\right) \\
&+ \left(\mathbf{p}.\widehat{\mathbf{h}}_s'\right) \left(\mathbf{p}.\widehat{\mathbf{v}}_s'\right) \left(\widehat{\mathbf{h}}_i'.\mathbf{q}\right) \left(\widehat{\mathbf{v}}_i'.\mathbf{q}\right) \left(\sigma_{v_s'v'h_s'h'}^{(1)} + \sigma_{v_s'v'h_s'h'}^{(12)} + \sigma_{v_s'v'h_s'h'}^{(21)} + \sigma_{v_s'v'h_s'h'}^{(2)}\right) \\
&+ \left(\mathbf{p}.\widehat{\mathbf{h}}_s'\right) \left(\mathbf{q}.\widehat{\mathbf{v}}_s'\right) \left(\widehat{\mathbf{h}}_i'.\mathbf{q}\right)^2 \left(\sigma_{v_s'h'h_s'h'}^{(1)} + \sigma_{v_s'h'h_s'h'}^{(12)} + \sigma_{v_s'h'h_s'h'}^{(21)} + \sigma_{v_s'h'h_s'h'}^{(2)}\right) \Big\rangle \qquad (3.117)
\end{aligned}
$$

where $\sigma_{p'q'}^{(1)}$ and $\sigma_{p'q'm'n'}^{(1)}$ are obtained from (3.110) & (3.111) and $\sigma_{p'q'}^{(2)}$ and $\sigma_{p'q'm'n'}^{(2)}$ are given by

$$
\begin{aligned}
\sigma_{p'q'}^{(2)} &= 4\pi K^6 \cos^2\theta_i' \cos^2\theta_s' \int_{-\infty}^{\infty}\int_{-\infty}^{\infty} W\left(k_{sx}-k_x, k_{sy}-k_y\right) W\left(k_x-k_{ix}, k_y-k_{iy}\right) \\
&\quad \alpha_{p'q'}^{(2)} \left[\alpha_{p'q'}^{*(2)} + \beta_{p'q'}^{*(2)}\right] dk_x dk_y \qquad (3.118)
\end{aligned}
$$

$$
\begin{aligned}
\sigma_{p'q'm'n'}^{(2)} &= 4\pi k^6 \cos^2\theta_i' \cos^2\theta_s' \int_{-\infty}^{\infty}\int_{-\infty}^{\infty} W\left(k_{sx}-k_x, k_{sy}-k_y\right) W\left(k_x-k_{ix}, k_y-k_{iy}\right) \\
&\quad \alpha_{p'q'}^{(2)} \left[\alpha_{m'n'}^{*(2)} + \beta_{m'n'}^{*(2)}\right] dk_x dk_y \qquad (3.119)
\end{aligned}
$$

the polarization dependent coefficients can be calculated using ((A.29)-(A.36)) at local angles. Note that while doing numerical simulations, for the sake of simplicity, we ignore the terms involving the product of first and second order fields i.e., $\sigma^{(12)}_{p'q'}$ and $\sigma^{(12)}_{p'q'm'n'}$.

Backscattering

In case of backscattering (3.117) reduces to

$$\begin{aligned}
\sigma^{2s}_{pq} \;=\; & \Big\langle \left(\mathbf{p}.\widehat{\mathbf{h}}'_s\right)^2 \left(\widehat{\mathbf{h}}'.\mathbf{q}\right)^2 \left(\sigma^{(1)}_{h'_s h'} + \sigma^{(2)}_{h'_s h'}\right) + \left(\mathbf{p}.\widehat{\mathbf{h}}'_s\right)^2 \left(\widehat{\mathbf{v}}'.\mathbf{q}\right)^2 \sigma^{(2)}_{h'_s v'} \\
& + \left(\mathbf{p}.\widehat{\mathbf{v}}'_s\right)^2 \left(\widehat{\mathbf{h}}'.\mathbf{q}\right)^2 \sigma^{(2)}_{v'_s h'} + \left(\mathbf{p}.\widehat{\mathbf{v}}'_s\right)^2 \left(\widehat{\mathbf{v}}'.\mathbf{q}\right)^2 \left(\sigma^{(1)}_{v'_s v'} + \sigma^{(2)}_{v'_s v'}\right) \\
& + \left(\mathbf{p}.\widehat{\mathbf{v}}'_s\right)^2 \left(\widehat{\mathbf{h}}'.\mathbf{q}\right) \left(\widehat{\mathbf{v}}'.\mathbf{q}\right) \sigma^{(2)}_{v'_s h' v'_s v'} + \left(\mathbf{p}.\widehat{\mathbf{v}}'_s\right)^2 \left(\widehat{\mathbf{h}}'.\mathbf{q}\right) \left(\widehat{\mathbf{v}}'.\mathbf{q}\right) \sigma^{(2)}_{v'_s v' v'_s h'} \\
& + \left(\mathbf{p}.\widehat{\mathbf{h}}'_s\right) \left(\mathbf{p}.\widehat{\mathbf{v}}'_s\right) \left(\widehat{\mathbf{v}}'.\mathbf{q}\right)^2 \sigma^{(2)}_{h'_s v' v'_s v'} + \left(\mathbf{p}.\widehat{\mathbf{h}}'_s\right) \left(\mathbf{p}.\widehat{\mathbf{v}}'_s\right) \left(\widehat{\mathbf{v}}'.\mathbf{q}\right)^2 \sigma^{(2)}_{v'_s v' h'_s v'} \\
& + \left(\mathbf{p}.\widehat{\mathbf{h}}'_s\right)^2 \left(\widehat{\mathbf{h}}'.\mathbf{q}\right) \left(\widehat{\mathbf{v}}'.\mathbf{q}\right) \sigma^{(2)}_{h'_s h' h'_s v'} + \left(\mathbf{p}.\widehat{\mathbf{h}}'_s\right)^2 \left(\widehat{\mathbf{h}}'.\mathbf{q}\right) \left(\widehat{\mathbf{v}}'.\mathbf{q}\right) \sigma^{(2)}_{h'_s v' h'_s h'} \\
& + \left(\mathbf{p}.\widehat{\mathbf{h}}'_s\right) \left(\mathbf{p}.\widehat{\mathbf{v}}'_s\right) \left(\widehat{\mathbf{v}}'.\mathbf{q}\right) \left(\widehat{\mathbf{h}}'.\mathbf{q}\right) \sigma^{(2)}_{v'_s h' h'_s v'} + \left(\mathbf{p}.\widehat{\mathbf{h}}'_s\right) \left(\mathbf{q}_s.\widehat{\mathbf{v}}'_s\right) \left(\widehat{\mathbf{h}}'.\mathbf{q}\right)^2 \sigma^{(2)}_{v'_s h' h'_s h'} \\
& + \left(\mathbf{p}.\widehat{\mathbf{h}}'_s\right) \left(\mathbf{p}.\widehat{\mathbf{v}}'_s\right) \left(\widehat{\mathbf{h}}'.\mathbf{q}\right)^2 \sigma^{(2)}_{h'_s h' v'_s h'} + \left(\mathbf{p}.\widehat{\mathbf{h}}'_s\right) \left(\mathbf{p}.\widehat{\mathbf{v}}'_s\right) \left(\widehat{\mathbf{v}}'.\mathbf{q}\right) \left(\widehat{\mathbf{h}}'.\mathbf{q}\right) \sigma^{(2)}_{h'_s v' v'_s h'} \\
& + \left(\mathbf{p}.\widehat{\mathbf{h}}'_s\right) \left(\mathbf{p}.\widehat{\mathbf{v}}'_s\right) \left(\widehat{\mathbf{h}}'.\mathbf{q}\right) \left(\widehat{\mathbf{v}}'.\mathbf{q}\right) \left(\sigma^{(1)}_{h'_s h' v'_s v'} + \sigma^{(2)}_{h'_s h' v'_s v'}\right) \\
& + \left(\mathbf{p}.\widehat{\mathbf{h}}'_s\right) \left(\mathbf{p}.\widehat{\mathbf{v}}'_s\right) \left(\widehat{\mathbf{h}}'.\mathbf{q}\right) \left(\widehat{\mathbf{v}}'.\mathbf{q}\right) \left(\sigma^{(1)}_{v'_s v' h'_s h'} + \sigma^{(2)}_{v'_s v' h'_s h'}\right) \Big\rangle \qquad (3.120)
\end{aligned}$$

and the reduced polarization dependent coefficients are obtained from (3.78)-(3.85) at local angles.

By comparing the first and second order bistatic scattering coefficients from 3.109 & 3.117 we can see that there are large number of terms which are present in 3.117 due to the inclusion of second order scattering effect by SPM2. Moreover, in the backscattering case the calculation of σ^{1s}_{pq} from 3.113 involves only co-polarization terms and all the first order cross-polarization coefficients and cross correlations become zero. However, in the calculation of σ^{2s}_{pq}, along with the co-polarization coefficients the cross-polarization coefficients and cross-correlation terms in local domain are calculated by second order coefficients. In previous section, by doing the comparisons between the numerical simulation by SPM1 and SPM2 we have seen that, for certain configurations, SPM2 give enhanced bistatic scattering and the cross polarization estimation by SPM2 is non-zero.

Hence, the addition of second order terms in TSM2 can produce enhanced bistatic scattering and the accurate depolarization predictions. However, on the other hand the inclusion of second order terms makes the problem computationally complex and

the calculation of many integral terms take long time to produce the results. We will check the bistatic scattering enhancement and cross polarization estimation by TSM2 in chapter 5 where the numerical results by TSM2 will be presented and compared with the results of other techniques and experimental data published in literature. We will give the application of TSM2 for sea and bare soil surfaces and evaluate the new method for a variety of conditions/configurations.

Chapter 4

Modeling of the rough surface

The diffusion of electromagnetic waves by the rough surface, being assimilated to a dielectric random rough surface, requires the knowledge of electromagnetic characteristics and the state of rough surface. Therefore it is essential to have a realistic description of the rough surface in order to estimate the diffused electromagnetic field. The principal objective of this chapter is to elaborate the modeling and statistical description of the sea and soil surface.

4.1 Introduction

The sea can be considered as a random physical system whose evolution is governed by the wind and gravity: more the wind is strong and blows for long time, more agitated is the sea. The waves at each point of a surface result from a summation of waves locally generated by the wind and waves coming from other directions and regions. These interactions make the phenomenon very difficult to quantify. The sea surface thus presents a chaotic state and its deterministic modeling is enough difficult, that's why a probabilistic (statistical) approach will be considered.

The soil surface is also complex to study due to the multitude of its physical, chemical, and biological characteristics. Soil is relative combination of sand, silt, and clay. The particles make up about 50 percent of the soil's volume. Pores containing air and/or water occupy the remaining volume [83].

To study the scattering of electromagnetic waves by the sea and soil surface it is necessary to consider the geometrical modeling and physical characteristics of these surfaces. In this chapter, we start by defining and analyzing the electromagnetic characteristics (permittivity and permeability) of sea and soil surface. Then the geometrical representation of these surfaces will be given.

4.1.1 Physical characteristics

A dielectric medium is generally described by its relative electric permittivity ε_r and its relative magnetic permeability μ_r [84].

Magnetic permeability

Dielectric surface can have an influence on the electromagnetic wave by the means of its magnetic permeability μ. However, in our study, the sea water will be supposed to be a nonmagnetic medium ($\mu_r = 1$). Thus, only its relative electric permittivity ε_r will be taken into account.

In case of soil surface, again we approximate the magnetic permeability to 1 to present the "diamagnetic (a relative permeability is slightly less than 1)" and "paramagnetic (a relative permeability is slightly greater than 1)" type of surfaces. The "ferromagnetic" type surfaces will not be considered in this thesis.

Electric permittivity for sea surface

The relative dielectric constant ε_r is defined as the ratio of the dielectric constant of the surface ε by the permittivity of a vacuum ε_0. For sea surface, it depends on the frequency of the wave $f = \omega/2\pi$, temperature T and salinity S of sea water whose average is about $S = 35\ \%_0(35g/l)$ [85].

In literature, two models are commonly used to define the permittivity of water: the model of Debye [86] and the model of Cole-Cole [87, 88].

Model of Debye According to Debye the value of ε_r of a given medium depends on the value of the frequency of the imposed magnetic field as well as the physical state of the medium. It may take into account the macroscopic variables such as the temperature and the pressure in terms of molecular properties [85, 86, 89]. One can therefore, expect that ε_r can also be expressed in term of these molecular properties. The distribution of electric charges in a molecule may give the properties of a dipole (or multipole for complex molecules) and the imposed electromagnetic field can act on the dipoles of the molecule in a classical manner according to the theory of the continuous medium. By using such reasoning Debye [86] showed that if one models a polar liquid by spherical oscillating dipoles in a continuous viscous medium, then the dependance of ε with the frequency of electromagnetic field is given by [86]

$$\varepsilon_r = \varepsilon_\infty + \frac{\varepsilon_s - \varepsilon_\infty}{1 + j\omega\tau} \tag{4.1}$$

In case of salted water we have:

$$\varepsilon_r = \varepsilon_\infty + \frac{\varepsilon_s - \varepsilon_\infty}{1 + j\omega\tau} - j\frac{\sigma}{\omega\varepsilon_0} \tag{4.2}$$

with $\varepsilon_0 = 8.854 \times 10^{-12} fm^{-1}$ is the permittivity of the free space, $\varepsilon_\infty = 4.9$ is the electric permittivity for very high frequency, $\omega = 2\pi f$, f is the frequency (in Hz.) of electromagnetic wave, ε_s and σ are the static permittivity and the ionic conductivity of sea water, respectively. The mathematical formulation of the functions $\varepsilon_s, \sigma$and τ is presented in Appendix B.

Behavior of a dialectic constant as a function of frequency Figure 4.1 represent the variation of the real part of the permittivity of sea water ε_r as a function of frequency, for different values of temperature and salinity. This part can be break

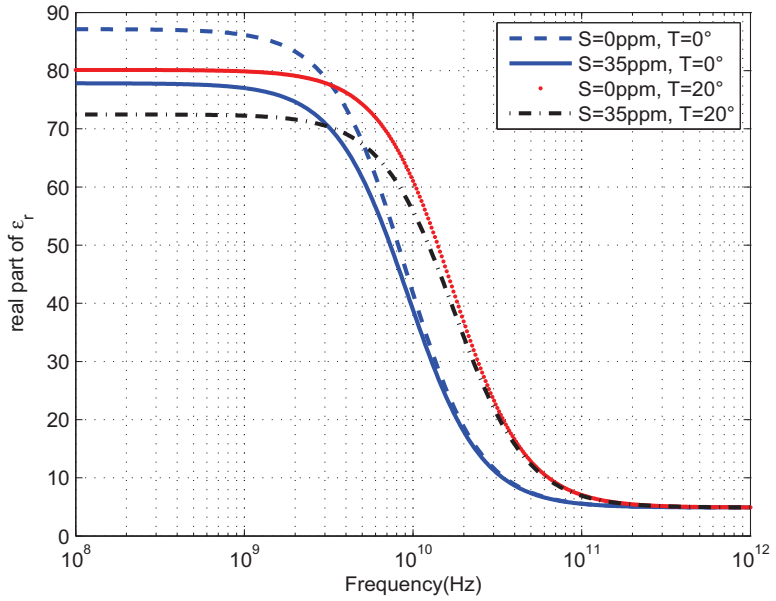

Figure 4.1: Evolution of the real part of the permittivity of sea water as a function of frequency

up into three domains according to the frequency.

- An approximately constant part corresponds to the zone of the low frequencies. In this part ε_r is approximately equal to static permittivity ε_s.

- A zone of abrupt transition correspond to the cut-off frequency from the real part of the permittivity ($f_c = \frac{1}{2\pi\sqrt{3t_r}}$)

- Finally a high frequency zone, correspond approximately to the limiting value of permittivity (ε_{ir}).

Every zone possesses a different behavior according to the temperature. Thus, in the first part, the effect of temperature is marked by a translation of curves towards the x-axis. This behavior explains by the predominance of the term of static permittivity. In the second part, the value of the cut of frequency moves towards the high frequencies when the temperature increases. In the last zone, the influence of the temperature remains negligible.

Next Fig. 4.2 represent the variation of the imaginary part of the permittivity of sea water ε_r as a function of frequency, for different values of temperature and salinity.

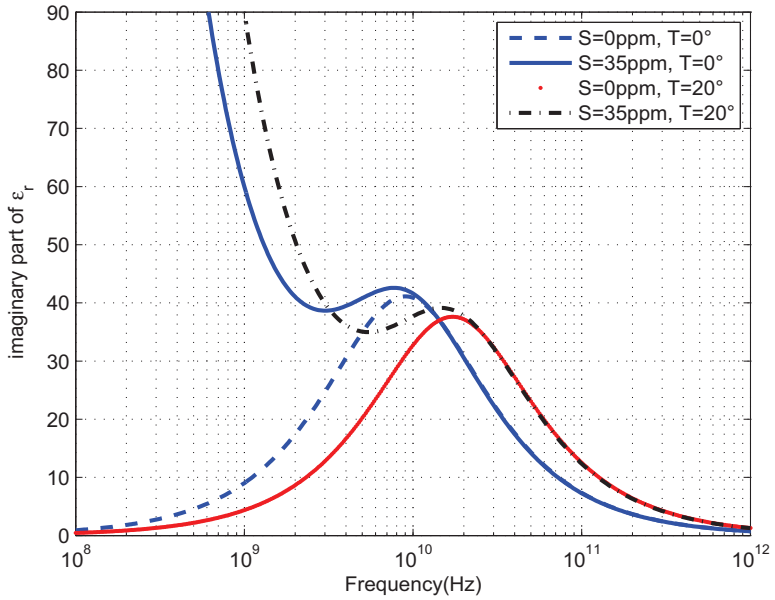

Figure 4.2: Evolution of the imaginary part of the permittivity of sea water as a function of frequency

The imaginary part of the permittivity presents three different behaviors according to the frequency:

- A fast reduction for low frequencies. In this case, an increase in temperature causes a translation of the curves towards the higher values.

- A transition zone with a relative maximum of which the behavior is inversely proportional to the temperature (As temperature decreases the maximum height increases).

- A decrease in the imaginary part for important frequencies has a similar behavior with respect to temperature and is identical to the first part.

The dielectric surface can equally have an influence on the electromagnetic wave because of his magnetic permeability μ. Nevertheless, in our study, sea water will be

supposed to be a non magnetic environment ($\mu = 1$). Thus, alone his relative electric permittivity ε_r will be taken into account.

Model of Cole-Cole The model of Cole-Cole is an empirical model that results from the model of Debye [87, 88]. For this model we added an empirical constant α, thus the model became

$$\varepsilon_r = \varepsilon_\infty + \frac{\varepsilon_s - \varepsilon_\infty}{1 + (j\omega\tau)^{1-\alpha}} \tag{4.3}$$

where $0 \leq \alpha \leq 1$. Its value is 0.02 estimated by Klein and Swift [85].

This function is known as the "distribution of Cole-Cole" is valid for freshwater. In case of salted water we have:

$$\varepsilon_r = \varepsilon_\infty + \frac{\varepsilon_s - \varepsilon_\infty}{1 + (j\omega\tau)^{1-\alpha}} - j\frac{\sigma}{\omega\varepsilon_0} \tag{4.4}$$

The representation of this model shows that there is not a significant difference with the model of Debye. The model of Debye is practically the only one that is based on clearly stated hypothesis and which reflects a rigorous dependence between ε, ω and physical parameters depending on the considered medium. In our calculations we use the dielectric constant given by model of Debye.

Electric permittivity for soil surface

The soil has a composition more complex than the sea and for this reason we use semi-empirical models for the electric permittivity of soil surface. The models of Topp and Dobson-Peplinsky, widely used in the literature are presented in this paragraph.

Topp's model According to Topp et al. [90], the humidity can be directly determined from the dielectric permittivity. These two parameters are linked by empirical polynomial functions, determined through a regression of order 3.

$$\begin{aligned} \varepsilon'' &= 3.03 + 9.3m_v + 146m_v^2 - 76.3m_v^{"} \\ m_v &= -5.3 \times 10^{-2} + 2.92 \times 10^{-2}\varepsilon' - 5.5 \times 10^{-4}\varepsilon'^2 + 4.3 \times 10^{-6}\varepsilon'^3 \end{aligned} \tag{4.5}$$

where $\varepsilon_r = \varepsilon' + j\varepsilon''$.

This model has the advantage of being independent of the frequency of observation, soil texture, temperature and its salinity. However, it is only valid for the frequency band [20 MHz - 1 GHz] and do not consider the imaginary part of dielectric constant.

Dobson-Peplinsky model The dielectric permittivity model most commonly used in the literature for soil surface was developed by Dobson et al. [91] . It is defined on the frequency range [1.4 GHz - 18 GHz] and more important than the model of Topp as it depends on the volumetric moisture content, the size of soil particles, the different components of soil, the dielectric constant of water and frequency.

This semi-empirical model based on the formula of multi-phase mixture containing randomly oriented inclusions [92] and experimental measurements. The dielectric permittivity is defined as:

$$\varepsilon' = \left[1 + \frac{\rho_b}{\rho_s}(\varepsilon_s^\alpha - 1) + m_v^{\beta'}\varepsilon_{f\omega}'^\alpha - m_v\right]^{\frac{1}{\alpha}} \tag{4.6}$$

$$\varepsilon'' = \left[m_v^{\beta''}\varepsilon_{f\omega}''^\alpha\right]^{\frac{1}{\alpha}} \tag{4.7}$$

where ρ_b is the density of ground-air mixture, $\rho_s \approx 2.66 g/cm^3$ is the density of soil particles, $\varepsilon_s \approx 4.7$ is the permittivity of the soil particles, $\alpha \approx 0.65$ is an empirical constant form factor and β' and β'' are two coefficients dependent on soil texture defined by:

$$\beta' = 1.2748 - 0.519S - 0.152A \tag{4.8}$$

$$\beta'' = 1.33797 - 0.603S - 0.1666A \tag{4.9}$$

where S and A represent respectively the rates of sand and clay content.

The frequency dependence occurs in the permittivity of free water, calculated in using the Debye equation.

For the frequency range [0.3 GHz - 1.3 GHz], this model underestimates the real part of the dielectric permittivity. Peplinsky [93] extended the validity of the Dobson model to this frequency domain by the following correction:

$$\varepsilon' = 1.15\varepsilon' - 0.68 \tag{4.10}$$

4.1.2 Geometrical characteristics

In this section we study the geometrical characteristics of sea and soil surface by using their slope distributions and rough surface spectrums.

Distribution of the slopes

In this paragraph two laws of distribution of the slopes are presented: Gaussian distribution and Cox & Munk distribution. We use the Gaussian distribution for soil surface and Cox & Munk slope distribution for sea surface.

Gaussian distribution The Gaussian distribution is defined by two parameters σ_u^2 and σ_c^2 which are the variances of the slopes of the surface of capillarity waves, respectively in the direction of wind and the transverse direction of wind. These two parameters were established by Cox & Munk [94] from the photographic measures of sun glitter on the sea. Thus an analytical expression (4.11) was proposed, it is given by

$$Pr(Z_x, Z_y) = \frac{1}{2\pi\sigma_u\sigma_c} e^{-\frac{1}{2}\left(\frac{Z_x^2}{\sigma_u^2}+\frac{Z_y^2}{\sigma_c^2}\right)} \tag{4.11}$$

with

$$\begin{aligned} \sigma_u^2 &= 0.005 + 0.78\ 10^{-3} U_{12.5} \\ \sigma_c^2 &= 0.003 + 0.84\ 10^{-3} U_{12.5} \end{aligned} \tag{4.12}$$

$U_{12.5}(m/s)$ is the wind speed at altitude 12.5 meters.

We note that this distribution is symmetric about mean value.For sea surface this does not correspond to the real phenomenon where one must have an asymmetry for the direction facing the wind. The phenomenon was considered in the works of Cox & Munk [94, 95].

Distribution of Cox & Munk Cox & Munk proposed a more complex model to translate the asymmetry of the slopes. The proposed distribution is given by [95] :

$$Pr(Z_x, Z_y) = \frac{F(Z_x, Z_y)}{2\pi\sigma_u\sigma_c} e^{-\frac{1}{2}\left(\frac{Z_x^2}{\sigma_u^2}+\frac{Z_y^2}{\sigma_{cu}^2}\right)} \tag{4.13}$$

with

$$\begin{aligned} F(Z_x, Z_y) &= 1 - \frac{C_{21}}{2}\left[\frac{Z_y^2}{\sigma_c^2 - 1}\right]\frac{Z_x}{\sigma_u} - \frac{C_{03}}{6}\left[\frac{Z_x^3}{\sigma_u^3 - 3\frac{Z_x}{\sigma_u}}\right] + ... \\ &\quad ... + \frac{C_{40}}{24}\left[\frac{Z_y^4}{\sigma_c^4 - 6\frac{Z_y^2}{\sigma_c^2}} + 3\right] + \frac{C_{22}}{4}\left[\frac{Z_y^2}{\sigma_c^2 - 1}\right]\left[\frac{Z_x^2}{\sigma_u^2 - 1}\right] + \frac{C_{04}}{24}\left[\frac{Z_x^4}{\sigma_u^4 - 6\frac{Z_x^2}{\sigma_u^2}}\right] \end{aligned} \tag{4.14}$$

C_{21}, C_{03}, C_{40}, C_{22} and C_{04} are the coefficients dependent upon the wind speed $U_{12.5}$ given to an altitude of 12,5m

$$\begin{aligned} C_{21} &= 0.01 - 0.0086.U_{12.5};\ C_{03} = 0.04 - 0.033.U_{12.5} \\ C_{40} &= 0.4;\ C_{22} = 0.12;\ C_{04} = 0.23 \end{aligned}$$

Z_x is the slope in the wind direction and Z_y is the slope in the crosswind direction. To identify the different parameters figured in the analytical equation (3.27), Cox & Munk took optical measurements on two types of surfaces

– SSM ≡ "Slick Sea Model", obtained from measures on a covered sea of an oil film to eliminate the effects of capillary waves,

$$\begin{aligned} \sigma_u^2 &= 0.005 + 0.78\ 10^{-3} U_{12.5} \\ \sigma_c^2 &= 0.003 + 0.84\ 10^{-3} U_{12.5} \end{aligned} \tag{4.15}$$

–CSM ≡ "Clean Sea Model", obtained according to a "clean" sea :

$$\begin{aligned} \sigma_u^2 &= 3.16 \times 10^{-3}{}_{12.5} \\ \sigma_c^2 &= 0.003 + 1.92 \times 10^{-3} U_{12.5} \end{aligned} \tag{4.16}$$

Such a distribution appears more probable owing to the fact that it highlights the asymmetry of the slopes as compared to the direction of the wind: the slopes in the direction “back wind” are on average stronger than in the direction “upwind ". A comparison of gaussian distribution and cox & munk is given in the following figure (Fig. 4.3) for upwind and crosswind direction.

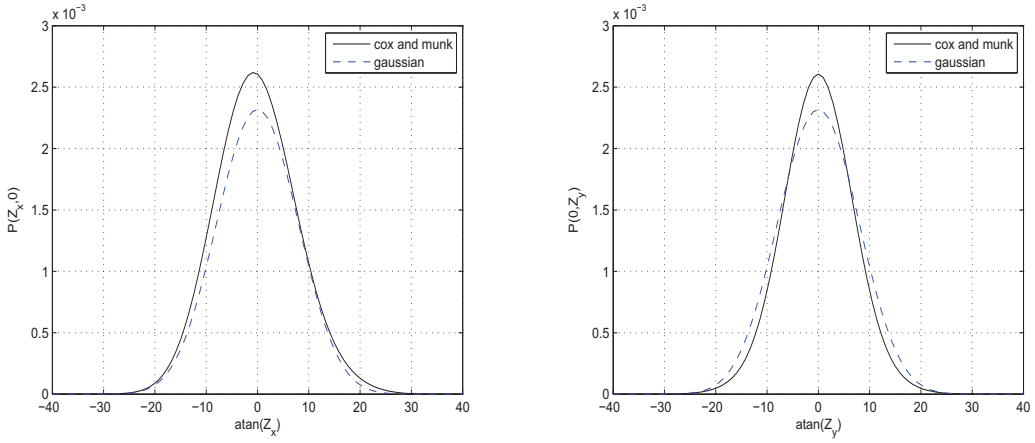

(a)upwind (b)crosswind

Figure 4.3: Slope distribution representation(wind speed U12.5=15m/s)

Surface spectrum models

Among statistical descriptions of waves, spectral formulation is generally privileged from the early work of Phillips [1958]. There is a wealth of theoretical and empirical studies detailing candidate equilibrium wind wave spectra in the literature [e.g., Toba, 1073; Hasselmannet al., 1973; Mitsuyasu and Honda, 1974; Kahma, 1981; Donelan et al., 1985]. Presently it is well-accepted that the long-wave spectrum resulting from the

Joint North Sea Wave Project [96] (JONSWAP[Hasselmann et al., 1973]) reasonably represents fetch-limited wind wave development. The spectrum of Apel is a synthesis the work carried out in the years 1980-1990. and more recently Elfouhaily [97] has proposed a spectrum by including physical criteria. This last model will be adopted in the study of the scattering phenomenon by the sea surface and exponential spectrum will be used for soil surface. Analysis of the behavior of these spectral models is approached in the following paragraph.

Gaussian spectrum This model is generally used in literature to characterize a random surface it probability density function can be written as

$$P(z) = \frac{1}{h\sqrt{2\pi}} e^{\frac{-z^2}{2h^2}} \tag{4.17}$$

where h is the variance of height. The autocorrelation function of Gaussian spectrum can be written as [79] :

$$\rho(R) = e^{\frac{-R^2}{l^2}} \tag{4.18}$$

where l is the correlation length. The spectrum is obtained by taking the Fourier transform of $\rho(R)$, its expression is given by

$$S(K) = \frac{l^2}{2} e^{\frac{-l^2}{4}K^2} \tag{4.19}$$

This expression can be extended to bidimensional case. It is sufficient to replace K by its components which gives

$$S(K_x, K_y) = \frac{l^2 h^2}{2} e^{\frac{-l^2}{4}\left(K_x^2 + K_y^2\right)} \tag{4.20}$$

The Gaussian model describes a random configuration of diffused surface.To define it its sufficient to precise the variance and correlation length. However these parameters are insufficient to describe the reality of marine surfaces which depends primarily on the force and the direction on the wind, from where need for the more realistic models.

Elfouhaily spectrum The Elfouhaily spectrum [97] establishes in 1997 is a synthesis of the whole work on the ocean behavior carried out since 1970 . He elaborated by taking in to account the experimental and theoretical facts which Pierson had not considered, like for example the slope model of Cox and Munk [95], moreover the fetch is also included. The bidirectional analytic expression is defined as a product of the isotropic part $S(K)$ with an angular distribution function $f(K, \varphi)$

$$S(K, \varphi) = S(K) f(K, \varphi)$$

The isotropic part is expressed in two terms, one depends on the capillary waves and the other on gravity waves. Their analytic expressions are given by

$$S(K) = K^{-3}\left[B_L(K) + B_H(K))\right] \tag{4.21}$$

where B_L and B_H represents the contribution of low and high frequency.

$$B_L(K) = \alpha_p F_p c(K_p)/2c(K) \tag{4.22}$$

The parameters in 4.21 depends on U_{10}, the wind speed at altitude $10m$ from the sea surface and $\Omega \approx c(K_p)/2c(K)$ is the inverse age of wave where $c(K)$ is the phase speed and K_p is the wave number for the maximum value of spectrum.

$$\alpha_p = 0.006\Omega^{\frac{1}{2}} \quad K_p = g\Omega^2/U_{10}^2 \quad c(K) = \left[g\left(1 + K^2/K_m^2\right)/K\right]^{\frac{1}{2}} \tag{4.23}$$

with $g = 9.81m/s^2$.

$$\Omega = 0.84 tanh\left[(X/X_0)^{0.4}\right]^{-0.75} \quad \text{with} \quad X_0 = 2.2 \times 10^4 \tag{4.24}$$

where X is the fetch of wind expressed in m. For a developed sea the value of fetch is relatively large. With $K_m = 370m^{-1}$, the function F_p in 4.22 is given by

$$F_p = \gamma^{\Gamma} \exp\left[-5\left(K_p/K\right)^2/4\right] \exp\left\{-\Omega\left[(K/K_p)^{\frac{1}{2}} - 1\right]/\sqrt{10}\right\} \tag{4.25}$$

where

$$\begin{aligned} \gamma &= 1.7 && 0.84 < \Omega \leq 1 \\ &= 1.7 + 6\log(\Omega) && 1 \leq \Omega < 5 \end{aligned}$$

$$\Gamma = \exp\left\{-\left[(K/K_p)^{\frac{1}{2}} - 1\right]^2/2\partial^2\right\} \qquad \partial = 0.08\left(1 + 4/\Omega^3\right)$$

The contribution of capillary waves in 4.21 is given by

$$B_H(K) = \alpha_m F_m c(K_m)/2c(K) \tag{4.26}$$

where

$$\alpha_m = 0.01\{ \begin{array}{ll} 1 + \ln\left[v_f/c(K_m)\right] & v_f \leq c(K_m) \\ 1 + 3\ln\left[v_f/c(K_m)\right] & v_f > c(K_m) \end{array} \tag{4.27}$$

The friction speed v_f is given by the relation$v_f = C_{10}^{\frac{1}{2}} U_{10}$ with

$$C_{10} = (0.8 + 0.065U_{10}) \times 10^{-3}$$

wherev_f and U_{10} are expressed in ms^{-1}.At the end

$$F_m = \exp\left[-\left(1 - K/K_m\right)^2/4\right] \exp\left[-5\left(K_p/K\right)^2/4\right] \tag{4.28}$$

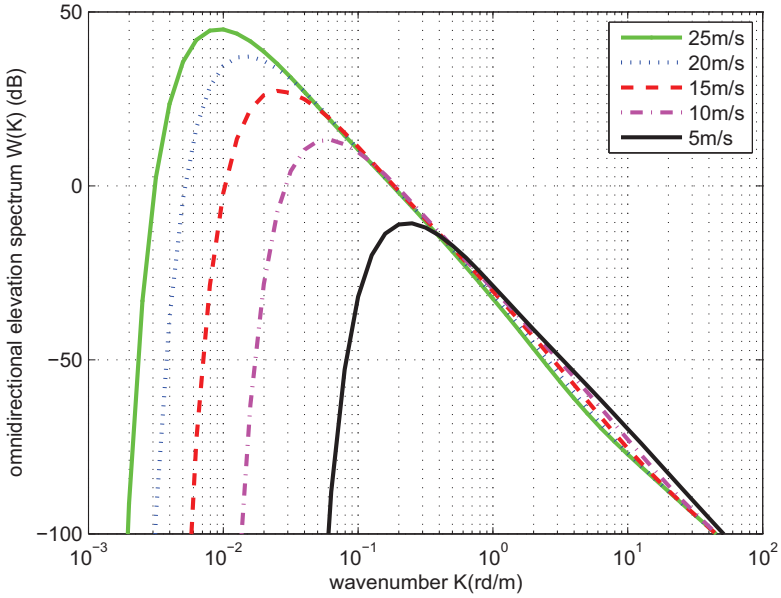

Figure 4.4: Elfouhaily sea surface spectra with different wind speeds

The omnidirectional spectrum for different wind speed is shown in the Fig. 4.4
The proposed angular function $f(K,\varphi)$ is given by

$$f(K,\varphi) = \frac{1}{2\pi}\left[1 + \Delta(K) \times \cos(2\varphi)\right] \tag{4.29}$$

The function $\Delta(K)$ proposed by Elfouhaily gives the transfer of energy from small waves towards long waves. When the wind speed increases it can be written as

$$\Delta(K) = \tanh\left[a_0 + a_g\left(\frac{c}{c_g}\right)^{2.5} + a_c\left(\frac{c_m}{c}\right)^{2.5}\right] \tag{4.30}$$

with

$$\begin{cases} a_0 = 0.173, \\ a_g = 4 \\ a_c = 0.13\frac{u_f}{c_m} \end{cases} \tag{4.31}$$

The variation of angular function for different wind speeds can be seen in the Fig. 4.5

Exponential Distribution The exponential correlation function is a more realistic choice for soil surface as fine-scale features that are more irregular than that of Gaussian correlation function and appear to match experimental data much better than Gaussian correlation functions [98, 99].

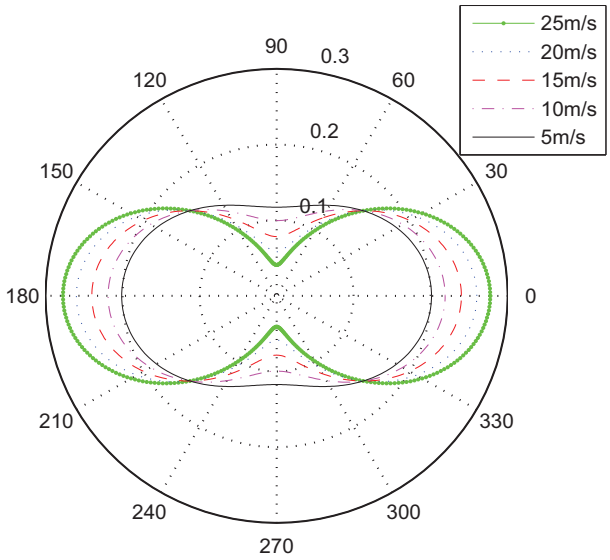

Figure 4.5: Variation of angular function for different wind speeds

For one and two dimensional surfaces the exponential spectrum are given respectively, by

$$S(K) = \frac{h^2 l}{\pi} \frac{1}{1 + K^2 l^2} \tag{4.32}$$

$$S(K) = \frac{h^2 l^2}{\pi} \frac{1}{1 + K_x^2 l^2} \frac{1}{1 + K_y^2 l^2} \tag{4.33}$$

where h is rms height, l is correlation length, and K is surface wave number.

Chapter 5

Applications and Numerical Simulations

To study the bistatic scattering enhancement at grazing angles and the exact depolarization estimation by TSM2, the numerical results and comparisons with experimental data and other analytical approximate techniques are presented in this chapter. The applications are given for sea and bare soil surface and the bistatic scattering coefficient is analyzed as a function of roughness parameters like incident and scattered angles, frequency, rms height and correlation length etc.

5.1 Introduction

Wave scattering by rough surfaces is an important issue in diverse areas of science such as measurements in medical, optics, acoustics, geophysics, communications and terrestrial or extraterrestrial remote sensing. Approximate models are still a necessity due to the insurmountable numerical complexity of realistic scattering problems. Even today's machines cannot cope with the enormous amount of computing demanded in the case of rigorous numerical calculations of the most general three-dimensional electromagnetic wave scattering from dielectric or conducting multi-scale surfaces.

This necessity has sprung the development of approximate models. Over the years considerable effort has been devoted to the development of such models which can predict accurately the bistatic scattering by rough surfaces. Among them, we can cite the Small Perturbation Method (SPM) [23]–[26],[69]–[71] the Kirchhoff Approximation (KA) [19]–[22], the Phase Perturbation Technique (PPT) [58, 100, 101], the Small Slope Approximation (SSA) [102]–[105], Weighted Curvature Approximation (WCA) [106]–[109] and the Two Scale Model (TSM) [1, 5], [27]–[30], [59, 60], [78]–[82] etc. However, these methods have restricted domain of validity and **it is difficult to find**

Methods	Example of methods	Advantages	Disadvantages
Exact	Method of moments Finite difference methods Boundary integral methods	(Quasi-) exact for the considered (deterministic) surface	very slow, memory occupation, complex
Approximate	**Specular reflection**: KA **Diffuse reflection**: SPM, TSM **Composite methods**: SSA1,WCA, PPT, LCA, IEM (KA+SPM1, SPM1+PO, ...)	very fast and stable while easy to implement (KA, SPM, TSM, SSA) relatively simple (other methods)	restricted validity domain, only average coefficient for an infinite surface, no depolarization prediction in incidence plane
Hybrid	weighted SPM/KA in local frame associated to a facet	Sufficiently fast	not rigorously exact

Table 5.1: Comparison of methods to calculate the scattering coefficient of a rough surface

a single approximation which is reliable over the whole range of scattering angles. A brief comparison of some of the existing models is given table 5.1.

The domain of validity of the most classical approximate models has been studied in [110]. Generally, the KA requires that the incident wavelength be much smaller than the radius of curvature of the surface and it accurately predicts incoherent scattering near the specular direction [21, 61, 77] . First-order perturbation theory (SPM1) is valid away from specular region when the surface standard deviation is small compared with the wavelength [21, 61, 73, 74, 111] . The SSA [102, 103] reconcile SPM1 and KA as a unifying theory and is applicable for a surface with small slope and moderate height. SSA1 considerably extends the validity domain of SPM, but remains outer performed by KA for large roughness in the domain where this last method is known to be accurate. PPT recover KA and SPM in the appropriate limits, and possess a wider validity domain than the standard approximations. It gives accurate predictions away from low scattered grazing angles ($|\theta_s| \leq 75°$) [112]. The WCA recently derived by Elfouhaily et al [106, 108] was shown to improve both KA and SSA1 in some range of moderate roughness and in co-polarization. One of the most popular approach which combines KA and SPM1 is the classical TSM (TSM1) [27, 29, 59, 113]. TSM1 has broader range of validity as compared to SPM1 and KA but it is inaccurate for grazing angles and there is a gap in regions of validity of SPM1 and KA. Moreover, the predictions for cross polarization in backscattering are not exact.

The particular problem of wave scattering at low grazing angles is of great interest because of its importance for the long-distance propagation of radio waves along the Earth's surface, radar observation of near surface objects, as well as solving many other fundamental and applied problems of remote sensing. In the third chapter we have

	Sea surface		Soil surface
Spectrum	Gaussian	Elfouhaily [97]	Exponential
Permittivity	Debye model [86], $4+i$	Debye model [86]	Peplinski model [93], Measured values [34]
Parameters	$kh: 0.1, 0.2, ..., 1$ $kl: 1, 2, ..., 6$	P-, L-, C-, X- and Ku-band, U10(m/s)=3,...,15	$h(cm) = 0.40, 1.12, 3.02$ $l(cm) = 8.4, 8.8$ f(GHz)=1.5, 4.75, 9.50
Comp. in Backscattering	MoM, SSA2 [37]	[33], [9], SSA1, MoM, WCA [38], [36]	[34], [35]
Comp. in Bistatic scattering	TSM1	TSM1	TSM1

Table 5.2: An overview of the methodology used to evaluate TSM2

seen that SPM, when studied up to second order, has larger domain of validity and the contribution of second order scattering give enhanced results for certain configurations, from moderate to large incident angles (small grazing angles). Moreover, SPM2 also produces non-zero results for cross polarization. These observations motivated us to develop an improved TSM (TSM2) by taking into account the contribution of second order scattering [31, 32]. We expect that the new developed model will be useful for remote sensing of the ocean and bare soil surfaces, especially when the transmitter is close to the surface and can produce better predictions for cross polarizations [39]-[42]. Due to the broader validity domain of SPM2, TSM2 has the ability to bridge the gap in the domains of validity of KA1 and SPM1. To check these hypothesis the simulation results using three different spectra are presented in this chapter and compared with the results obtained from other analytical approximate techniques, measured data published in literature and the results calculated by using the software FEKO [114], which is based on the numerically exact method MoM [115, 116].

In this chapter, initially we use the MoM to test the accuracy and validity domains of TSM2 for a surface with Gaussian spectrum. Then the applications are given for sea surface obeying the Elfouhaily et al. spectrum. Section 3 is devoted to the applications of TSM2 for bare soil surface. A comparison of model predictions with experimental data for cross polarization is presented in section 4. Finally, the conclusions of this work are reported.

5.2 Application to Sea Surface

In this section numerical results are presented for Gaussian and sea spectra and compared with MoM, measured data and other approximate analytic techniques.

Historically normalized radar cross section of vertical polarization σ_{vv} has been known to be rather well explained by Bragg scattering augmented by a composite, or two-scale, sea surface over the range of incidence angles from approximately 20° to 60° and probably at even higher incidence angles, into the so called LGA regime [1, 117]. On the other hand, there is a need to study σ_{hh} in more detail. It is appeared to be fairly well predicted by Bragg/TSM1 surface scattering from 20° to 45° incidence but at larger incident angles this intensity is considerably stronger than that expected from theoretical computation. Many non-Bragg scattering mechanisms attributable to wave breaking have been suggested to explain the strong radar returns. The Doppler property of horizontal polarization (HH) return is also found to be very different from the VV return [10, 11]. However there are other mechanisms e.g., fading [9] and higher order scattering etc. that are responsible for strong backscatter intensity. To get improved intensity of at larger incident angles we have developed TSM2 by taking into account the contribution of second order scattering at small scale. In this section we investigate σ_{hh} by using TSM2 from moderate to large incident angles.

5.2.1 Numerical results using Gaussian spectrum

For our first experiment and to check how TSM2 perform on a single scale surfaces, we have chosen the prototype of surfaces with Gaussian spectrum. These are parameterized only by the rms height h and the correlation length l. In backscattering direction, we examine the accuracy of TSM2 by comparing the numerical results with MoM. Then we use the TSM2 to predict the surface scattering in bistatic configuration and compare the results with SSA2.

Monostatic configuration

This configuration is omnipresent in the literature, it is simple to implement since the emitter is in the same time the receiver. It is used in many applications as classic radars, SAR images and GBR...

To fulfill the backscattering configuration conditions, incident angles in emission and reception are taken identical and the corresponding azimuth difference equal to π. We have been working on surfaces numbered from 1 to 15, whose parameters are summarized in table 5.3.

The numerical results for MoM have been obtained by using FEKO [114]for perfectly conducting surface. For each surface the scattering coefficient is estimated by averaging over 1000 samples. Note that in MoM simulations we have used one-dimensional (1D) surface embedded in a two-dimensional (2D) space in order to avoid the computational complexity involved in the 2D surface embedded in a three-dimensional

Surface	kh	kl	Figure
1	0.2	1	5.1(a)
2	0.5	1	5.1(b)
3	1	1	5.1(c)
4	0.2	2	
5	0.5	2	
6	1	2	
7	0.2	3	5.2(a)
8	0.5	3	5.2(b), 5.5, 5.6, 5.7, 5.8
9	1	3	5.2(c)
10	0.2	4	5.3(a)
11	0.5	4	5.3(b)
12	1	4	5.3(c)
13	0.2	5	
14	0.5	5	
15	1	5	

Table 5.3: Summary of roughness parameters

(3D) space. Furthermore, scattering results obtained for 1D profiles also give a good indication of scattering dependence on 2D surface parameters [118]. Figures 5.1(a)-(c) display the monostatic NRCS σ_{hh} versus the incidence angle for MoM, TSM1, TSM2, SPM1 and SPM2 for three surfaces $S1$, $S2$ and $S3$ with $kl = 1$ and kh ranging from 0.2 to 1.The value of relative permittivity is calculated by using Debye's model [86].

Surface 1 falls into the validity domain of SPM1. At this roughness level (i.e., when $kh = 0.2$ & $kl = 1$) the predictions by SPM2 are much weaker than SPM1 at all incident angles and the contribution of second order scattering does not seems to be important. The results of TSM1 and TSM2 coincide and are in agreement with MoM. However, it can be observed from Figs 5.1(b) and 5.1(c) that the second order scattering effects are becoming strong and SPM2 approaches to SPM1 as the rms height increases and the addition of SPM2 in SPM1 starts giving enhanced results for scattering coefficient computed by TSM2. For $S3$ (Fig. 5.1(c)) the TSM2 results are slightly greater than TSM1 and the comparison with MoM shows that both TSM1 and TSM2 start overestimating the scattered power as the incident angle increases. It is to be noted that the roughness parameters for this surface are chosen outside the validity domain of SPM1 and SPM2.

Figures 5.2(a)- (c) shows angular responses of σ_{hh} for surfaces $S7$, $S8$, and $S9$ with $kl = 3$ and $kh = 0.2$, 0.5 and 1, respectively.

We notice that as the correlation length is increased, SPM2 gives enhanced backscattered power than SPM1 from intermediate to small grazing angles and become more significant as the rms height increases. Hence the contribution of second order scatter-

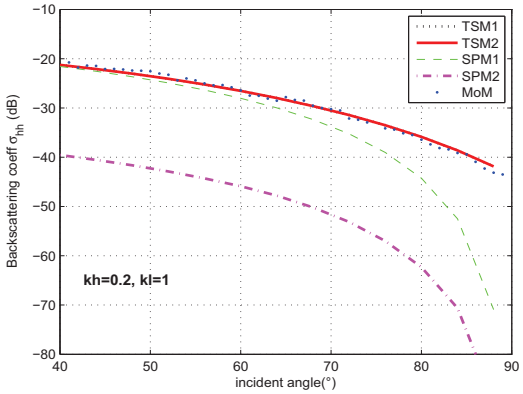

(a)

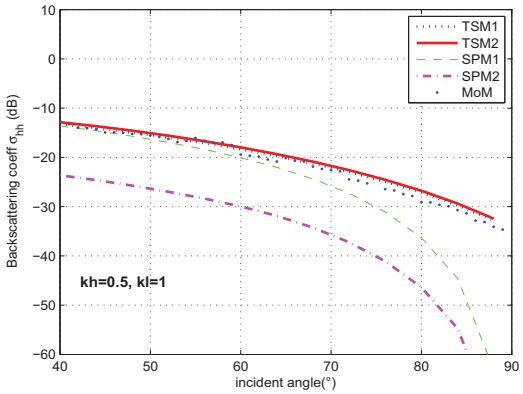

(b)

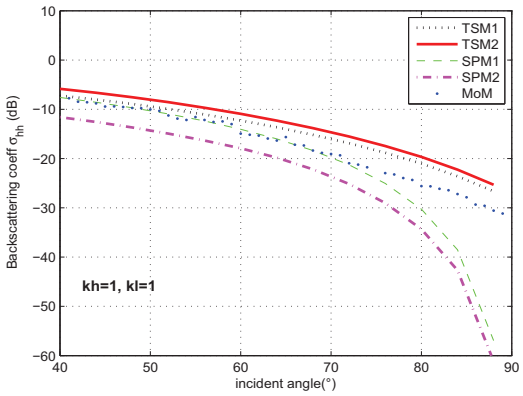

(c)

Figure 5.1: Backscattering coefficient: Comparison of TSM1, TSM2, SPM1 and SPM2 with the MoM, Gaussian spectrum,(a)$kh = 0.2$, $kl = 1$; (b)$kh = 0.5$, $kl = 1$; (c)$kh = 1$, $kl = 1$

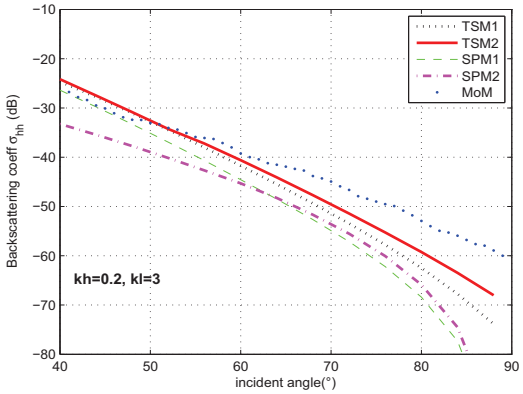

(a)

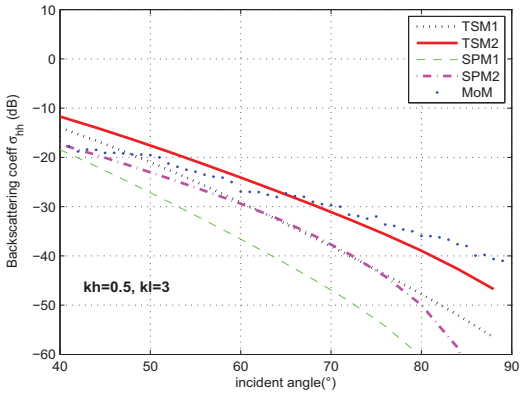

(b)

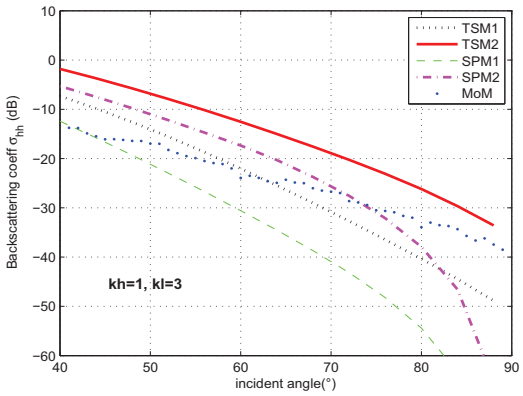

(c)

Figure 5.2: Backscattering coefficient: Comparison of TSM1, TSM1, SPM2 and SPM2 with the MoM, Gaussian spectrum,(a)$kh = 0.2$, $kl = 3$; (b)$kh = 0.5$, $kl = 3$; (c)$kh = 1$, $kl = 3$

ing results in improved TSM (TSM2). The comparisons with MoM in Figs. 5.2(a) and 5.2(b) shows that for these roughness conditions (i.e., $kh = 0.2$, $kl = 3$ & $kh = 0.5$, $kl = 3$), TSM2 is in better agreement, from moderate to large incident angles. However, Fig. 5.2(c) shows that for a point chosen outside the validity domain of SPM2, SPM2 and hence TSM2 overestimate the scattered power. We also found the same type of results for surfaces $S4$, $S5$, and $S6$.

These observations are further verified by viewing the comparisons of three more relatively rough surfaces $S8$, $S9$, and $S10$ in Figs. 5.3(a)-(c).

Hence in general, we found that when roughness of the surface increases, TSM2 predicts enhanced backscatter returns and provide reasonable accuracy from moderate to large incident angles. However, when one increases the rms height to leave the domain of validity of the SPM1 and SPM2 ($S3$, $S6$, $S9$ and $S12$), TSM2 start overestimating the backscattered intensity limiting the effectiveness of TSM2 for surfaces with Gaussian spectrum.

In the last example of this section the comparisons between TSM2 and SSA2 [37] are illustrated in Fig. 5.4(a) and (b). The roughness parameters are chosen as $kh = 0.5$, $kl = 3$ and $kh = 1$, $kl = 6$ respectively and a relative permittivity of $4 + i$ [37].

Again we observe that as the rms height increases the predictions by SSA2 and TSM2 become identical from moderate to large incident showing the efficiency of TSM in this domain.

Bistatic configuration

Now lets move on to bistatic scattering. Figure 5.5 illustrates in-plane bistatic HH polarized results for rough surface $S8$ ($kh = 0.5$ & $kl = 3$) with relative permittivity $4+i$. The incident angle in the emission is fixed to 50° Fig. 5.5(a) and then to 80° Fig. 5.5(b), while the received one varies from $-90°$ to $-40°$ and 40° to 90°. As can be seen, the contribution of second order term is more appreciable on backward grazing angles and the difference between TSM1 and TSM2 increases with the increase in incident and/or observed angle.

The next two figures 5.6 & 5.7 are plotted against observed angle, for fully bistatic case by setting the received azimuth to 45° and then to 135°. There incident angle is chosen as 50° and 80° whereas, the observed angles varies from intermediate to small grazing angles. No enhancement is observed in the first case when $\varphi_s = 45°$ however TSM2 gives enhanced results for the second case i. e., when $\varphi_s = 135°$ and this enhancement increases as the incident angle increases 5.7(b).

A more clear picture of the enhancement given by TSM2 can be seen in figure 5.8 where we present the numerical comparisons between TSM1 and TSM2 by changing

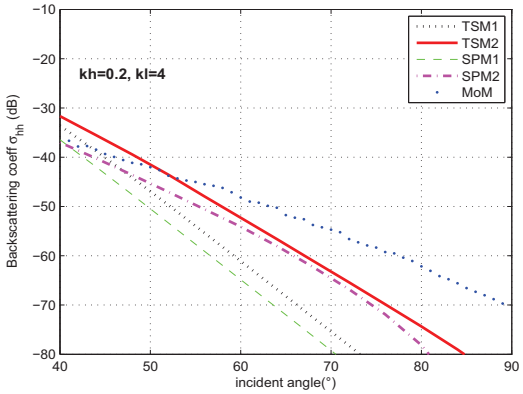

(a)

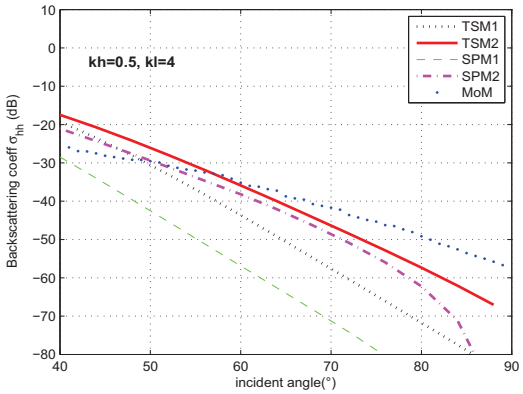

(b)

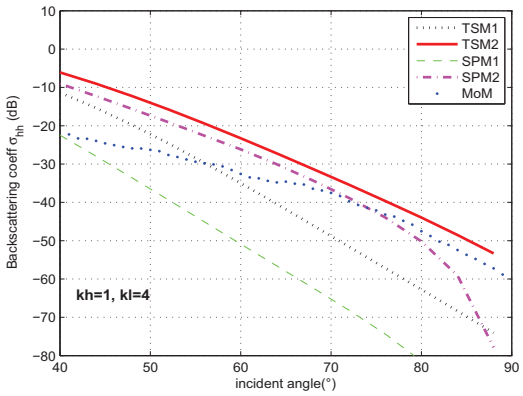

(c)

Figure 5.3: Backscattering coefficient: Comparison of TSM1, TSM2, SPM1 and SPM2 with the MoM, Gaussian spectrum,(a)$kh = 0.2$, $kl = 4$; (b)$kh = 0.5$, $kl = 4$; (c)$kh = 1$, $kl = 4$

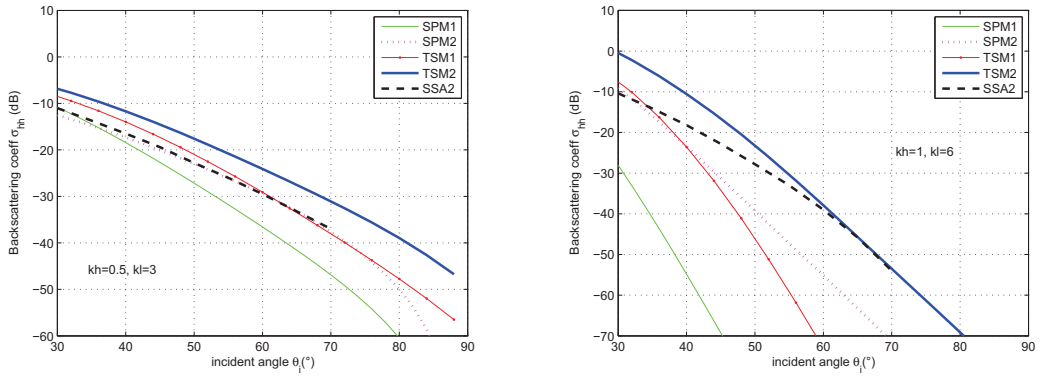

(a) (b)

Figure 5.4: Backscattering coefficient: Comparisons of TSM2 with SSA2, TSM1, SPM1 and SPM2, Gaussian spectrum, $\varepsilon_r = 4 + i$ [37]; (a)$kh = 0.5$, $kl = 3$; (b)$kh = 1$, $kl = 6$.

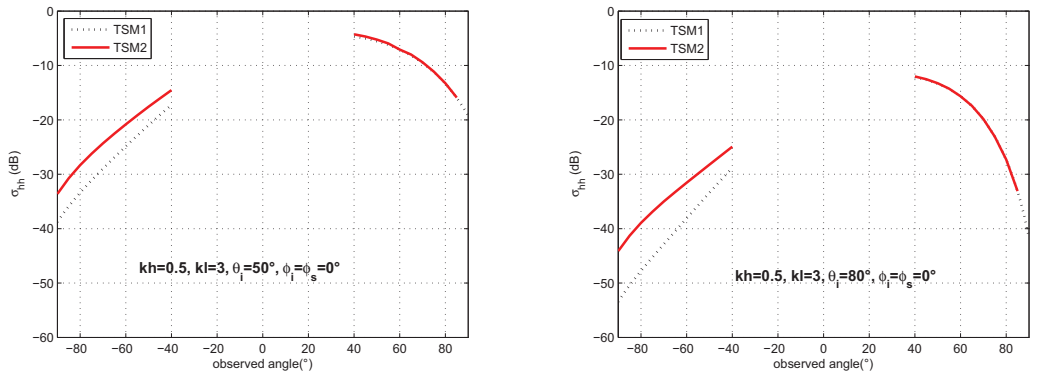

(a) (b)

Figure 5.5: Forward scattering coefficient: Comparisons of TSM1 and TSM2, Gaussian spectrum, $kh = 0.5$, $kl = 3$, $\varphi_i = \varphi_s = 0°$, (a)$\theta_i = 50°$; (b)$\theta_i = 80°$.

the scattering azimuth direction. Incident angle is fixed to 50° Fig. 5.8(a) and then to 80° Fig. 5.8(b) and the observed angle is equal to incident angle for both cases.

5.2.2 Numerical results using Elfouhaily spectrum

We now study the case of multi-scale surface using a more realistic sea spectrum developed by Elfouhaily et al. [97]. We begin by validating TSM2, in monostatic configuration, by comparing our results with those published in literature. We also analyze

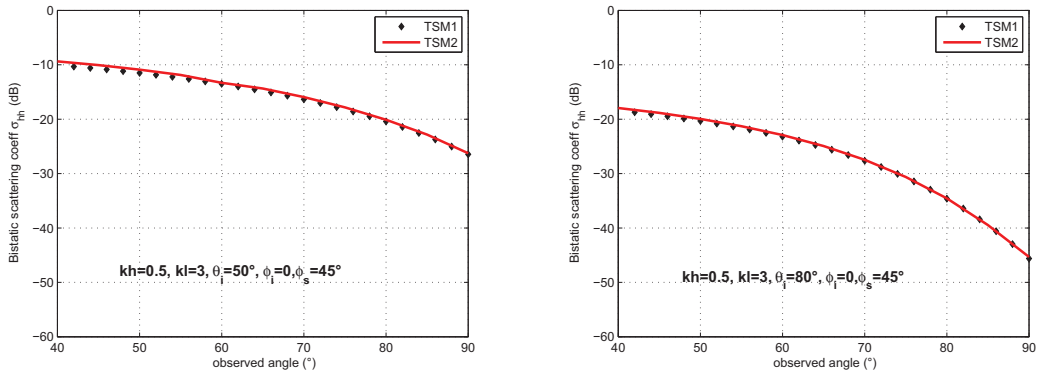

(a) (b)

Figure 5.6: Bistatic scattering coefficient: Comparisons of TSM1 and TSM2, Gaussian spectrum, $kh = 0.5$, $kl = 3$, $\varphi_i = 0°$, $\varphi_s = 45°$, (a)$\theta_i = 50°$; (b)$\theta_i = 80°$.

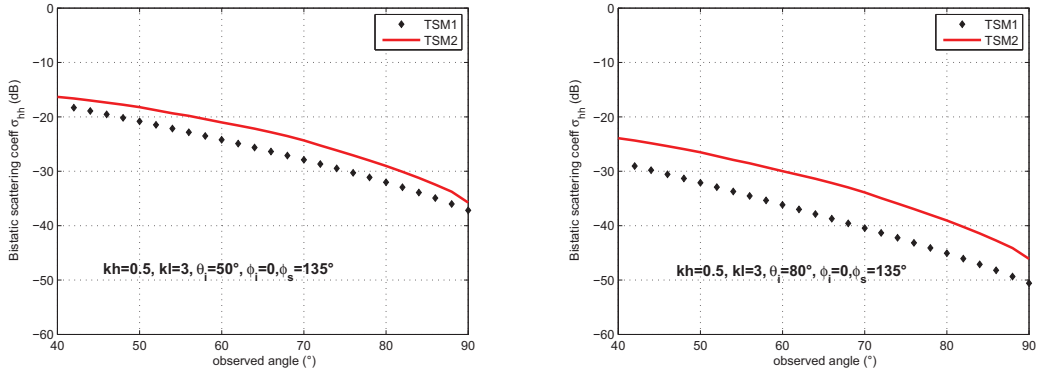

(a) (b)

Figure 5.7: Bistatic scattering coefficient: Comparisons of TSM1 and TSM2, Gaussian spectrum, $kh = 0.5$, $kl = 3$, $\varphi_i = 0°$, $\varphi_s = 135°$, (a)$\theta_i = 50°$; (b)$\theta_i = 80°$.

the behavior of scattering coefficient by varying several parameters (emitted frequency, wind speed, geometry ...) for backscattering case. Then we present the predictions by TSM2 in different bistatic configurations and compare them with TSM1 and SSA1.

Monostatic configuration

Most of the classic applications of radar are based on monostatic configuration i.e., where $\theta_s = \theta_i$ and $\varphi_s = \varphi_i + \pi$. Therefore, monostatic scattering problem has been

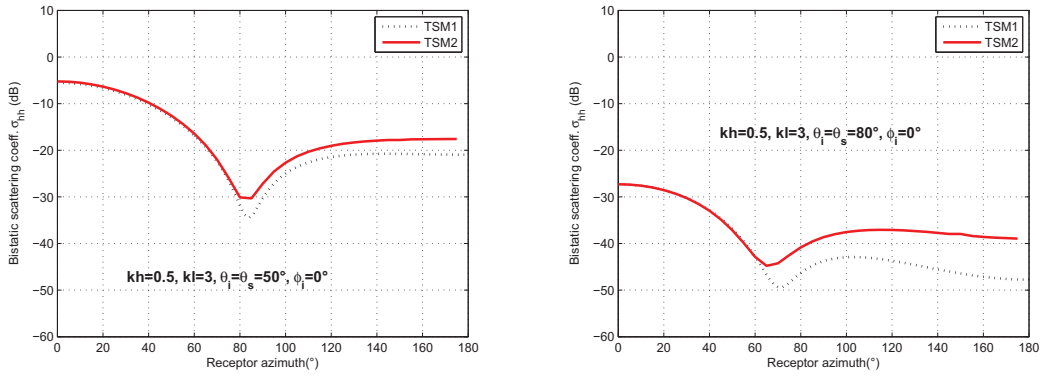

(a) (b)

Figure 5.8: Bistatic scattering coefficient: Comparisons of TSM1 and TSM2, Gaussian spectrum, $kh = 0.5$, $kl = 3$, $\varphi_i = 0°$, (a)$\theta_i = \theta_s = 50°$; (b)$\theta_i = \theta_s = 80°$.

well studied in literature and several campaigns were conducted to experimentally validate the theoretically developed models. To that, we present the simulation results by TSM2 obtained in the monostatic case and compare them with experimental data and other models as a function of incident angle, emitted frequency and wind speed.

Variations of scattering coefficient as a function of incident angle In this part we will fix all the geometric and physical parameters with the exception of the incidence angle (same angle of observation) and that will vary from 40° to 90°.

At first the comparisons are realized with respect to the results published by NW Guinard et al. [33] and WJ Plant [9]. For horizontal polarization, the variation of backscattering coefficient is taken over the frequency range from UHF to Ku-band as a function of grazing angle and sea state. The relative permittivity is calculated by using Debye's model [86] at a water temperature of 20° C and salinity of 35 ppm for each frequency band.

In Fig. 5.9, the comparison between TSM1, TSM2 and the acquired data [33] at P-band is shown. This frequency band does not fall in the usual radar bands. However, due to the availability of experimental data and to see the behavior of TSM2 on the low frequency, we have done the calculations at this band. The model values are calculated using two wind speeds 4 m/s and 12 m/s (measured at 10 m height) whereas the experimental data is given for a variety of wind speeds from $0 - 24$ m/s. For a wind speed of 4 m/s, a small enhancement is observed in TSM2 from TSM1 as the grazing angle become large. However, as the wind speed increases to 12 m/s the difference between two models increases and TSM2 predictions are in good agreement

with experimental data from small to moderate grazing angles. On the other hand TSM2 predictions are found to exceed those of TSM1 by 15 to 20 dB for grazing angles 30° to 50° but we believe that with the cancelation effects of σ_{22} and σ_{13} as defined in [72] this difference will be reduced and TSM2 will remains valid for moderate angles also.

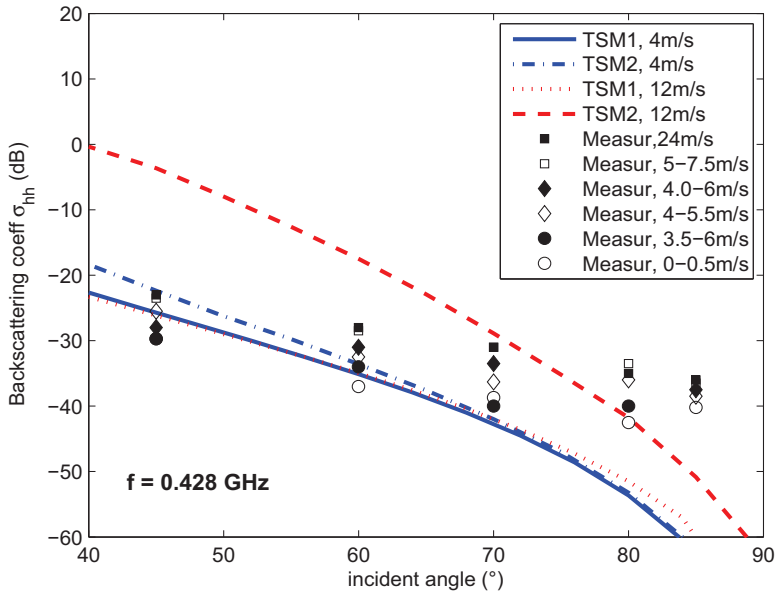

Figure 5.9: Backscattering coefficients: Comparison of TSM2 with experimental data [33] and TSM1 for HH polarization at different wind speeds, f=0.428 GHz.

Figures 5.10 and 5.11 compares the numerical models TSM1 and TSM2 with experimental data at L- and C-band respectively. The simulated results are given for a wind speed of 6 m/s whereas the experimental data is taken over various wind speeds i.e., $3.5 - 7.5$ m/s. It is found that TSM2 give improved backscattered results and the comparison with experimental data demonstrate its validity at grazing angles. It is also noticed that for the same wind speed the second order predictions become stronger as the frequency increases.

Figure 5.12 illustrate the comparison between the newly developed model TSM2, TSM1 and measured data at X-band. The wind speeds for numerical models and experimental data are chosen same as given in Fig. 5.9. For the low wind speed of 4 m/s the newly developed model produce enhanced backscattered results and comparisons with data show reasonable accuracy up till grazing angle of 20° and can be further improved to large grazing angles by including the complete second order scattering effects (i. e., by including the effects of σ_{13} and σ_{31} in σ_{22}). However as the wind

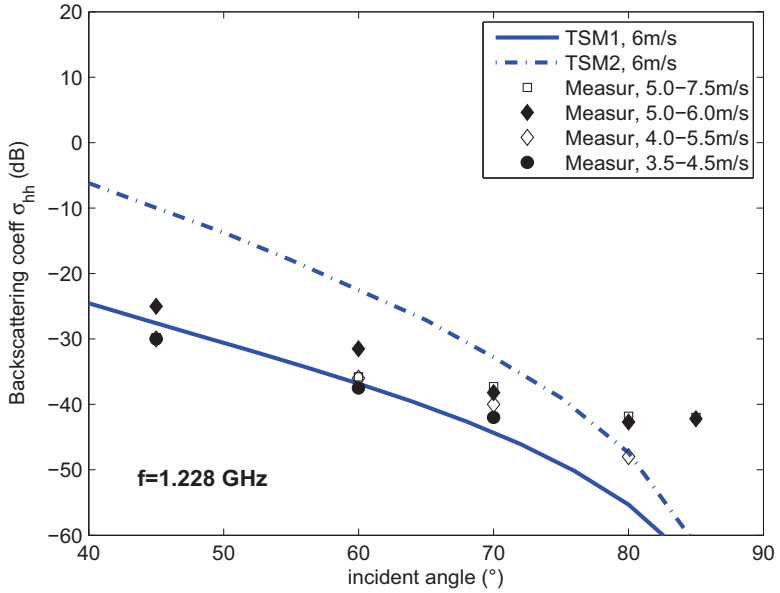

Figure 5.10: Backscattering coefficients: Comparison of TSM2 with experimental data [33] and TSM1 for HH polarization at different wind speeds, f=1.228 GHz.

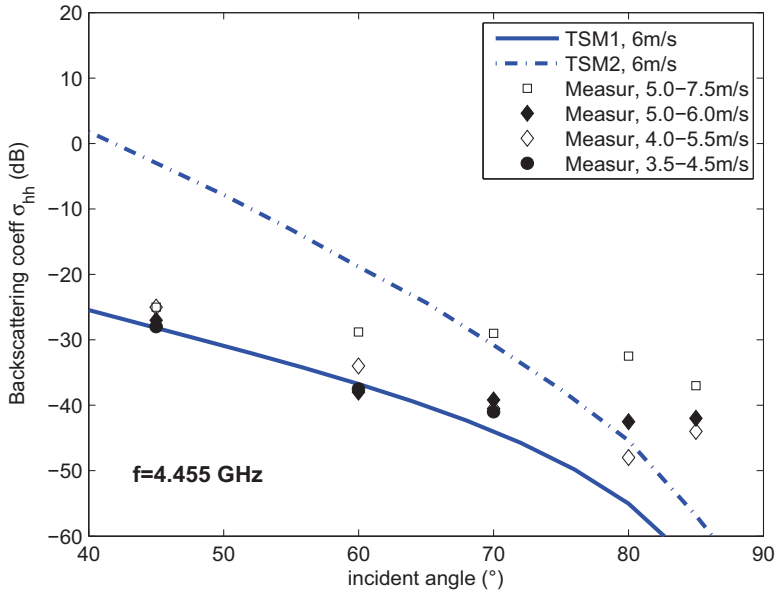

Figure 5.11: Backscattering coefficients: Comparison of TSM2 with experimental data [33] and TSM1 for HH polarization at different wind speeds, f=4.455 GHz.

speed increases to 12 m/s TSM2 shows good results only from 3° to 10° and seems to start over predicting for moderate and higher incident angles.

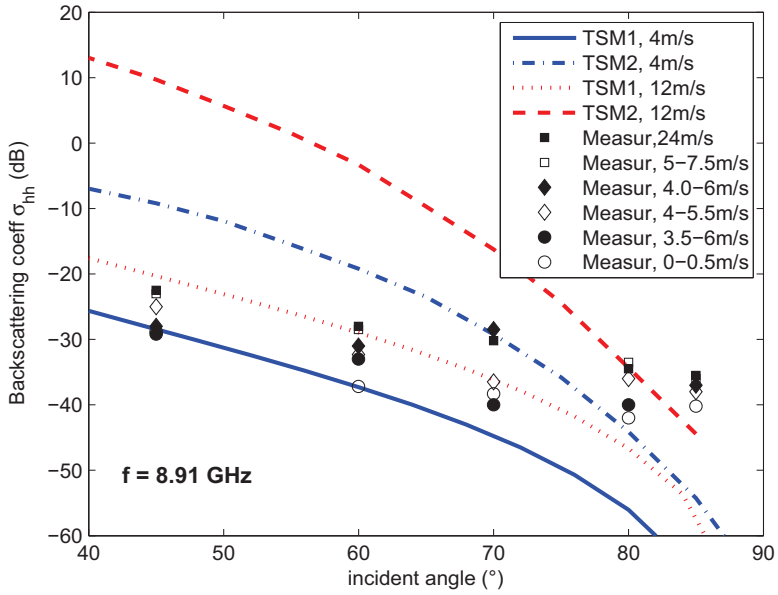

Figure 5.12: Backscattering coefficients: Comparison of TSM2 with experimental data [33] and TSM1 for HH polarization at different wind speeds, f=8.91 GHz.

This observation is further confirmed by seeing the comparison at Ku-band with a wind speed of 6 m/s (see Fig. 5.13(a)). The TSM2 results are only good only for grazing angles from 5° to 10° and overestimate otherwise. The backscattering results at Ku-band with a wind speed of 12 m/s show a significant departure from experimental data even at small grazing angles. We conclude that SPM2 and hence TSM2 starts over predicting the backscattered intensity as the surface become rougher, limiting the applicability of TSM2 for microwave frequencies higher than X-band.

To study further the consistency and validity of TSM2, we compare our results with MoM, WCA and SSA1 [38] in Fig. 5.14 which is plotted at L-band ($f = 1.228$ GHz) with wind speeds of 3 and 7 m/s. The relative permittivity is set to $30 + 30i$ [38]. The comparison with MoM shows that SSA1 results underestimate the scattered intensity at grazing angles for all wind speeds and TSM2 results are in good agreement at small grazing angles but start overestimating as the wind speed and grazing angle increases. TSM2 results are also consistent with those of WCA and this consistency will further be increased for moderate incident angles by including the complete second order scattering effects.

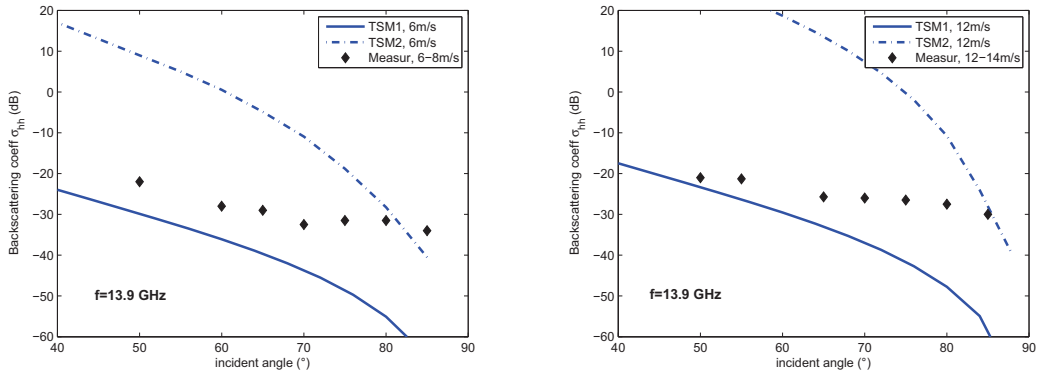

(a) (b)

Figure 5.13: Backscattering coefficient: Comparisons of TSM2 with experimental data [9] and TSM1, f=13.9 GHz (a)wind speed=6m/s; (b)wind speed=12m/s.

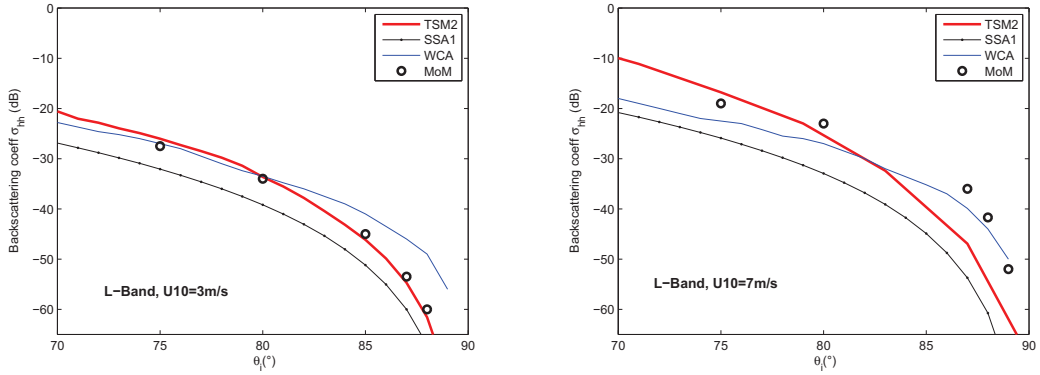

(a) (b)

Figure 5.14: Backscattering coefficient: Comparisons of TSM2 with WCA and SSA1 f=1.5 GHz (a)wind speed=3m/s; (b)wind speed=7m/s.

Variations as a function of frequency As shown in the preceding paragraph, frequency is a significant parameter in the scattering problem. In this paragraph, in order to see the impact of the inclusion of second order scattering effects on frequency we present the numerical results of backscattering coefficient σ_{hh} as a function of frequency.

Figure 5.15 shows the variations of the backscattering coefficient by TSM1 and TSM2, as a function of frequency for three wind speeds 3 m/s, 7 m/s and 12 m/s at an incident angle equal to 80°.

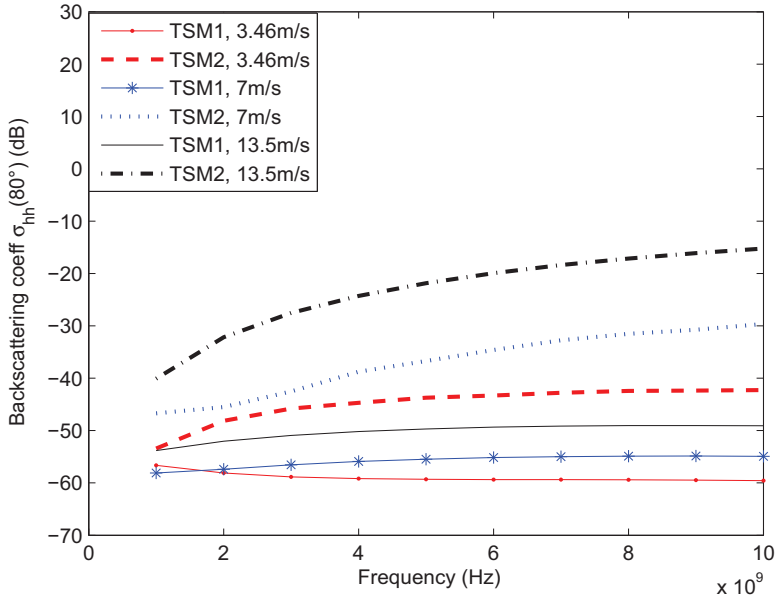

Figure 5.15: Backscattering coefficients as a function of wind speed: Comparison of TSM2 and TSM1 at different wind speeds, $\theta_i = \theta_s = 80°$;

Analysis of the curves shows that for a low wind speed of 3 m/s there is a small enhancement in TSM2 at L-band. The difference between TSM2 and TSM1 then increases linearly uptill 3 GHz and remain almost constant for subsequent frequencies. However for higher wind speeds of 7 m/s and 12 m/s a significant enhancement of about 8 dB and 10 dB respectively is found at L-band and the difference between two curves increases continuously as the frequency increases, resulting in the over estimation at higher frequencies. The same type of behavior is shown in Fig. 5.16 at an incident angle of 70° where the enhancement is more rapid than shown for the earlier case (ref Fig. 5.15). It is to be noted that for lower frequencies than 1 GHz the second order scattering effects are weaker than first order scattering and give no improvement or slight enhancement in backscattered intensity depending on the wind speed.

Variations as a function of wind speed The wind speed plays an important role in the roughness of sea surface and this leads to an automatic change in its electromagnetic behavior. In this paragraph, we study the behavior of backscattering coefficient σ_{hh} by TSM2 as a function of wind speed.

Figures 5.17 and 5.18 plots σ_{hh} obtained from TSM2 and TSM1 at incident angles of 80° and 70°, respectively as a function of wind speed. The results are presented for three different frequency bands i.e., L-, C-, and X-band. By examining the two

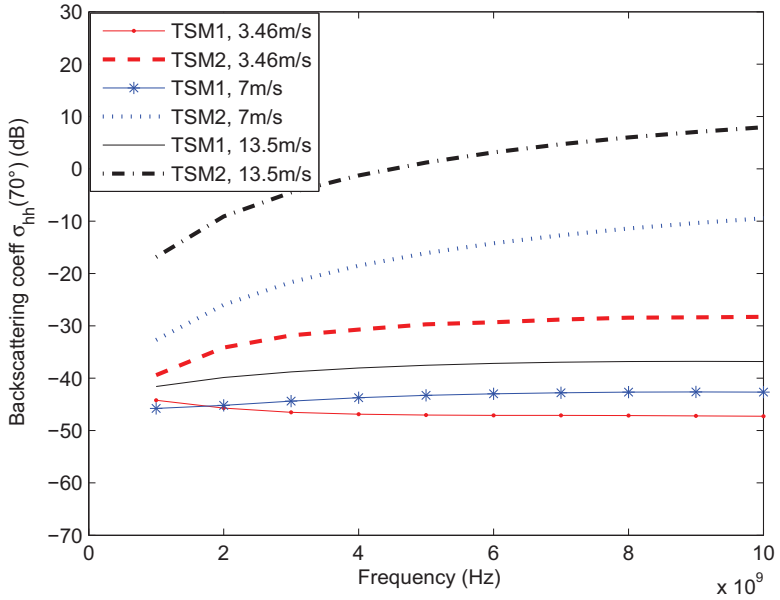

Figure 5.16: Backscattering coefficients as a function of frequency: Comparison of TSM2 and TSM1 at different wind speeds, $\theta_i = \theta_s = 70°$.

figures 5.17 and 5.18 we note that backscattering coefficient augment rapidly as the wind speed increases and is more sensitive to wind speed than frequency.

Bistatic configuration

Various bistatic configurations, where receiver location is separate from the transmitter location, can be a great source of information for remote sensing applications. In order to study the influence of the contribution of second order scattering on bistatic scattering coefficient at grazing angles we present some simulation results obtained from TSM2 and TSM1. The simulations are performed using an electromagnetic frequency of 1.228 GHz (L-band) and for two wind speeds i.e., 3 m/s and 7 m/s. We assume that the salinity and the temperature of the sea water are 35 ppm and 20° C, respectively and employ Debye formula [86] to model relative permittivity ε_r.

Figures 5.19 and 5.20 describe the variation of bistatic scattering coefficient for horizontal polarization as a function of observed angle from intermediate to small grazing angles ($50° - 88°$). The incident angle in the emission is fixed 80° and then to 70° and the received azimuth is set to 45°.

It is seen that TSM2 predict enhanced results with the increase in wind speed and/or grazing angle. The same type of effects are observed for two other configurations

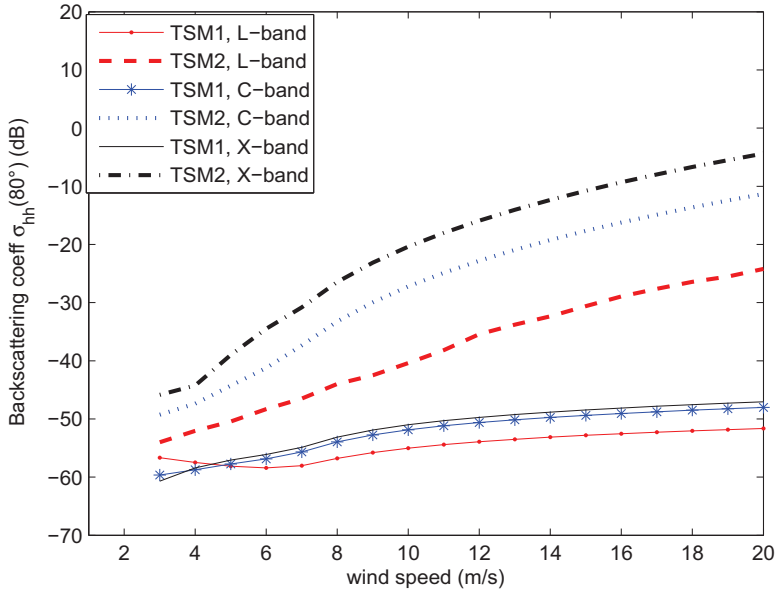

Figure 5.17: Backscattering coefficients as a function of wind speed: Comparison of TSM2 and TSM1 at L-, C- and X-band, $\theta_i = \theta_s = 80°$

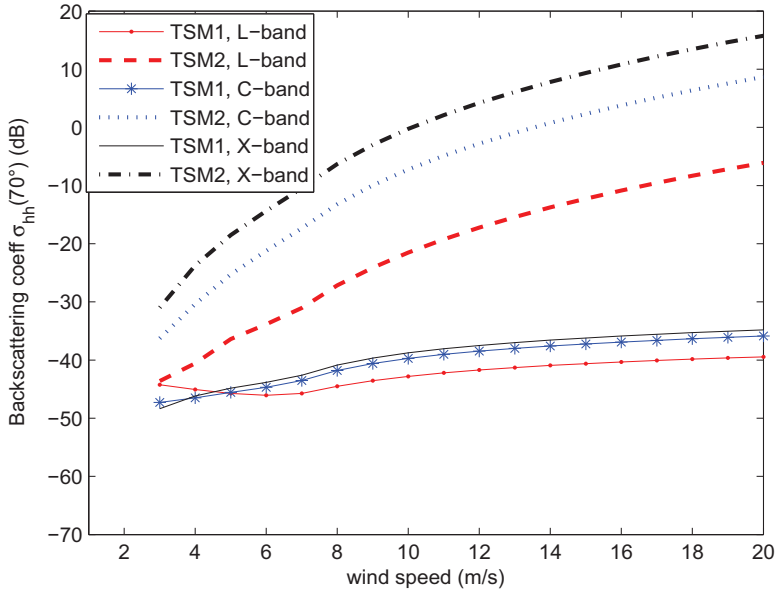

Figure 5.18: Backscattering coefficients as a function of wind speed: Comparison of TSM2 and TSM1 at L-, C- and X-band, $\theta_i = \theta_s = 70°$;

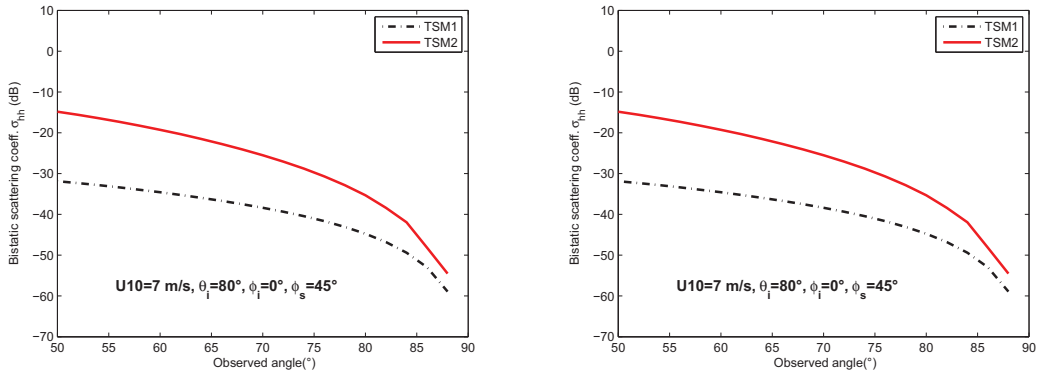

(a) (b)

Figure 5.19: Bistatic scattering coefficient: Comparisons between TSM2 and TSM1, f=1.228 GHz, $\varphi_i = 0°$, $\varphi_s = 45°$, $\theta_i = 80°$(a)wind speed=3m/s; (b)wind speed=7m/s.

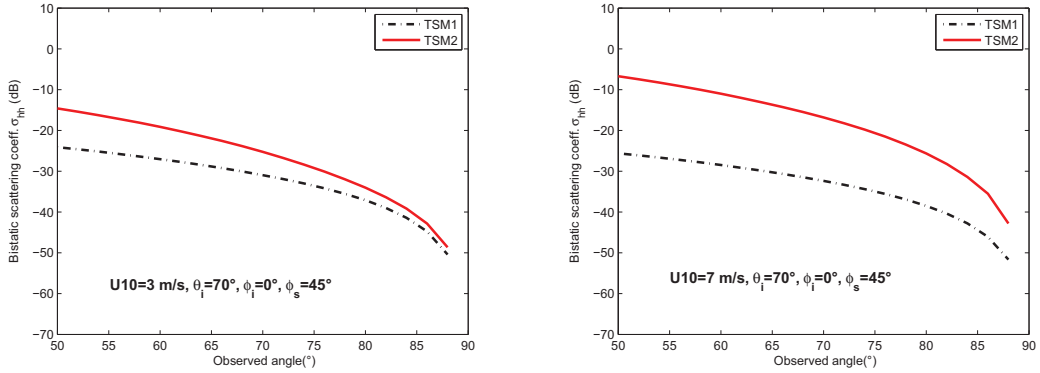

(a) (b)

Figure 5.20: Bistatic scattering coefficient: Comparisons between TSM2 and TSM1, f=1.228 GHz, $\varphi_i = 0°$, $\varphi_s = 45°$, $\theta_i = 70°$(a)wind speed=3m/s; (b)wind speed=7m/s.

(see Figs. 5.21 and 5.22) where the received azimuth is set to 135° and rest of the parameters are same as in Figs 5.19 and 5.20, respectively.

To further examine the efficiency of TSM2 in a case where the variation of receptor azimuth is considered by fixing all the other parameters we plot the bistatic scattering coefficient σ_{hh} as a function of φ_s in Fig. 5.23. The emitteris set to ($\theta_i = 80°$, $\varphi_i = 0°$) and the observation angle θ_s is identical to incident angle θ_i. For the considered example, there is a negligible/slight difference between TSM2 and TSM1 when $\varphi_i = \varphi_s$. However, as receptor azimuth goes away from the emitter azimuth the enhancement

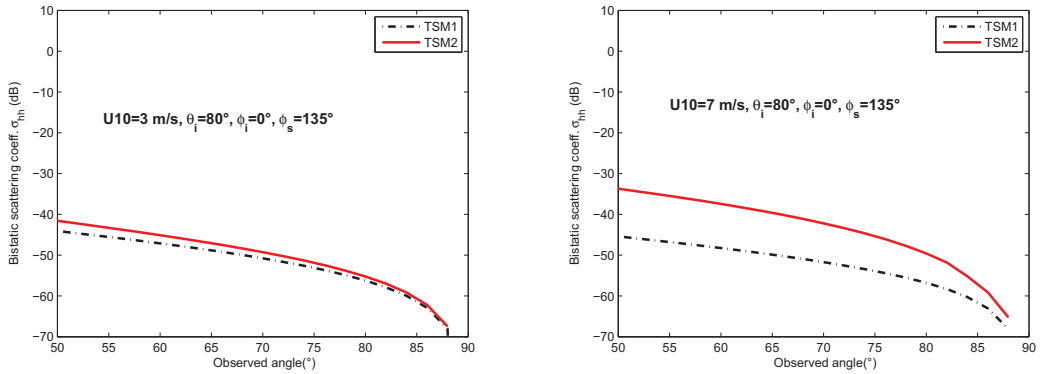

(a) (b)

Figure 5.21: Bistatic scattering coefficient: Comparisons between TSM2 and TSM1, f=1.228 GHz, $\varphi_i = 0°$, $\varphi_s = 135°$, $\theta_i = 80°$(a)wind speed=3m/s; (b)wind speed=7m/s.

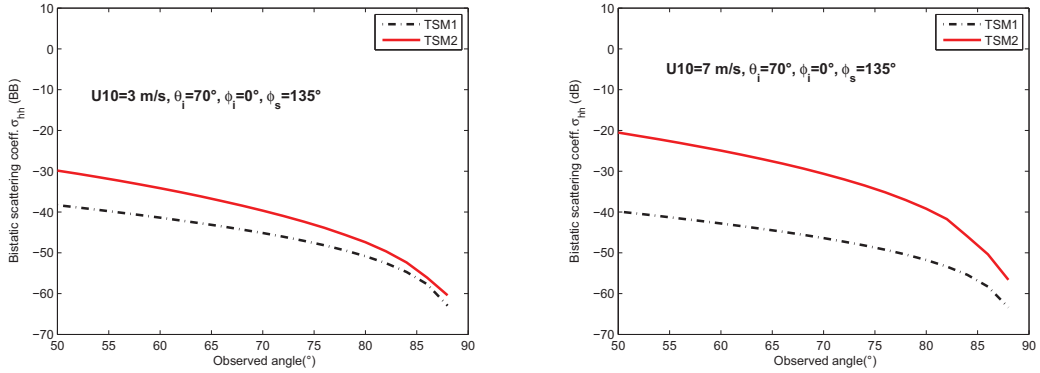

(a) (b)

Figure 5.22: Bistatic scattering coefficient: Comparisons between TSM2 and TSM1, f=1.228 GHz, $\varphi_i = 0°$, $\varphi_s = 135°$, $\theta_i = 70°$(a)wind speed=3m/s; (b)wind speed=7m/s.

gradually increases and then remain constant for intermediate angles. Next, the incident angle θ_i is decreased to 70° and simulations are done with two wind speeds 3 m/s (Fig. 5.24(a)) and 7 m/s (Fig. 5.24(b)). A small enhancement, as compared to Fig. 5.23 is found due to the change in incident angle and the behavior of scattering coefficient is same as for the previous configuration.

The simulations are done at other frequencies bans by varying observed angle, receptor azimuth angle and wind speeds and we do not find any significant difference of interpretation versus L-band. So we only present the results at L-bnad in this

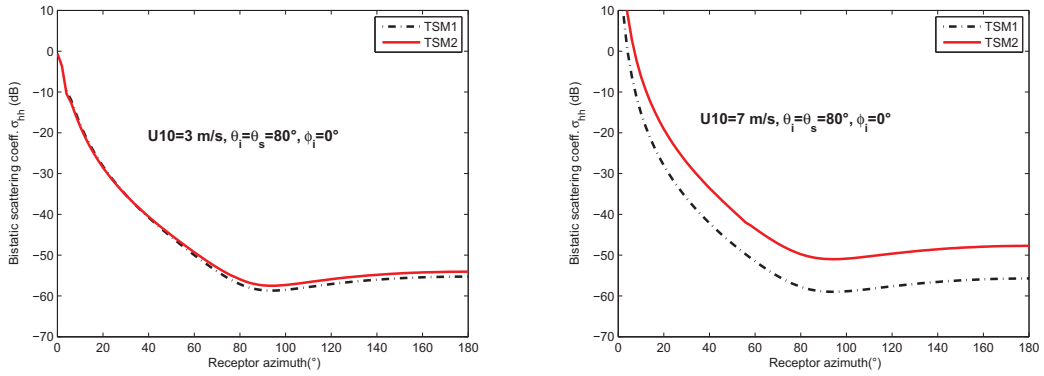

(a) (b)

Figure 5.23: Bistatic scattering coefficient: Comparisons between TSM2 and TSM1, f=1.228 GHz, $\varphi_i = 0°$,$\theta_i = \theta_s = 80°$, (a)wind speed=3m/s; (b)wind speed=7m/s.

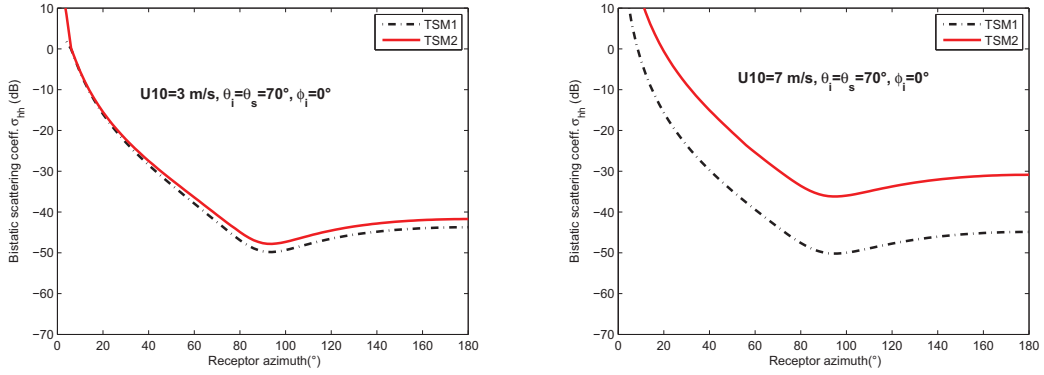

(a) (b)

Figure 5.24: Bistatic scattering coefficient: Comparisons between TSM2 and TSM1, f=1.228 GHz, $\varphi_i = 0°$,$\theta_i = \theta_s = 70°$, (a)wind speed=3m/s; (b)wind speed=7m/s.

section.

5.3 Application to Bare Soil Surface

Microwave remote sensing of land has been theoretically and experimentally studied for many years [21, 50], [119]–[124] and found in many practical applications, such as soil moisture estimation, retrieval of surface parameters like the root mean square (rms) surface height and correlation length, ice and snow cover mapping from SSMI,

Surface	h (cm)	l (cm)	Freq(GHz)	Relative permittivity	
			1.50	15.57+i3.71	L1
1	0.40	8.4	4.75	15.42+i2.15	C1
			9.50	12.31+i3.55	X1
			1.50	15.34+i3.66	L2
2	1.12	8.4	4.75	15.23+i2.12	C2
			9.50	13.14+i3.85	X2
			1.50	8.92+i2.24	L3
3	3.02	8.8	4.75	9.64+i1.19	C3
			9.50	7.57+i1.99	X3

Table 5.4: The surface roughnes parameters and the relative permittivities of wet soil

AMSR-E sensors, etc.

To analyze the wave scattering from bare soil surface with random roughness analytically, TSM can be used by splitting the surface into two scales [21, 125]: a large and small one related to the incident wave. In this section, we examine the validity and efficiency of TSM2 from a bare soil surface with exponential correlation function. Exponential correlations are more appropriate since the surfaces with exponential correlation functions have fine-scale features that are more irregular than that of Gaussian correlation function and appear to match experimental data much better than Gaussian correlation functions [98, 99].

5.3.1 Monostatic configuration

In this section, numerical simulations are carried out to compute the backscattering coefficient from bare soil surfaces with exponential correlation function. Because exponential correlation function surfaces have a fine-scale structure, it has larger backscattering. The results by TSM2 are presented at L-, C- and X-band frequencies with intermediate to large incident angles and compared with those from TSM1 and measured data [34]. The same physical roughness parameters of three surfaces are used for L-, C- and X-band frequencies. The rough-surface parameters and relative permittivities of wet soil are listed in Table 5.4.

Figure 5.25 is plotted for σ_{hh} for a slightly rough surface S1 at L-band (L1). The simulated results from TSM2 show very good agreement with measured data and TSM1. In fact this roughness condition (i.e., where $kh = 0.13$ & $kl = 2.6$) fall within the region of validity of SPM1 and SPM2 results are much weaker than SPM1(for this roughness condition), hence the contribution of second order scattering do not give any significant effect and the results of TSM1 and TSM2 match exactly for all incident angles.

In Figs. 5.26(a) and 5.26(b), the results are illustrated for the same surface S1

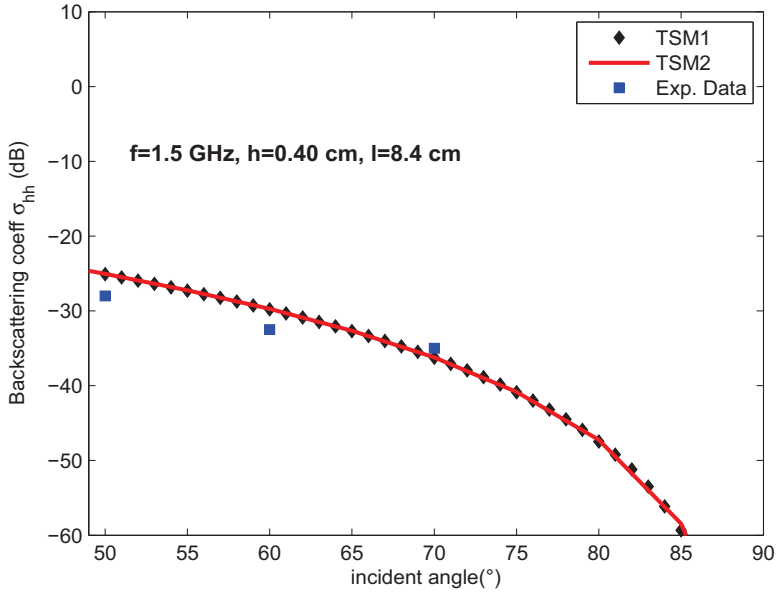

Figure 5.25: Backscattering coefficient: Comparison of TSM1 and TSM2 with measured data [34] using exponential spectrum, $kh = 0.13$, $kl = 2.6$.

at C- and X-band frequencies. These points (i.e., $kh = 0.40$, $kl = 8.4$ & $kl = 0.80$, $kl = 16.7$ for C1 & X1 respectively) lies outside the validity domain of SPM1. Due to SPM2 contribution TSM2 shows a slight enhancement for both frequncy bands and the results are in good agreement with measured data. smaller. Figure 5.27 compares the simulated results by TSM1 and TSM2 for a relatively rough surface S2 at three frequency bands. A small improvement is observed for L2, whereas the inclusion of second order scattering gives significant enhancement for C2 and X2.

The comparisons between numerical results computed with TSM1 and TSM2 and measured data for a very rough surface S3 are presented in Figs. 5.28(a)-(c). At L-band we get a little enhancement for backscattering coefficient σ_{hh} by TSM2 and the results are not so far from the measured data. However, a significant enhancement is observed at C- and X-band and clearly TSM2 overestimates. Infact for larger value of kh (e.g., $kh \geq 1$) SPM2 start overestimating the scattering intensity which also limit the validity of TSM2 for large values of kh. On the other hand, as shown in considered examples it can be used for longer correlation lengths.

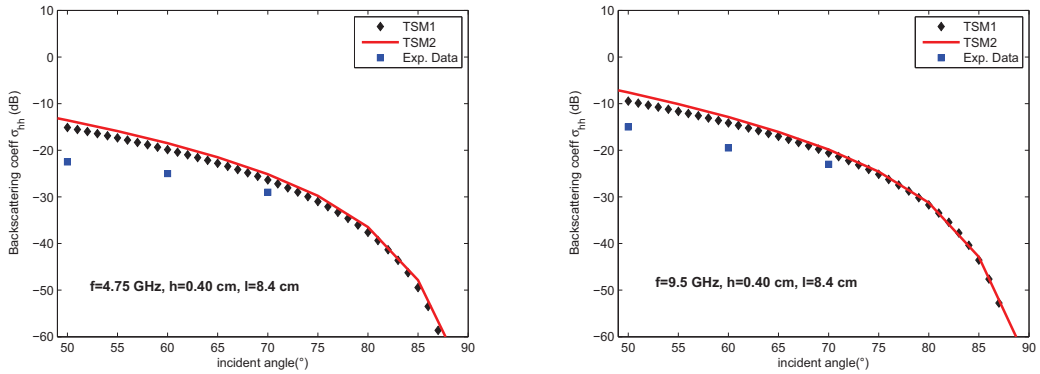

(a) (b)

Figure 5.26: Backscattering coefficient: Comparison of TSM1 and TSM2 with measured data [34] using exponential spectrum, (a)$kh = 0.40$, $kl = 8.4$; (b)$kh = 0.80$, $kl = 16.7$.

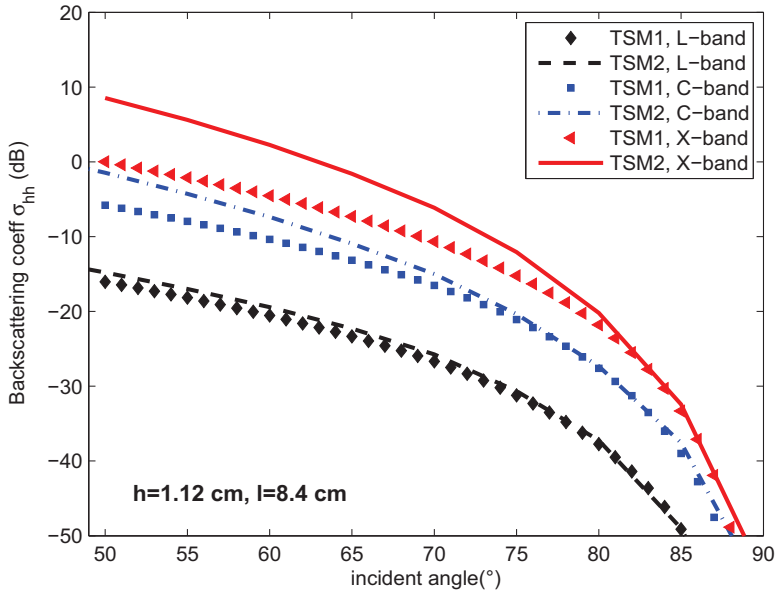

Figure 5.27: Backscattering coefficient: Comparison of TSM1 and TSM2 for surface $S3$ using exponential spectrum.

5.3.2 Bistatic configuration

In this section we present the simulation results of the bistatic scattering coefficient σ_{hh} for bare soil surfaces based on exponential correlation function. The dielectric

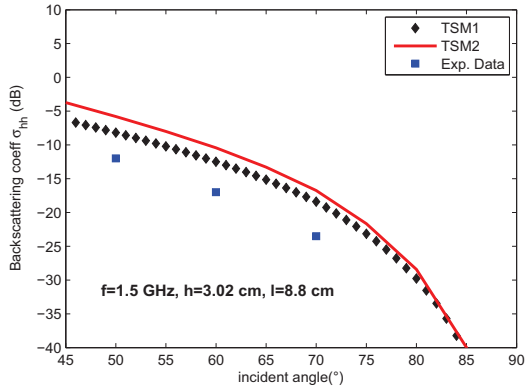

(a)

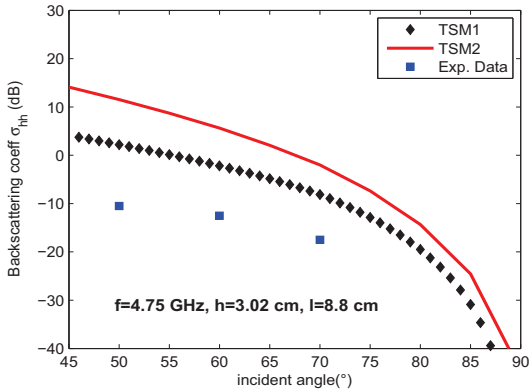

(b)

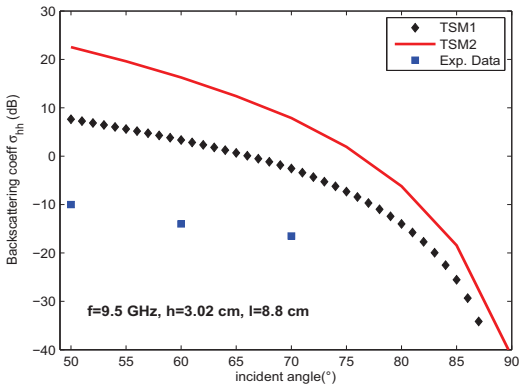

(c)

Figure 5.28: Backscattering coefficient: Comparison of TSM1 and TSM2 with measured data [34] using exponential spectrum, (a)$kh = 0.95$, $kl = 2.8$; (b)$kh = 3.00$, $kl = 8.8$; (c)$kh = 3.00$, $kl = 8.8$.

constants are calculated by using Peplinski [93] and Dobson [91] models, respectively. We examine the inclusion of second order scattering effects in TSM at L- and X-band frequencies and the numerical results are computed for two rough surfaces $S1$ and $S3$ (i.e., a slightly rough and a very rough surface).

Figure 5.29 shows the comparison between TSM1 and TSM2 in the forward scattering direction. The incident angle is set to 80° and the results are given for forward and backward grazing angles. At L-band (Fig.5.29(a)) the results are almost same for both surfaces, however, TSM2 gives significant enhancement at X-band frequency for a very rough surface S3.

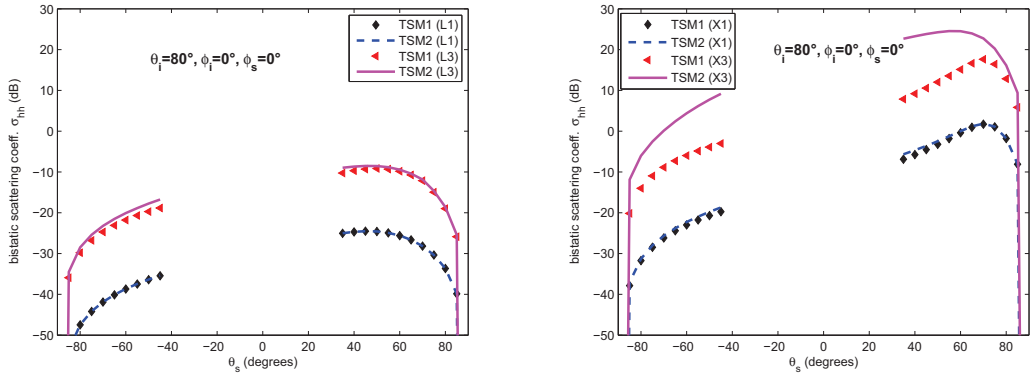

(a) (b)

Figure 5.29: Forward scattering coefficient: Comparisons of TSM1 and TSM2 using exponential spectrum for $S1$ and $S3$, $\theta_i = 80°$, $\varphi_i = \varphi_s = 0°$, (a)L-band; (b)X-band.

In next two figures 5.30 and 5.31 the bistatic scattering coefficient σ_{hh} is plotted against scattered angle by setting the azimuth angle φ_s to 45° and then to 135°. The incident angle is taken as 80°. It can be seen that, as observed in backscattering case, the bistatic scattering intensity increases by increasing frequency and/or roughness level. However, the increase in roughness level (or rms height) gives stronger effect than the increase in frequency or correlation length.

The variation of bistatic scattering coefficient as a function of receptor azimuth is illustrated in Fig. 5.32. The emitter and receiver incident angle is set to 80°. The previous observations for the effect of adding the second order scattering effects on backscattering, forward scattering and bistatic scattering are confirmed by this figure. The greater enhancement occurs when φ_s varies from 90° to 180°.

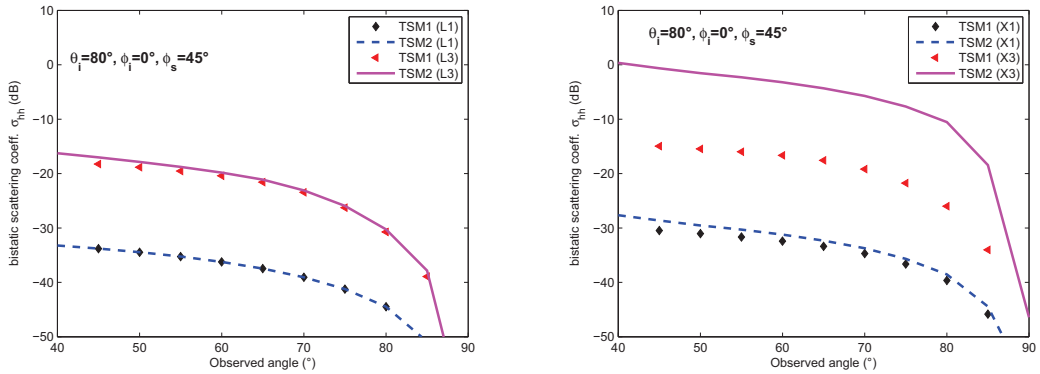

(a) (b)

Figure 5.30: Bistatic scattering coefficient: Comparisons of TSM1 and TSM2 using exponential spectrum for $S1$ and $S3$, $\theta_i = 80°$, $\varphi_i = 0°$, $\varphi_s = 45°$, (a)L-band; (b)X-band.

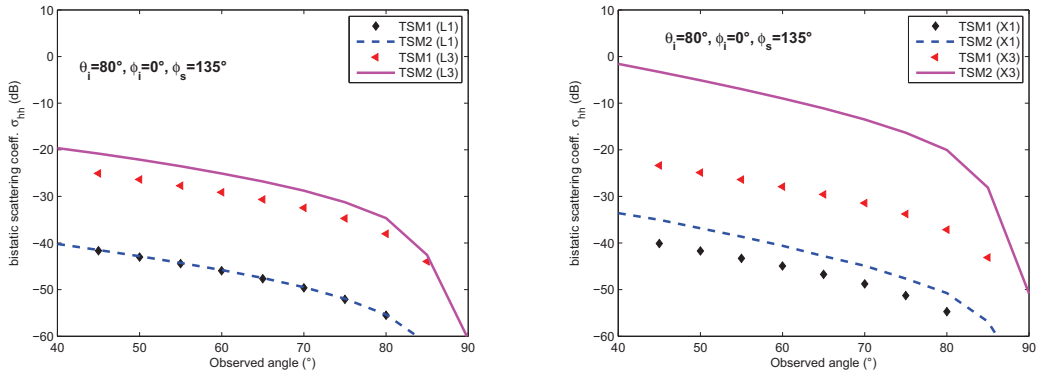

(a) (b)

Figure 5.31: Bistatic scattering coefficient: Comparisons of TSM1 and TSM2 using exponential spectrum for $S1$ and $S3$, $\theta_i = 80°$, $\varphi_i = 0°$, $\varphi_s = 135°$, (a)L-band; (b)X-band.

5.3.3 Conclusion

In the first part of this chapter we have analyzed the TSM2, from intermediate to small grazing angles, for horizontal polarization. For sea surface the simulated results are compared with those of MoM, SSA2, WCA and with measurements published in literature by using Gaussian and elfouhaily spectrum. Backscattering enhancement is found at grazing angles and the comparisons showed the validity of TSM2 up till

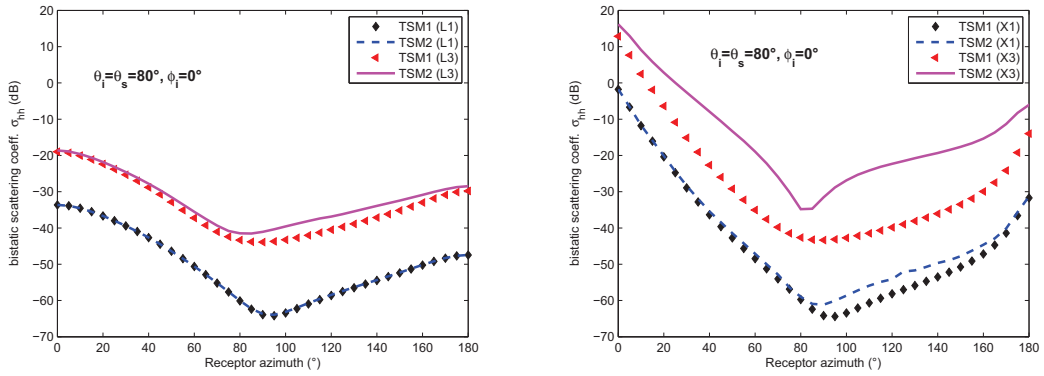

(a) (b)

Figure 5.32: Bistatic scattering coefficient: Comparisons of TSM1 and TSM2 using exponential spectrum for $S1$ and $S3$, $\theta_i = \theta_s = 80°$, $\varphi_i = 0°$, (a)L-band; (b)X-band.

certain limits. For example in case of Gaussian spectrum TSM2 can be effectively used as far as the value of kh remains less than 1. On the other hand, using a more realistic elfouhaily spectrum we found the good results for relatively low wind speeds and it starts overestimating the scattering intensity for wind speeds higher than 7 m/s and a frequency greater than 9 GHz (X-band). The analysis as a function of frequency and wind speed is also given.

Secondly, the applications have been given for bare soil surface where comparisons with measurements were presented for a variety of roughness conditions. The results are validated at L-, C- and X-band in backscattering direction. For soil surface, similar type of limitations were observed as in the case of gaussian spectrum.

5.4 Depolarization Estimation

Depolarization i.e., the change of the polarization of an electromagnetic wave from one state to another, brought about by the interaction of the wave with some material agent resulting in the corruption of desired signal. However the study of depolarization in conjunction with co-polarization information can be used to retrieve the surface roughness parameters [16, 17] and gives deeper insight into physical phenomena.

Cross polarization in a radar return from a rough surface has been observed experimentally [15, 126]. First order Small Perturbation Method (SPM1) [23]–[26] and Kirchhoff Approximation (KA) [19]–[22] does not predict this phenomenon. In order to account for observed cross polarization most theoreticians have used the methods of Advanced Integral Equation Model (AIEM) [127]–[130], Second order Small

Slope Approximation (SSA2) [37], Second order Small Perturbation Method (SPM2) [15, 71, 126], Two Scale Model (TSM) [1, 27, 59] and Empirical models [34] etc. In the classical TSM [27, 59] it is assumed that the short wavelength waves are riding on the larger waves and thus tilted with respect to the horizontal surface. It uses SPM1 at small scale i.e. for short wavelength waves and the effect of long wavelength part is taken into account by averaging over tilt angles. Hence by using the classical TSM based on first order theory, depolarization is basically due to the tilt of reflecting plane. Due to this reason the simple TSM needs to be improved.

Since the mechanism of multi-scattering due to target surface roughness also causes depolarization [15], hence this observation motivates us to develop an improved TSM by taking into account the contribution of higher order scattering (up to second order) at small scale. The purpose of this paper is to present the mathematical development of the improved TSM. In addition, we assume that the bare soil surface can be modeled as having two average sizes of roughness, this model is then applied to depolarization case. In backscattering configuration, we assess the performance of this improved model by comparing the numerical results with the measured data [34], AIEM [35] and SSA2 [37]. Finally, the simulation results are presented for bistatic case.

5.4.1 Numerical Results for sea Surface

Depolarization (or cross-polarization) predictions by TSM2 are presented in this section for backscattering and bistatic scattering case. Due to the unavailability of published experimental data at grazing angles for cross polarization the comparisons are given with the results obtained from TSM1. The parameters used here for simulation purpose are almost same as already used in the previous section for co-polarization (HH) case and the calculations are done by using Elfouhaily sea spectrum [97], Cox and Munk [94, 95] slope distribution and Debye's equation [86] for dielectric constant.

In Fig. 5.33, the comparison between TSM1and TSM2 is shown at P-band (0.428 GHz) using two wind speeds 4 m/s and 12 m/s. For a wind speed of 4 m/s a small enhancement is observed from TSM1 to TSM2 as the grazing angle become large. However, as the wind speed increases to 12 m/s the enhancement by TSM2 also increases.

Figures 5.34-5.36 present the comparisons of depolarized backscattering coefficient σ_{hv} by TSM1 and TSM2 at L-, C- and X-band, respectively for different wind speeds. We note that the second order scattering effects become stronger as the wind speed and/or the frequency increases and after a certain limit the SPM2 and hence TSM2 start overestimating the scattering coefficient which is shown in the next figure (Fig. 5.37).

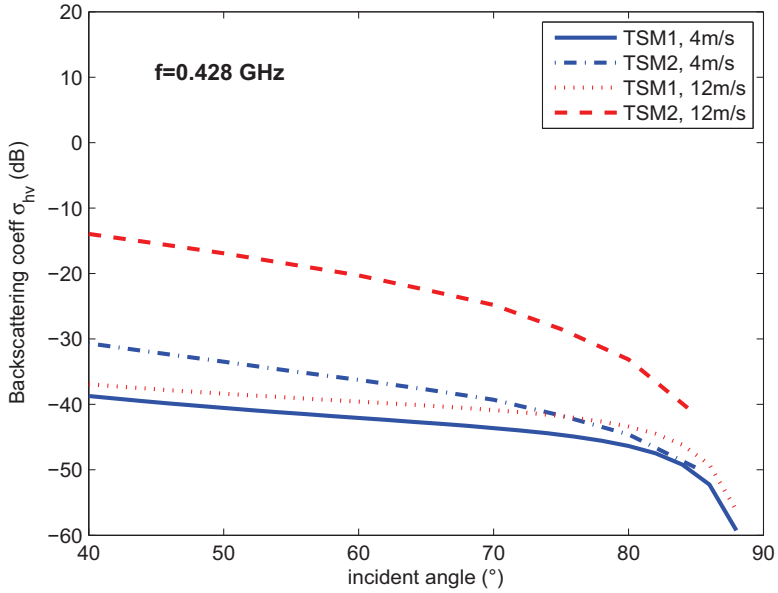

Figure 5.33: Backscattering coefficient: Comparison of TSM1 and TSM2 for HV polarization at P-band.

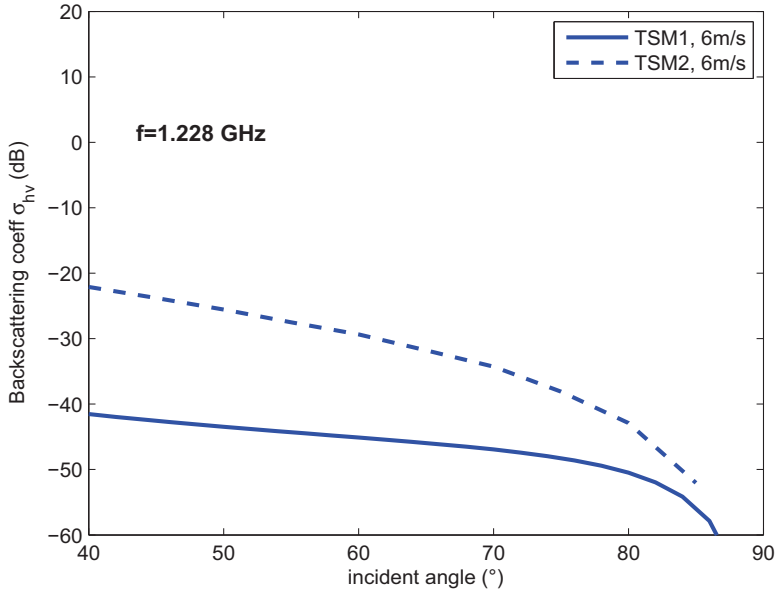

Figure 5.34: Backscattering coefficient: Comparison of TSM1 and TSM2 for HV polarization at L-band.

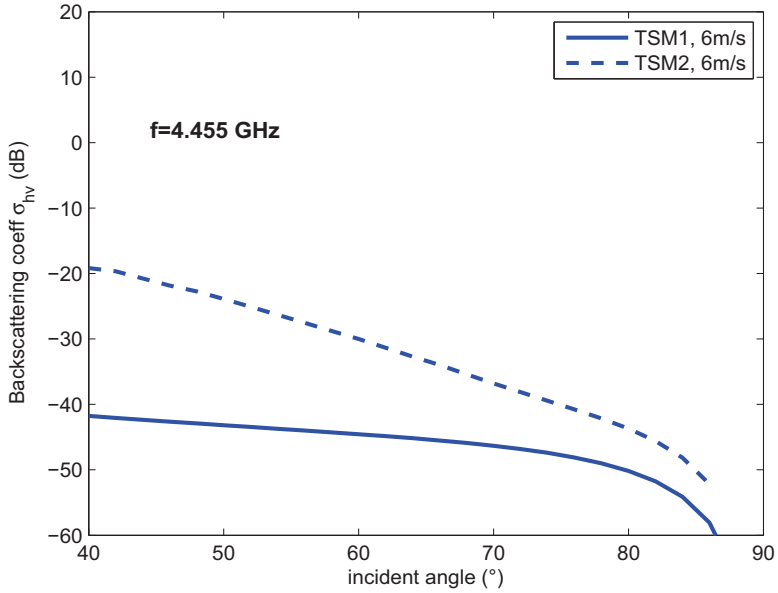

Figure 5.35: Backscattering coefficient: Comparison of TSM1 and TSM2 for HV polarization at C-band.

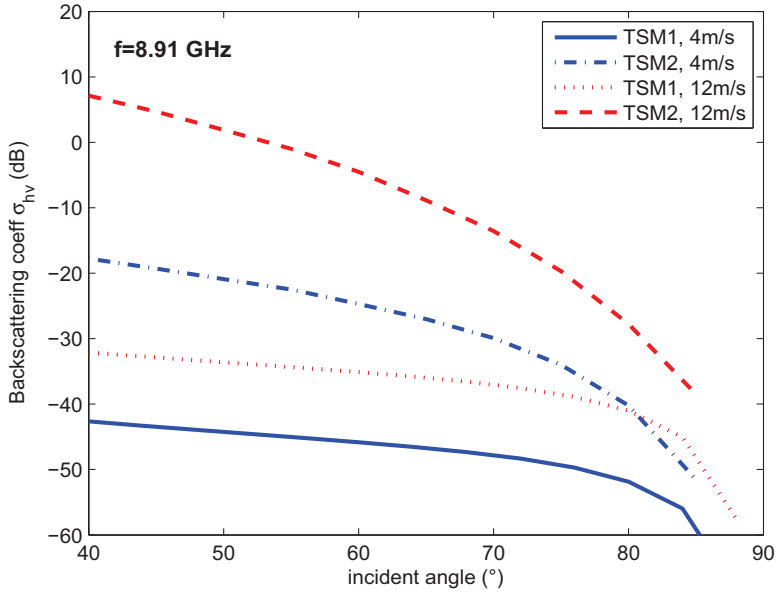

Figure 5.36: Backscattering coefficient: Comparison of TSM1 and TSM2 for HV polarization at X-band.

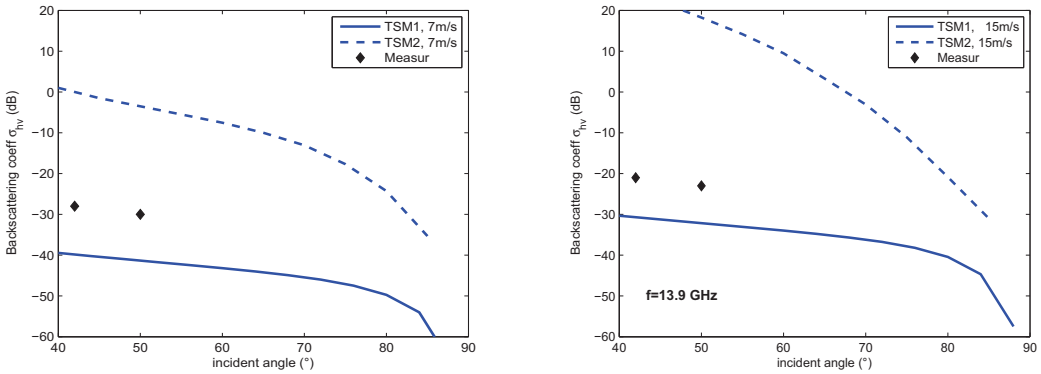

(a) (b)

Figure 5.37: Backscattering coefficient: Comparisons of TSM2 with experimental data [36] and TSM1, f=13.9 GHz (a)wind speed=7m/s; (b)wind speed=15m/s.

The variation of bistatic scattering coefficient σ_{hv} as a function of observed angle is given in Fig. 5.38 at L-band. The incident angle in the emission is fixed 80°, the received azimuth is set to 135° and the wind speed is taken as 3 m/s and then to 7 m/s. In the last figure (Fig. 5.39) of this section the bistatic scattering coefficient σ_{hv} is plotted against receptor azimuth. The emitters set to ($\theta_i = 80°$, $\varphi_i = 0°$), the observation angle θ_s is identical to incident angle θ_i and the comparisons are given for two wind speeds i.e., 3 m/s and 7 m/s at L-band. We note that the enhancement by TSM2 increases with the increase of wind speed and the comparisons on other frequency bans showed that the enhancement also increases by increasing the frequency.

5.4.2 Numerical Results for Bare Soil Surface

In this section, initially we illustrate the numerical simulation results of the cross polarized backscattering coefficient (σ_{hv}). The bistatic case is represented at the end of this section.

Figures 5.40 and 5.41 show the angular dependence of σ_{hv} for a bare soil surface with rms height (h) of 0.40 cm and correlation length (l) of 8.4 cm. For all three plots, the values of frequencies and relative dielectric constants are taken as 1.5 GHz,15.57 (L1); 4.75 GHz, 15.42 (X1) and 9.5 GHz, 12.31 (X1), respectively. The simulation results of TSM2 are compared with SPM2, TSM1 and measured data [34]. It is observed that the TSM2 give enhanced results which are in good agreement with the measured data.

We carry on the comparison between TSM1 and TSM2 for a relatively rough surface

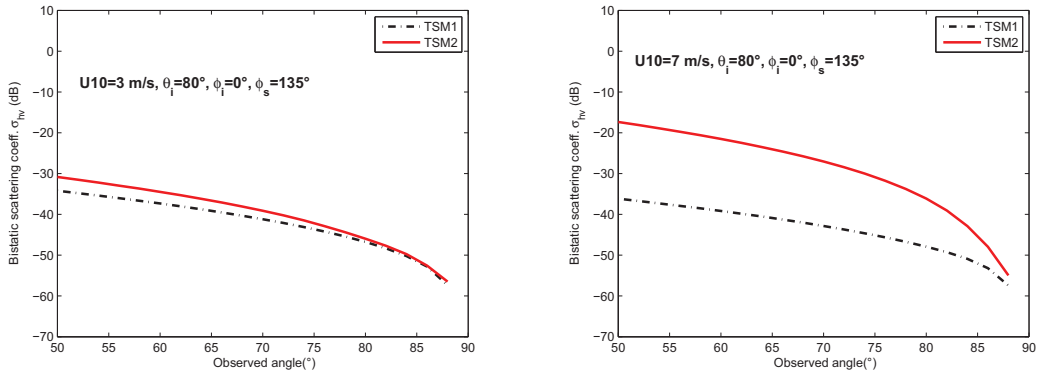

(a) (b)

Figure 5.38: Bistatic scattering coefficient: Comparisons between TSM1 and TSM2, f=1.228 GHz, $\varphi_i = 0°$, $\varphi_s = 135°$, $\theta_i = 80°$ for HV polarization,(a)wind speed=3m/s; (b)wind speed=7m/s.

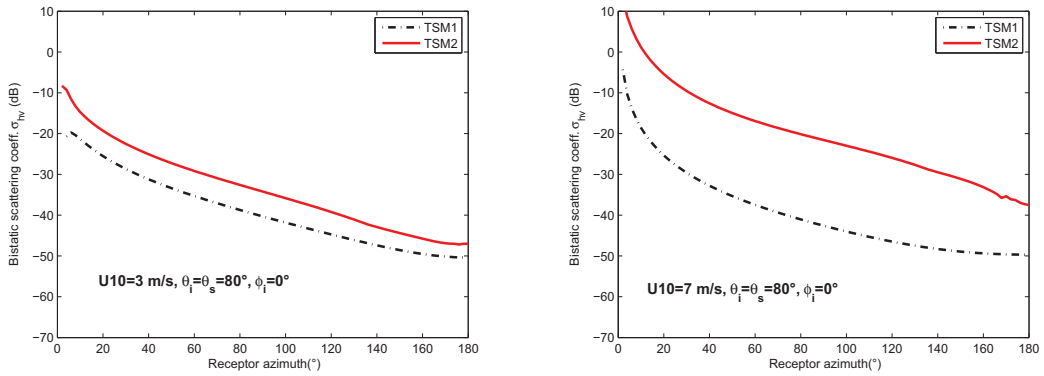

(a) (b)

Figure 5.39: Bistatic scattering coefficient: Comparisons between TSM1 and TSM2, f=1.228 GHz, $\varphi_i = 0°$,$\theta_i = \theta_s = 80°$, for HV polarization (a)wind speed=3m/s; (b)wind speed=7m/s.

with $h = 1.12$ cm and $l = 8.4$ cm at L2 ($f = 1.5$ GHz, $\varepsilon_r = 15.34$), C2 ($f = 4.75$ GHz, $\varepsilon_r = 15.23$) and X2 ($f = 9.5$ GHz, $\varepsilon_r = 13.14$) and found that the difference between two models increases as the roughness of the surface increases.

In Figs. 5.42 - 5.44 the comparison with measured data is given for a very rough surface with $h = 3.02$ cm and $l = 8.8$ cm at L3 ($f = 1.5$ GHz, $\varepsilon_r = 8.92$), C3 ($f = 4.75$ GHz, $\varepsilon_r = 9.64$) and X3 ($f = 9.5$ GHz, $\varepsilon_r = 7.57$). For L3 we are not so far from the

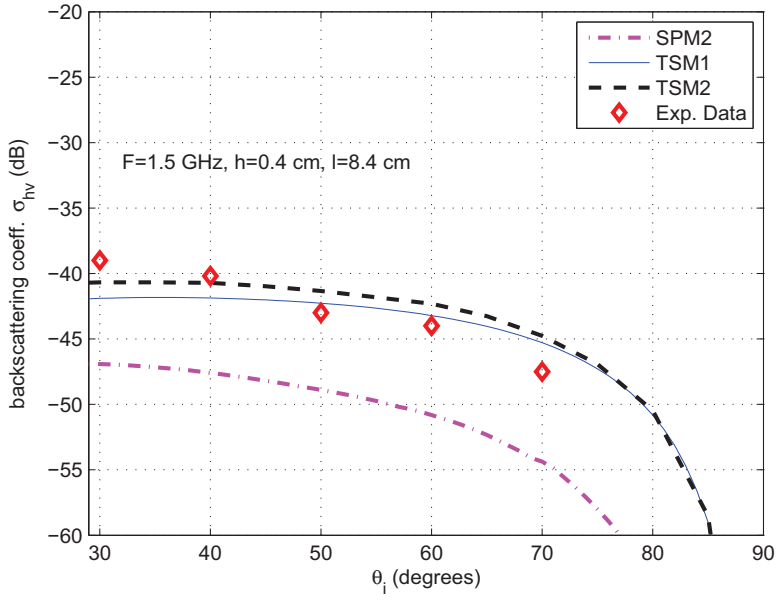

Figure 5.40: Backscattering coefficient: TSM2 compared to the measured data [34], SPM2 and TSM1 for $h = 0.40$ cm and $l = 8.4$ cm at L-band.

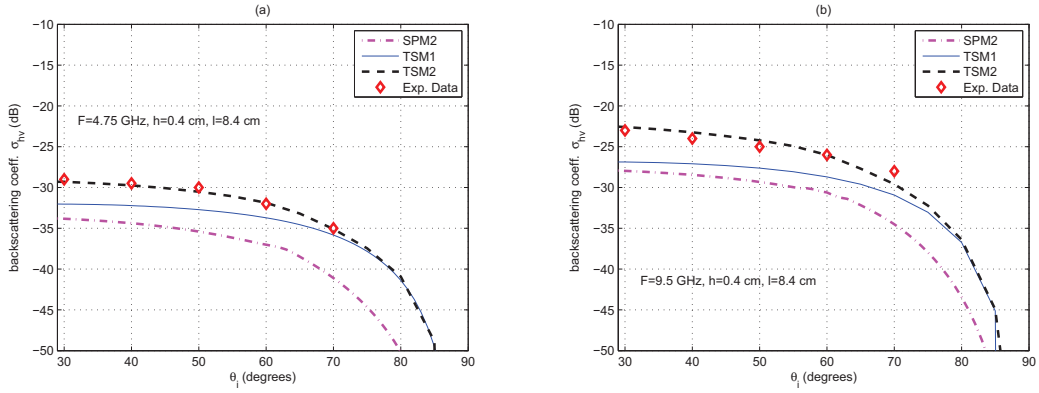

Figure 5.41: Backscattering coefficient: TSM2 compared to the measured data [34], SPM2 and TSM1 for $h = 0.40$ cm and $l = 8.4$ cm at (a) C-band, (b) X-band.

measured data but for the other two frequencies (i.e., C3 and X3) TSM2 over-estimates.

Next, to study further the consistency and validity of TSM2, we compare our results with AIEM and experimental data [35] in Fig. 5.45(a) which is plotted at S-band ($f = 3$ GHz) with $h = 1.045$ cm, $l = 19.47$ cm and $\varepsilon_r = 11.5$. Again the predictions by TSM2 are in better agreement with the measured data and AIEM.

To evaluate the applicability of TSM2, the locations of considered points are iden-

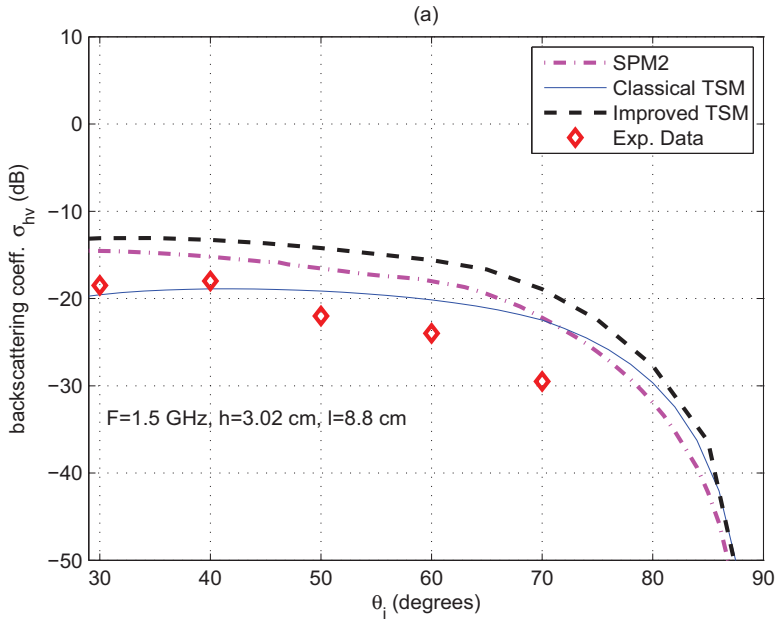

Figure 5.42: Backscattering coefficient: TSM2 compared to the measured data [34], SPM2 and TSM1 for $h = 3.02$ cm and $l = 8.8$ cm at L-band.

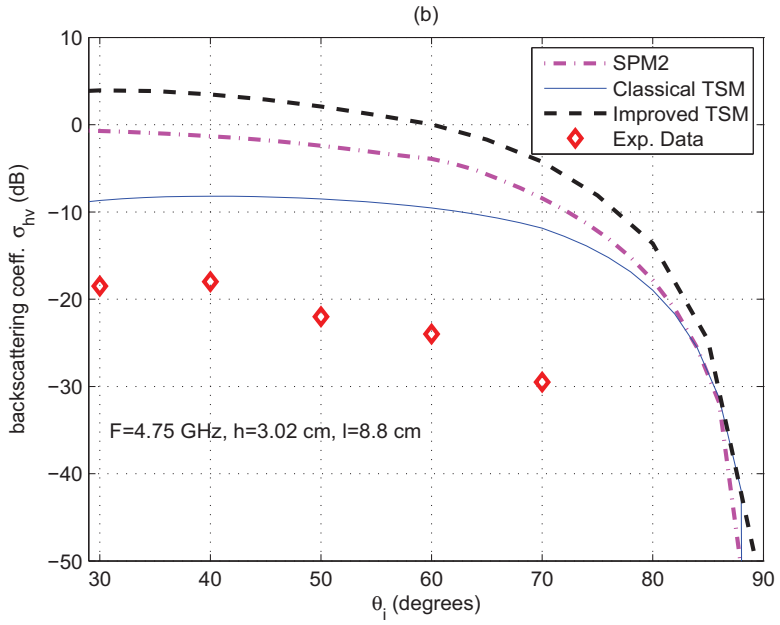

Figure 5.43: Backscattering coefficient: TSM2 compared to the measured data [34], SPM2 and TSM1 for $h = 3.02$ cm and $l = 8.8$ cm at C4-band.

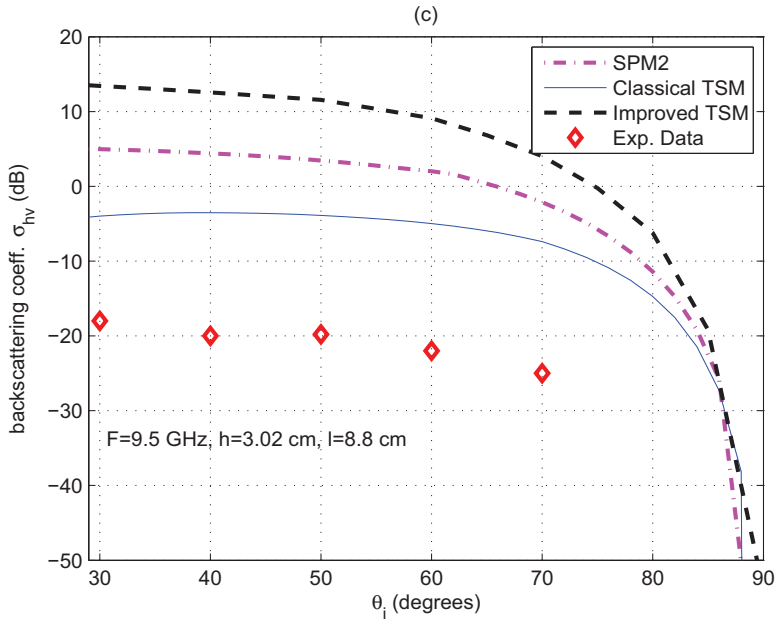

Figure 5.44: Backscattering coefficient: TSM2 compared to the measured data [34], SPM2 and TSM1 for $h = 3.02$ cm and $l = 8.8$ cm at X4-band.

tified in $ks - kl$ space in Fig. 5.45(b) along with the qualitative regions of validity of SPM1, SPM2 [72], PO (Physical Optics) and GO (Geometrical Optics) models. It is observed that TSM2 predictions are good/reasonable as far as $kh \leq 1$ and it overestimates otherwise. It is quite logical because actual estimation of cross polarized coefficients are due to the inclusion of second order scattering by SPM2 which is valid till $kh < 0.6$ [72], for moderate incident angles. On the other hand TSM2 can be used successfully for longer correlation lengths.

Furthermore, the comparison of TSM2 with SSA2 is also presented in Figs 5.46(a) and 5.46(b) for $kh = 0.5$, $kl = 3$ and $kh = 1$, $kl = 6$. TSM2 gives enhanced results as compared to SSA2 which is due to the fact that TSM also includes the averaging effects over slope distribution for long scale waves along with the scattering coefficient calculations by SPM for small scale waves.

Finally, Figs. 5.47(a) and (b) show the angular responses of the hv-polarized bistatic scattering coefficient (σ_{hv}). The incident angle is fixed at 45° while the received one varies from −90° to 90° and received azimuth is set at 45°.The numerical results are given for L1, L3, X1 and X3. It can be observed that the difference between two models increases with the increase in frequency and roughness level.

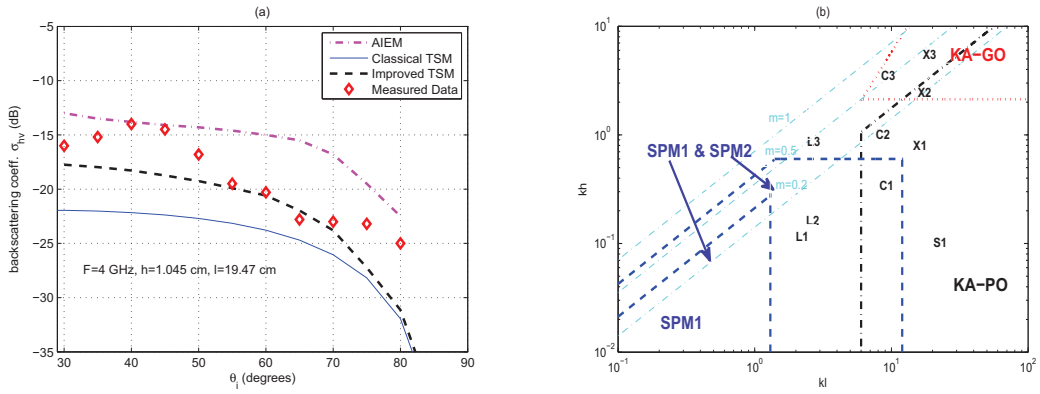

Figure 5.45: (a)Backscattering coefficient: TSM2 compared with AIEM, measured data [35] and TSM1 for $h = 3.02$ cm and $l = 8.8$ cm at S-band; b) roughness parameters and the qualitative region of validity of SPM1, SPM2, PO and GO models.

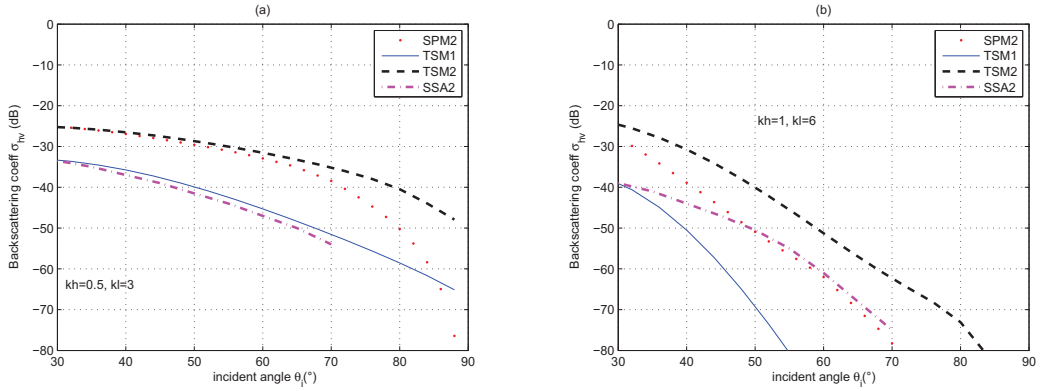

Figure 5.46: Backscattering coefficient: Comp. of SPM2, TSM1 and TSM2 with SSA2 (a)$kh = 0.5$, $kl = 3$; (b)kh=1, $kl = 6$.

5.4.3 Conclusion

In the second part of this chapter TSM2 has been analyzed for the cross polarization predictions in the backscattering and bistatic scattering directions. Again the application have been considered both for sea and soil surfaces. In the case of sea surface, due to the absence of measured data at grazing angles the comparisons are given only between TSM1 and TSM2. However, in the case of bare soil surface comparisons of numerical results with measured data and with other scattering models shows that TSM2 gives better predictions of depolarized components up to certain roughness limits. In bistatic case the comparisons are given by varying the observed and azimuthal angles.

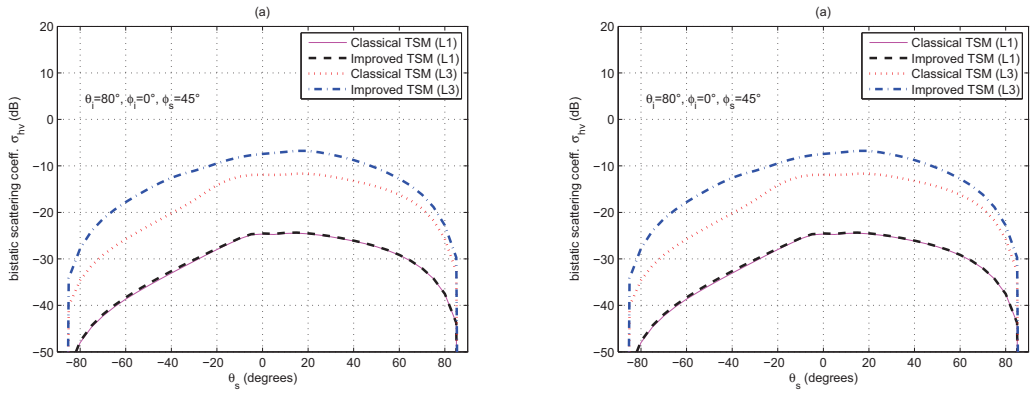

Figure 5.47: Bistatic scattering coefficient: Comp. of TSM1 and TSM2 (a) L-band (b) X-band.

5.5 Conclusion

In this chapter we have analyzed and validated the TSM2 by comparing its simulated results with measured and published results in literature. In the first part of the chapter, TSM2 has been used to study the bistatic scattering enhancement at grazing angles for horizontal polarization and its applications are given for sea and bare soil surfaces. For both surfaces the simulations has been performed by taking into account the geometrical representation (spectral representation and slope distribution) and physical characteristics (electric permittivity and magnetic permeability) and the comparisons are presented as a function of different parameters (incident and observed angles, emitted frequency, wind speed). We found that, in case of Gaussian and exponential spectrum, TSM2 can be used adequately to estimate the scattering coefficient from moderate to small grazing angles as far as the value of kh remains less than or nearly equal to 1. On the other hand it can be used for longer correlation lengths. Similarly, the comparisons base on Elfouhaily spectrum showed that TSM2 predictions at grazing angles are good for relatively low wind speeds and emitted frequency up to X-band.

In the second part of the chapter we have shown that, due to the inclusion of second order scattering effects while in the development of TSM2, it has the ability to predict accurately the depolarization in case of backscattering and bistatic scattering. The evaluation and validity limits of TSM2 for sea and soil surface is presented.

On the other hand, due to the four integrals involved in the calculation of scattering coefficient by using TSM2 it is computationally complex and take long time to give the results so there is a need to devise the methods to accelerate the results.

Chapter 6

Conclusions and Prospectives

The major contribution of this thesis have been the development of an improved Two-Scale Model (TSM2) by taking into account the contribution of second order (multiple) scattering effects from a random rough surface. The TSM2 was used, on the one hand, to study the bistatic scattering enhancement at grazing angles and on the other hand, to the accurate depolarization estimation. The applications of TSM2 were considered both for sea and bare soil surfaces and the newly developed model was validated by comparing the results with experimental measurements published in literature and with those obtained from other analytical approximate methods like Small Slope Approximation (SSA) and Weighted Curvature Approximation (WCA). Besides these major accomplishments the development, analysis and limitations of classical scattering models were also studied.

In the second chapter, after introducing the fundamental concepts of electromagnetism necessary to understand the effects of surface roughness on a scattering coefficient we recalled the equations of a monochromatic plane wave and then the diffraction and diffusion of electromagnetic waves by a rough surface is studied. We clarified the concepts of polarization with different states (linear, elliptical and circular). Furthermore, the statistical description of a random rough surface by using its geometrical characteristics (height distribution, function autocorrelation function characteristic spectral representation and distribution slopes) is given at end of this chapter.

The third chapter is devoted to the study of scattering models. The calculation of vector electromagnetic field scattered by a rough surface is not easy and there does not exist any exact solution which is valid for all configurations. Indeed, each method has its limitations, advantages and disadvantages, and the estimation of scattered field depends on the surface roughness with respect to emitted electromagnetic wavelength and the chosen geometrical configuration. Keeping this in mind three classically used scattering models i.e. Kirchhoff Approximation (KA), Small Perturbation Model

(SPM) and Two Scale Model (TSM) were presented. We started by reviewing the KA, which is applicable mainly for the calculation of specular component. The principle of this method is to assimilate the surface by a tangent plane at the incident point of transmitted wave. However, KA is no longer valid when the short wavelength waves dominate the surface. For a slightly rough surface SPM has been studied in detail. By using extended boundary condition method this method has been extended up to second order. A detailed comparison between SPM1 and SPM2 showed that due to the multiple scattering nature of SPM2, it possess bistatic scattering enhancement at grazing angles for certain configurations. Moreover, SPM2 produced non-zero results for backscattering direction as opposed to SPM1 and has larger validity domain.

The two studied models are valid for surfaces to a single scale of roughness i.e., a large and a small related to the incident wavelength. However, the natural surfaces are characterized by several scales of roughness. Since it is impossible to consider all scales, a model called two scales (TSM1) was studied. In this approach, the surface is characterized by two average scales of roughness, one small and the other a more significant as compared to the wavelength. It uses SPM1 at small scale i.e. for short wavelength waves and the effect of long wavelength part is taken into account by averaging over the tilt angles. Hence, TSM1 has larger domain of validity as compared to SPM1 and KA, but it is inaccurate for grazing angles and there is a gap in the domains of validity of SPM1 and KA. Moreover, the depolarization estimation by TSM1 are due to the tilt of reflecting plane and not an actual phenomena since both KA and SPM do not give predictions for depolarization in backscattering case when studied to first order. Hence there was a need to improve this model. Motivated by the observations of SPM2 we developed TSM2 by including the second order scattering effects into first order at small scale. The detail development has been presented at the end of the third chapter.

Mathematical modeling of the marine and soil surface, which is the key step in estimating the scattered field, was presented in fourth chapter. Thus, we focused on the physical and geometrical representation of the surfaces through different models published in literature.

To validate the developed model at grazing angles, the scattering coefficients of the ocean and soil surface have been estimated for horizontal polarization and compared with published results and measurements in the literature in fifth chapter. A study of depolarization for both surfaces at grazing angles was conducted in the second part of this chapter. The comparisons were based primarily on the monostatic configuration (backscattering). As for the bistatic configuration, unfortunately there does not exist many results in literature. A qualitative validity limit for each case was also given.

Various prospectives of this work can be considered. First, in this manuscript the

calculations by second order scattering field i. e., $\left\langle \mathbf{E}^{(2)}\mathbf{E}^{*(2)} \right\rangle$ has been considered while in the development of TSM2. As a result we obtained enhanced bistatic scattering at grazing angles and for other configurations enhanced results for all incident angles, resulting in over estimation at intermediate angles. To include the complete second order scattering effects, the contribution by third order field i. e., $\left\langle \mathbf{E}^{(1)}\mathbf{E}^{*(3)} \right\rangle$ & i. e., $\left\langle \mathbf{E}^{(3)}\mathbf{E}^{*(1)} \right\rangle$ should be considered. Since the third order field gives the negative effect at moderate angles so by including this part the validity domain of TSM2 can be extended for intermediate and small grazing angles. However, as we have already discussed that the calculation of scattering coefficient by TSM2 involves four integrals so it takes long time to compute the results. The computation and inclusion of third order field will make it more computationally complex. As a second prospective of this work some techniques should be proposed to reduce the number of numerical integrations to make the computation numerical implementation easier as given in [131, 132] for SSA2 (second order Small Slope Approximation) [37, 103, 105] and LCA2 (second order Local Curvature Approximation) [107, 133].

Third, as in the case composite TSM1, the scale dividing parameter k_d is always a challenging task for composite TSM2 to make it useful/utilizable in the whole angular domain. The selection of for composite TSM2 is more difficult than composite TSM1 because the calculations of SPM2 involves the convolution of two spectrums as opposed to SPM1, so its an open question to solve. Last but not the least is that we have considered second order (or multiple) scattering to get the enhanced bistatic scattering at grazing angles. The other phenomena like shadowing, wave breaking and fading should also be considered simultaneously for the accurate predictions of scattering coefficient at small grazing angles.

Chapter 7

Publications during Thesis

7.1 International Journals

- N. Sajjad, A. Khenchaf, A. Coatanhay, Depolarization of Electromagnetic waves from Bare Soil Surface, to appear in SCEE 2010 post-conference book (Mathematics in Industry by Springer).
- N. Sajjad, A. Khenchaf, A. Coatanhay, Electromagnetic wave scattering based on an improved two-scale model, submitted to IEEE Transactions on Antennas and Propagation, april 2010.

7.2 International Conferences

- N. Sajjad, A. Khenchaf, A. Coatanhay and A. Awadah, "An improved two scale model for the ocean surface bistatic scattering," IGARSS, Boston, USA, 6-11 July, 2008.
- N. Sajjad, A. Khenchaf and A. Coatanhay, "Electromagnetic wave scattering from sea and bare soil surface based on an improved two scale model, " invited paper, Radar 2009, Bordeaux, France, 12-16, October 2009.
- N. Sajjad, A. Khenchaf and A. Coatanhay, "Electromagnetic wave scattering from ocean surface at low grazing angles," IGARSS, Cap Town, South Africa, 13-17 July, 2009.
- N. Sajjad, A. Khenchaf, A. Coatanhay, "Depolarization of Electromagnetic waves from Sea Surface," OCOSS 2010, Brest, France, June 2010.
- N. Sajjad, A. Khenchaf, A. Coatanhay, "Depolarization of Electromagnetic waves from Bare Soil Surface," SCEE 2010, Toulouse, France, September 2010.

Bibliography

[1] J. W. Wright, "A new model for sea clutter," *IEEE Trans. Antennas Propagat.*, vol. AP-16, no. 2, pp. 217–223, 1968.

[2] M. F. Werby, and S. A. Chin-Bing, "A Study of High Order Born Approximations for Low Grazing Angle High Frequency Rough Interface Scattering," Naval Ocean Research and Development Activity NSTL Station MS, Rep. Accession no. ADA191963, 1988.

[3] D. J. McLaughlin et al., "High resolution polarimetric radar scattering measurements of low grazing angle sea clutter," *IEEE J. Ocean. Eng.*, vol. 20, no. 3, pp. 166–178,. Jul. 1995.

[4] M.I. Charnotskii, "Wave scattering by periodic surface at low grazing angles: Single grazing mode," *Progress in Electromagnetic Research, PIER* 26, pp. 1-42, 2000.

[5] G. R. Valenzuela, "Theories for the interaction of electromagnetic and oceanic waves — A review," *Boundary-layer Meteorology*, vol. 13, pp. 61-85, 1978.

[6] D. E. Barrick. "Near-grazing illumination and shadowing of rough surfaces,". *Radio Science*, 30 , pp. 563–580, May 1995.

[7] D. M. Milder, "Surface shadowing at small grazing angle," *Waves Random Media*, vol. 13, Issue 2, pp. 89-94, 2003.

[8] C. Bourlier, "Unpolarized infrared emissivity with shadow from anisotropic rough sea surfaces with non-Gaussian statistics," *Applied Optics,* 44 (20), 4335-4349, 2005.

[9] W. J. Plant, "Microwave sea return at moderate to high incidence angles," *Waves Random Media*, vol. 13, no. 3, pp. 339-354, Oct. 2003.

[10] V. W. Pidgeon, "Doppler dependence of radar sea return," *J. Geophys. Res.*, vol. 73, pp. 1333-1341, 1968.

[11] W. Keller, W. Plant, and G. Valenzuela, "Observations of breaking ocean waves with coherent microwave radar," in *Wave dynamics and radio probing of the sea surface*, ed. O. M. Phillips and K. Hasselmann, Plenum, New York, pp. 295-293, 1986.

[12] L. B. Wetzel, "Sea clutter, in Radar Handbook, 2nd ed, M. I Skolnik, Ed. New York: McGraw-Hill, 1990.

[13] P. H. Y. Lee et al., "What are the mechanisms for non-Bragg scattering from water wave surfaces," *Radio Sci.*, vol. 34, no.1, pp. 123–138, 1999.

[14] D. Walker, "Experimentally motivated model for low grazing angle Doppler spectra of the sea surface," *Proc. Inst. Elect. Eng.—Radar, Sonar, Navigat.*, vol. 147, no. 3, pp. 114–120, 2000.

[15] G. R. Valenzuela, "Depolarization of EM waves by slightly rough surfaces," *IEEE Trans. Ant. and Prop.*, vol. 15, pp. 552–557, 1967.

[16] Yisok Oh, "Comparison of two inversion methods for retrieval of soil moisture and surface roughness from polarimetric radar observation of soil surfaces," *Proc. IGARSS 04*. vol. 2, Issue , pp. 807 - 810. 2004.

[17] Yisok Oh, "Quantitative retrieval of soil moisture content and surface roughness from mulitipolarized radar observations of bare soil surfaces". *IEEE Trans. Geosci. Remote Sens.*, vol. 42, pp. 596-601, 2004.

[18] P. Beckmann, *The Depolarization of Electromagnetic Waves*, Golem Press, 1968.

[19] P. Beckman, and A. Spizzichino, *The Scattering of Electromagnetic Waves from Rough Surfaces*, Pergamon, New York, USA, 1963.

[20] D. E. Barrick, "Rough surface scattering based on the specular point theory," *IEEE Transactions on Antennas and Propagation*, vol. 16, issue 4, pp. 449-454, 1968.

[21] F. T. Ulaby, R. K. Moore, and A. K. Fung, *Microwave Remote Sensing: Active and Passive, vol. II, Radar Remote Sensing and Surface Scattering and Emission Theory*, Artech House, Inc., Norwwod, MA, 1986.

[22] Ogilvy, J. A. T*heory of Scattering from Random Rough Surfaces*, Adam Hilger, Bristol, England, 1991.

[23] L. Rayleigh, *The theory of sound*, vol. 2, dover, New York, 1945.

[24] S. O. Rice, "Reflection of electromagnetic waves from slightly rough surfaces," *Commun. Pure Appli. Math.* vol. 4, pp. 351-378,1951.

[25] G.S. Agarwal, "Interaction of electromagnetic waves at rough dielectric surfaces," *Phys. Rev.* B 15(4) 2371-2383, 1977.

[26] L. Tsang, and J.A. Kong, *Scattering of Electromagnetic Waves, Theories and Applications*, John Wiley & Sons, Inc. 2000.

[27] F. G. Bass, and I. M. Fuks, *Wave Scattering from Statistically Rough Surfaces*, Pergamon, 418-442, Pergamon Press Oxford, New York, 1979.

[28] A. K. Fung, Z. Li, and K. S. Chen, "Backscattering from a randomly rough dielectric surface," IEEE Trans. Geosci. Rem. Sens. 30, 356–369, 1992.

[29] A. Khenchaf, F. Daout, and J. Saillard, "The two-scale model for random rough surface scattering," *IEEE Supp. Proc. Oceans 96*, Ft Lauderdale, Florida, pp.50-54. 1996.

[30] A. Khenchaf, and O. Airiau, "Bistatic radarmoving returns from sea surface," *IEICE Trans. Elect.* vol. E83, pp.1827–1835, 2000.

[31] N. Sajjad, A. Khenchaf, A. Coatanhay, and A. Awada, "An improved two scale model for the ocean surface bistatic scattering", *IGARSS 08*, Boston, USA, 2008.

[32] N. Sajjad, A. Khenchaf, and A. Coatanhay, "Electromagnetic Wave Scattering From Sea and Bare Soil Surfaces Based On An Improved Two-Scale Model," *invited paper*, *International Radar Conference*, Bordeaux, October 2009.

[33] N.W. Guinard, and J.C. Daley, "An experimental study of a sea-clutter model," *Proc. IEEE* , 58, (4). pp. 543-550, 1970.

[34] Yisok Oh, Kamal Sarabandi, and Fawwaz T.Ulaby, "An Empirical Model and an Inversion Technique for Radar Scattering from Bare Soil Surfaces," *IEEE TGRS*, vol. 30, pp. 370–381, 1992.

[35] Liu et al. "Study on the backscattering characteristic of typical earth substances in northwest of Chaina," I*GARSS 09*, Cape Town, South Africa, july 12–17, 2009.

[36] R.K. Moore, A.K. Fung, "Radar determination of winds at sea," Proc. IEEE, vol. 67, pp. 1504–1521, Nov. 1979.

[37] M. S. Gilbert, and J. T. Johnson, "A study of the higher-order small-slope approximation for scattering from a Gaussian rough surface," *Waves Random Media*, vol. 13, pp. 137–149, 2003.

[38] P. Spiga, G. Soriano, and M. Saillard, "Modelling surface scattering at grazing incidence", *International Radar Conference*, Bordeaux, October 2009.

[39] N. Sajjad, A. Khenchaf, and A. Coatanhay, "Electromagentic wave from ocean surface at low grazing angles," *IGARSS 09*, Cape Town, South Africa, 2009.

[40] N. Sajjad, A. Khenchaf, and A. Coatanhay, " Depolarization of Electromagnetic Waves from Sea Surface," *Ocean & Coastal Observation : Sensors and Systems*, Eurpean conference, Brest, France, June 2010.

[41] N. Sajjad, A. Khenchaf, and A. Coatanhay, "Depolarization of Electromagnetic Waves From Bare Soil Surfaces," *Scientific Computing in Electrical Engineering (SCEE)*, Toulouse, France, 2010.

[42] N. Sajjad, A. Khenchaf, and A. Coatanhay, "Depolarization of Electromagnetic Waves From Bare Soil Surfaces" to appear in journal of Mathematics in industry by Springer (SCEE 2010 post conference book).

[43] R. E. Collin, *Foundations for Microwave Engineering.* Mc Graw-Hill International Editions, second edition edition, 1992.

[44] M. Born, and E. Wolf, *Principles of Optics,* 7th edition, Cambridge university press, New york, 1999.

[45] J.-P. Faroux, and J. Renault, *Electromagnétisme2:Equations de Maxwell et phénomènes d'induction.* Dunod, 1998.

[46] J. A. Stratton. *Electromagnetic theory.* Mc Gray-Hill, 1941.

[47] A. Sommerfled, Optics. New York : Academic Press, 1954.

[48] A. Ishimaru, *Electromagnetic Wave Propagation, Radiation, and Scattering*, Prentice Hall, New Jersey, 1991.

[49] C. T. Tai, *Dyadic Green's Functions in Electromagnetic Theory*, The 2nd edition, IEEE Press, Piscataway, New Jersey, 1994.

[50] L. Tsang, J. A. Kong, and R. Shin, *Theory of Microwave Remote Sensing*, Wiley-Interscience, New York, 1985.

[51] E. Wolf, "A generalized extinction theorem and its role in scattering theory" in *Coherence and Quantum Optics*, L. Mandel and E. Wolf, Editors, Plenum Press, New York, p. 339, 1973.

[52] R. S. Longhurst . *Geometrical and Physical Optics*, 2nd Edition. London: Longmans, 1968.

[53] P.P. Ewald. Ann. Phys. 49, 1, 1915.

[54] C.W. Oseen. Ann. Phys. 48, 1, 1915.

[55] M. Boerner, and W. L. Yan, "Introduction to Radar Polarimetry with Assesments of Historical Development and of the Current Stat-of-the-Art." In Journées Internationales de la polarimétrie Radar, Nantes, Mars 1990.

[56] G. Sinclair, "The transimission and reception of elliptically polarized waves," In *IRE*, vol. 38, pages 148–151, Ferbruary 1950.

[57] H. Mott," Antennas for Radar and communications: a polarimetric approach," *Wiley Series in microwave and optical Engineering* - Kai Chang, Seris Editor,1992.

[58] F. T. Ulaby, and C.Elachi, *Radar polarimetry for geoscience application*, artech House, 1990.

[59] A. Khenchaf, "Bistatic scattering and depolarization by randomly rough surface: application to the natural rough surface in X-band," Waves Random Media, vol.11, pp. 61–87, 2001.

[60] A. Khenchaf, "Bistatic reflection of electromagnetic waves from random rough surfaces: Application to the sea surface and snowy-covered," *European Physical Journal-Applied Physics* vol. 14(1): pp. 45-62, 2001.

[61] E. I. Thorsos, and D. R. Jackson, "Studies of scattering theory using numerical methods," *Waves Random Media*, vol. 3, pp. S165–S190, 1991

[62] S. Silver. *Microwave antenna theory and designe*. Mc Gray-Hill, 1947.

[63] A. Khenchaf, *Modélisation Electromagnétique; Radar Bistatique et Traitement de l'Information*, thèse de doctorat de l'université de Nantes, December 2000.

[64] P. C. Waterman, Phys. Rev. D 3, 825, 1971.

[65] P. C. Waterman, "Matrix formulation of electromagnetic scattering," *Proc. IEEE* 53, 805–812, 1965.

[66] M. Nieto-Vesperinas, "Depolarization of EM waves scattered from slightly rough random surfaces: a study by means of the extinction theorem," *J. Opt. Soc.Am.*72, 539-547, 1982.

[67] F. Toigo, A. Marvin, V. Celli, and N. R. Hill, "Optical properties of rough surfaces: General theory and the small roughness limit," *Phys. Rev.* B 15(12), 5618–5626,1977.

[68] J.M. Soto-Crespo, M. Nieto-Vesperinas, and A.T. Friberg, "Scattering from slightly rough random surfaces: a detailed study on the validity of the small perturbation method," *J. Opt. Soc. Am.* A 7, 1185-1201, 1990.

[69] S. H. Yueh, R. Kwok, F. K. Li, S. V. Nghiem, and W. J. Wilson, "Polarimetric passive remote sensing of ocean wind vectors," *Radio Sci.* 29, 799–814, 1994.

[70] J. T. Johnson, R. T. Shin, J. A. Kong, L. Tsang, and K. Pak, "A numerical study of ocean polarimetric thermal emission," "*IEEE Trans. Geosc. Rem. Sens.* , Jan 1999.

[71] L. Tsang, and J.A. Kong, *Scattering of Electromagnetic Waves, Advanced Topics*, John Wiley & Sons, Inc. 2001.

[72] E. I. Thorsos, and D. R. Jackson, "The validity of the perturbation approximation for rough surface scattering using a Gaussian roughness spectrum," *J. Acoust. Soc. Amer.*, vol. 86, pp. 261–277, 1989.

[73] M.-J. Kim, and A. J. Stoddart, "The region of validity of perturbation theory," *Waves Random Media*, vol. 3, pp. 325–342, 1993.

[74] M.-J. Kim, H. M. Berenyia, R. E. Burgea and S. Tajbakhsha, "Region of validity of perturbation theory for dielectrics and finite conductors," *Waves Random Media*, vol. 5, Issue 3, pp. 305 - 327, 1995.

[75] D. E. Barrick, and R. Fitzgerald, "The Failure of "Classic" Perturbation Theory at a Rough Neumann Boundary Near Grazing," *IEEE Trans. Antennas Propagat.* vol. 48, no. 9, 2000.

[76] GUO Li-Xin, WEI Guo-Hui, Kim Cheyoung and WU Zhen-Sen, "Modification of Classical SPM for Slightly Rough Surface Scattering with Low Grazing Angle Incidence", *Commun. Theor. Phys.* vol. 44, pp. 901–907, 2005.

[77] E. Thorsos, "The validity of the Kirchhoff approximation for rough surface scattering using a Gaussian roughness spectrum," *Journal of the Acoustical Society of America*, vol. 83, pp. 78–92, Jan. 1988.

[78] H. L. Chan, and A. K. Fung, "A theory of sea scatter at large incident angles," *J. Geophys. Res., vol.* 82, pp. 3439–3444, 1977.

[79] G. S. Brown, "Backscattering from a Gaussian-distributed perfectly conducting rough surface," *IEEE Trans. Antennas. Propagat.*, AP-26(3) :472–482, 1978.

[80] A. K. Fung, and K. K. Lee "A semi-empirical sea-spectrum model for scattering coeffcient estimation," *IEEE Jou. Ocean. Engine.*, 7(4) :166–176, 1982.

[81] Plant, W. J., "A Two-Scale Model of Short Wind-Generated Waves and Scatterometry," *J. Geophys. Res.*, vol. 91(C9), pp.10735–10749, 1986.

[82] W.J. Plant, "Bragg scattering of electromagnetic waves from air/sea interface," *Surfaces Waves and Fluxes*, G.L. Geerne art and W.J. Plant, Editors, vol 2, Kluwer Academic, pp.41-108, 1990.

[83] , J. R. Jensen, *Remote Sensing of the Environment: An Earth Resource Perspective* New Jersey: Prentice Hall, 2000.

[84] A. Khenchaf, *Modélisation électromagnétique Radar bistatique et traitement de l'information.* HDR, Ecole polytechnique de l'université de Nantes, 2000.

[85] L. A. Klein, and C. T. Swift, "An improved model for the dielectric constant of sea water at microwave frequencies," *IEEE Trans. Antennas. Propagat.*, AP-25 N°1 :104–111, 1977.

[86] P. Debye. *Polar molecules.* Chemical cathalog compagny, New York, 1929.

[87] K. S. Cole, and R. H. Cole, "Dispersion and absorption in dielectrics I. Alternating current characteristics," *Journal of chemilcal physics,* 9 :341–351, April 1941.

[88] K. S. Cole, and R. H. Cole, "Dispersion and absorption in dielectrics II. Direct current characteristics," *Journal of chemilcal physics*, 10 :98–105, February 1942.

[89] K. Lamkaouchi. *L'eau : étalon diélectrique. Etude de lois diélectriques appliquées à l'eau et à des émulsions de pétrole mesurées en micro-ondes.* thèse, l'université bordeau I, 1992.

[90] G.C. Topp, J.L. Davis, and A.P. Annan, "Electromagnetic Determination of soil water content: Measurements in Coaxial Transmission Lines", *Water Ressources Research*, 16.3, pp 574-582, 1980.

[91] M.C. dobson, F.T. Ulaby, M.T. Hallikainen and El-Rayes, "Microwave Dielectric Behavior of Wet Soil - Part II - Dielectric Mixing Models", *IEEE Trans. GRS,* 23.1, pp 35-46, 1985.

[92] G.P. Deloor, "Dielectric properties of heterogeneous mixtures containing water", *J.Microwave Power*, 3.2, pp 67-73,1968.

[93] N. R. Peplinski, F. T. Ulaby, and M. C. Dobson, "Dielectric properties of soils in the 0.3–1.3 GHz range,' IEEE Trans. Geosci. Remote Sensing, vol. 33, pp. 803–807, May 1995.

[94] C. Cox, and W. Munk, "Statistics of the sea surface derived from sun glitter," J. *Mar. Res*, 13 :198–226, 1954.

[95] C. Cox, and W. Munk, "Slopes of the sea surface deduced from photographs of sun glitter," *Bull. Scripps. Inst. of Oceanog.*, 6 :401–488, 1956.

[96] K. Yoshimori, K. Itoh, and Y. Ichioka, "Optical characteristics of a wind-roughned water surface : a two dimensinoal theory," *Applied Optics*, 34(27) :6236–6247, 1995.

[97] T. Elfouhaily, B. Chapron, K. Katsaros, and D. Vandemark, "A unified directional spectrum for long and short wind-driven waves," *J. Geophys. Res.*, 102(C7) :781–796, 1997.

[98] Mattia, F., T. Le Toan, J. Souyris, G. Carolis, N. Floury, F. Posa, and G. Pasquariello, "The effect of surface roughness on multifrequency polarimetric SAR data," *IEEE TGRS.*, vol. 35, no. 4, pp. 954-966, Jul. 1997.

[99] M. W. J. Davidson et al., "On the characterization of agricultural soil roughness for radar remote sensing studies," *IEEE TGRS.*, vol. 38, no. 2, pp. 630-640, Mar. 2000.

[100] A. Ishimaru, *Wave Propagation and Scattering in Random Media*, IEEE Press, New York,1997 (Reprint of the 1978 original, with a foreword by Gary S. Brown, An IEEE/OUP Classic Reissue.)

[101] D.P. Winebrenner, and A. Ishimaru, "Investigation of a surface field phase perturbation technique for scattering from rough surfaces," *Radio Science* 20, pp.161-170, 1985.

[102] A. G. Voronovich ,"Small-slope approximation in wave scattering from rough surfaces," *Sov. Phys. JETP*, vol. 62, pp.65 - 70 , 1985.

[103] A. G. Voronovich, "Small-slope approximation for electromagnetic wave scattering at a rough interface of two dielectric half-spaces," *Waves Random Media*, vol. 4, pp. 337–367, 1994.

[104] S. T. McDaniel, "A small-slope theory of rough surface scattering,". *J. Acoust. Soc. Am.* vol. 95, pp.1858-1864, 1994.

[105] A. G. Voronovich, *Wave Scattering from Rough Surfaces*, Springer Series on Wave Phenomena. Berlin, Germany: Springer-Verlag, 1999.

[106] T. Elfouhaily, S. Guignard, and D. R. Thompson,"Formal tilt invariance of the local curvature approximation" *Waves Random Media* 13, L7–11, 2003.

[107] T. Elfouhaily, S. Guignard, R. Awadallah, and D. R. Thompson,"Local and non-local curvature approximation: a new asymptotic theory for wave scattering", *Waves Random Media* 13, pp 321–338, 2003.

[108] C.A. Guérin, G. Soriano, and T. Elfouhaily, "Weighted curvature approximation: numerical tests for 2D dielectric surfaces," *Waves in Random and Complex Media*, vol. 14(3), pp. 349–363, 2004.

[109] C. Bourlier, N. Dechamps, and G. Berginc, "Comparison of asymptotic backscattering models (SSA, WCA, and LCA) from one-dimensional Gaussian ocean-like surfaces," *IEEE Transactions on Antennas and Propagation*, vol. 53(5), pp. 1640–1652, 2005.

[110] T. Elfouhaily, and C. -A. Guérin, "A critical survey of approximate wave theories from random rough surfaces," *Waves Random Media*, vol. 14, pp. R1–R40, 2004.

[111] J. M. Soto-Crespo, M. Nieto-Vesperinas and A. T. Fridberg, "Scattering from slightly rough random surfaces: a detailed study on the validity of the small perturbation method," JOSA A, Vol. 7, Issue 7, pp. 1185-1201, 1990.

[112] S. Broschat, "The phase perturbation approximation for rough surface scattering from a Pierson–Moskowitz sea surface," *IEEE TGRS.*, vol. 31, pp. 278–283, Jan. 1993.

[113] S. T. Wu, and A. K. Fung, "A noncoherent model for microwave emissions and backscattering from the sea surface," *J.Geophys. Res.* 77, 5917–5929, 1972.

[114] EM Software & Systems-S.A. (Pty) Ltd, "FEKO Product Overview", Web site: www.feko.info.

[115] D. Colton, and R. Kress, *Integral Equations in Scattering Theory*, New York: Wiley-Interscience, 1983.

[116] J. J. H. Wang, *Generalized Moment Method in Electromagnetics*, New York: Wiley-Interscience, 1991.

[117] F. G. Bass et al., A."Very high frequency radiowave scattering by a disturbed sea surface Part II: Scattering from an actual sea surface," IEEE Trans. Antenna and Propagation, AP- 16(5), pp. 560-568, 1968.

[118] G. Franceschetti, A. Iodice and D. Riccio, "Scattering from dielectric random fractal surfaces via method of moments," *IEEE Trans. Geosci. Remote Sensing*, vol. 38, pp. 1644–1655, Sept. 2000.

[119] J. R. Wang, and B. J. Choudhury, "Remote sensing of soil moisture content over bare fields at 1.4 GHz frequency," *J. Geophys. Res.*, Vol. 86, pp. 5277–5282, 1981.

[120] Tsang, L. and R. W. Newton, "Microwave emissions from soils with rough surfaces," *J. Geophy. Res.*, Vol. 87, No. 11, 9017–9024, 1982.

[121] Wang, J. R. P. E. O'Neill, T. J. Jackson, and E. T. Engman, "Multi-frequency measurements of the effects of soil moisture, soil texture and surface roughness," *IEEE Transactions on Geoscience and Remote Sensing*, Vol. 21, 44–51, 1983.

[122] J. C. Shi, J. Wang, A. Y. Hsu, P. E. O'Neill, and E. T. Engman, "Estimation of bare surface soil moisture and surface roughness parameter using L-band SAR image data," *IEEE Transactions on Geoscience and Remote Sensing*, Vol. 35, 1254–1266, Sep. 1997.

[123] J. Shi, K. S. Chen, Q. Li, T. J. Jackson, P. E. O'Neill, and L. Tsang, "A parameterized surface reflectivity model and estimation of bare-surface soil moisture with L-band radiometer," *IEEE Transactions on Geoscience and Remote Sensing*, Vol. 40, No. 12, 2674–2686, 2002.

[124] J. C. Shi, L. M. Jiang, L. X. Zhang, K. S. Chen, J.-P. Wigneron, and A. Chanzy, "A parameterized multifrequency-polarization surface emission model," *IEEE Transactions on Geoscience and Remote Sensing*, Vol. 43, No. 12, 2831–2841, 2005.

[125] M. Davidson, et al."A validation of multi-scale surfaces roughness dscription for the modelling of rdara backscattering from bare soils", I1 Intern. Work. on Retr. of Geo-physical Param. from SAR data for Land Applic., Estec, The Netherlands, 21-23 Oct. 1998.

[126] H. R. Raemer, and D.D. Preis, "Aspects of Parallel-Polarized and Cross-Polarized Radar Returns from a Rough Sea Surface," *IEEE Trans. on EM Compat.*, vol. 22, Issue 1, pp. 29–44, 1980.

[127] A. K. Fung, *Microwave Scattering and Emission Models and Their Applications*, Artech House, Norwood, MA, 1994.

[128] T.-D. Wu and K. S. Chen,"A reappraisal of the validity of the IEM model for backscattering from rough surfaces," *IEEE TGRS*, vol.42, no. 4, pp. 743Ű-753, 2004.

[129] H. W. Lee et al., "Extension of Advanced Integral Equation Model for Calculations of Fully Polarimetric Scattering Coefficient from Rough Surface," *IGARSS*, July 23–28, 2007.

[130] T. D. Wu, K.S. Chen, J. C. Shi, H. W. Lee and A. K. Fung, "A study of AIEM Model for Bistatic Scattering from Randomly Surfaces," *IEEE TGRS*, vol.46(9), pp. 2584–2598, 2008.

[131] C. Bourlier, "Azimuthal harmonic coefficients of the microwave backscattering from a non-Gaussian ocean surface with the first-order SSA model," *IEEE Trans. Geos. Rem. Sensing*, vol. 42, no. 11, pp. 2600-2611, 2004.

[132] C. Bourlier, and N. Pinel, "Numerical implementation of local unified models for backscattering from random rough sea surfaces," *Waves Random Complex Media*, vol. 19, no. 3, pp. 455-479, 2009.

[133] T. M. Elfouhaily, and J. T. Johnson, "Extension of the local curvature approximation to third order and full tilt invariance," *Waves Random Complex Media*, vol. 16, no. 2, pp. 97-119, 2006.

Appendix A

SPM simplified scattering coefficients

A.1 SPM1

The bistatic scattering coefficient for SPM1 is given by (eqs. $(1.2.56a)$ and $(1.2.56b)$)[71]

$$\begin{aligned}\sigma^{(1)}\left(\widehat{\mathbf{K}}_s,\widehat{\mathbf{K}}_i\right) &= 4\pi K^2\cos^2\theta_s W\left(\mathbf{k}_s-\mathbf{k}_i\right)\left\{\left|f_{ee}^{(1)}\left(\mathbf{k}_s,\mathbf{k}_i\right)\left(\widehat{e}\left(-k_{iz}\right).\widehat{e}_i\right)\right.\right. \\ &\quad \left.\left.+f_{eh}^{(1)}\left(\mathbf{k}_s,\mathbf{k}_i\right)\left(\widehat{h}\left(-k_{sz}\right).\widehat{e}_i\right)\right|^2\right\} \qquad (A.1)\end{aligned}$$

for scattered wave in $\widehat{e}\left(k_{sz}\right)$ i.e., horizontal polarization (according to the convention used in [71]) and

$$\begin{aligned}\sigma^{(1)}\left(\widehat{\mathbf{K}}_s,\widehat{\mathbf{K}}_i\right) &= 4\pi K^2\cos^2\theta_s W\left(\mathbf{k}_s-\mathbf{k}_i\right)\left\{\left|f_{he}^{(1)}\left(\mathbf{k}_s,\mathbf{k}_i\right)\left(\widehat{e}\left(-k_{iz}\right).\widehat{e}_i\right)\right.\right. \\ &\quad \left.\left.+f_{hh}^{(1)}\left(\mathbf{k}_s,\mathbf{k}_i\right)\left(\widehat{h}\left(-k_{sz}\right).\widehat{e}_i\right)\right|^2\right\} \qquad (A.2)\end{aligned}$$

for scattered wave in $\widehat{h}\left(k_{sz}\right)$ i.e.,vertical polarization, where $f_{pq}^{(1)}$ are polarization dependent terms defined as

$$f_{ee}^{(1)}\left(\mathbf{k}_s,\mathbf{k}_i\right)=\frac{\left(K_1^2-K^2\right)}{k_{sz}+k_{1zs}}\frac{2k_{iz}}{k_{iz}+k_{1zi}}\cos\left(\phi_s-\phi_i\right) \qquad (A.3)$$

$$f_{eh}^{(1)}\left(\mathbf{k}_s,\mathbf{k}_i\right)=\frac{K_1^2-K^2}{k_{sz}+k_{1zs}}\frac{2Kk_{iz}k_{1zi}}{K^2k_{1zi}+K_1^2k_{iz}}\sin\left(\phi_s-\phi_i\right) \qquad (A.4)$$

$$f_{he}^{(1)}\left(\mathbf{k}_s,\mathbf{k}_i\right)=\frac{\left(K_1^2-K^2\right)k_{1zs}K}{K_1^2k_{sz}+K^2k_{1zs}}\frac{2k_{iz}}{k_{iz}+k_{1zi}}\sin\left(\phi_s-\phi_i\right) \qquad (A.5)$$

$$f_{hh}^{(1)}(\mathbf{k}_s,\mathbf{k}_i) = \frac{K_1^2-K^2}{K_1^2k_{sz}+K^2k_{1zs}}\frac{2K^2k_{iz}}{K^2k_{1zi}+K_1^2k_{iz}} \cdot\left\{-k_{1zs}k_{1zi}\cos(\phi_s-\phi_i)+k_{\rho s}k_{\rho i}\frac{K_1^2}{K^2}\right\} \quad (A.6)$$

Note that $\sigma^{(1)}\left(\widehat{\mathbf{K}}_s,\widehat{\mathbf{K}}_i\right) = \gamma^{(1)}\left(\widehat{\mathbf{K}}_s,\widehat{\mathbf{K}}_i\right).\cos\theta_i$. Assume that $f^{(1)}(\mathbf{k}_s,\mathbf{k}_i) = 4K^2\cos^2\theta_i\alpha^{(1)}(\mathbf{k}_s,\mathbf{k}_i)$ and replace the indices $e \leftrightarrow h$, $h \leftrightarrow v$ i.e., according to the convention used in our thesis to represent the horizontal and vertical polarization. Now for horizontaly polarized incident wave, by putting $\widehat{e}_i = \widehat{e}(-k_{iz})$ in (A.1) and (A.2) we obtain

$$\sigma_{hh}^{(1)} = 16\pi\left|K^2\cos\theta_i\cos\theta_s\alpha_{hh}^{(1)}\right|^2 W(k_{sx}-k_{ix},k_{sy}-k_{ix}) \quad (A.7)$$

$$\sigma_{vh}^{(1)} = 16\pi\left|K^2\cos\theta_i\cos\theta_s\alpha_{vh}^{(1)}\right|^2 W(k_{sx}-k_{ix},k_{sy}-k_{ix}) \quad (A.8)$$

Similarly for vertically polarized incident wave, by putting $\widehat{e}_i = \widehat{h}(-k_{iz})$ in (A.1) and (A.2)we obtain

$$\sigma_{hv}^{(1)} = 16\pi\left|K^2\cos\theta_i\cos\theta_s\alpha_{hv}^{(1)}\right|^2 W(k_{sx}-k_{ix},k_{sy}-k_{ix}) \quad (A.9)$$

$$\sigma_{vv}^{(1)} = 16\pi\left|K^2\cos\theta_i\cos\theta_s\alpha_{vv}^{(1)}\right|^2 W(k_{sx}-k_{ix},k_{sy}-k_{ix}) \quad (A.10)$$

Hence in generale, the bistatic scattering coefficient for SPM1 is given as

$$\sigma_{pq}^{(1)} = 16\pi\left|K^2\cos\theta_i\cos\theta_s\alpha_{pq}^{(1)}\right|^2 W(k_{sx}-k_{ix},k_{sy}-k_{ix}) \quad (A.11)$$

where the polarization dependent terms $\alpha_{pq}^{(1)}$ can be obtained in simplified form from (A.3)-(A.6) by using (2.19), (3.30) and the following transformations

$$\begin{cases} k_{sx} = K\sin\theta_s\cos\phi_s \\ k_{sy} = K\sin\theta_s\sin\phi_s \\ k_{sz} = K\cos\theta_s \\ k_{s\rho} = K\sin\theta_s \\ k_{1zs} = \sqrt{K_1^2-k_{s\rho}^2} = K\sqrt{\varepsilon_r-\sin^2\theta_s} \end{cases} \quad (A.12)$$

as

$$\alpha_{hh}^{(1)} = \frac{(\varepsilon_r - 1)\cos(\varphi_s - \varphi_i)}{\left(\cos\theta_s + \sqrt{\varepsilon_r - \sin^2\theta_s}\right)\left(\cos\theta_i + \sqrt{\varepsilon_r - \sin^2\theta_i}\right)} \tag{A.13}$$

$$\alpha_{hv}^{(1)} = \frac{(\varepsilon_r - 1)\sqrt{\varepsilon_r - \sin^2\theta_i}\sin(\varphi_s - \varphi_i)}{\left(\cos\theta_s + \sqrt{\varepsilon_r - \sin^2\theta_s}\right)\left(\varepsilon_r\cos\theta_i + \sqrt{\varepsilon_r - \sin^2\theta_i}\right)} \tag{A.14}$$

$$\alpha_{vh}^{(1)} = \frac{(\varepsilon_r - 1)\sqrt{\varepsilon_r - \sin^2\theta_s}\sin(\varphi_s - \varphi_i)}{\left(\varepsilon_r\cos\theta_s + \sqrt{\varepsilon_r - \sin^2\theta_s}\right)\left(\cos\theta_i + \sqrt{\varepsilon_r - \sin^2\theta_i}\right)} \tag{A.15}$$

$$\alpha_{vv}^{(1)} = \frac{(\varepsilon_r - 1)\left\{\sqrt{\varepsilon_r - \sin^2\theta_s}\sqrt{\varepsilon_r - \sin^2\theta_i}\cos(\varphi_s - \varphi_i) - \varepsilon_r\sin\theta_i\sin\theta_s\right\}}{\left(\varepsilon_r\cos\theta_s + \sqrt{\varepsilon_r - \sin^2\theta_s}\right).\left(\varepsilon_r\cos\theta_i + \sqrt{\varepsilon_r - \sin^2\theta_i}\right)} \tag{A.16}$$

A.2 SPM2

The bistatic scattering coefficient for SPM2 is given by eqs. (1.3.64*a*)-(1.3.64*d*)[71]

$$\sigma_{pq}^{(2)} = 4\pi K^2\cos^2\theta_s \int_{-\infty}^{\infty} d\mathbf{k}_d W(\mathbf{k}_s - \mathbf{k}_d) W(\mathbf{k}_d - \mathbf{k}_i)\,\alpha_{pq}^{(2)}(\mathbf{k}_s, \mathbf{k}_d, \mathbf{k}_i) \cdot \left[\alpha_{pq}^{(2)*}(\mathbf{k}_s, \mathbf{k}_d, \mathbf{k}_i) + \beta_{pq}^{(2)*}(\mathbf{k}_s, \mathbf{k}_s - \mathbf{k}_d + \mathbf{k}_i, \mathbf{k}_i)\right] \tag{A.17}$$

where (eq. (1.3.60)[71])

$$\alpha_{pq}^{(2)}(\mathbf{k}_s, \mathbf{k}_d, \mathbf{k}_i) = \alpha_{pqa}^{(2)}(\mathbf{k}_s, \mathbf{k}_i) + \alpha_{pqb}^{(2)}(\mathbf{k}_s, \mathbf{k}_d, \mathbf{k}_i) \tag{A.18}$$

and the second order polarization dependent terms $\alpha_{pqa}^{(2)}$ and $\alpha_{pqb}^{(2)}$ can be obtained from eqs. (1.2.75*b*)-(1.2.75*i*)[71] as

$$\alpha_{hha}^{(2)} = \frac{k_{iz}}{k_{iz} + k_{1zi}}\left(\frac{K_1^2 - K^2}{k_{1zs} + k_{sz}}\right)\left\{\cos(\phi_s - \phi_i)(k_{1zi} + k_{1zs})\right\} \tag{A.19}$$

$$\alpha_{hhb}^{(2)} = \frac{-2k_{iz}}{k_{iz} + k_{1zi}}\left(\frac{K_1^2 - K^2}{k_{1zs} + k_{sz}}\right)\left(K_1^2 - K^2\right) \cdot \left[-\sin(\phi_s - \phi_k')\sin(\phi_k' - \phi_i)\frac{k_z' k_{1z}'}{K_1^2 k_z' + K^2 k_{1z}'} + \cos(\phi_s - \phi_k')\cos(\phi_k' - \phi_i)\frac{1}{k_{1z}' + k_z'}\right] \tag{A.20}$$

$$\alpha_{hva}^{(2)} = \frac{K_1^2 - K^2}{k_{1zs} + k_{sz}}\frac{K k_{iz}}{K_1^2 k_{iz} + K^2 k_{1zi}}\left\{\sin(\phi_s - \phi_i)\left(K_1^2 + k_{1zs}k_{1zi}\right)\right\} \tag{A.21}$$

$$\begin{aligned}\alpha_{hvb}^{(2)} &= -\frac{2K_1^2-K^2}{k_{1zs}+k_{sz}}\frac{Kk_{iz}}{K_1^2k_{iz}+K^2k_{1zi}}\Big[\sin\left(\phi_s-\phi_{dk}\right)\frac{K_1^2k_{d\rho}k_{\rho i}}{k_{d\rho}^2+k_{dz}k_{d1z}}\\ &+\frac{\left(K_1^2-K^2\right)k_{1zi}}{K_1^2k_{dz}+K^2k_{d1z}}\left(\sin\left(\phi_s-\phi_{dk}\right)\cos\left(\phi_{dk}-\phi_i\right)k_{dz}k_{d1z}\right.\\ &\left.+\cos\left(\phi_s-\phi_{dk}\right)\sin\left(\phi_{dk}-\phi_i\right)\left(k_{d\rho}^2+k_{dz}k_{d1z}\right)\right)\Big] \qquad \text{(A.22)}\end{aligned}$$

$$\alpha_{vha}^{(2)}=\frac{K}{k_{sz}}\frac{\left(K_1^2-K^2\right)}{\left(K_1^2k_{sz}+K^2k_{1zs}\right)}\frac{k_{sz}k_{iz}}{\left(k_{iz}+k_{1zi}\right)}\sin\left(\phi_s-\phi_i\right)\left(K_1^2+k_{1zs}k_{1zi}\right) \qquad \text{(A.23)}$$

$$\begin{aligned}\alpha_{vhb}^{(2)} &= -\frac{2K}{k_{sz}}\frac{\left(K_1^2-K^2\right)}{\left(K_1^2k_{sz}+K^2k_{1zs}\right)}\frac{k_{sz}k_{iz}}{k_{iz}+k_{1zi}}\Big[\sin\left(\phi_k'-\phi_i\right)\frac{K_1^2k_{s\rho}k_\rho'}{k_\rho'^2+k_z'k_{1z}'}\\ &+\frac{k_{1zs}\left(K_1^2-K^2\right)}{\left(K_1^2k_z'+K^2k_{1z}'\right)}\left(k_z'k_{1z}'\cos\left(\phi_s-\phi_k'\right)\sin\left(\phi_k'-\phi_i\right)\right.\\ &\left.+\left(k_\rho'^2+k_z'k_{1z}'\right)\sin\left(\phi_s-\phi_k'\right)\cos\left(\phi_k'-\phi_i\right)\right)\Big] \qquad \text{(A.24)}\end{aligned}$$

$$\begin{aligned}\alpha_{vva}^{(2)} &= -\frac{K}{k_{sz}}\frac{\left(K_1^2-K^2\right)}{\left(K_1^2k_{sz}+K^2k_{1zs}\right)}\frac{1}{\left(K_1^2k_{iz}+K^2k_{1zi}\right)}\cos\left(\phi_s-\phi_i\right)\\ &.\left(k_{1zi}+k_{1zs}\right)K_1^2Kk_{sz}k_{iz} \qquad \text{(A.25)}\end{aligned}$$

$$\begin{aligned}\alpha_{vvb}^{(2)} &= -\frac{2K}{k_{sz}}\frac{\left(K_1^2-K^2\right)}{\left(K_1^2k_{sz}+K^2k_{1zs}\right)}\frac{1}{\left(K_1^2k_{iz}+K^2k_{1zi}\right)}k_{sz}k_{iz}\\ &\Big[Kk_{1zs}k_{1zi}\frac{\left(K_1^2-K^2\right)}{\left(k_{1z}'+k_z'\right)}\sin\left(\phi_s-\phi_k'\right)\sin\left(\phi_k'-\phi_i\right)\\ &+\frac{1}{\left(K_1^2k_z'+K^2k_{1z}'\right)}\left(\frac{K_1^2}{K}\left(K_1^2-K^2\right)k_{\rho s}k_{\rho i}k_\rho'^2\right.\\ &-k_{s\rho}k_\rho'KK_1^2\left(k_z'+k_{1z}'\right)k_{1zi}\cos\left(\phi_k'-\phi_i\right)\\ &-k_{\rho i}k_\rho'KK_1^2\left(k_z'+k_{1z}'\right)k_{1zs}\cos\left(\phi_s-\phi_k'\right)\\ &\left.-Kk_z'k_{1z}'\left(K_1^2-K^2\right)k_{1zs}k_{1zi}\cos\left(\phi_k'-\phi_i\right)\cos\left(\phi_s-\phi_k'\right)\right)\Big] \qquad \text{(A.26)}\end{aligned}$$

Now to make the scattering coefficient (A.17) and polarization dependent terms (A.6)-(A.6) in more comprehensible and explicit form we use (2.19), (3.30), (A.12) and

$$\begin{cases} k_{dx}=K\sin\theta_d\cos\varphi_d\\ k_{dy}=K\sin\theta_d\sin\varphi_d\\ k_{dz}=K\cos\theta_d\\ dk_{dx}dk_{dy}=K^2\sin\theta_d\cos\theta_d d\theta_d\varphi_d\\ k_{d\rho}=K\sin\theta_d\\ k_{d1z}=\sqrt{K_1^2-k_{d\rho}^2}=K\sqrt{\varepsilon_r-\sin^2\theta_d} \end{cases} \qquad \text{(A.27)}$$

and after simplifying them we get

$$\begin{aligned}\sigma_{pq}^{(2)} &= 4\pi K^4 \cos^2\theta_s \int_0^{2\pi}\int_0^{\pi/2} \sin\theta_d \cos\theta_d d\theta_d d\varphi_d W\left(\mathbf{k}_s - \mathbf{k}_d\right) W\left(\mathbf{k}_d - \mathbf{k}_i\right) \\ &\quad .\alpha_{pq}^{(2)}\left[\alpha_{pq}^{(2)*} + \beta_{pq}^{(2)*}\right] \end{aligned} \tag{A.28}$$

and

$$\begin{aligned}\alpha_{hh}^{(2)} &= \frac{K^2 \cos\theta_i \left(\varepsilon_r - 1\right)}{\left(\cos\theta_i + \sqrt{\varepsilon_r - \sin^2\theta_i}\right)\left(\cos\theta_s + \sqrt{\varepsilon_r - \sin^2\theta_s}\right)} \\ &\quad \left[\cos\left(\varphi_s - \varphi_i\right)\left(\sqrt{\varepsilon_r - \sin^2\theta_i} + \sqrt{\varepsilon_r - \sin^2\theta_s}\right) - 2\left(\varepsilon_r - 1\right)\right. \\ &\quad \left\{\frac{-\sin\left(\varphi_s - \varphi_d\right)\sin\left(\varphi_d - \varphi_i\right)\cos\theta_d \sqrt{\varepsilon_r - \sin^2\theta_d}}{\varepsilon_r \cos\theta_d + \sqrt{\varepsilon_r - \sin^2\theta_d}}\right. \\ &\quad \left.\left. + \frac{\cos\left(\varphi_s - \varphi_d\right)\cos\left(\varphi_d - \varphi_i\right)}{\cos\theta_d + \sqrt{\varepsilon_r - \sin^2\theta_d}}\right\}\right] \end{aligned} \tag{A.29}$$

$$\begin{aligned}\beta_{hh}^{(2)} &= \frac{\varepsilon_r - 1}{\left(\cos\theta_i + \sqrt{\varepsilon_r - \sin^2\theta_i}\right)\left(\cos\theta_s + \sqrt{\varepsilon_r - \sin^2\theta_s}\right)} \\ &\quad \left[\cos\left(\phi_s - \phi_i\right)\left(\sqrt{\varepsilon_r - \sin^2\theta_i} + \sqrt{\varepsilon_r - \sin^2\theta_s}\right) + 2\left(\varepsilon_r - 1\right)\right. \\ &\quad \left.\left\{\frac{\sin\left(\phi_s - \phi_1\right)\sin\left(\phi_1 - \phi_i\right) C\sqrt{\varepsilon_r - A^2 - B^2}}{\varepsilon_r C + \sqrt{\varepsilon_r - A^2 - B^2}} - \frac{\cos\left(\phi_s - \phi_1\right)\cos\left(\phi_1 - \phi_i\right)}{\sqrt{\varepsilon_r - A^2 - B^2} + C}\right\}\right] \end{aligned} \tag{A.30}$$

$$\begin{aligned}\alpha_{hv}^{(2)} &= \frac{K^2 \cos\theta_i}{\left(\cos\theta_s + \sqrt{\varepsilon_r - \sin^2\theta_s}\right)\left(\varepsilon_r \cos\theta_i + \sqrt{\varepsilon_r - \sin^2\theta_i}\right)} \\ &\quad .\left[\left(\varepsilon_r - 1\right)\sin\left(\varphi_s - \varphi_i\right)\left(\varepsilon_r + \sqrt{\left(\varepsilon_r - \sin^2\theta_s\right)\left(\varepsilon_r - \sin^2\theta_i\right)}\right)\right. \\ &\quad - \left(2\varepsilon_r - 1\right)\left[\frac{\varepsilon_r \sin\theta_d \sin\theta_i \sin\left(\varphi_s - \varphi_d\right)}{\sin^2\theta_d + \cos\theta_d \sqrt{\varepsilon_r - \sin^2\theta_d}}\right. \\ &\quad + \frac{\left(\varepsilon_r - 1\right)\sqrt{\varepsilon_r - \sin^2\theta_i}}{\varepsilon_r \cos\theta_d - \sqrt{\varepsilon_r - \sin^2\theta_d}}\Big(\sin\left(\varphi_s - \varphi_d\right)\cos\left(\varphi_d - \varphi_i\right) \\ &\quad .\cos\theta_d \sqrt{\varepsilon_r - \sin^2\theta_d} + \cos\left(\varphi_s - \varphi_d\right)\sin\left(\varphi_d - \varphi_i\right) \\ &\quad \left.\left.\left.\left. .\left(\sin^2\theta_d + \cos\theta_d \sqrt{\varepsilon_r - \sin^2\theta_d}\right)\right)\right]\right] \end{aligned} \tag{A.31}$$

$$\beta_{hv}^{(2)} = \frac{1}{\left(\cos\theta_s + \sqrt{\varepsilon_r - \sin^2\theta_s}\right)\left(\varepsilon_r\cos\theta_i + \sqrt{\varepsilon_r - \sin^2\theta_i}\right)}$$
$$\left[(\varepsilon_r - 1)\sin(\phi_s - \phi_i)\left(\varepsilon_r + \sqrt{\left(\varepsilon_r - \sin^2\theta_s\right)\left(\varepsilon_r - \sin^2\theta_i\right)}\right)\right.$$
$$-(2\varepsilon_r - 1)\left[\frac{\varepsilon_r\sqrt{A^2+B^2}\sin\theta_i\sin(\phi_s-\phi_1)}{(A^2+B^2)+C\sqrt{\varepsilon_r - A^2 - B^2}} + \frac{(\varepsilon_r-1)\sqrt{\varepsilon_r - \sin^2\theta_i}}{\varepsilon_r C + \sqrt{\varepsilon_r - A^2 - B^2}}\right.$$
$$\left(\sin(\phi_s-\phi_1)\cos(\phi-\phi_i)\,C\sqrt{\varepsilon_r - A^2 - B^2}\right.$$
$$\left.\left.\left.+\cos(\phi_s-\phi_1)\sin(\phi_1-\phi_i)\left(\left(A^2+B^2\right)+C\sqrt{\varepsilon_r - A^2 - B^2}\right)\right)\right]\right] \quad \text{(A.32)}$$

$$\alpha_{vh}^{(2)} = \frac{K^2(\varepsilon_r - 1)\cos\theta_i}{\left(\varepsilon_r\cos\theta_s + \sqrt{\varepsilon_r - \sin^2\theta_s}\right)\left(\cos\theta_i + \sqrt{\varepsilon_r - \sin^2\theta_i}\right)}$$
$$\left[\sin(\varphi_s - \varphi_i)\left(\varepsilon_r + \sqrt{\varepsilon_r - \sin^2\theta_s}\sqrt{\varepsilon_r - \sin^2\theta_i}\right)\right.$$
$$-2\left(\sin(\varphi_d - \varphi_i)\frac{\varepsilon_r\sin\theta_s\sin\theta_d}{\sin^2\theta_d + \cos\theta_d\sqrt{\varepsilon_r - \sin^2\theta_d}}\right.$$
$$+\frac{\sqrt{\varepsilon_r - \sin^2\theta_s}(\varepsilon_r - 1)}{\left(\varepsilon_r\cos\theta_d + \sqrt{\varepsilon_r - \sin^2\theta_d}\right)}$$
$$.\left(\cos\theta_d\sqrt{\varepsilon_r - \sin^2\theta_d}\cos(\varphi_s - \varphi_d)\sin(\varphi_d - \varphi_i)\right.$$
$$\left.\left.\left.+\left(\sin^2\theta_d + \cos\theta_d\sqrt{\varepsilon_r - \sin^2\theta_d}\right)\sin(\varphi_s - \varphi_d)\cos(\varphi_d - \varphi_i)\right)\right)\right] \quad \text{(A.33)}$$

$$\beta_{vh}^{(2)} = \frac{\varepsilon_r - 1}{\left(\varepsilon_r\cos\theta_s + \sqrt{\varepsilon_r - \sin^2\theta_s}\right)\left(\cos\theta_i + \sqrt{\varepsilon_r - \sin^2\theta_i}\right)}$$
$$\left[\sin(\phi_s - \phi_i)\left(\varepsilon_r + \sqrt{\varepsilon_r - \sin^2\theta_s}\sqrt{\varepsilon_r - \sin^2\theta_i}\right)\right.$$
$$-2\left(\frac{\sin(\phi_1 - \phi_i)\,\varepsilon_r\sin\theta_s\sqrt{A^2+B^2}}{(A^2+B^2)+C\sqrt{\varepsilon_r - A^2 - B^2}} + \frac{\sqrt{\varepsilon_r - \sin^2\theta_s}(\varepsilon_r - 1)}{\left(\varepsilon_r C + \sqrt{\varepsilon_r - A^2 - B^2}\right)}\right.$$
$$\left(C\sqrt{\varepsilon_r - A^2 - B^2}\cos(\phi_s - \phi_1)\sin(\phi_1 - \phi_i)\right.$$
$$\left.\left.\left.+\left(\left(A^2+B^2\right)+C\sqrt{\varepsilon_r - A^2 - B^2}\right)\sin(\phi_s - \phi_1)\cos(\phi_1 - \phi_i)\right)\right)\right] \quad \text{(A.34)}$$

$$
\begin{aligned}
\alpha_{vv}^{(2)} = {} & \frac{K^2\left(\varepsilon_r-1\right)\cos\theta_i}{\left(\varepsilon_r\cos\theta_s+\sqrt{\varepsilon_r-\sin^2\theta_s}\right)\left(\varepsilon_r\cos\theta_i+\sqrt{\varepsilon_r-\sin^2\theta_i}\right)} \\
& .\Big[-\varepsilon_r\cos\left(\varphi_s-\varphi_i\right)\left(\sqrt{\varepsilon_r-\sin^2\theta_i}+\sqrt{\varepsilon_r-\sin^2\theta_s}\right) \\
& -2\Big[\sqrt{\varepsilon_r-\sin^2\theta_s}\sqrt{\varepsilon_r-\sin^2\theta_i}\frac{\left(\varepsilon_r-1\right)\sin\left(\varphi_s-\varphi_d\right)\sin\left(\varphi_d-\varphi_i\right)}{\left(\cos\theta_d+\sqrt{\varepsilon_r-\sin^2\theta_d}\right)} \\
& +\frac{1}{\left(\varepsilon_r\cos\theta_d+\sqrt{\varepsilon_r-\sin^2\theta_d}\right)}.\Big(\varepsilon_r\left(\varepsilon_r-1\right)\sin\theta_s\sin\theta_i\sin^2\theta_d \\
& -\sin\theta_s\sin\theta_d\varepsilon_r\left(\cos\theta_d+\sqrt{\varepsilon_r-\sin^2\theta_d}\right)\sqrt{\varepsilon_r-\sin^2\theta_i}\cos\left(\varphi_d-\varphi_i\right) \\
& -\sin\theta_i\sin\theta_d\varepsilon_r\left(\cos\theta_d+\sqrt{\varepsilon_r-\sin^2\theta_d}\right)\sqrt{\varepsilon_r-\sin^2\theta_s}\cos\left(\varphi_s-\varphi_d\right) \\
& -\cos\theta_d\left(\varepsilon_r-1\right)\sqrt{\varepsilon_r-\sin^2\theta_d}\sqrt{\varepsilon_r-\sin^2\theta_s}\sqrt{\varepsilon_r-\sin^2\theta_i} \\
& .\cos\left(\varphi_d-\varphi_i\right)\cos\left(\varphi_s-\varphi_d\right)\Big)\Big]\Big]
\end{aligned} \tag{A.35}
$$

$$
\begin{aligned}
\beta_{vv}^{(2)} = {} & \frac{\left(\varepsilon_r-1\right)}{\left(\varepsilon_r\cos\theta_s+\sqrt{\varepsilon_r-\sin^2\theta_s}\right)\left(\varepsilon_r\cos\theta_i+\sqrt{\varepsilon_r-\sin^2\theta_i}\right)} \\
& \Big[-\varepsilon_r\cos\left(\phi_s-\phi_i\right)\left(\sqrt{\varepsilon_r-\sin^2\theta_i}+\sqrt{\varepsilon_r-\sin^2\theta_s}\right) \\
& -2\Big[\sqrt{\varepsilon_r-\sin^2\theta_s}\sqrt{\varepsilon_r-\sin^2\theta_i}\frac{\left(\varepsilon_r-1\right)\sin\left(\phi_s-\phi_1\right)\sin\left(\phi_1-\phi_i\right)}{\left(\sqrt{\varepsilon_r-A^2-B^2}+C\right)} \\
& +\frac{1}{\left(\varepsilon_r C+\sqrt{\varepsilon_r-A^2-B^2}\right)}\Big(\varepsilon_r\left(\varepsilon_r-1\right)\sin\theta_s\sin\theta_i\left(A^2+B^2\right) \\
& -\sin\theta_s\sqrt{A^2+B^2}\varepsilon_r\left(C+\sqrt{\varepsilon_r-A^2-B^2}\right)\sqrt{\varepsilon_r-\sin^2\theta_i}\cos\left(\phi_1-\phi_i\right) \\
& -\sin\theta_i\sqrt{A^2+B^2}\varepsilon_r\left(C+\sqrt{\varepsilon_r-A^2-B^2}\right)\sqrt{\varepsilon_r-\sin^2\theta_s}\cos\left(\phi_s-\phi_1\right) \\
& -C\sqrt{\varepsilon_r-A^2-B^2}\left(\varepsilon_r-1\right)\sqrt{\varepsilon_r-\sin^2\theta_s}\sqrt{\varepsilon_r-\sin^2\theta_i} \\
& \cos\left(\phi_1-\phi_i\right)\cos\left(\phi_s-\phi_1\right)\Big)\Big]\Big]
\end{aligned} \tag{A.36}
$$

where

$A=\sin\theta_s\cos\phi_s-\sin\theta\cos\phi+\sin\theta_i\cos\phi_i$

$B=\sin\theta_s\sin\phi_s-\sin\theta\sin\phi+\sin\theta_i\sin\phi_i$

$C=\cos\theta_s-\cos\theta+\cos\theta_i$

$\phi_1=\tan^{-1}B/A$

Appendix B

Debye's Model

B.1 Mathematical formulation

In this paragraph the functions, $\varepsilon_s, \sigma$and τ are presented.

B.1.1 Static permittivity

As for the static permittivity ε_s, it depends on salinity S and temperature T of water. It can be written as

$$\varepsilon_s(T,S) = \varepsilon_s(T,0)a(T,S) \tag{B.1}$$

This expression is valid for a sea of salinity ranging between 4 and 35 ppm where

$$\begin{aligned} \varepsilon_s(T,0) &= 87.134 - 1.949 \times 10^{-1}T - 1.276 \times 10^{-2}T^2 + 2.491 \times 10^{-4}T^3 && \text{(B.2)} \\ a(T,S) &= 1.0 + 1.613 \times 10^{-5}TS - 3.656 \times 10^{-3}S + 3.210 \times 10^{-5}S^2 \\ &\quad -4.232 \times 10^{-7}S^3 && \text{(B.3)} \end{aligned}$$

B.1.2 Relaxation time

τ is the time of relaxation, it is given by

$$\tau(T,S) = \tau(T,0)b(T,S) \tag{B.4}$$

This expression is valid for $0 \leq S \leq 157$ and for $0 \leq T \leq 40°C$ with

$$\begin{aligned} 2\pi\tau(T,0) &= 1.1109 \times 10^{-10} - 3.824 \times 10^{-12}T + \\ &\quad 6.938 \times 10^{-14}T^2 - 5.096 \times 10^{-16}T^3 && \text{(B.5)} \\ b(T,S) &= 1.0 + 2.282 \times 10^{-5}TS - 7.638 \times 10^{-4}S \\ &\quad -7.760 \times 10^{-6}S^2 + 1.105 \times 10^{-8}S^3 && \text{(B.6)} \end{aligned}$$

B.1.3 Static conductivity

σ is the static conductivity of the salted water expressed in $\Omega^{-1}m^{-1}$ and is given by

$$\sigma(T,S) = \sigma(25,S)e^{-\Pi} \tag{B.7}$$

This expression is valid for $0 \leq S \leq 40$ with

$$\sigma(25,S) = S[0.18252 - 1.4619 \times 10^{-3}S + 2.093 \times 10^{-5}S^2 - 1.282 \times 10^{-7}S^3] \tag{B.8}$$

$$\begin{aligned} \Pi &= \triangle[2.033 \times 10^{-2} + 1.266 \times 10^{-4} \triangle + 2.464 \times 10^{-6} \triangle^2 && \text{(B.9)} \\ &\quad -S(1.849 \times 10^{-(} - 2.551 \times 10^{-7}\Delta + 2.551 \times 10 - 8\Delta^2 && \text{(B.10)} \end{aligned}$$

and

$$\triangle = 25 - T$$

Appendix C

Résumé en français

L'estimation de la surface équivalente radar (SER) des fouillis de mer et terrestre est essentielle pour la conception et l'amélioration des performances des systèmes de télédétection et d'observation de la planète. Le problème particulier de la diffusion des ondes en configuration à angle rasant est de grand intérêt à cause de son importance pour la surveillance longue portée de radar, suivi de cible, la communication et les systèmes de navigation fonctionnant au dessus de la surface rugueuse. La surface équivalente radar d'une surface rugueuse devient très faible en incidence rasante puisque la plus grande partie de la puissance incidente est diffusée dans la direction spéculaire (selon le degré de rugosité de la surface). De plus, les mécanismes principaux de diffusion sont différents aux angles rasants, par exemple, les effets de diffusion multiple (ou de diffusion d'ordre supérieur) [1]–[4], l'ombrage [5]–[8], fading [9] et les mécanismes liés au déferlement des vagues [10]–[14] sont particulièrement présents dans une telle configuration. Par conséquent, c'est dans ce contexte que s'intègre les travaux de recherche développés dans cette thèse. Ceci en développant le modèle deux échelles à l'ordre 2 permettant ainsi de contribuer à l'estimation des coefficients de diffusion bistatique par les surfaces rugueuses avec l'application de ce modèle aux surfaces maritime et terrestre.

Le mécanisme de la diffusion multiple en raison de la rugosité de surface provoque également la dépolarisation de l'onde émise (changement d'état de polarisation ou polarisation croisée) [15]. Cette dépolarisation due à la rugosité de la surface et son observation en configuration bistatique entrainent l'estimation des quatre coefficients de la matrice de diffusion. Et l'information issue des termes en polarisation croisée ajoutée à celle extraite des termes en co-polarisation peuvent être exploitée pour récupérer différents paramètres et notamment de rugosité de surface [16, 17], aussi des propriétés diélectriques de la surface, ... etc [18]. En conséquence, l'étude de la dépolarisation ne peut être utilisée que pour mettre en évidence des phénomènes physiques mis en jeu

lors de la propagation et la diffusion mais aussi pour des objectifs de caractérisation, de détection et de reconnaissance d'objets présents sur la surface.

Dans ce contexte, l'objectif de cette thèse est d'étudier la problématique de dépolarisation des ondes par les surfaces rugueuses observées en configuration bistatique et particulièrement dans la zone de rasance. Ainsi, l'extension à l'ordre 2 du modèle de diffusion à deux échelles TSM1 a été proposée. Afin d'effectuer l'évaluation de ce modèle, des modèles et approximations souvent utilisés qui sont l'Approximation de Kirchhoff (KA) [19]–[22], méthode des petites perturbations à l'ordre un (SPM1- first order Small Perturbation Method) [23]–[26] et le modèle à deux échelles (TSM- Two Scale Model) [1, 27, 28, 29, 30] ont été présentés dans un premier temps. Il est à noter que le modèle TSM1 qui combine KA et SPM1 possède un domaine de validité plus important et il a été appliqué avec succès dans différentes configurations et applications. Cependant, ce modèle utilise le modèle SPM1 dont les coefficients de diffusion croisés sont nuls en configuration monostatique. D'où la nécessité d'étendre le modèle TSM1 en utilisant le modèle SPM2. Dans l'objectif d'effectuer cette extension, nous avons étudié et comparé les résultats de simulation obtenus par SPM1 et SPM2. Cette comparaison est effectuée en utilisant d'abord une surface décrite par un spectre Gaussien. En dehors des termes croisés non nuls en monostatique pour SPM2, les résultats obtenus pour ce type de surface et pour certaines configurations montrent une amélioration des coefficients de rétrodiffusion et notamment pour des angles d'incidence importants. Ensuite, après développement du modèle TSM2, des applications sont présentées pour les surfaces maritime et terrestre en utilisant respectivement le spectre de Elfouhaily et le spectre exponentiel [31, 32]. Les résultats de simulation obtenus sont comparés avec des données réelles publiées dans la littérature [9, 33, 34, 35, 36] et aussi avec ceux obtenus via d'autres techniques approchées comme SSA (Small Slope Approximation) [37] et WCA (Weight Curvature Approximation) [38]. Cette évaluation et ces différentes comparaisons démontrent la pertinence et la validité du modèle TSM2, en particulier pour des angles rasants [39, 40, 41, 42].

Après le premier chapitre dédié à une introduction présentant le contexte et les objectifs de la problématique traitée, les travaux de recherche réalisés dans le cadre de cette thèse sont organisés en cinq chapitres.

Le deuxième chapitre de ce manuscrit rappelle certains concepts fondamentaux liés à la théorie des ondes électromagnétiques, les définitions et les notations utilisées par la suite dans les autres chapitres. Puis nous présentons les différentes techniques de description statistique d'une surface rugueuse aléatoire.

Dans le troisième chapitre, d'abord nous étudions et présentons les modèles de diffusion EM par les surfaces rugueuses utilisées classiquement (KA et SPM), qui sont caractérisés par un domaine de validité angulaire limitée. Puis, en utilisant la méthode

d'extension des conditions aux limites « extended boundary condition method » (la méthode des conditions de frontière étendue) nous avons étudié le modèle SPM jusqu'au second ordre. Ensuite, en considérant une surface décrite par un spectre gaussien, différentes simulations ont été effectuées en comparant les résultats obtenus à l'aide de SPM2 avec ceux obtenus via SPM1. Ce chapitre se termine en commençant par examiner le modèle TSM1en remplaçant dans l'écriture de TSM1 le modèle SPM1 par le modèle SPM à l'ordre 2 (SPM1 + SPM2). Cette analyse permet de présenter le développement du modèle TSM2.Cette description est ensuite utilisée pour estimer le champ électromagnétique diffusé par ces surfaces. Ainsi, nous avons caractérisé la surface maritime en utilisant soit un spectre Gaussien soit le spectre d'Elfouhaily. Concernant la distribution des pentes, nous avons retenu, selon l'application traitée, soit un modèle Gaussien soit la représentation de Cox&Munk. Pour la surface terrestre, le spectre exponentiel et la distribution des pentes Gaussienne sont utilisés. De même, nous présentons dans ce chapitre les expressions analytiques de modèle de Debye et le modèle de Peplinski pour la permittivité électrique respectivement de l'eau de mer et le sol.

Le cinquième et dernier chapitre présente les résultats numériques obtenus en utilisant le modèle TSM2. Dans la première partie de ce chapitre, l'application de TSM2 est réalisée en considérant les surfaces maritime et terrestre, observées notamment aux angles rasants. Les résultats obtenus en monostatique sont comparés avec les données expérimentales publiés, et aussi avec ceux obtenus via les approches TSM1, SSA et WCA. Ensuite, les résultats de simulation sont donnés pour le cas bistatique et comparés avec ceux obtenus à l'aide de TSM1. La prédiction de la dépolarisation (ou polarisation croisée) par TSM2 sont évaluées dans la deuxième partie de ce chapitre. La limite de validité dans chaque cas est également proposée.

Enfin, une conclusion permettant de dresser un bilan des travaux réalisés est présentée. Elle est suivie par un ensemble de perspectives offertes au travail réalisé.

Mots clés: modèle de deux échelles à l'ordre 2, coefficients de diffusion bistatique, surfaces rugueuses, surface maritime, surface terrestre, incidence rasante, polarisation croisée.